CLERMONT AUVERGNE INP
uca
Ecole doctorale Sciences Pour l'Ingénieur

Calcul à haute performance, répétabilité et reproductibilité des résultats numériques et des mesures de performance

LIMOS

Université Clermont Auvergne, LIMOS, Aubière, France
Benjamin Antunes et David Hill

Problématique

Au fil des années, l'utilisation d'ordinateurs s'est totalement démocratisée dans la recherche scientifique. Pour répondre aux besoins toujours croissants de la science et des connaissances, des machines de plus en plus puissantes sont développées, avec des architectures de plus en plus complexes. C'est ce que l'on nomme des supercalculateurs.
Sur ces machines, nous pouvons faire tourner de très grosses simulations, paralléliser des programmes et essayer de percer les mystères de l'univers. Une question qui peut paraitre triviale se pose : L'informatique a t-elle permis de faire avancer la science ? Sans conteste, il est très probable que oui. Les outils que nous avons aujourd'hui nous permettent d'aller beaucoup plus vite et loin que ce que nous pouvions faire auparavant.
Néanmoins, certains problèmes sont apparus : Des problèmes de reproductibilité. L'ordinateur va agir comme une boite noire, et l'article publié dans un journal ne permettra pas de reproduire les résultats. Ben Marwick titre un article : "How computers broke science – and what we can do to fix it" [1]. La reproductibilité, défini par Karl Popper comme étant un des critères différenciant la Science de la Pseudo-science, concerne toute la production scientifique. On peut citer John P.A Ioannidis ayant écrit un article nommé "Why most published research findings are false" [2].
Dans le cadre de ma thèse, je vais étudier comment le monde du calcul haute performance a des problèmes de reproductibilité.

Exemples de problèmes en informatique

$$(10^{-3} + 1) - 1 \sim 0$$
$$10^{-3} + (1 - 1) = 10^{-3}$$

```
1 >>> (pow(10,-3)+1)-1
2 0.0009999999999998899
3 >>> pow(10,-3)+(1-1)
4 0.001
5 >>>
```

Problèmes d'hyperthreading sur SkyLake et KabyLake

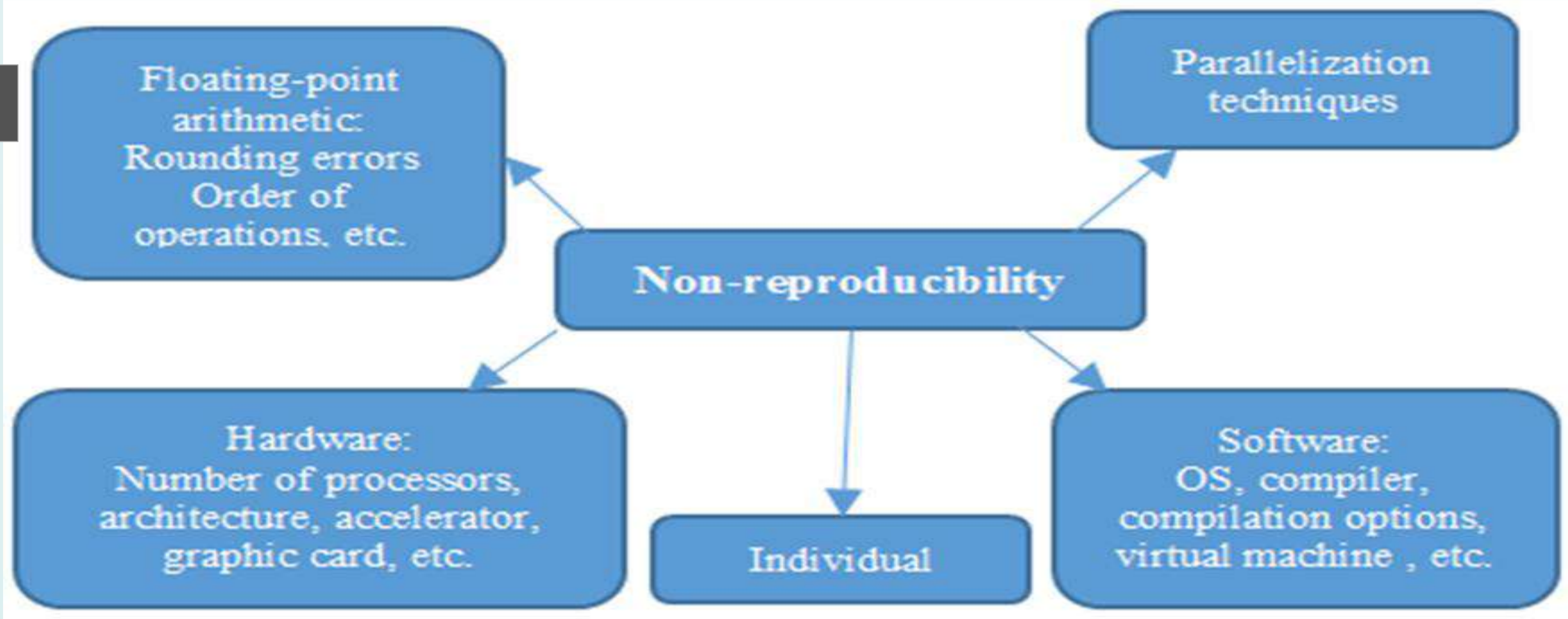

Différents cas d'études de reproductibilité des résultats et des performances

Modèles épidémiques du Covid19

Article publié à la conférence JFMS 2022 [3].

- Sur 20 modèles permettant de simuler une épidémie, un seul reproductible.
- Proposition d'un modèle reproductible et parallélisable, développé en C++
- Utilisable à l'échelle d'une ville, d'une région ou d'un pays

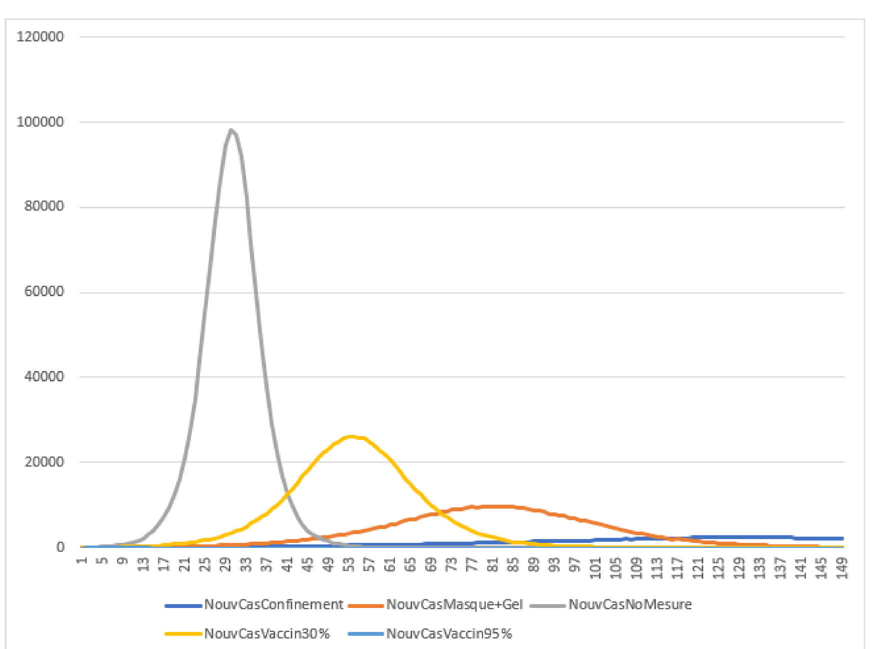

Figure 2 : Courbes comparatives des nouveaux cas sans mesures sanitaires ou avec (confinement, masques et gel, vaccin efficace à 95% ou à 30%).

Lois d'Amdhal et Gustafson

- La loi d'Amdhal : $S_{\text{latence}}(s) = \dfrac{1}{1 - p + \frac{p}{s}}$

Cette loi prédit une accélération (nommée speedup) d'un même programme, en fonction du nombre de processeurs et de la proportion parallélisable du programme (une partie de celui-ci étant obligatoirement séquentielle).

- La loi de Gustafson : $S_{\text{latence}}(s) = 1 - p + sp,$

Cette loi revisite Amdhal, en prédisant que l'on peut dans un temps de calcul donné, augmenter le speedup indéfiniment en augmentant le nombre de processeurs et la taille du problème simultanément.

Qu'en est-il avec l'architecture actuelle des processeurs ?

Les machines quantiques

- L'informatique est probabiliste par essence. Ainsi, nous n'aurons jamais la répétabilité numérique que l'on doit avoir sur des machines classiques.
- Néanmoins, la reproductibilité des résultats et des temps de calcul doit être atteinte.
- Plusieurs acteurs proposent des solutions pour accéder à des machines quantiques, avec différentes conceptions.

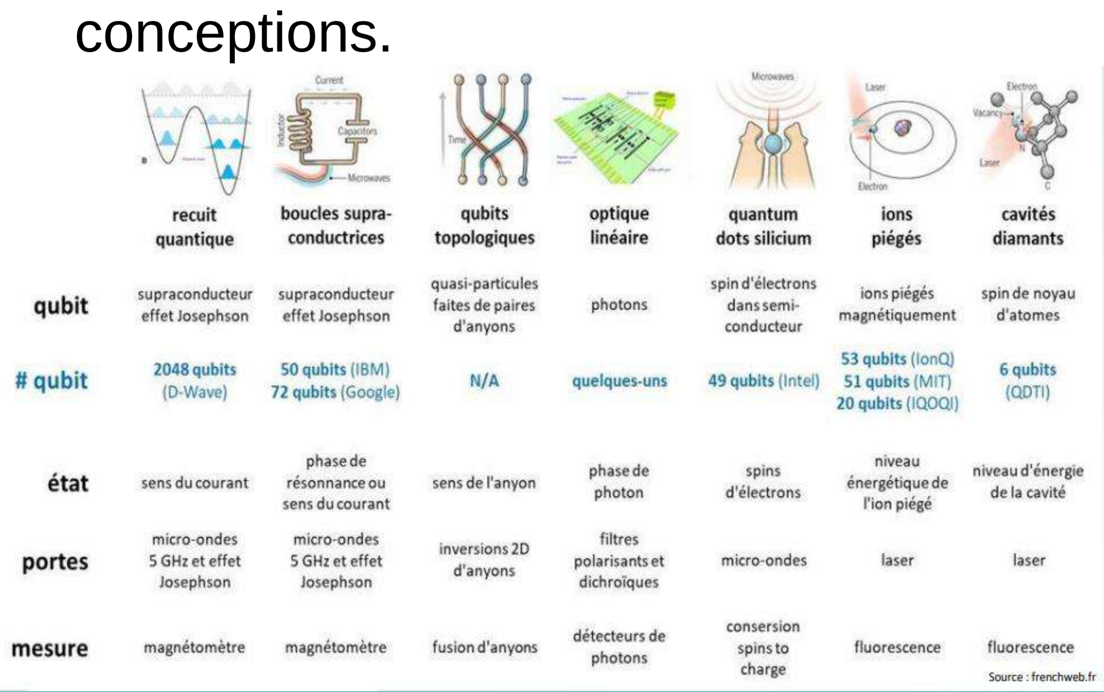

	recuit quantique	boucles supra-conductrices	qubits topologiques	optique linéaire	quantum dots silicium	ions piégés	cavités diamants
qubit	supraconducteur effet Josephson	supraconducteur effet Josephson	quasi-particules faites de paires d'anyons	photons	spin d'électrons dans semi-conducteur	ions piégés magnétiquement	spin de noyau d'atomes
# qubit	2048 qubits (D-Wave)	50 qubits (IBM) 72 qubits (Google)	N/A	quelques-uns	49 qubits (Intel)	53 qubits (IonQ) 51 qubits (MIT) 20 qubits (IQOQI)	6 qubits (QDTI)
état	sens du courant	phase de résonnance ou sens du courant	sens de l'anyon	phase de photon	spins d'électrons	niveau énergétique de l'ion piégé	niveau d'énergie de la cavité
portes	micro-ondes 5 GHz et effet Josephson	micro-ondes 5 GHz et effet Josephson	inversions 2D d'anyons	filtres polarisants et dichroïques	micro-ondes	laser	laser
mesure	magnétomètre	magnétomètre	fusion d'anyons	détecteurs de photons	consersion spins to charge	fluorescence	fluorescence

Source : frenchweb.fr

Conclusion

La reproductibilité est un élément essentiel de la science. Dans le domaine du calcul haute performance, il existe énormément de cas à étudier. L'objectif serait d'établir des méthodes, des bonnes pratiques ou des outils pour faciliter la mise en place de la recherche reproductible. Un changement des mentalités est également nécessaire, et passe par une prise de conscience de l'importance du problème. Cette thèse étudiera certains éléments précis comme décrit ci-dessus, mais il existe de nombreux autres sujets très intéressant à étudier.

Références

[1] : MARWICK, Ben. How computers broke science–and what we can do to fix it, Nov. 2015. URL http://theconversation. com/how-computers-broke-science-and-what-we-can-doto-fix-it-49938.[p 14], 2015.
[2] : IOANNIDIS, John PA. Why most published research findings are false. PLoS medicine, 2005, vol. 2, no 8, p. e124.
[3] : HILL D.R.C., ANTUNES B.A., " Reproductibilité et modèles Covid – un modèle multi-agents", Journées Francophones de la Modélisation et de la Simulation (JFMS 2022) – Cargèse, 28 mars au 2 avril 2022, pp. 35-53.

benjamin.antunes@uca.fr

Advanced Design of Robots Under High Dynamic Loading by a Mechatronic Approach

Hyunjun BAE, Thu Thuy DANG, Benjamin BOUDON, Chedli BOUZGARROU

M3G-MRSI, Institut Pascal UMR-CNRS 6602

Objectives

Accurate modeling, analysis and validation of **the coupling between the electrical actuator and the robot**, for simulation and control. This thesis is focused on the research of the mechatronic designs of robots to emphasize their benefits in the control design of **agile robots** (machining robots, rapid handling robots, collaborative robots, exoskeletons, or cable robots), in order to guarantee their operational performances.

Issues

- **Multi-physical model** should be considered for the mastery of the robot control subjected to high dynamical interactions.
- **Parameter identification** will improve the accurate multi-physical model.
- The novel design of **advanced control law** can be proposed with the use of multi-physical model.

Development

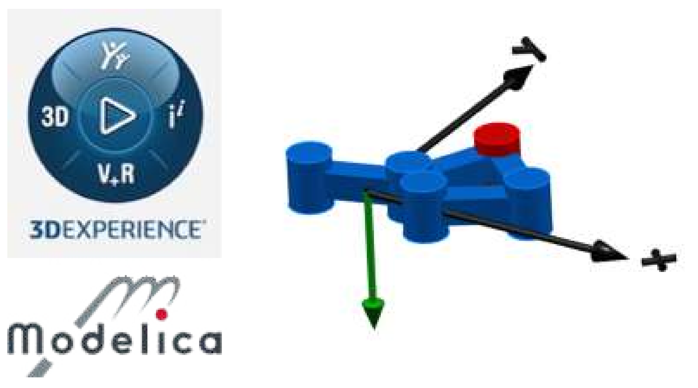

Figure 1: Modelica language model

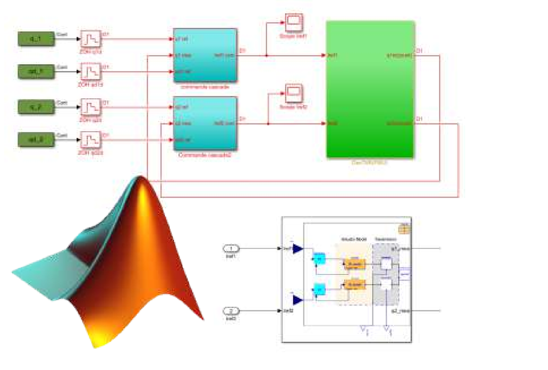

Figure 2: Matlab/Simulink model

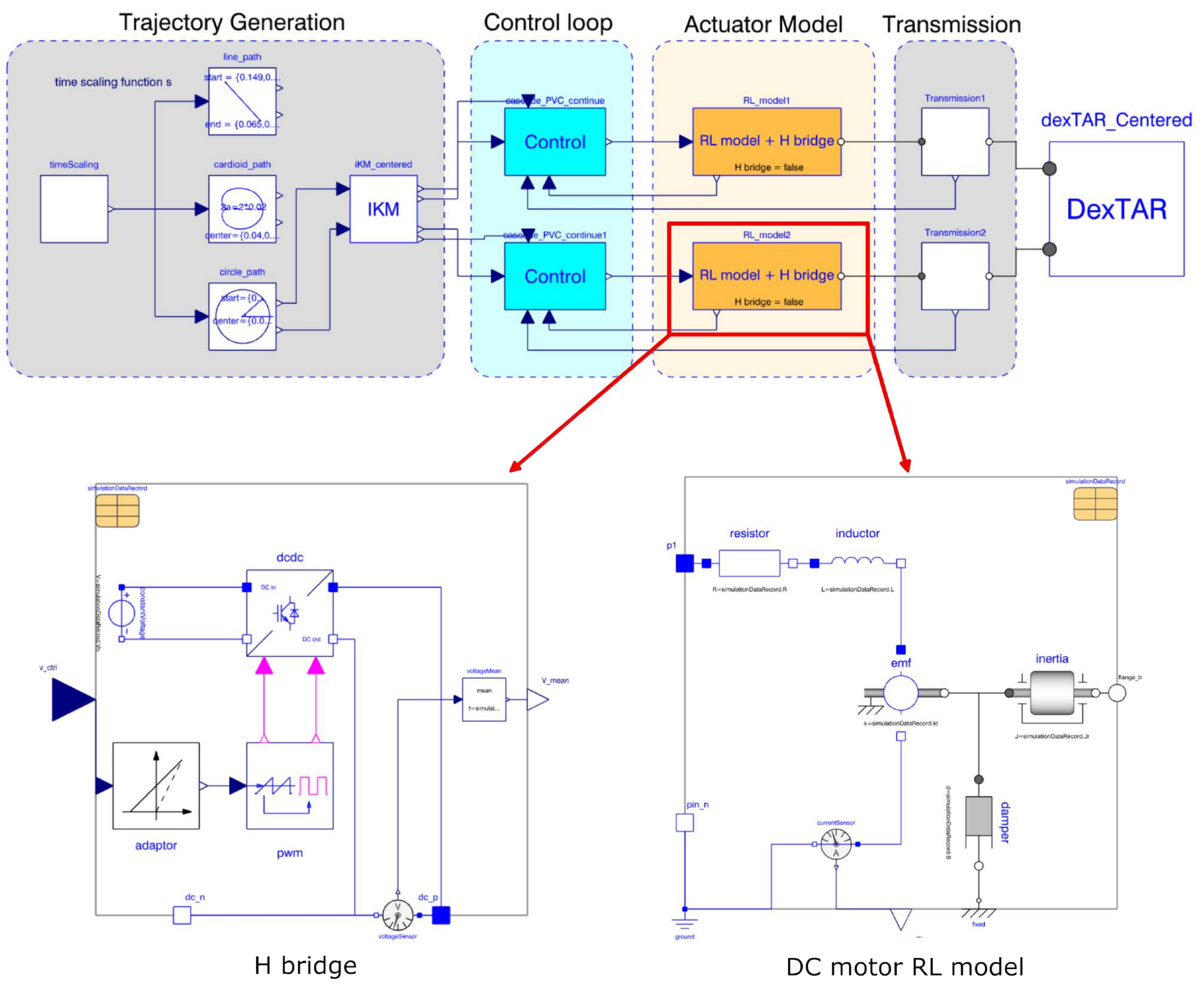

Figure 3: Control structure: Different models or scenarios can be tested

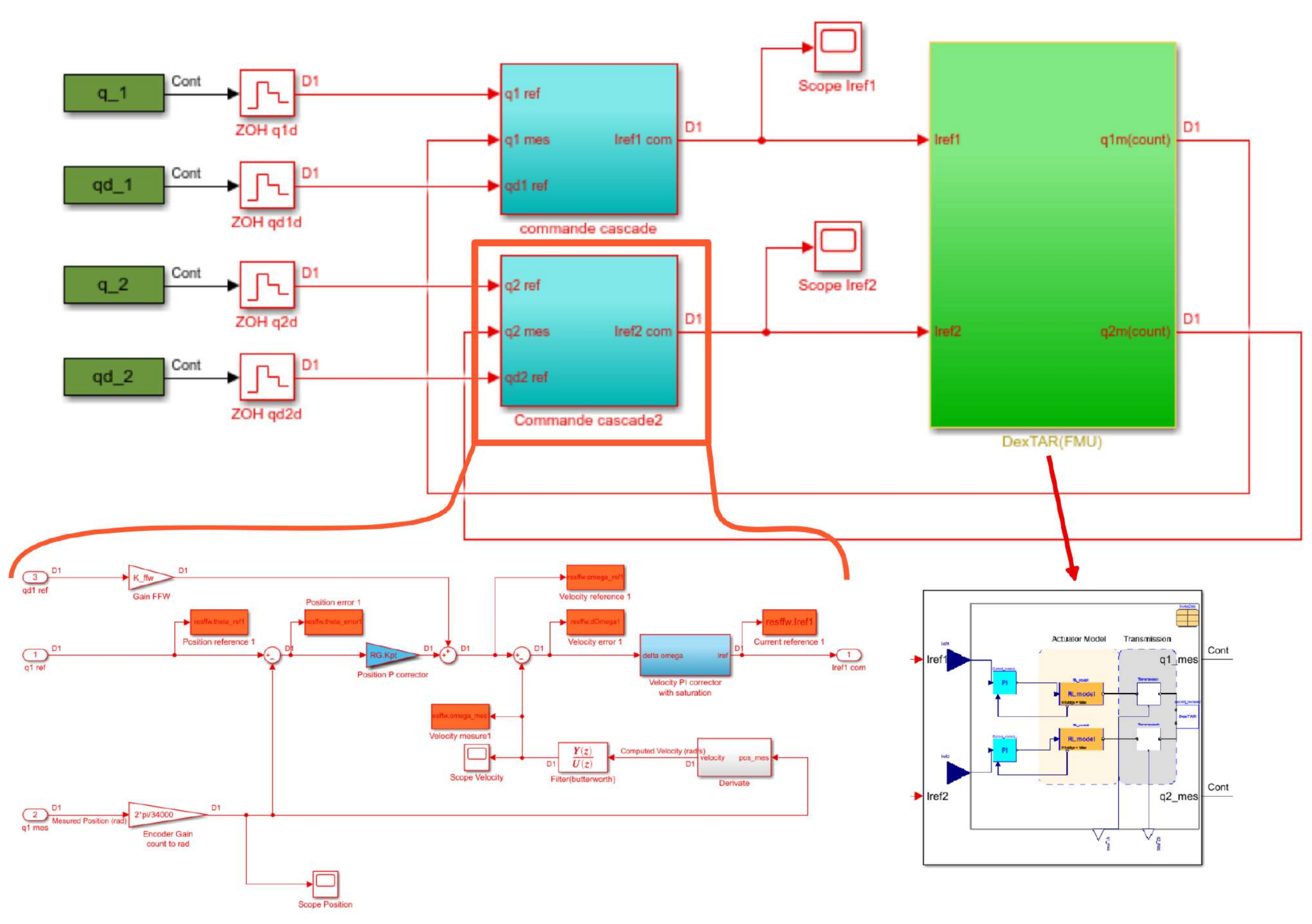

Figure 4: Cascade control implemented in Simulink environment

Methods

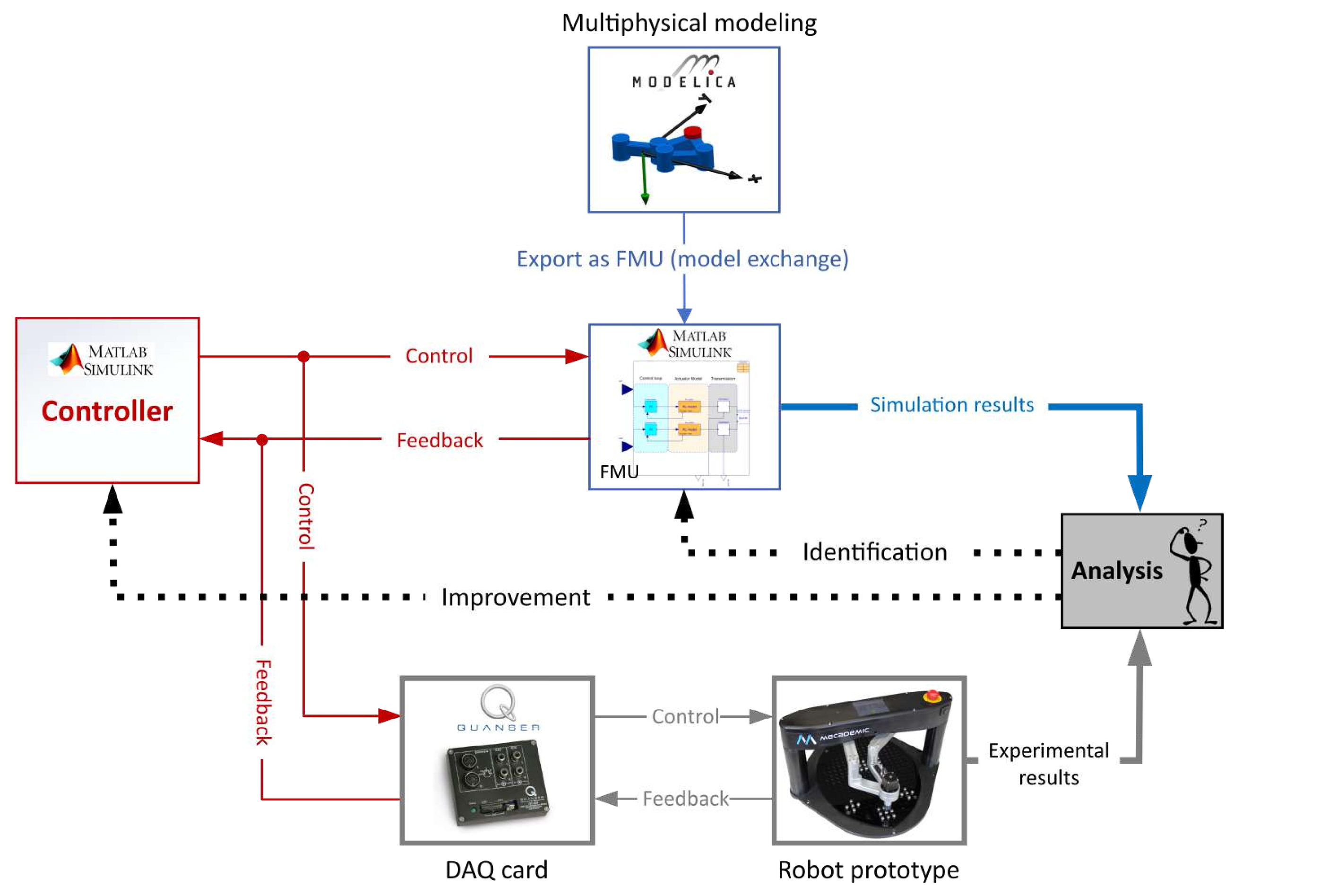

Figure 5: Macroscopic view of simulation and experimentation with DexTAR robot

Results: Graphics

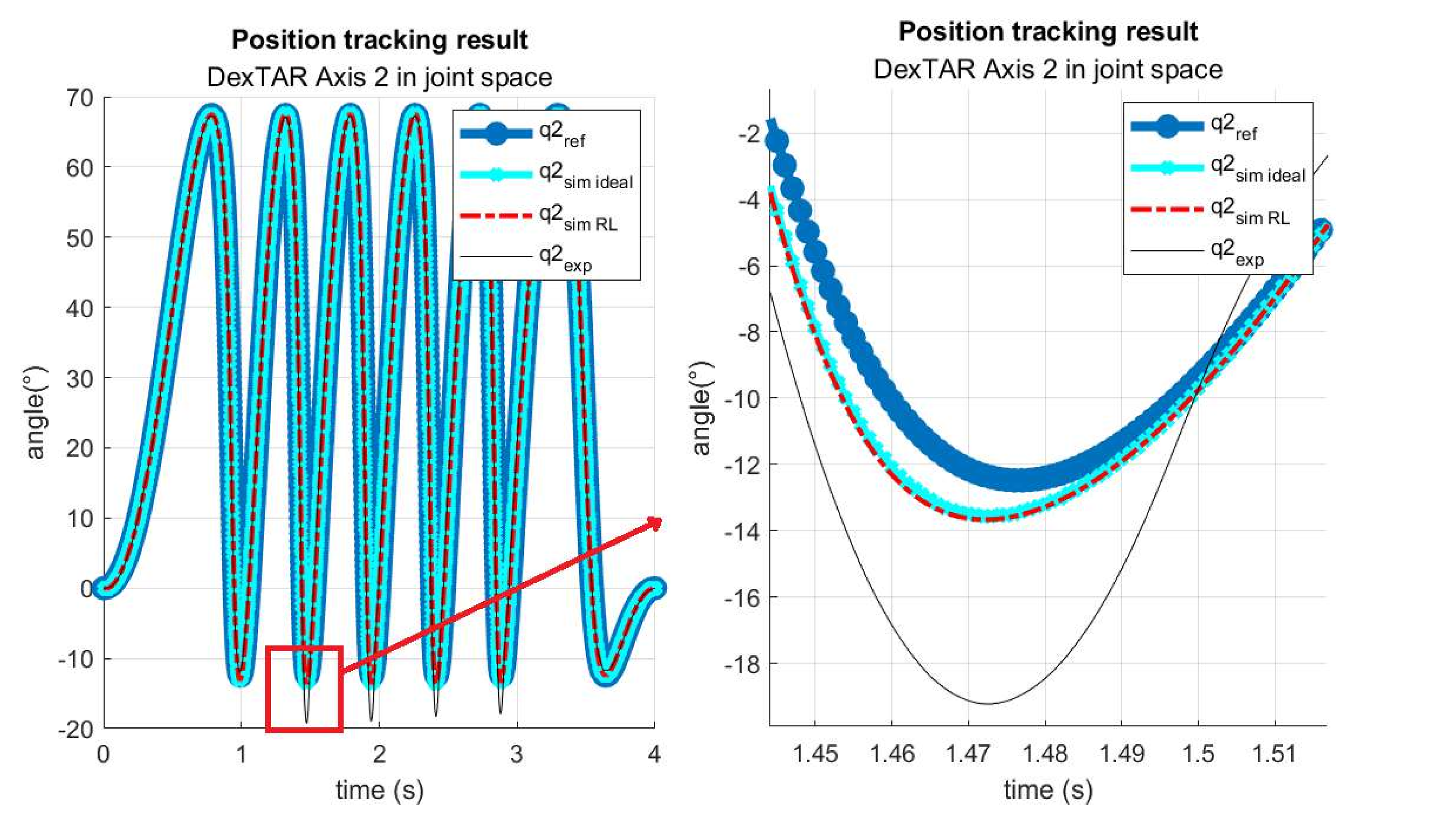

Figure 6: Comparison between simulation and experimentation result for trajectory tracking

Conclusion

- A multi-physical model of a parallel five-bar robot (DexTAR) has been built in Modelica language considering the actuator's modeling with various degrees of accuracy : ideal model or RL circuit-model for DC motor associated with a PWM H-bridge model.
- Experimental set-up with DexTAR robot enabled the validation of the simulation results.
- To guarantee the identical control design on both simulation and experimentation, a Modelica-based exported FMU model of the robot system has been imported in the Matlab/Simulink environment. Cascade control is applied for each axis, yields good effector's position tracking results.
- Further aspects of the multi-physical design remain to be studied: parameter identification of the robot, improvement of the control law, different types of trajectory tracking with even higher dynamic loading, etc.

Acknowledgments

- This research was financed by the French government IDEX-ISITE initiative 16-IDEX-0001 (CAP 20-25).

References

[1] Francis Bourbonnais, Pascal Bigras, and Ilian A. Bonev. Minimum-Time Trajectory Planning and Control of a Pick-and-Place Five-Bar Parallel Robot. *IEEE/ASME Transactions on Mechatronics*, 20(2):740–749, apr 2015.

[2] Pierre-Jean Barre. *Stratégies de commande pour un axe numérique de machine-outil a usinage très grande vitesse.* PhD thesis, L'ÉCOLE NATIONALE SUPÉRIEURE D'ARTS ET MÉTIERS, 1995.

[3] Adrien Koessler. *Contribution à l'agrandissement de l'espace de travail opérationnel des robots parallèles. Vérification du changement de mode d'assemblage et commande pour la traversée des singularités.* PhD thesis, Université Clermont Auvergne, 2019.

Communicating image sensors with low energy consumption, Application to the monitoring of the interaction between river dynamics and vegetation

A.Yaya Balde[1],E. Bergeret[1],D. Cajal[1], J-P. Toumazet[23]
[1]UCA/CNRS/LPC/F-63000 Clermont-Ferrand/France
[2]UCA/CNRS/GEOLAB/F-63000 Clermont-Ferrand/France
[3]LTSER- Zone Atelier Loire – CNRS INEE – France

Introduction

The objective is to perform a 4D monitoring (3-D modeling + temporal monitoring) of the river configuration (sandbanks and associated vegetation which benefits from this substrate settle and contributes to stabilizing it by its root network). Several studies of this type have already been conducted ([1] and [2]), with the 3D monitoring carried out by a photogrammetry technique using aerial images. This analysis is efficient, but it only provides a posteriori view of a flood or an intense drought effect, without information on the different steps that led to this result; the overflights are carried out with an annual periodicity. The proposed approach makes it possible to solve this problem, by installing in situ a device made up of several image sensors allowing the 3D reconstitution and triggered by other sensors (vibration, moisture, temperature) to provide data when each major event occurs by using LPWAN technology.

Current Consumption

Characteristics of the measurement:

- Shooting definition : UXGA (1600 x 1200)
- In [3], he shows that the number of pixels has an impact on the current consumed.
- Image capturing : 0.3 to 0.4 s
- Image saving : 132 mA for 3.8 second
- Image sending: 376 mA for 2.91 second

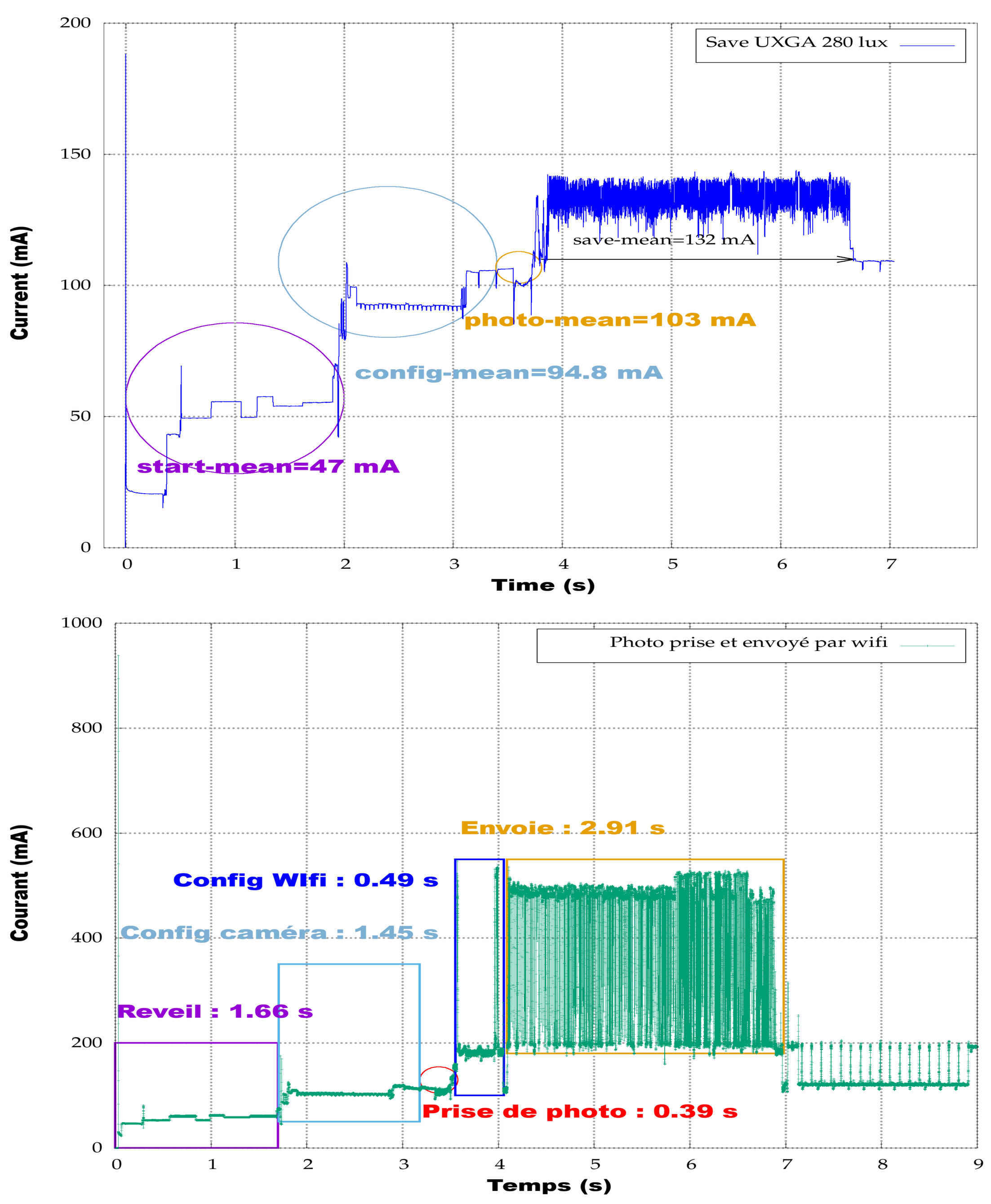

Figure 2: Image saved in memory (above), image sent by wifi (below)

Optimisation of sensor position

First, we determined the parameters of sensor boards (ESP32-Cam), and how to locate them relatively to each other.[a] in figure 1 represents the location of the sensor boards.

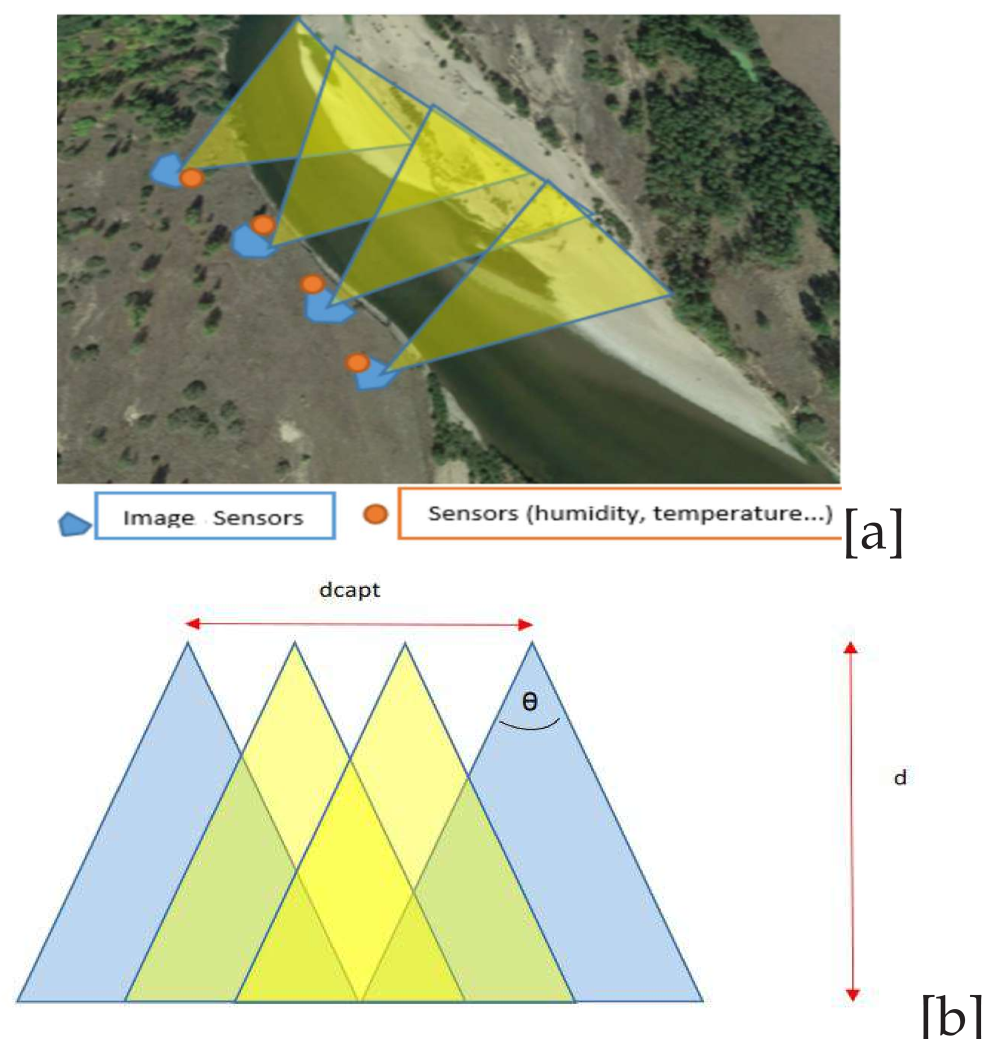

Figure 1: Sensor location

Based on [b] in figure 1, we established these formula used to locate sensors.

- $S_1S_2(\text{Gap of sensors}) = 70\% * AC$
- $\theta = \frac{\text{AFOV (Angle field of view)}}{2}$
- $BC(\text{Overlap}) = CS_2 * 2 * \tan\theta - S_1S_2$

Results for a 6-meter focus distance, with θ=25° for OV2640.

S1S2 (%)	S1S2 (m)	BC (m)	BC (%)
50,0	3,0	2,6	43,3
41,7	2,5	3,1	51,6
33,3	2,0	3,6	59,9
25,0	1,5	4,1	68,3
16,7	1,0	4,6	76,6

Table 1: Data for sensor location

Photogrammetric reconstruction

- Space between sensors : 3 meters
- Software : Agisoft Metashape
- Number of images : 10
- Dense point cloud : 5 538 069 points

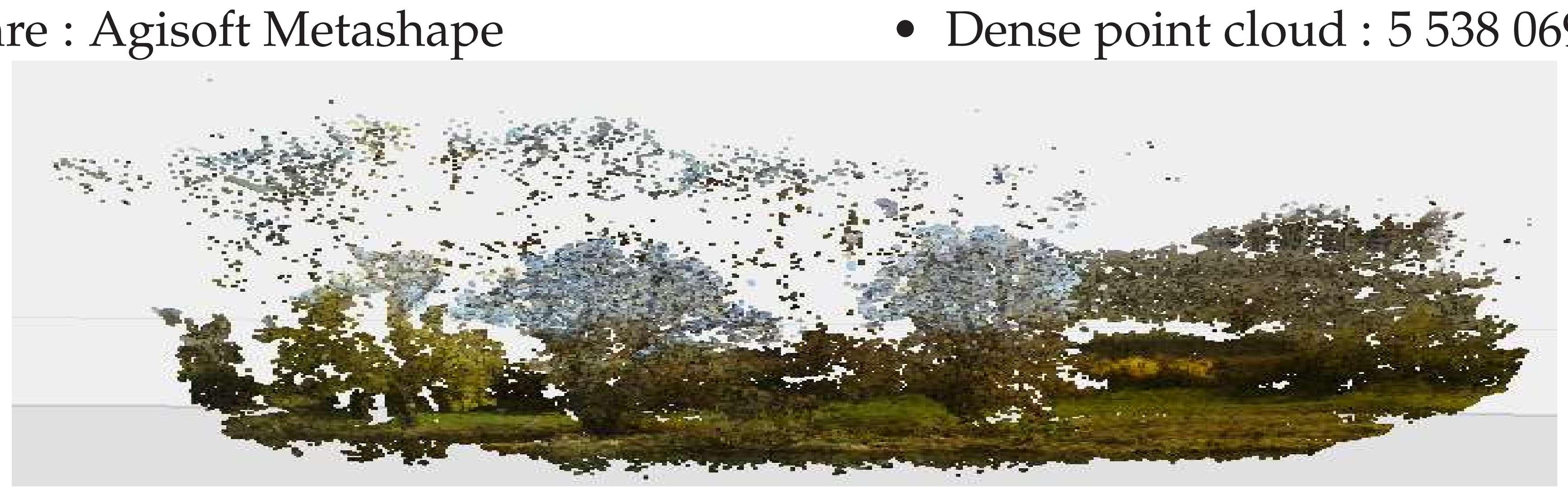

Figure 3: Photogrammetric reconstruction

Conclusion

We have defined two scenarios based on the different experiments

First scenario:

- Human intervention is necessary
- It takes too long to get the data
- More resources needed

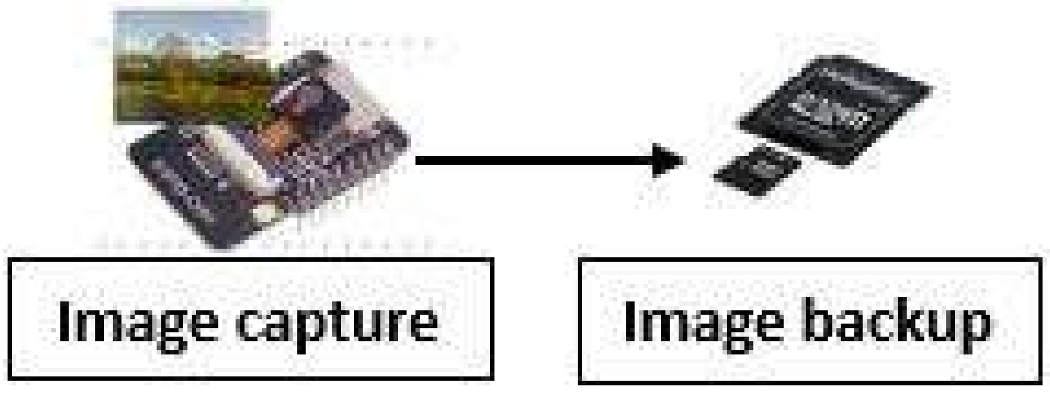

Second scenario:

- Power consumption is higher in scenario 2
- Standalone system

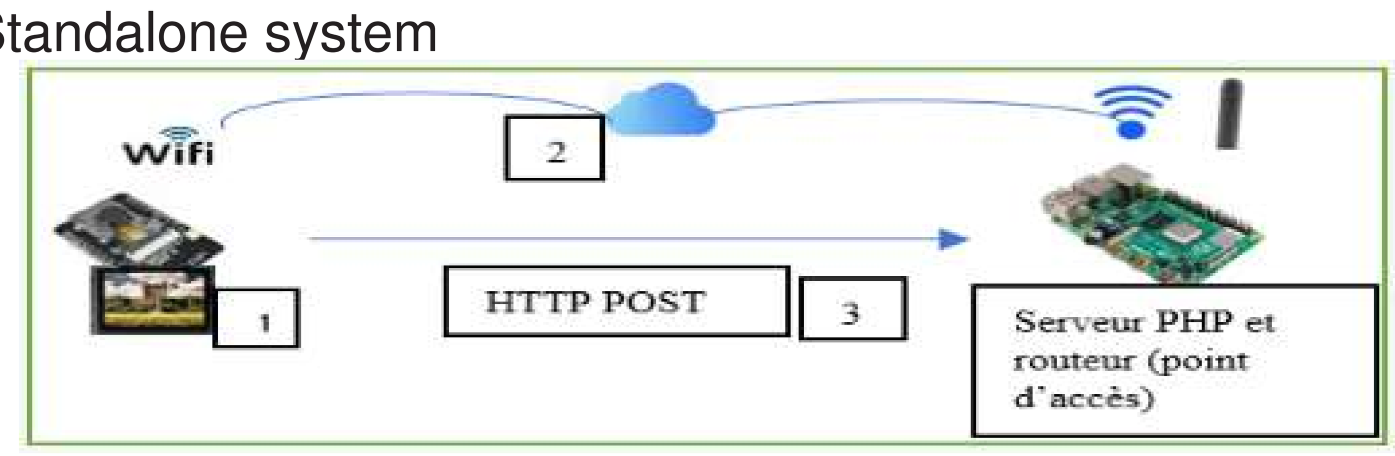

For the next test we will have to:

- Optimize the algorithm of scenario 2 for a better synchronisation
- Perform a new test with LoRa instead of Wifi as transmission protocol to establish a comparaison on the consumption of the two protocols.

References

[1] Hortobágyi. A multi-scale approach of fluvial biogeomorphic dynamics using photogrammetry,. *Journal of environmental management*, 2017.
[2] Vautier. Monitoring and reconstructing past biogeomorphic succession within fluvial corridors using stereophotogrammetry. *Wiley online library*, 2016.
[3] R. LikamWa. Energy characterization and optimization of image sensing toward continuous mobile vision. *Proceeding of the 11th annual international conference*, 2013.

alpha_yaya.balde@doctorant.uca.fr

Géométrie Cérébrale et Stimulation Cérébrale Profonde

Clermont Auvergne INP
Ecole doctorale Sciences Pour l'Ingénieur

Directeur de thèse : Jean Jaques LEMAIRE _ Encadrant : Adrien Wohrer

Maha BEN SALAH
maha26bensalah@gmail.com
+33 0665659849

CHU Clermont-Ferrand — Institut Pascal — Fondation de l'Avenir, Accélérateur de progrès médical

Introduction

La maladie de Parkinson est une maladie neurodégénérative caractérisé par la destruction des neurones à dopamine. Symptômes : tremblements, la lenteur des mouvements et la raideur musculaire.

La stimulation cérébrale profonde (SCP): une technique chirurgicale réduit les tremblements et améliore la qualité de vie chez le malade.

Objectif

- Etudier les relations entre la géométrie des structures cérébrales à stimuler, l'amélioration et les effets indésirables.
- Identifier la meilleure zone à stimuler afin d'améliorer le mieux possible l'état du patient sans risque de causer des effets indésirables.

Données

Données géométriques

(issues de la planification opératoire)

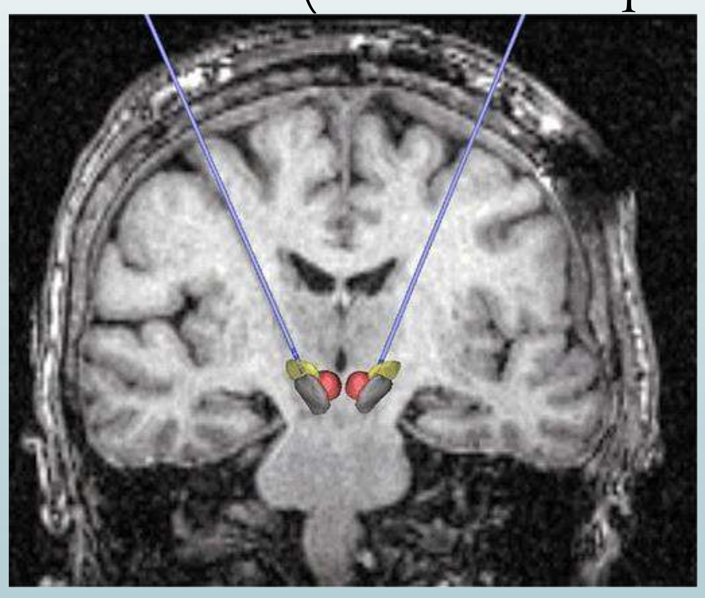

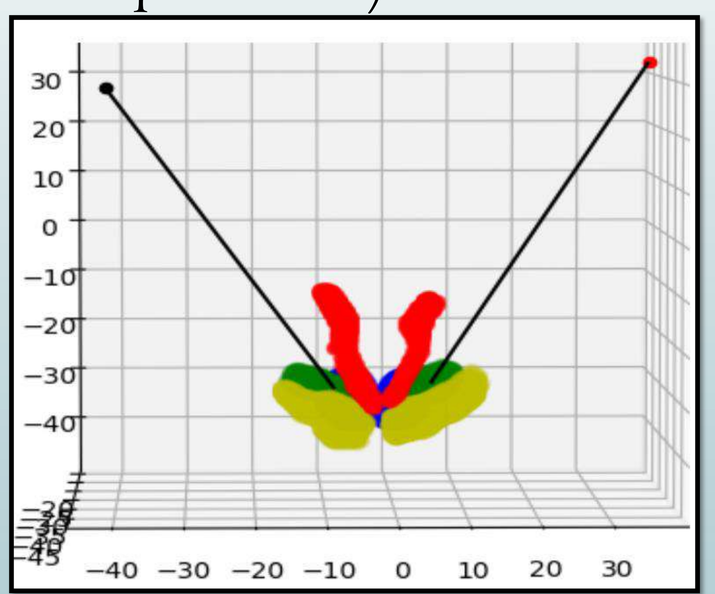

8 structures cérébrales et 2 trajectoires des électrodes implantées

Données peropératoires

(enregistrés au cours de l'opération)

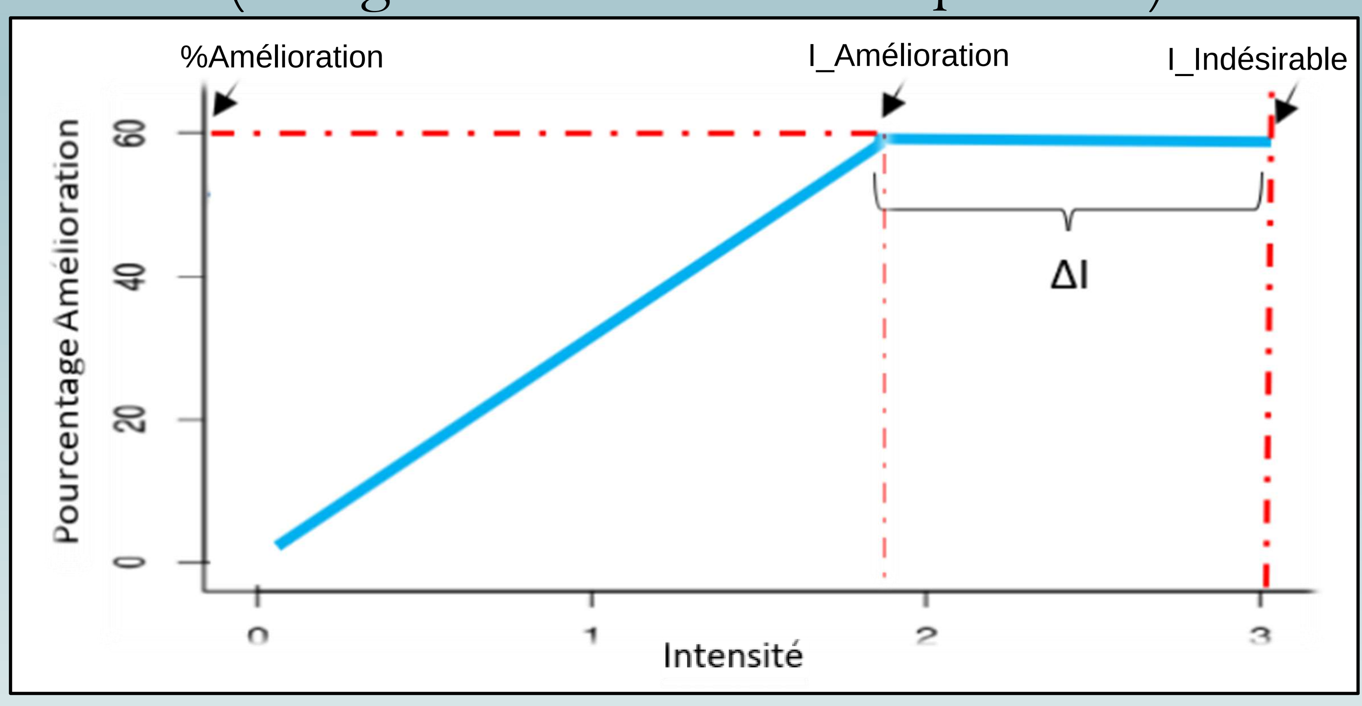

Pourcentage d'Amélioration: % amélioration de l'état du patient.
Intensité d'Amélioration: L'intensité de stimulation à la quelle est enregistrée un pourcentage d'amélioration.
Intensité indésirables: L'intensité de stimulation à la quelle est apparu un effet secondaire.

Cartographie cérébrale et production des données

Recalage et Clustering

Recaler les différents cerveaux dans un espace commun.
Identifier des sous-régions communes entre les patients.

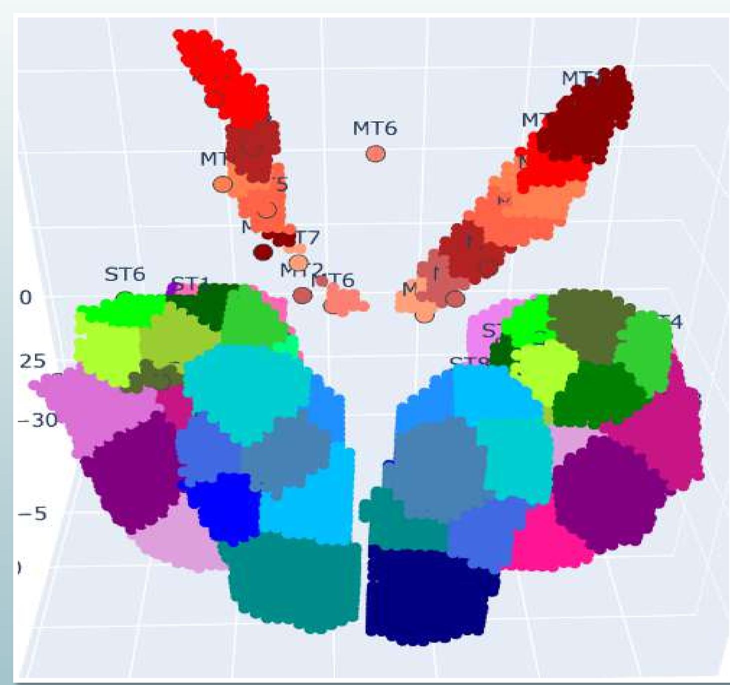

Algorithmes utilisés :

*Coherent Point Drift-Andriy Myronenko and Xubo Song 2010
*Feature Registration Framework using Mix-ture Models-Rangarajan 2000
*A Generative Model for the Joint Registration of Multiple Point Sets - Georgios Evangelidis, Dionyssos Kounades-Bastian, Radu Horaud 2014
*Joint Alignment of Multiple Point Sets with Batch and Incremental Expectation-Maximization - Georgios D. Evangelidis and Radu Horaud 2017

Un échantillon statistique correspond à une position de stimulation testée chez un patient dans un hémisphère donné, convertie en un ensemble de 32 distances, et les mesures cliniques associées.

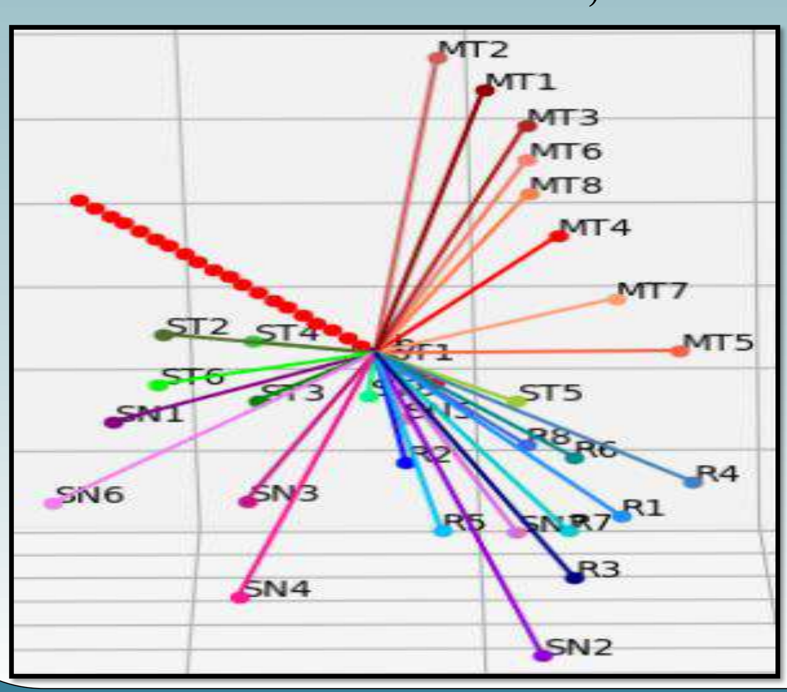

	% Amélioration	I_Amélioration	Effet Indesirable	I_indesirable	Δ Intensité	MT1	MT2	MT3	MT4	MT5	...
0	0.0	6.0	0.0	6.0	0.0	NaN	NaN	NaN	5.948941	9.766723	...
1	1.5	3.0	1.0	5.8	2.8	NaN	NaN	NaN	5.758090	9.004842	...
2	2.5	2.8	1.0	5.2	2.4	NaN	NaN	NaN	5.737709	8.293702	...
3	2.5	1.6	1.0	4.8	3.2	NaN	NaN	NaN	5.889568	7.647470	...
4	3.0	0.8	1.0	5.0	4.2	NaN	NaN	NaN	6.201025	7.083933	...
...	...	...	...	...	...	...	...	...	...	...	...
523	2.0	0.8	0.0	3.0	2.2	12.201372	13.267219	10.611474	7.011603	9.777973	...
524	2.0	1.2	0.0	3.0	1.8	12.897702	14.037102	11.231295	7.064620	9.087019	...
525	2.0	1.4	0.0	3.0	1.6	13.631873	14.834466	11.902965	7.256387	8.458078	...
526	2.0	1.6	0.0	3.0	1.4	14.398098	15.655111	12.618209	7.576374	7.905962	...
527	2.0	2.8	NaN	NaN	NaN	15.191526	16.495565	13.370033	8.009228	7.447779	...

Etude Statistique

En faisant une Analyse en Composantes Principales (ACP) on remarque que le %Amélioration est faiblement corrélé avec la 3éme composante alors que les effets indésirables sont fortement liés à la 3éme composante et faiblement liés a la 1ere composante. Donc on peut trouver une zone ou une direction pour prévenir les effets secondaires et qui favorise un pourcentage d'amélioration important.

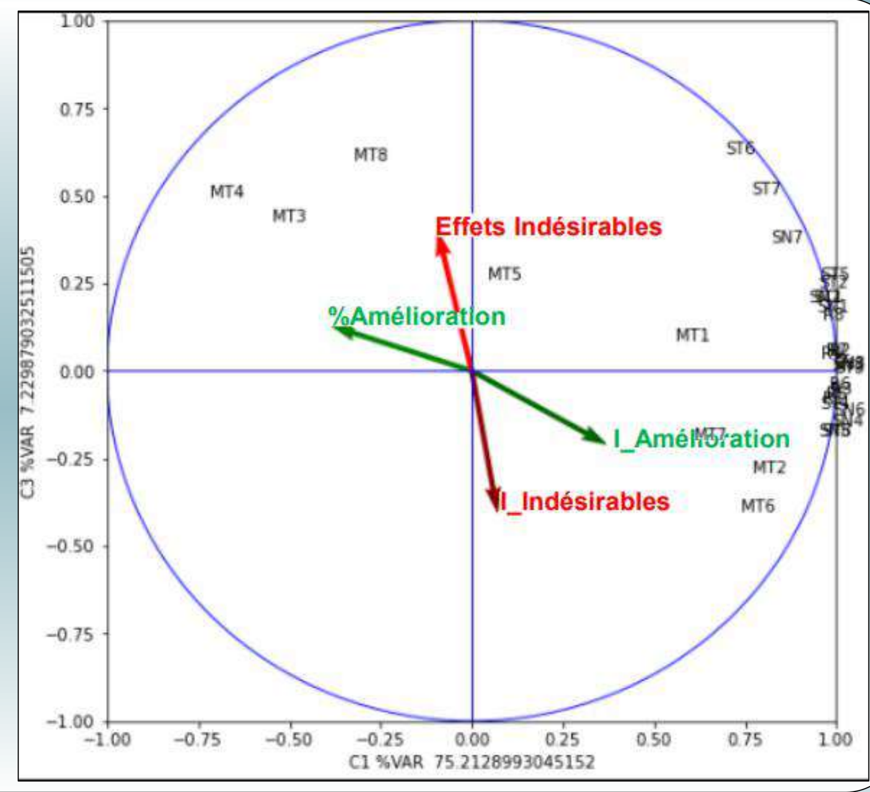

Prédiction avec les modèles de machine learning

Les différents modèles de machine learning (KNN, SVM, Reseaux de neurones, Random Forest, Decision Trees, Quadratic Discriminant Analysis, …) ont abouti à des résultats cohérents et semblables.

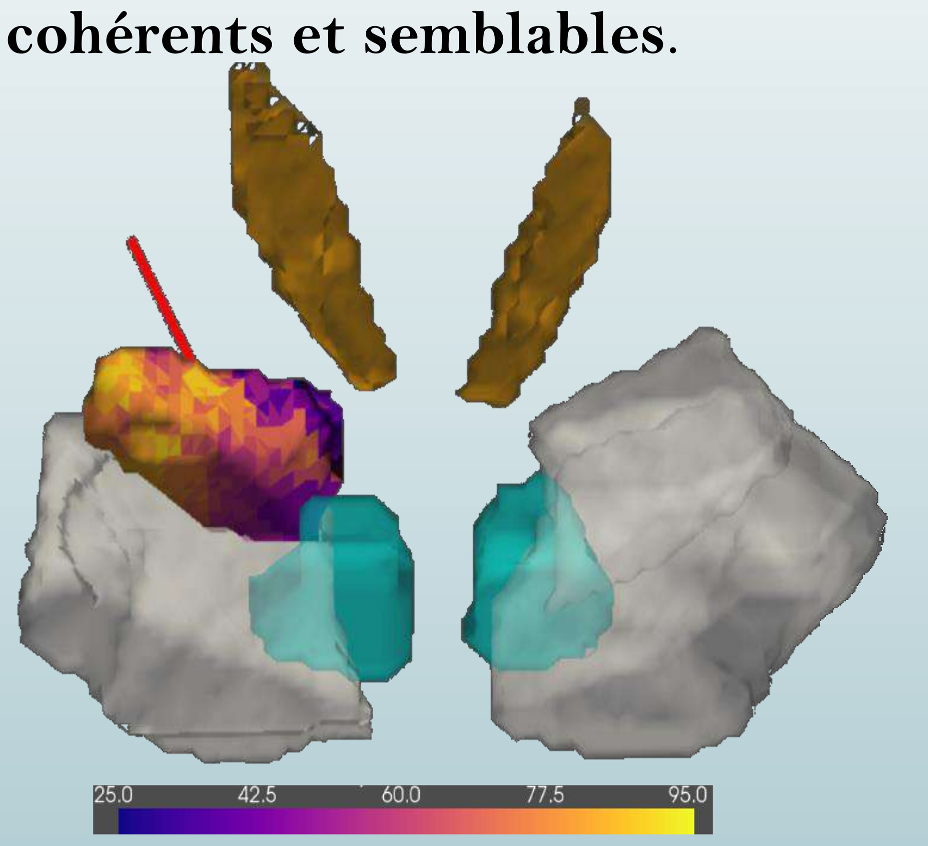

Prédiction du %Amélioration

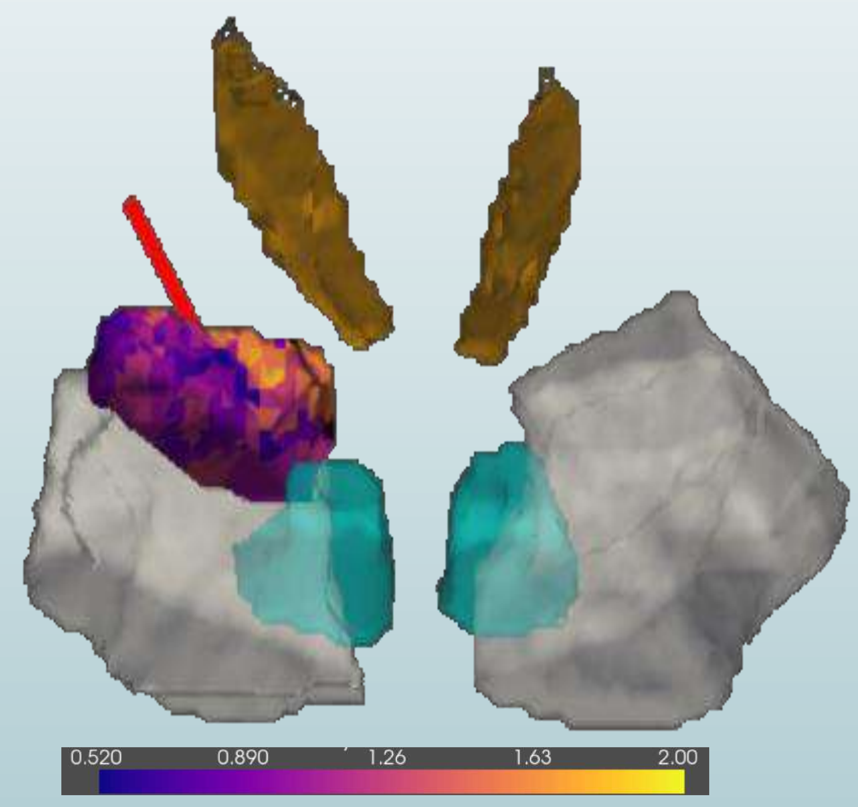

Prédiction d'Intensité d'amélioration

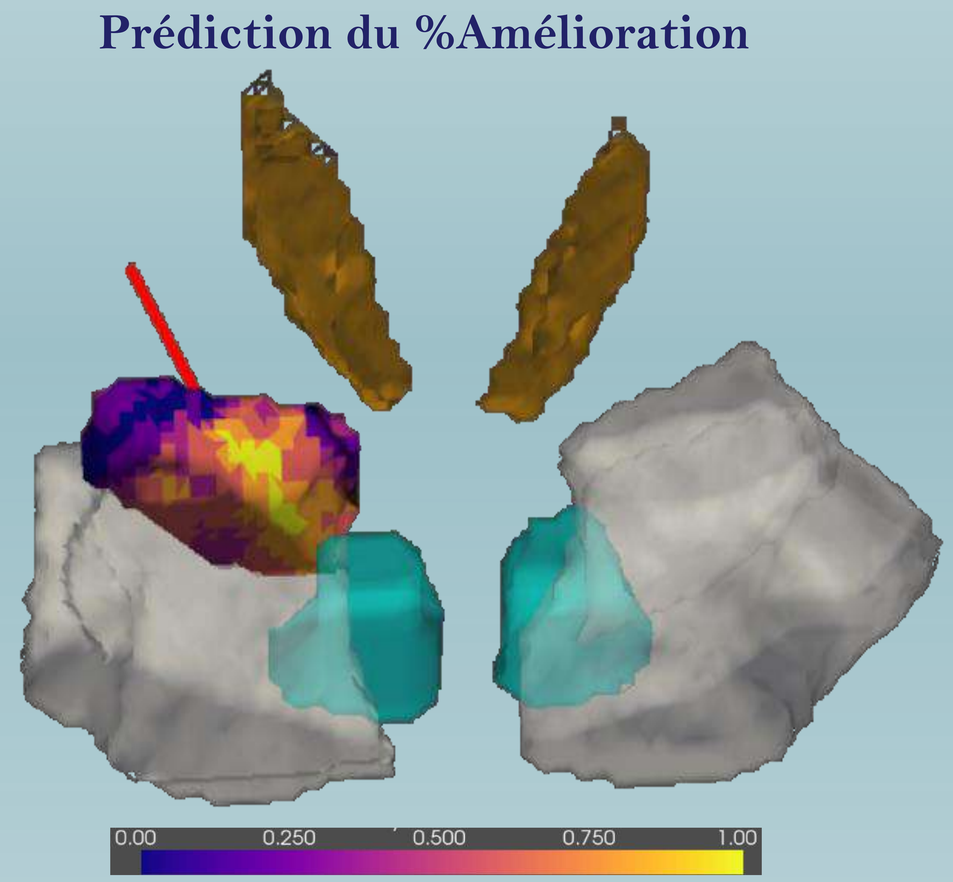

Prédiction d'Effets Indésirables

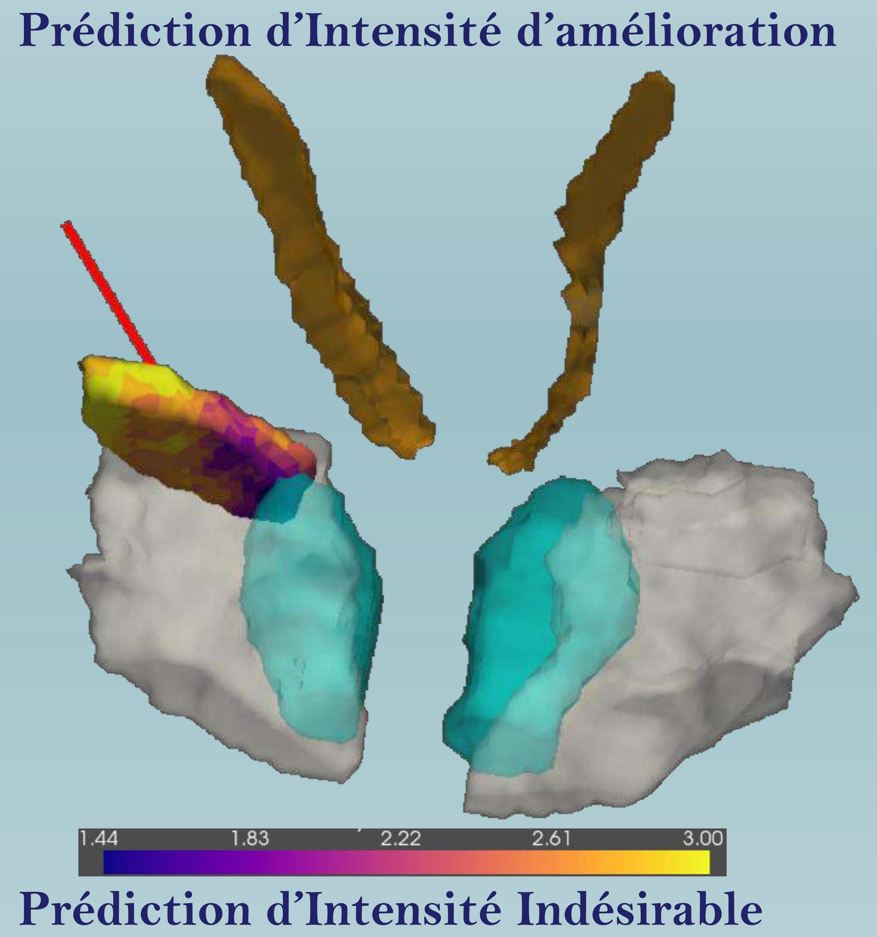

Prédiction d'Intensité Indésirable

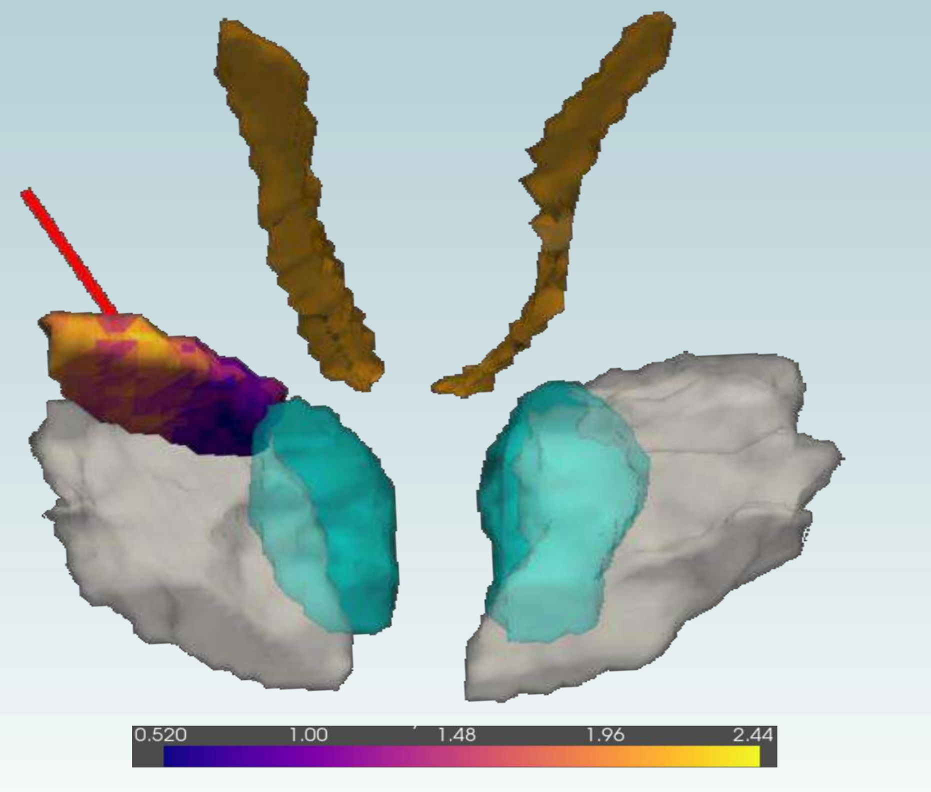

Prédiction ΔI

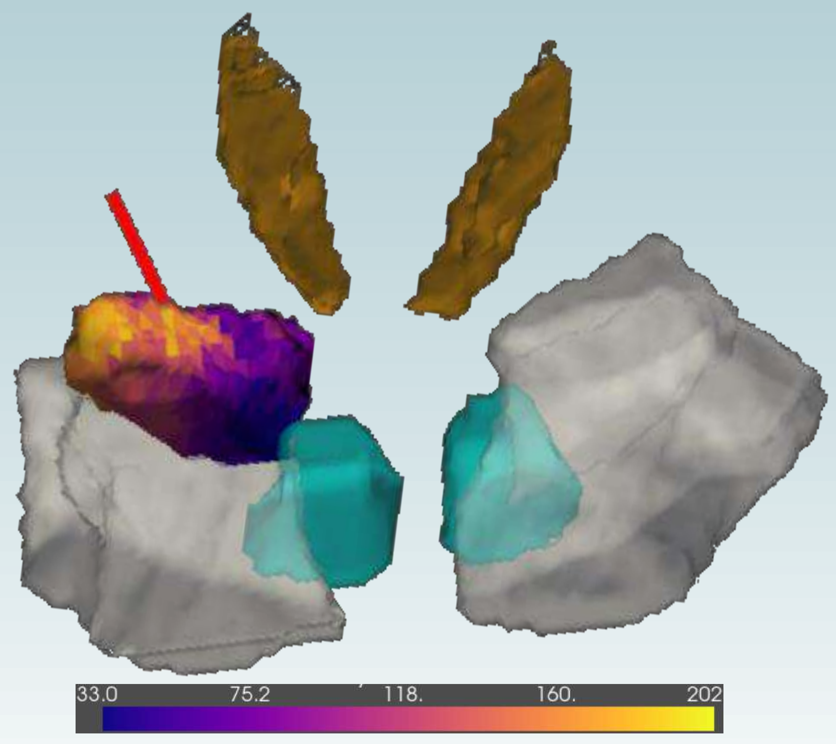

Prédiction de l'aire de la partie sous la courbe (%Amel *ΔI)

Conclusion: On a trouvé que la partie supérieure postérieure du STN est favorable pour un pourcentage d'amélioration important avec un faible risque d'avoir des effets secondaires.

Impression 3D de Biocéramiques Dopées pour l’ingénierie tissulaire osseuse

Florian BIOTTEAU[1], Charlotte VICHERY[1], Stéphane DESCAMPS[1], David MARCHAT[2], Jean-Marie NEDELEC[1]

[1] Université Clermont Auvergne, Clermont Auvergne INP, CNRS, ICCF, F-63000 Clermont-Ferrand, France
[2] Mines Saint-Etienne, Univ Lyon, Univ Jean Monnet, INSERM, U 1059 Sainbiose, Centre CIS, Saint-Etienne, France

Institut de Chimie de Clermont-Ferrand

Introduction

Présentation

Lorsque le manque d’os est trop important pour une réparation naturelle, il est nécessaire d’avoir recours à l’implantation d’un comblement osseux pour permettre le rétablissement de l’intégrité structurelle du squelette. Pour cela, différents matériaux existent qu’ils soient synthétiques ou naturels (autogreffe, allogreffe ou xénogreffe). Les seconds ont des problèmes de disponibilité et de compatibilité d’où la nécessité de développer des biocéramiques synthétiques. Cependant ces biocéramiques synthétiques ne préviennent pas, encore, des risques usuels tel que les rejets, les infections bactériennes, …

Objectifs

Nos objectifs sont d’améliorer l’intégration dans le corps humain d’implants osseux par leur structuration et l’ajout d’ions dopants (Sr^{2+}, Cu^{2+}, Cu^{+}) précédemment étudiés dans l’équipe [1,2] présentant des intérêts biologiques. Le but final est de proposer des implants sur-mesure personnalisés pour chaque patient et chaque défaut tout en réduisant les risques post-opératoires.

Méthodologie

Pour cela, nous avons réalisé un dopage cuivre sur un mélange de biocéramiques de la famille des phosphates de calcium : le phosphate tricalcique (ß-TCP) et l’hydroxyapatite (HAP). Le premier à l’avantage d’être totalement résorbable par le corps humain et le second d’être bio-intégré à la structure osseuse de par sa similarité de composition et de propriétés. Le dopage et la structuration ont également pour but d’améliorer la prolifération cellulaire, le développement des vaisseaux sanguins [3] et réduire les risques de contamination bactérienne.

Identification du défaut

Imagerie médicale

Scanner puis reconstruction 3D de la zone du défaut

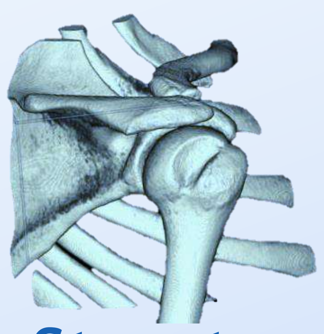

Dessin du comblement

Construction 3D de l’implant sur Blender

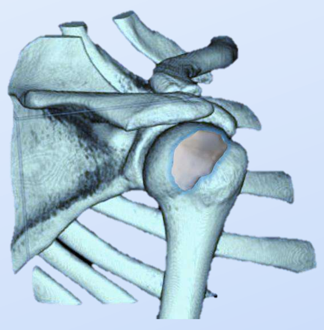

Structuration de l’implant

Choix de la zone à texturer

Il peut être intéressant d’avoir différentes structures en fonction des contraintes qui seront appliquées à l’implant. La zone extérieure est donc laissée relativement dense alors que l’intérieur va être macrostructuré.

Choix du motif répété 3D

Afin d’appliquer cette macrostructure, Rhino 7 et son module de géométrie paramétrique par nœud, Grasshopper, ont été utilisés. De nombreux motifs sont possibles [4], des plus simples en formes de croix à des structures bien plus complexes, en passant par des motifs triplement périodiques tels que les gyroides comme on peut le voir sur l’image ci-dessous.

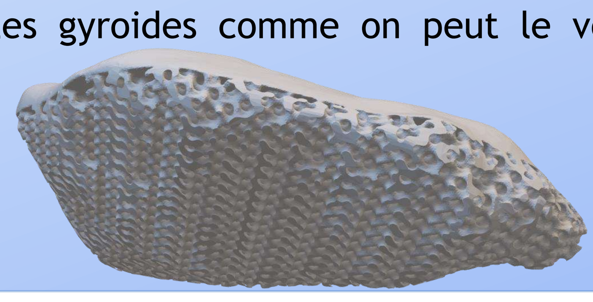

Synthèse de la biocéramique

Différentes voies de synthèse

En fonction du dopage voulu, les poudres ont été synthétisées de différentes manières : Précipitation (non dopé), Hydrolyse d’une brushite (dopé Cu) ou Sol-Gel (dopé Sr) :

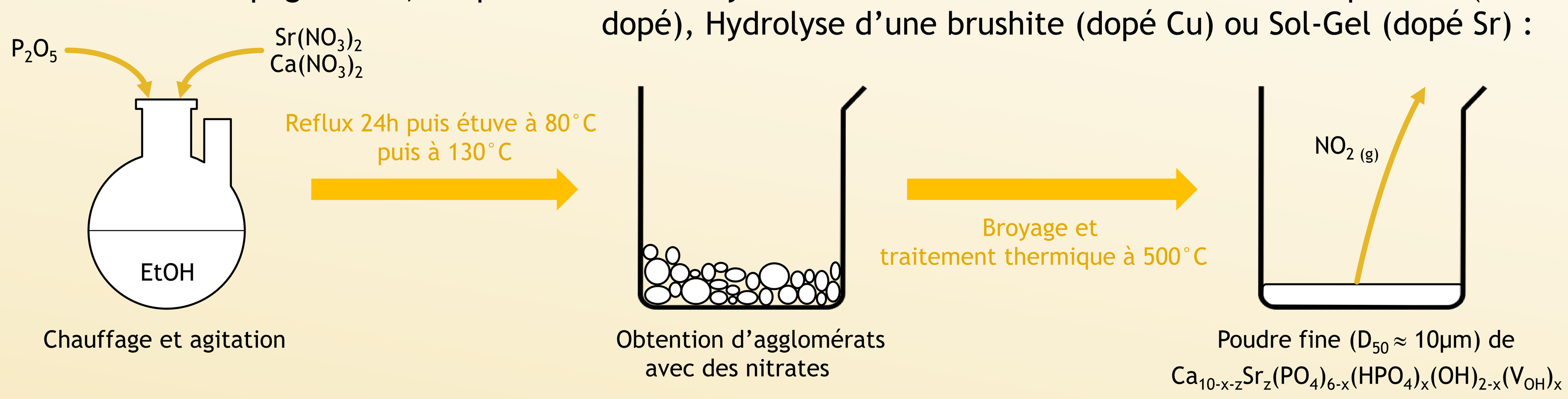

Le dopage et la proportion des phases ont été suivis par MP-AES et DRX avec affinement de Rietveld.

Préparation et mélange

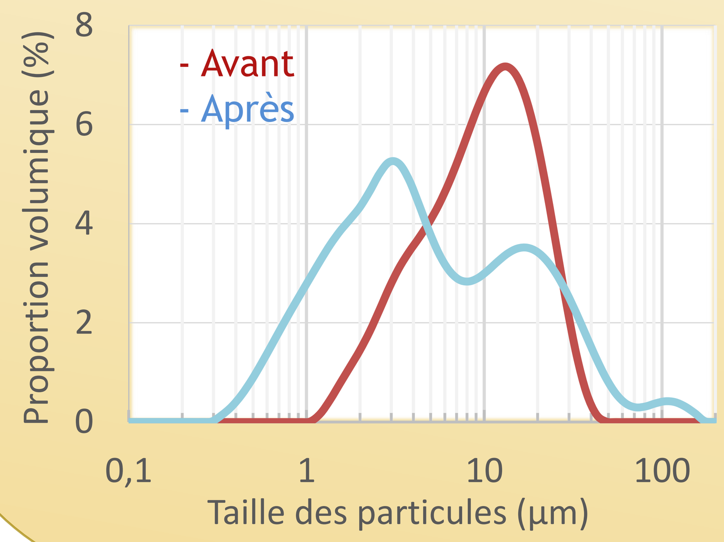

Pré-traitement de la poudre

La poudre a été chauffée à 900°C afin d’obtenir un mélange HAP/ß-TCP (75/25).

Mélange avec la résine photopolymérisable

Différents tests ont été réalisés afin d’accroitre son taux d’incorporation dans la résine ce qui permet un plus faible retrait par la suite et plus homogène.
Pour cela, la granulométrie des particules a été réduite grâce à un broyeur à bille afin de monter à environ 40% en masse de céramique dans le mélange.

Mise en forme

Mélange photosensible

Piège des particules dans une résine polymérisée

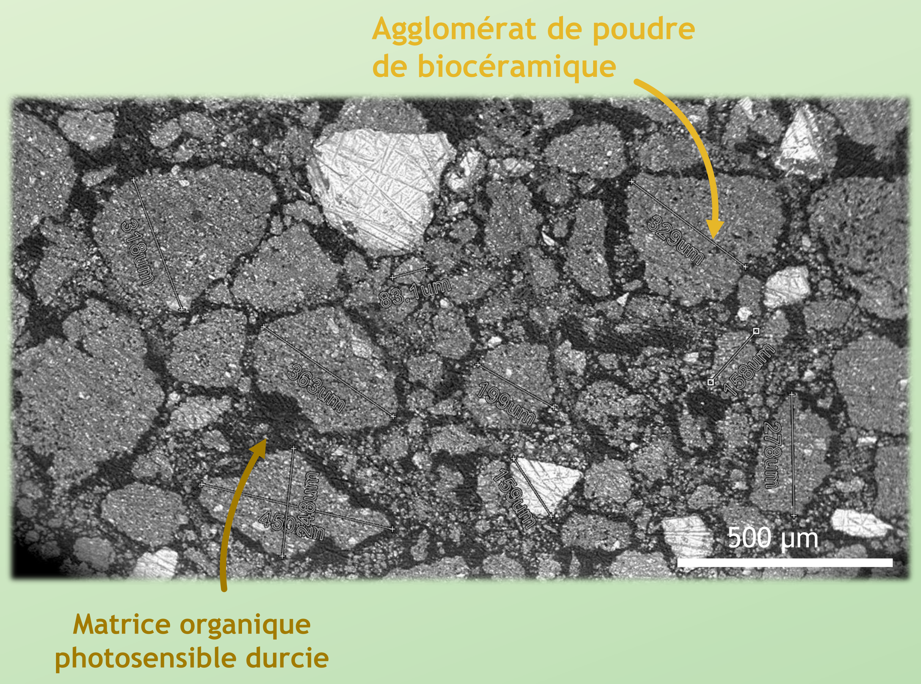

Principe de fonctionnement de la technologie DLP Céramique

Durcissement de la matrice organique sous l’action d’un éclairage UV localisé

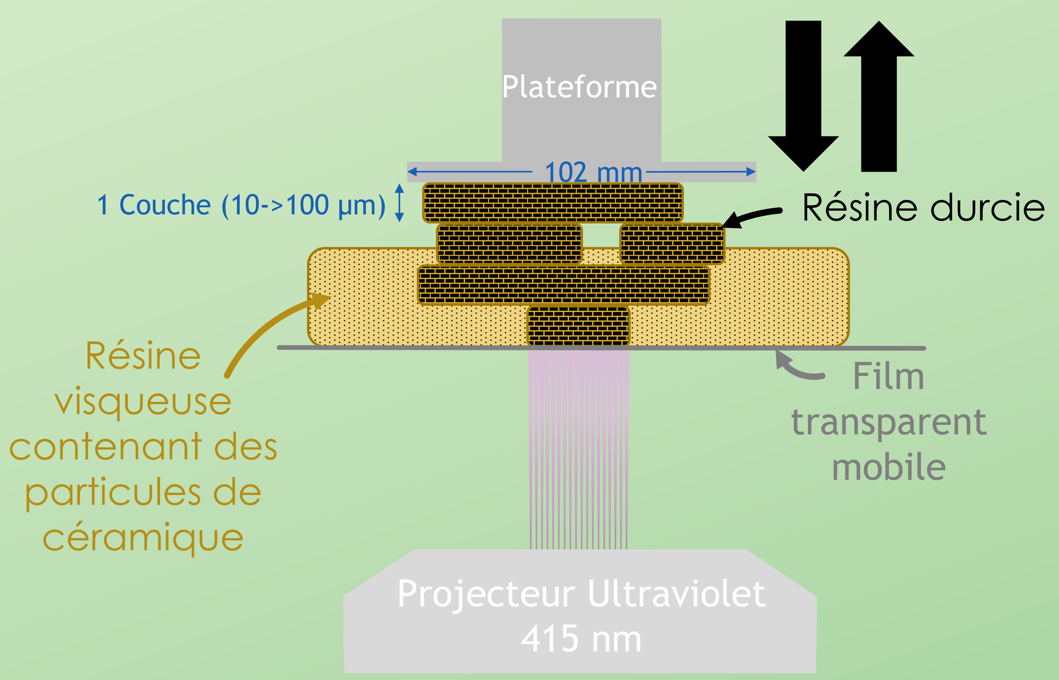

Pièces 3D produites

Retrait de la base et de la résine non polymérisée

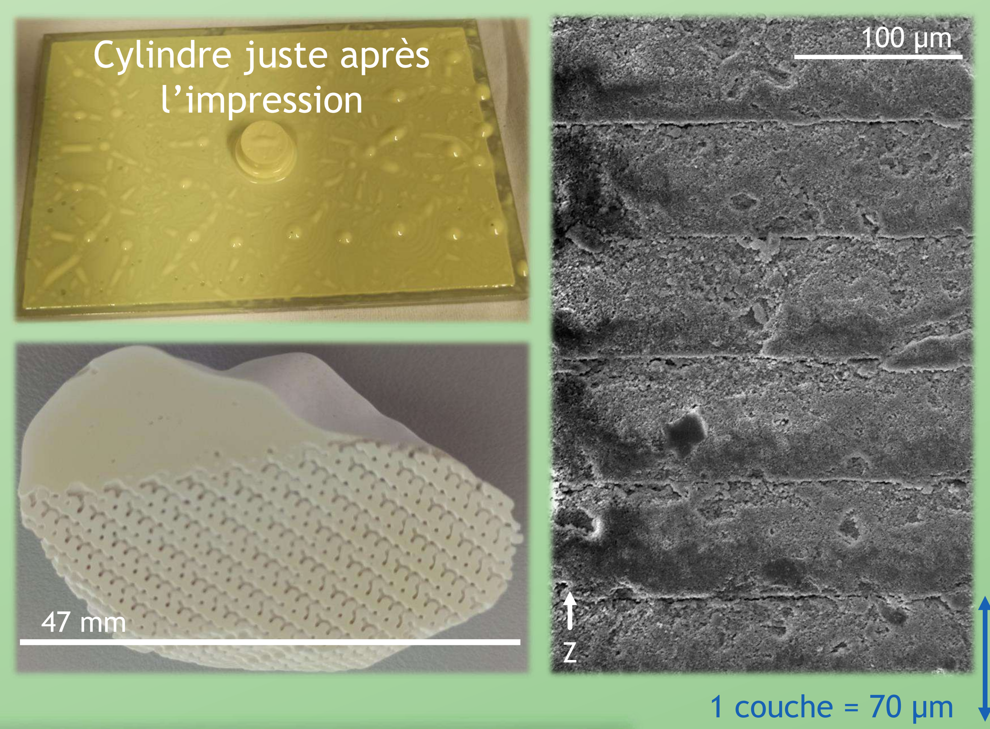

Post-traitement

Déliantage

- Suppression de la matrice organique par dégradation thermique
- Oxydation haute température du carbone ($C+O_2$ -> CO_2)

Pour les résines commerciales :
Perte de masse ≈ 30%
Retrait XYZ < 1 %

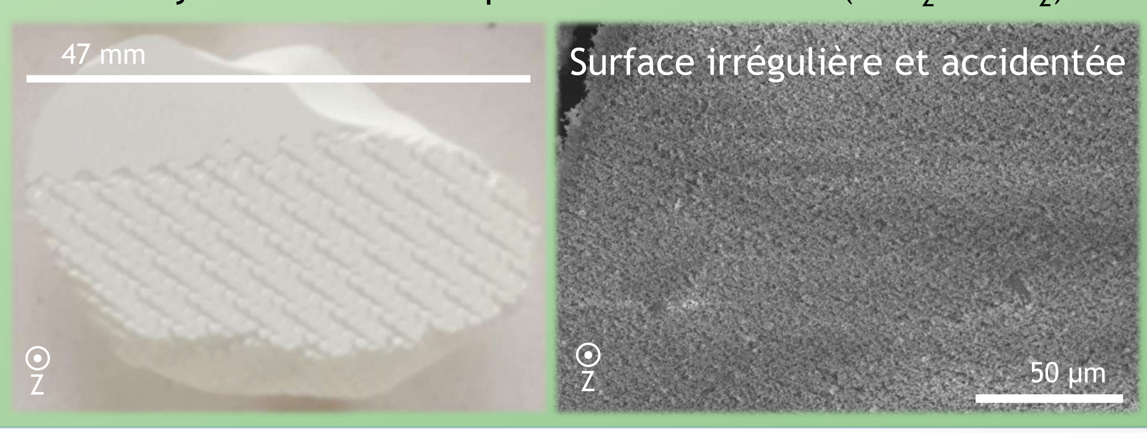

Frittage

- Création de liaisons entre les différents grains : assure la tenue mécanique de la pièce
- Densification

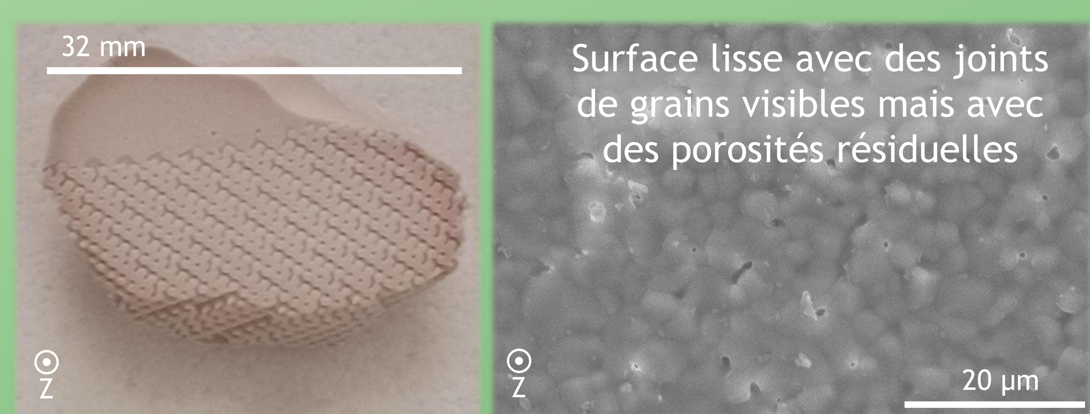

Pour les résines commerciales :
Perte de masse < 5 %
Retrait XYZ ≈ 25 %

Conclusions et perspectives

L’impression 3D est un outil extrêmement intéressant pour le domaine médical. Alliée à de nouveaux matériaux et des macrostructures favorables, une reconstruction sur-mesure et adaptée est envisageable.
Cependant, préparer une résine chargée en biocéramique est ardu : beaucoup d’étapes critiques peuvent conduire à une multitude de défaillances de l’implant (mauvais nettoyage, une couche ratée, …).
Une fois nos préparations stables et chargées en céramique à hauteur des résines commerciales (70% en masse), nous seront amenés à réaliser des tests mécaniques, biologiques et de relargages afin de déterminer l’influence des structures 3D sur celles-ci. Dans l’objectif de proposer, bientôt, aux chirurgiens orthopédistes, notamment de l’équipe, de nouvelles solutions à leurs besoins et de meilleurs implants osseux à leurs patients.

Références
[1] : G. Renaudin, S. Gomes, J-M. Nedelec. First-Row Transition Metal Doping in Calcium Phosphate Bioceramics: A Detailed Crystallographic Study. Materials 2017, 10, 92.
[2] : Jacobs, A.; Renaudin, G.; Charbonnel, N.; Nedelec, J.-M.;Forestier, C.; Descamps, S. Copper-Doped Biphasic Calcium Phosphate Powders: Dopant Release, Cytotoxicity and Antibacterial Properties. Materials 2021, 14, 2393.
[3] : Barralet, J.E.; Gbureck, U.; Habibovic, P.; Vorndran, E.; Gerard, C.; Doillon, C.J. Angiogenesis in Calcium Phosphate Scaffolds by Inorganic Copper Ion Release. Tissue Eng. Part A **2009**, 15, 1601–1609.
[4] : Y. Yao, W. Qin, B. Xing, N. Sha, T. Jiao, Z. Zhao. High performance hydroxyapatite ceramics and a triply periodic minimum surface structure fabricated by digital light processing 3D printing. Journal of Advanced Ceramics 2021, 10 (1) : 39-48.

Université Clermont Auvergne · CNRS · CHU Clermont-Ferrand · Clermont Auvergne INP · École Doctorale des Sciences pour l’Ingénieur · L’Europe s’engage en région Auvergne-Rhône-Alpes avec le FEDER

Graph learning methods to analyze and support industrial resilience

Kévin CORTIAL
Supervisors : Adélaïde ALBOUY KISSI – Frédéric CHAUSSE
Open Studio – Institut Pascal – Université Clermont Auvergne - CNRS - Clermont Auvergne INP

Context

Graphs are increasingly used to describe interactions between entities. They are based on a simple formalism that nevertheless allows complex systems to be modelled. Thus, in many domains, graphs can represent different aspects of the real world. In this context and **based on open source data, knowledge graphs representing industrial ecosystems have been built.**

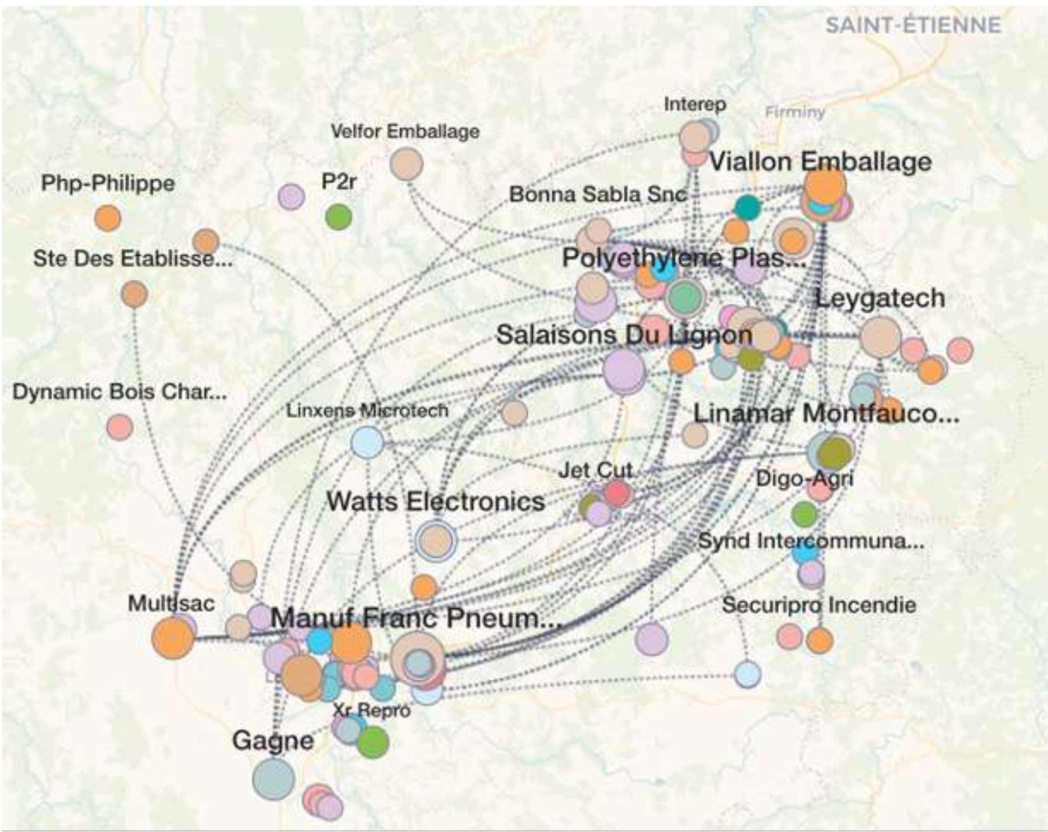

Learning on graphs requires **revisiting the usual artificial intelligence methods, as these unstructured data are complex to analyse.** Economics already uses methods from graph theory to describe and study the relationships between economic agents in networks. In this PhD, **we develop new learning methods for economic graphs** with the latest advances in graph learning.

Objectives

– **Classification of nodes** will allow identification of key players in economic network.

– **Clustering** to group and detect industrial communities with similar properties.

– **Prediction of links** that do not yet exist between two nodes. Predicting a connection between two entities could be seen as a recommendation system.

Methods

Machine and deep learning methods for graphs compute vector embeddings for each node to obtain better representations in their environment. With this new data for each node, graph learning is effective for many tasks, such as link prediction, community detection and node classification.

Graph Neural Networks

GNNs have made the hypothesis that many pieces of node's information reside in its neighborhoods. To store this data, we use node embedding which gathers the neighborhoods information with neural network.

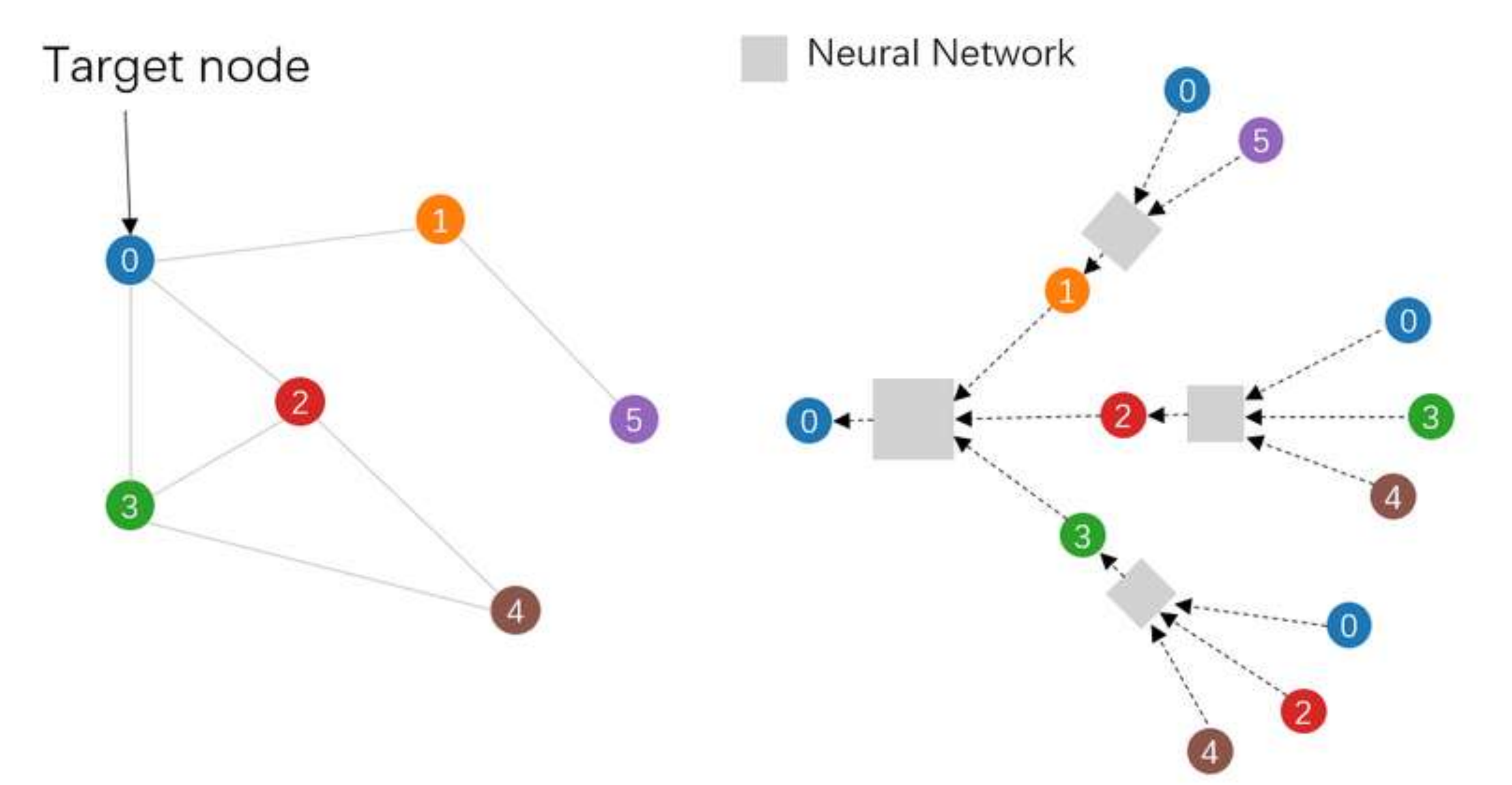

(a) Input graph (b) Neighborhood aggregation

Graph Attention Networks

Like GNN, Graph Attention Networks (GAT) use data contained in these neighbors to create embeddings for each node. The difference in GATs is the use of the **attention mechanism to select the importance to be given to each neighbor** (like Transformer models).

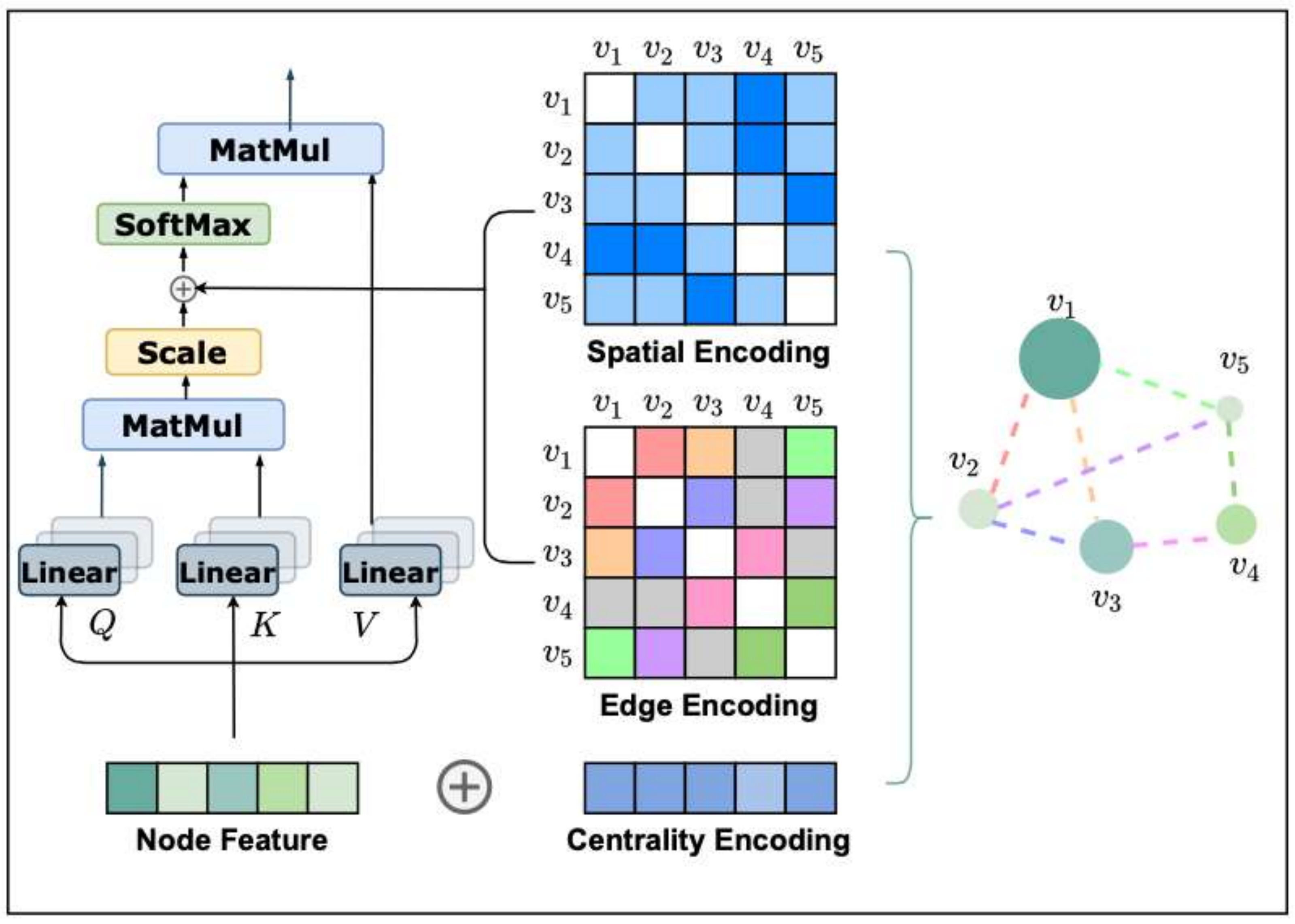

GAT aggregates information present in the neighborhood of a node by a weighted sum as an attention mechanism.

- First, GAT calculates an attention coefficient for each neighbor of the node in question (node features).
- Then, GAT must integrate edge data according to their number (centrality).
- Finally, if the nodes position in the graph is important, GAT will consider this position data (spatial encoding).

The adaptation of the GAT architecture, presented above, requires the addition of all graph's information at self-attention layer.

Perspectives

If we have historical data over several years, we can work on the analysis and evolution over time of economic graphs. In this context, we could investigate **Temporal Graph Networks** (TGNs), a deep learning model on dynamic graphs represented as sequences of timed events.

During this PhD, we could test combinations of new artificial intelligence or statistical concepts into GNN. The goal would be to improve the performance perhaps but especially to make graph learning models more explainable and interpretable for the economic world.

There are many research perspectives on these methods and their fields of application. For example, chemistry and biology use these models to analyse molecular graphs. **Social networks** are already using these methods for their **recommendation systems** but also in e-commerce.

Bibliography

Kipf, Thomas N., et Max Welling. 2017. « Semi-Supervised Classification with Graph Convolutional Networks »

Schlichtkrull, Michael et al. 2018. « Modeling Relational Data with Graph Convolutional Networks »

Vaswani, Ashish et al. 2017. « Attention Is All You Need »

Veličković, Petar et al. 2018 « Graph Attention Networks »

Ying, Chengxuan et al. 2021. « Do Transformers Really Perform Bad for Graph Representation ? »

Zhang, Muhan et Yixin Chen. 2018. « Link Prediction Based on Graph Neural Networks »

Process modelling and expression of performance indicators

Ecole doctorale Sciences Pour l'Ingénieur

Ricardo Viola[1 2], Emmanuel Duc[1 2], Xavier Balandraud[1], Pierre Michaud[2], Fabien Poulhaon[2]

[1]Univ. Clermont Auvergne, CNRS, SIGMA Clermont, Institut Pascal, F-63000 Clermont-Ferrand
[2]ESTIA Institute of Technology, F-64210 Bidart

Context

The application of additive manufacturing in industry still faces several challenges. In order to be able to make a precise comparison between the manufacturing process of a part using robotized WAAM and other so-called standard processes, it is necessary to create a techno-economic model. Such a model must be based in the performance indicators. The indicators in the present study are correlated to the robot kinematics and the thermal behavior during manufacturing.

Manufacturing Process

The Direct Energy Deposition wire arc (DED-WA) commonly known as wire arc additive manufacturing (WAAM) was the process chosen for the study. The WAAM process uses an electric arc as a heat source to melt the metallic wire on a substrate. In the present study, the molten metal was deposited using trajectories performed by a 6-axis robot.

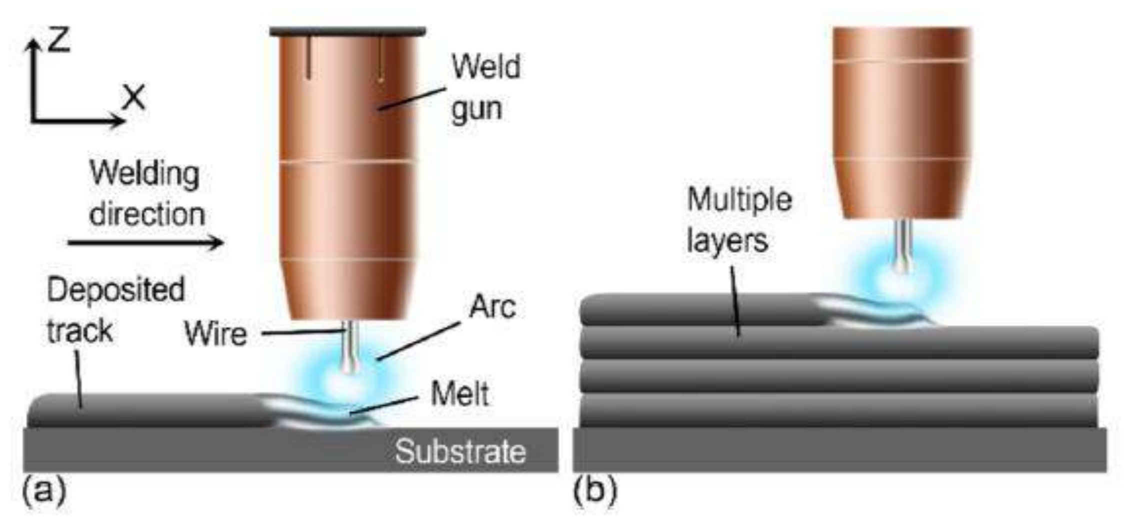

Illustration of Wire Arc Additive Manufacturing (a) initial single layer; (b) subsequent multiple layers [Näsström et al, « Laser enhancement of wire arc additive manufacturing », *Journal of Laser Applications*, vol. 31, nº 2, p. 022307, May 2019]

Kinematic Study

Due to the enormous influence of the robot on the process, it was necessary to study the robot's behavior. The transitions between deposition and non-deposition of metal along the toolpath (so-called arc transition) was analyzed. The phases of acceleration, constant velocity and deceleration of the robot are also analyzed. Eight different strategies (Figure A) were used with two speeds in order to simulate the filling of two sizes of objective rectangles (O.R.). Some results are shown in Figure B.

Strategies

Figure A

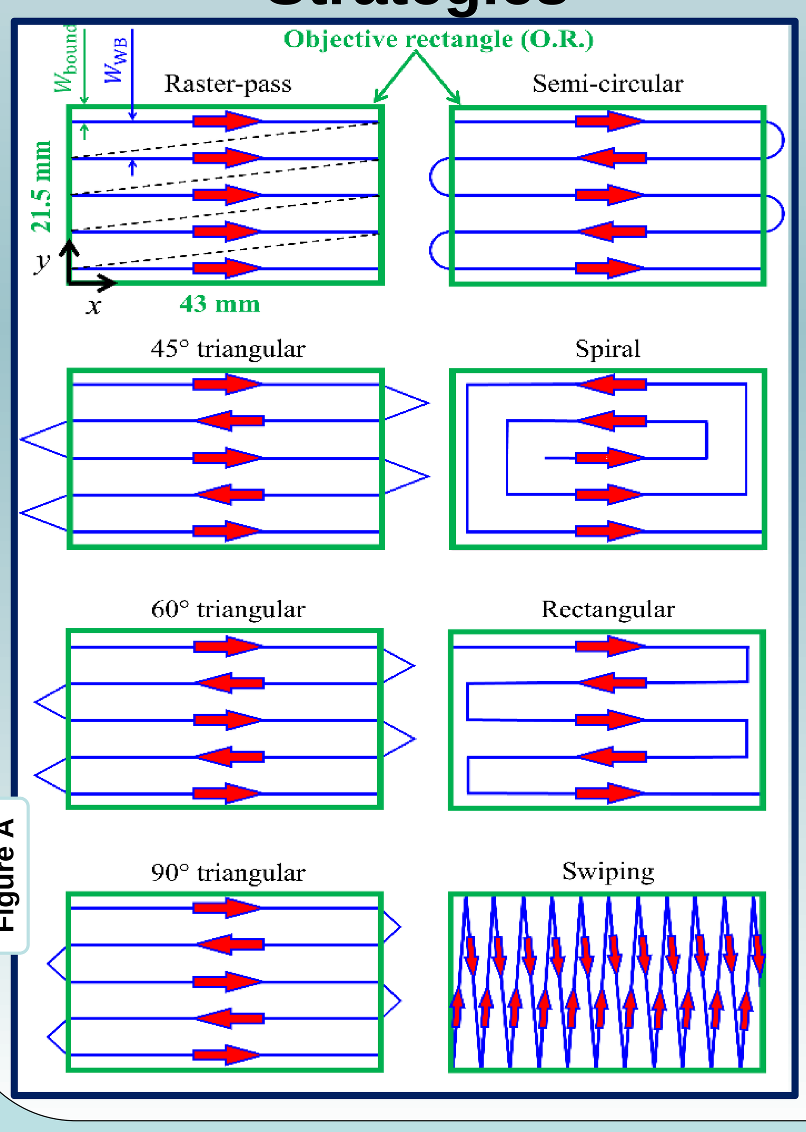

Results

Figure B

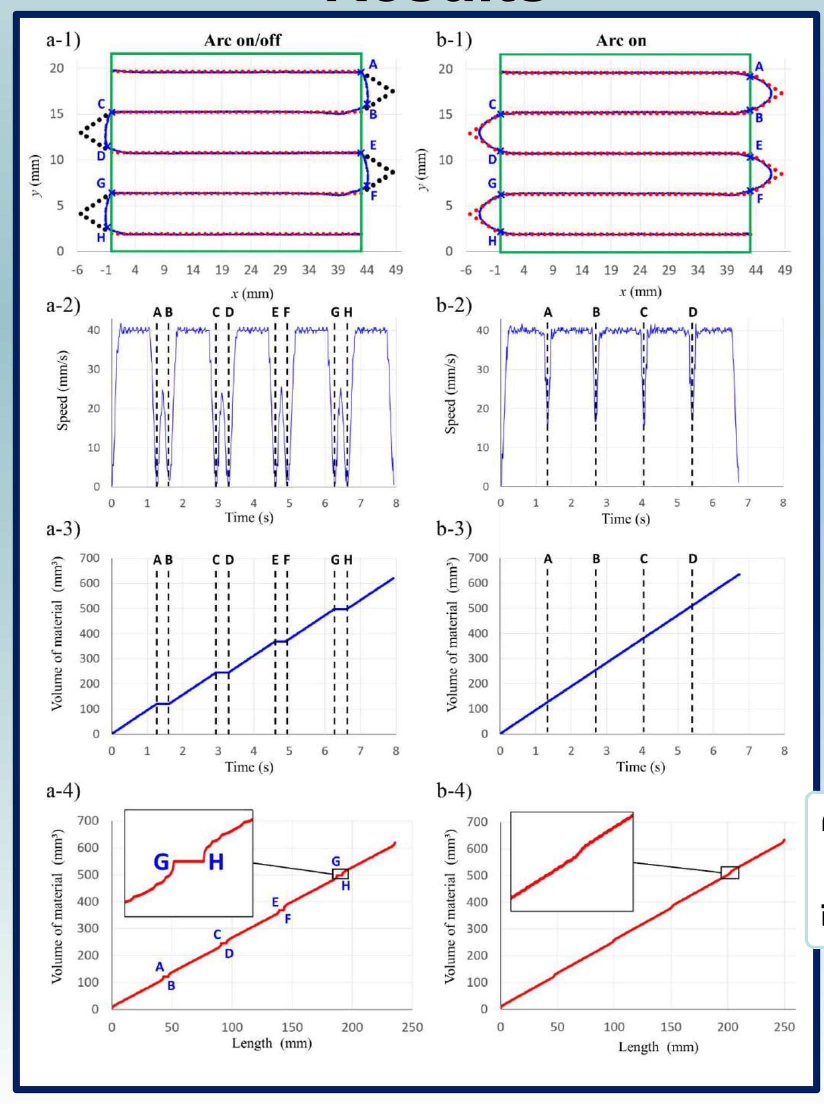

Data collected

Thermo-Kinematic Model

This model was developed in order to obtain thermal indicators along the entire length of the trajectory, thus allowing deposition strategies to be compared. Some trajectories can originate "hot spots", which have an influence on the microstructure achieved and therefore on the quality of the material and its mechanical properties. Four deposition strategies 1, 2, 3 and 4 (Figure C) were simulated to test the model and verify that the results obtained were representative of each trajectory.

Strategies

Figure C

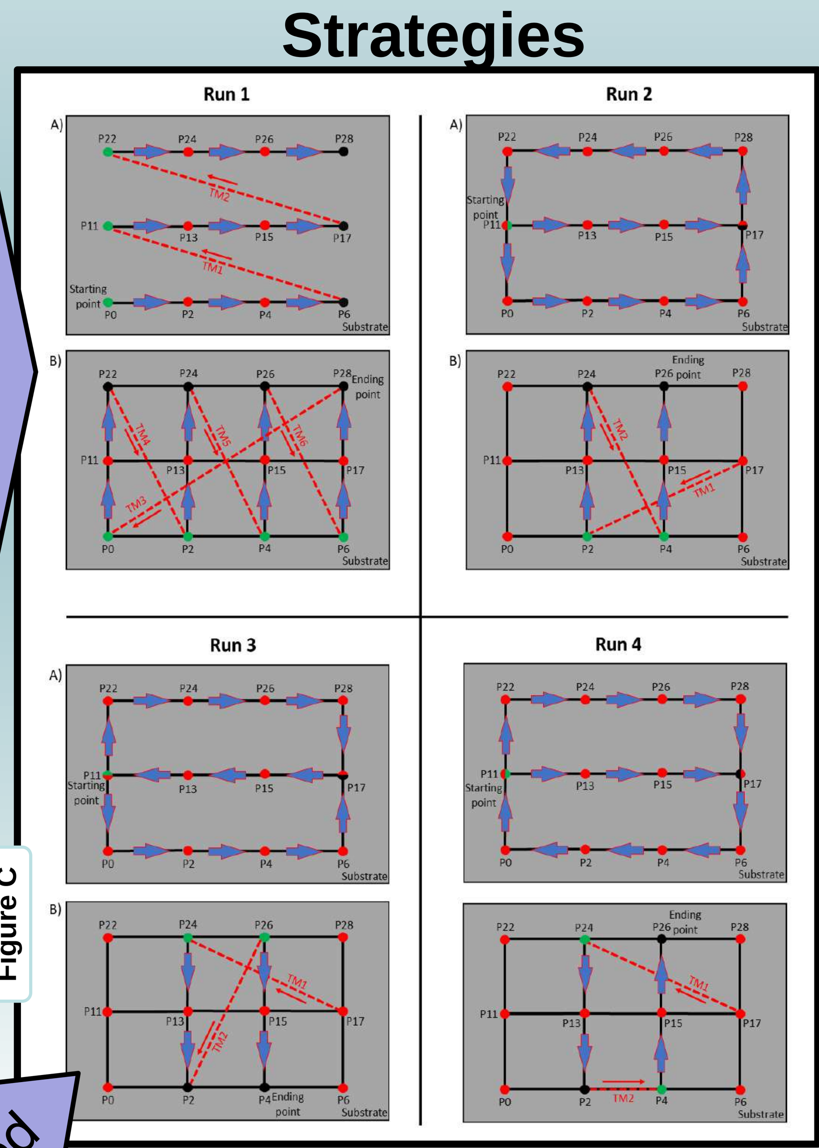

Results

Figure D

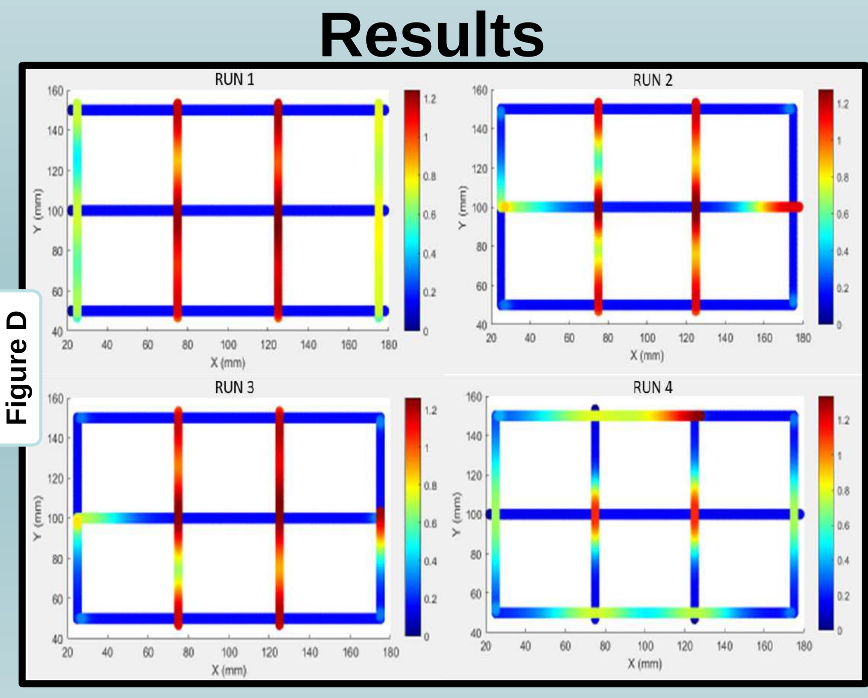

- It was possible to identify thermal indicators consistent with the FEM simulation
- In all 4 strategies tried, this model allowed to identify, in ascending order, the one with the lowest thermal gradient relative to the one with the highest thermal gradient

Correlated

Material Quality

The quality of the deposited material depends not only on the process parameters, but also on the thermal history that it is subject to. Experiments with different interlayer temperature (150°C and 350°C) were carried out in order to analyze the impact of thermal history on material quality . The temperature data collected by a pyrometer, FLIR thermal camera and thermocouples will allow to establish a relationship between the cooling curve of each layer, their position in the wall and the quality of the material achieved. The walls built under different cooling conditions will provide samples for tensile tests, hardness, microhardness and also fatigue tests instrumented by infrared thermography will be performed.

Monitoring

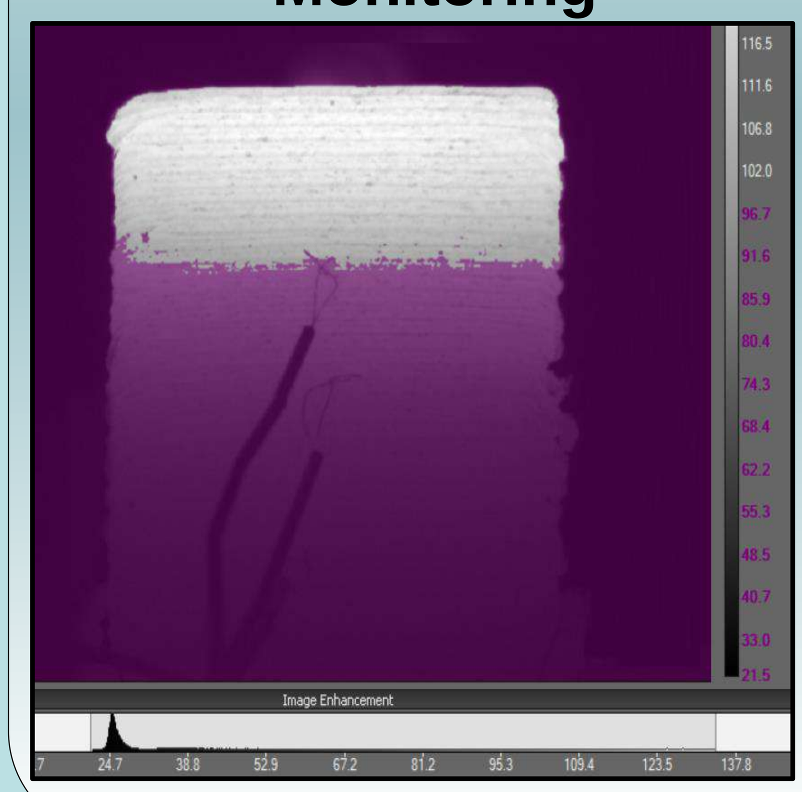

Results

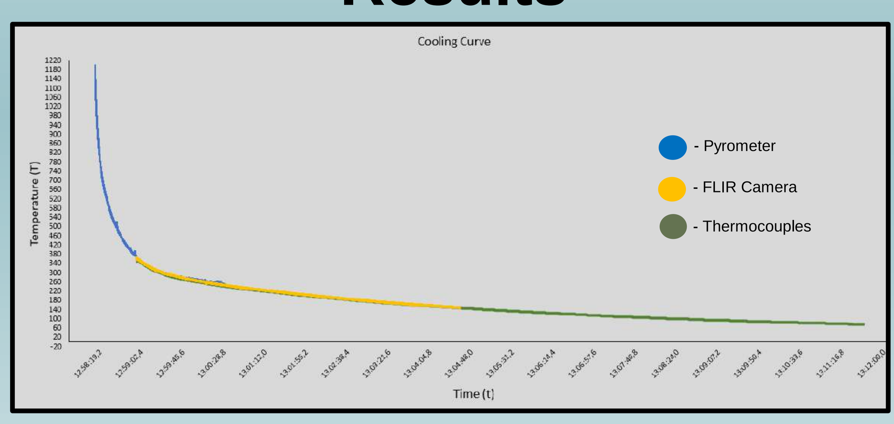

By cross-referencing the collected cooling curves with the Continuous Cooling Transformation diagram (CCT) of the material used, it will be possible to identify if the time period during which the material is exposed to certain temperatures is sufficient to generate detrimental phases.

Expected Conclusions

This study will permit to obtain a general indicator based on 4 key process indicators: 1 economic, 1 temporal, 1 quality and 1 geometrical. The general indicator should allow a quick perception of the suitability of the process to manufacture or not a certain part. The 4 key process indicators should fully represent the different aspects of the same process. The final thermo-kinematic model will provide an advanced estimation of the manufacturing time for different parts with the same characteristics. The time indicator will be included in the production cost calculation model. As a result, a direct comparison of production time and cost with standard processes would be possible. The quality indicator will provide the expected mechanical characteristics considering the production time .

Future work

There is another indicator that should be considered and has not yet been properly studied: the geometric indicator. This indicator should cross information on the angles that can be reached during the process as well as the geometric limitations to be considered.

Authentication Attacks on Projection Based Cancelable Biometric Schemes

DURBET Axel, GROLLEMUND Paul-Marie, LAFOURCADE Pascal, MIGDAL Denis and THIRY-ATIGHEHCHI

Université Clermont-Auvergne, CNRS, Mines de Saint-Étienne, LIMOS, LMBP France

SCAN ME

Objectives

1. Contruct an impersonation attack on CB scheme.
2. Formalize how to consider the filter in such attack.
3. Show attacks on some projection-based cancelable biometric schemes.

Introduction

- Biometric authentication is widely used.
- It is more convenient and quicker.
- Biometric characteristics cannot be lost.
- Biometric characteristics cannot be forgotten.
- This solution are not exempt from vulnerabilities.
- The projection-based cancelable biometric schemes are very common.
- Some theoretical attacks are provided.

Materials

- Python 3.9.
- Gurobi 9.1.2.
- Debian 11.
- EPYC 7F72 dual processor (48 cores).
- 256GB RAM.

Attacked Scheme

- The attacked CB instantiation, described in our Algorithm, is based on a uniform random projection (*URP*). Such a projection serves as an embedding of a high-dimensional space into a space of much lower dimension while preserving approximately the distances between all pairs of points.
- Here is the attacked algorithm based on Sobel filter:

Algorithm 1 [URP-SOBEL]

Inputs : biometric data I; token parameter P
Output : BCV vector $T = (t_1, \dots, t_m)$

1: Apply Sobel filter on I to produce an n-sized feature vector: $F = (f_1, \dots, f_n)$.
2: Generate with the token P a family V of m pseudorandom vectors $V_1, \dots, V_m$ of size n according to a uniform law $\mathcal{U}([-0.5, 0.5])$.
3: Arrange the family V as a matrix M of size $n \times m$.
4: Compute T as the matrix-vector product $F \times M$.
5: **for** t_i in T **do**
6: **if** $t_i < 0$ **then** $t_i = 0$ **else** $t_i = 1$
7: **end for**
8: **return** T

Mathematical Section

- Assume that $I_A = (o_{i,j})_{n \times m}$ is the attacker's original image, $I' = (x'_{i,j})_{n \times m}$ the modified original image and $X = (x_{i,j})_{n \times m}$ its augmented form. Let $\mathcal{K}_1$ be all indices where the template is equal to 0 and $\mathcal{K}_2$ all other indices. Let $M = (a_{i,j})_{(n*m) \times \ell}$ be the projection matrix. Let Y_{flat} be the flattened form of the matrix Y where rows are concatenated in a single vector.
- The attack consists of solving following problem for Sobel filter:
  - Minimize: $\|X - I_A\|^2$
  - Subject to the following constraints:

$$\begin{cases} Y^2 = \left[(G_1 * X)^2 + (G_2 * X)^2\right] \\ Y_{flat} M_i < 0, \forall i \in \mathcal{K}_1 \\ Y_{flat} M_j \geq 0, \forall j \in \mathcal{K}_2 \\ x_{i,j} \in \{0, \dots, 255\}, \forall (i,j) \end{cases}$$

Sobel Filter Example

Attack Overview

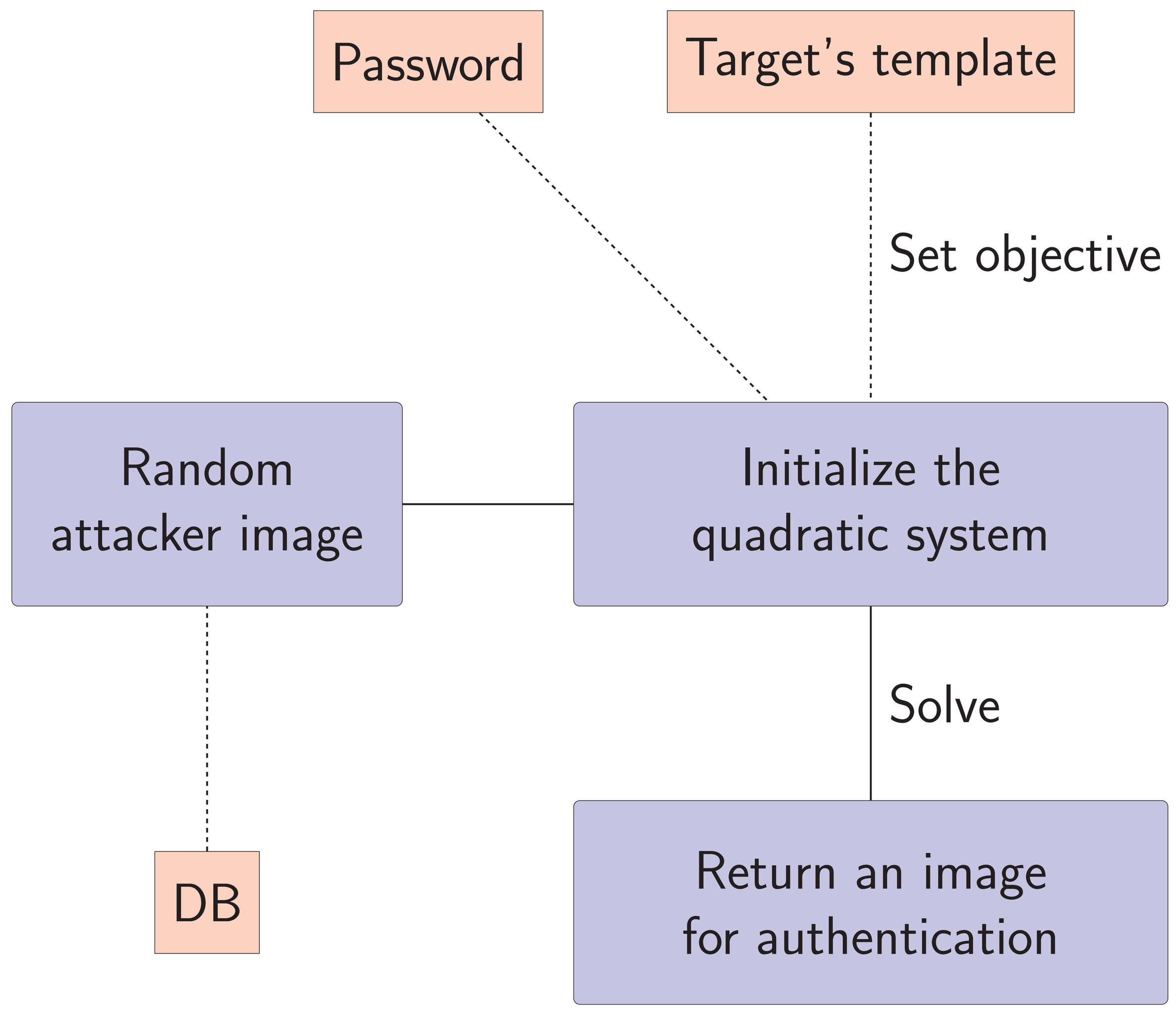

Beginning of Result

Image Size	Mean Distance	Mean Time (s)
2×2	99	0.14
2×3	117	32.76
3×3	133	150.0
4×3	144	146.67
4×4	177	150.0

Table 1:Summary of the experiments for a 50-bit template.

Conclusion

- Several authentication attacks on a popular CB scheme has been presented.
- Attacks are conducted on a complete chain of treatments.
- Two ways for the attacker to impersonate several legitimate persons has been presented.
- The modification of the attacker's image is minimal.

Future Work and How to Ensure the Scaling of the Attack

- Code optimization.
- System relaxation.

Acknowledgments

The authors acknowledges the support of the French Agence Nationale de la Recherche (ANR), under grant ANR-20-CE39-0005 (project PRIVABIO).

Contact Information

- Web: PRIVABIO Project on: https://privabio.limos.fr/
- Email: axel.durbet@uca.fr

The use of machine learning and grey-box models to solve complex time-consuming RBDO problems

Application to mass production mechanical systems

Alessio Faraci[1], Pierre Beaurepaire[1], Nicolas Gayton[1]

[1]SIGMA Clermont - 63178 Aubière Cedex, France

Objectives

1. Develop an efficient approach for reliability estimation
2. Apply this method in a multi-fidelity modelling context
3. Apply zero-order optimization problem based on machine learning separators
4. Apply developments to production processes in collaboration with Radiall

Introduction

Context

- Structural design goal: to be optimal, reliable regarding uncertainties
- Applying grey-box approaches for reliability analysis, optimizing and controlling of production process and systems

Grey-box modelling

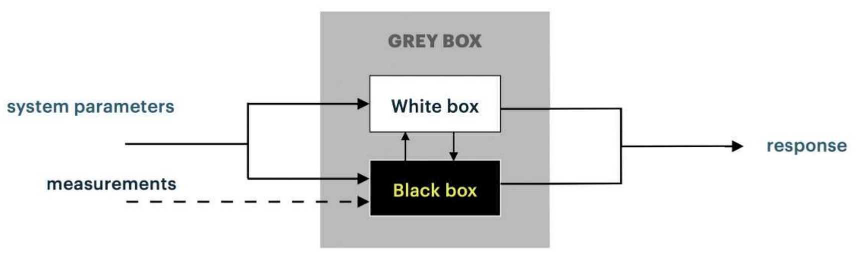

- **white box**: physics-based computational models
- **black box**: mathematical models based on ML approaches built from observational data
- **grey box**: fusing information to relax the need to exactly model the underlying physics, while requiring considerably less data

Methodology

RBDO formulation

- Optimization under reliability constraints: aim to identify admissible design with optimal performance
- Minimizing a cost function f while satisfying the performance function g
- Optimal solutions lie on the boundaries of the admissible space

$$\text{Find:} \quad \bar{X}_{OptRel} = \arg\min_{\bar{X}} f\left(\bar{X}, P^{(k)}\right)$$

$$\text{Subject to:} \quad Prob\Big(g\big(X(\bar{X}, \omega), P(\omega)\big) \leqslant 0\Big) \leqslant P_{target}$$

- **Main problem**: computational time consuming
  - ↳ Metamodel-based strategy → Adaptive Kriging
  - ↳ Classify a MC sample using ML separators defined in an augmented-space and 0-order algorithms (e.g. Genetic Algorithm)

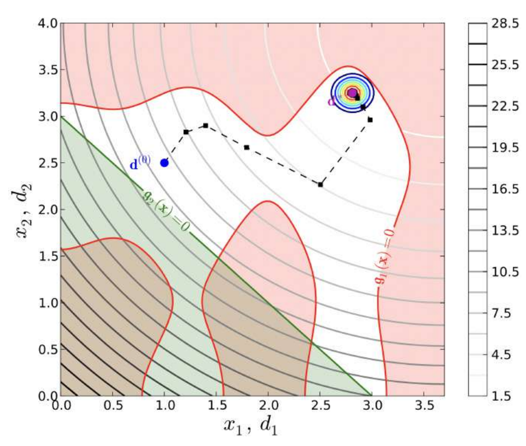

First investigation: review on Python toolboxes for Kriging

1. Focus on:
   - ↳ comparing the various settings available for each library
   - ↳ to ascertain how they perform and differ under similar assumptions
2. Comparison on:
   - ↳ computational time-cost for different size of ED
   - ↳ prediction accuracy by means of Mean of the Squared Errors (MSE)

$$MSE = \frac{1}{n}\sum_{i=1}^{n}\left(Y(x_i^*) - \tilde{Y}(x_i^*)\right)^2$$

Benchmark case-study

- FE model: rectangular shell plate (1.5m×1m) clamped at the four edges
- Load: pressure of 100 Pa uniformly applied at the surface
- Fiber orientation: $x = \{x_1, \dots, x_m\}$ where $m \in [2, 4, 8, 16, 32]$
- MC sampling: input space with a uniform distribution between 0° and 180°
- QoI: displacement Y at the center of the plate
- Kriging surrogate: $\tilde{Y}(x) = \sum_{j=1}^{p} \beta_j f_j(x) + Z(x)$
- Matérn 3/2 kernel: $R(x, x'; \theta) = \left(1 + \sqrt{3}\frac{|x-x'|}{\theta}\right) exp\left[-\sqrt{3}\frac{|x-x'|}{\theta}\right]$

Benchmark case-study results

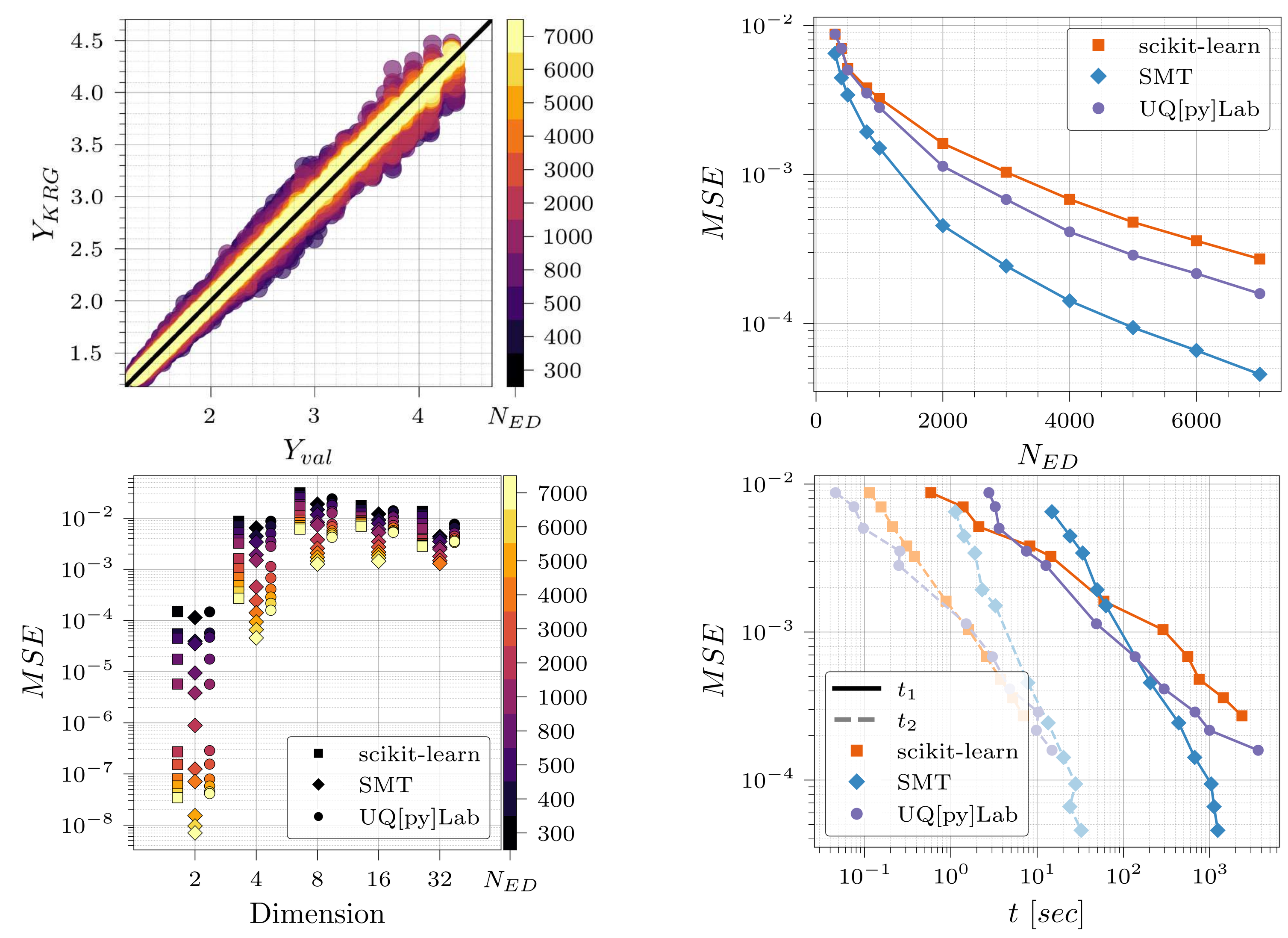

Figure 1: North-West: Cross-validation plot for SMT, dimension 4; North-East: MSE for increasing value of N_{ED}; South-West: MSE at different dimensionality; South-East: MSE vs time.

Industrial applications

Applications to product cost reduction in mass production

Discussion and future work

- Discrepancies have been observed among various Python packages
- The review will be extended to more packages and scenarios (e.g. different kernel types and other optimization algorithms)
- Zero-order algorithm will be investigated to deal with RBDO problems
- Multifidelity computer codes with different confidence levels will be investigated and applied to decrease the global optimization time

References

[1] C. K. Williams and C. E. Rasmussen, *Gaussian processes for machine learning*. MIT press Cambridge, MA, 2006, vol. 2, no. 3.

[2] V. Dubourg, "Méta-modèles adaptatifs pour l'analyse de fiabilité et l'optimisation sous contrainte fiabiliste," Ph.D. dissertation, Clermont-Ferrand 2, 2011.

[3] B. Echard, N. Gayton, and M. Lemaire, "Ak-mcs: an active learning reliability method combining kriging and monte carlo simulation," *Structural Safety*, vol. 33, no. 2, pp. 145–154, 2011.

[4] N. Lelièvre, P. Beaurepaire, C. Mattrand, N. Gayton, and A. Otsmane, "On the consideration of uncertainty in design: optimization-reliability-robustness," *Structural and Multidisciplinary Optimization*, vol. 54, no. 6, pp. 1423–1437, 2016.

Acknowledgments

This project has received funding from the European Union's Horizon 2020 research and innovation programme under the Marie Skłodowska-Curie grant agreement No. 955393.

Contacts

Website: https://www.greydient.eu
Linkedin: https://www.linkedin.com/company/itngreydient
Twitter: https://www.twitter.com/ITNGreydient

alessio.faraci@sigma-clermont.fr

Détection faiblement supervisée de pathologies vasculaires

Guillaume Garret[1], Antoine Vacavant[1], Carole Frindel[2]
[1]CaVITI - Institut Pascal, Université Clermont Auvergne, Clermont-Ferrand, France
[2]CREATIS, Université de Lyon, Lyon, France
Projet Région Défi Imagerie / IA-DAISIES — École Doctorale des Sciences pour l'Ingénieur

Objectifs

1. Développer des outils de compréhension de modèles IA déjà existants pour des tâches de segmentation médicale.
2. Développer des méthodes faiblement supervisées en exploitant le rehaussement vasculaire et la reconstruction d'un arbre vasculaire à partir d'une portion initiale complétée par données précliniques.
3. Confronter les modèles *machine learning* à la présence de lésions dans les tissus.

Introduction

- Excellentes performances des IA $\Rightarrow$ implantation massive dans la vision par ordinateur.
- La nature "boite noire" des IA entraîne la réticence des secteurs critiques - comme l'imagerie médicale.
- La reconstruction numérique du système vasculaire du foie est parfois nécessaire avant diagnostique médical ou préparation d'intervention. Obtenue grâce aux IA, l'explicabilité et l'interprétabilité est presque nulle.
- Nous développons des méthodes d'explicabilité qui visent la confiance, l'éthique et la traçabilité des modèles de segmentation du système vasculaire du foie.

Matériels

- Modèle *Dense-UNet* entraîné à segmenter le système vasculaire du foie [1].

Figure 1:Reconstruction 3D vascularisation d'un foie (base IRCAD).

- Ensemble de données *Liver segmentation 3D-IRCADb-01* [2]. Images tomographiques du foie de 20 patients, en 3D.

Méthode

Parmi les approches d'explicabilité : les cartes d'attributions. Elles indiquent la contribution marginale d'une caractéristique d'entrée sur la sortie.

- Cartes d'attributions par la méthode *Integrated Gradients* IG [3]
  - Génération d'une ligne de base x'.
  - Interpolation de l'entrée x le long d'un chemin linéaire allant de x' à x.

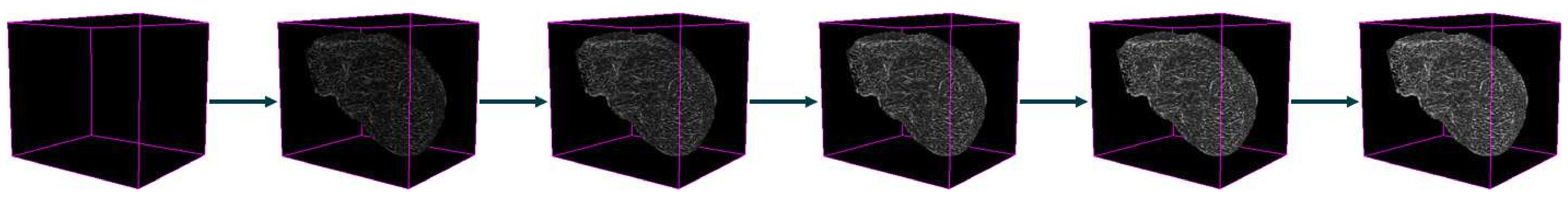

Figure 2:Représentation des images interpolées le long du chemin linéaire $x' \longrightarrow x$.

  - Accumulation des gradients des images interpolées.
  - Intégration des gradients entre la ligne de base x' et l'entrée x.
- Génération d'un graphe représentant la topologie du système vasculaire du foie (selon la vérité terrain).

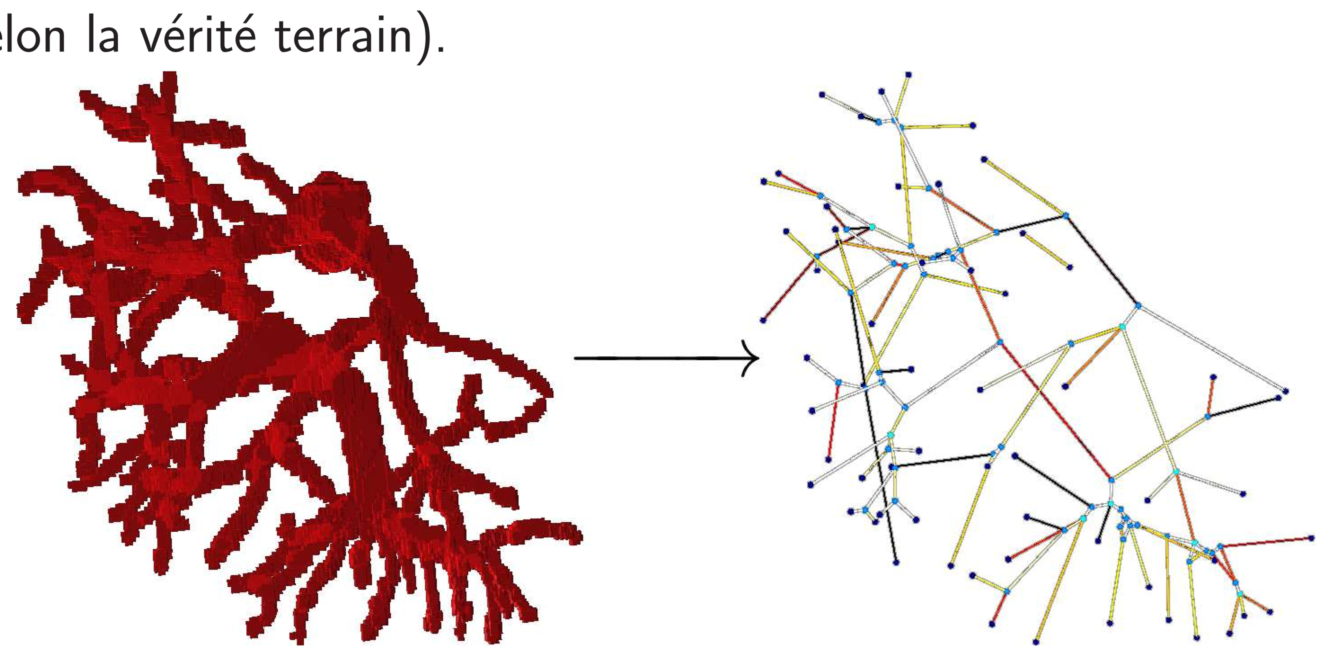

Figure 3:Graphe de la topologie du système vasculaire du foie.

- Etude des *Integrated Gradients* aux noeuds du graphe :
  - Perspective par rapport à la performance du modèle.
  - Perspective par rapport à la topologie vasculaire.

Formalisme d'explicabilité

- *Integrated Gradients* [3]
  - Méthode axiomatique (sensibilité et invariance à l'implémentation).

$$IG_i(x) = (x_i - x_i') \times \int_{\alpha=0}^{1} \frac{\partial F(x' + \alpha \times (x - x'))}{\partial x_i} d\alpha$$

  - Où i une fonctionnalité, x l'entrée, x' la ligne de base et α la constante d'interpolation.
- En pratique, sur données numériques discrètes,

$$IG_i^{approx}(x) = (x_i - x_i') \times \sum_{k=1}^{m} \frac{\partial F(x' + \frac{k}{m} \times (x - x'))}{\partial x_i} \times \frac{1}{m}$$

  - Où i un voxel individuel, x le tenseur image, x' le tenseur ligne de base, k la constante de perturbation et m le nombre d'étapes dans l'approximation de la somme de Riemann.

Résultats qualitatifs

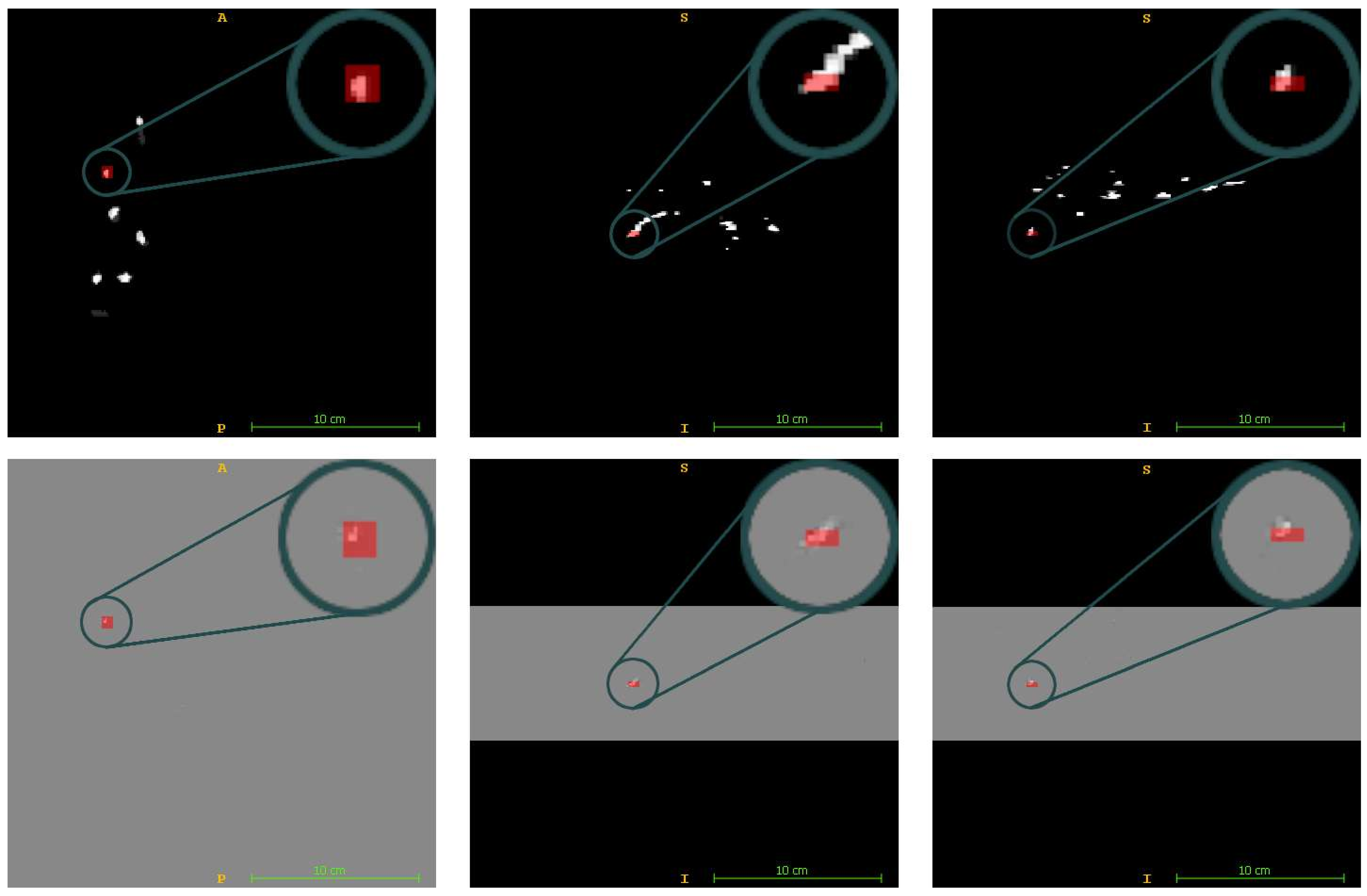

Figure 4:De gauche à droite : plan axial, coronal, sagital. En haut : vérité terrain. En bas : carte d'attributions. Zone rouge : fenêtre d'observation. On observe sur la carte d'attributions une contribution positive des pixels correspondants aux vaisseaux sur la vérité terrain.

Bilan et perspectives

- La nature performante mais non explicable des algorithmes d'apprentissage profond freine leur utilisation dans l'imagerie médicale.
- Nous travaillons à expliquer le comportement des réseaux de segmentation du système vasculaire du foie au travers de cartes d'attributions, obtenues par la méthode des *Integrated Gradients*. Cette méthode axiomatique repose sur un socle théorique fondamental.
- Les vaisseaux dans l'image contribuent positivement à la prédiction de vaisseaux lors de la segmentation.

- Mettre en perspective les cartes d'attributions par rapport à d'autres caractéristiques (diamètre du vaisseau, courbure, etc.)
- Enrichir l'explicabilité via d'autres méthodes (*DeepLIFT*, *DASP*.)
- Utiliser des cartes d'attributions pour superviser l'apprentissage.

Références

[1] A. Affane, A. Kucharski, P. Chapuis, S. Freydier, M.-A. Lebre, A. Vacavant, and A. Fabijańska.
Segmentation of Liver Anatomy by Combining 3D U-Net approaches.
2021.

[2] 3D-IRCADb-01 dataset.
www.ircad.fr/research/data-sets/liver-segmentation-3d-ircadb-01/.

[3] M. Sundararajan, A. Taly, and Q. Yan.
Axiomatic Attribution for Deep Networks.
2017.

 Guillaume.GARRET@uca.fr

Commande robuste d'objets déformables avec robots manipulateurs et application à des procédés industriels

CLERMONT AUVERGNE INP

Ecole doctorale Sciences Pour l'Ingénieur

Directeur :
Chedli Bouzgarou

Co-directeur :
Youcef Mezouar

Co-directeur :
Erol Ozgür

Victor Giraud

SOFT MAN BOT

INSTITUT PASCAL
sciences de l'ingénierie et des systèmes

Problématique

- **Les objets déformables** sont partout : textiles, plastique, nourriture, tissus humains… On les classifie génralement en **Linéaire**, comme les cordes et les poutres, **Thin-shell**, comme les feuilles de papier, et **Volumétrique**, comme une éponge.

- **La manipulation d'objets déformables** est un problème ouvert, notamment pour les applications industrielles

- **Les challenges sont multiples** pour une commande en boucle fermée. Les objets et stratégies sont variées, mais les points communs sont un besoin de **perception**, de **modélisation** et de **contrôle.**

- **Contributions :** Proposition d'une **architecture logicielle** commune aux différents membres du projet, et d'une stratégie de commande intelligente

Commande Optimale

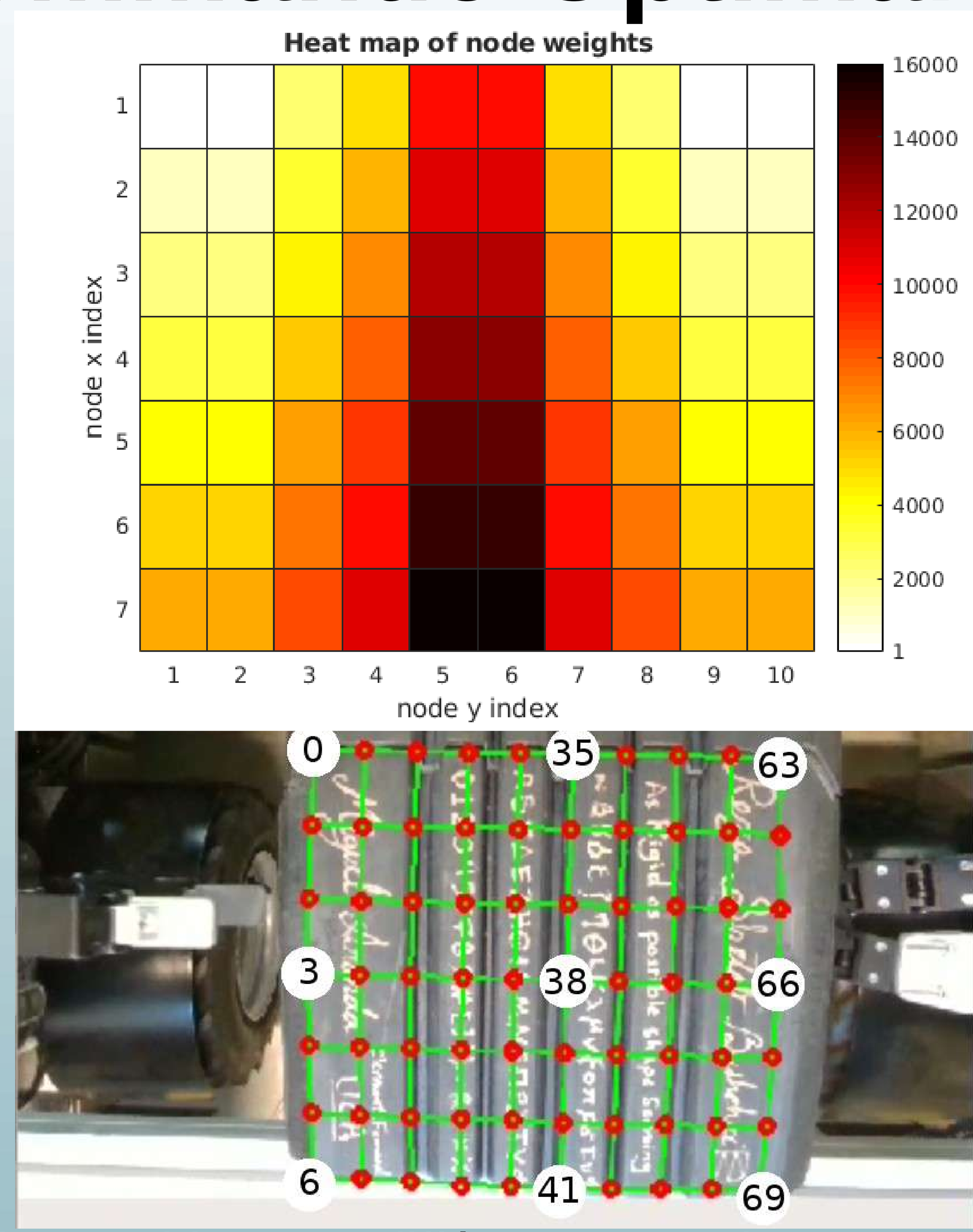

On donne des "poids" aux différents noeuds pour prioriser les zones de convergences afin de générer une trajectoire de tâche en boucle fermée. Le calcul de la régulation se fait sur un horizon de temps.

Architecture proposée

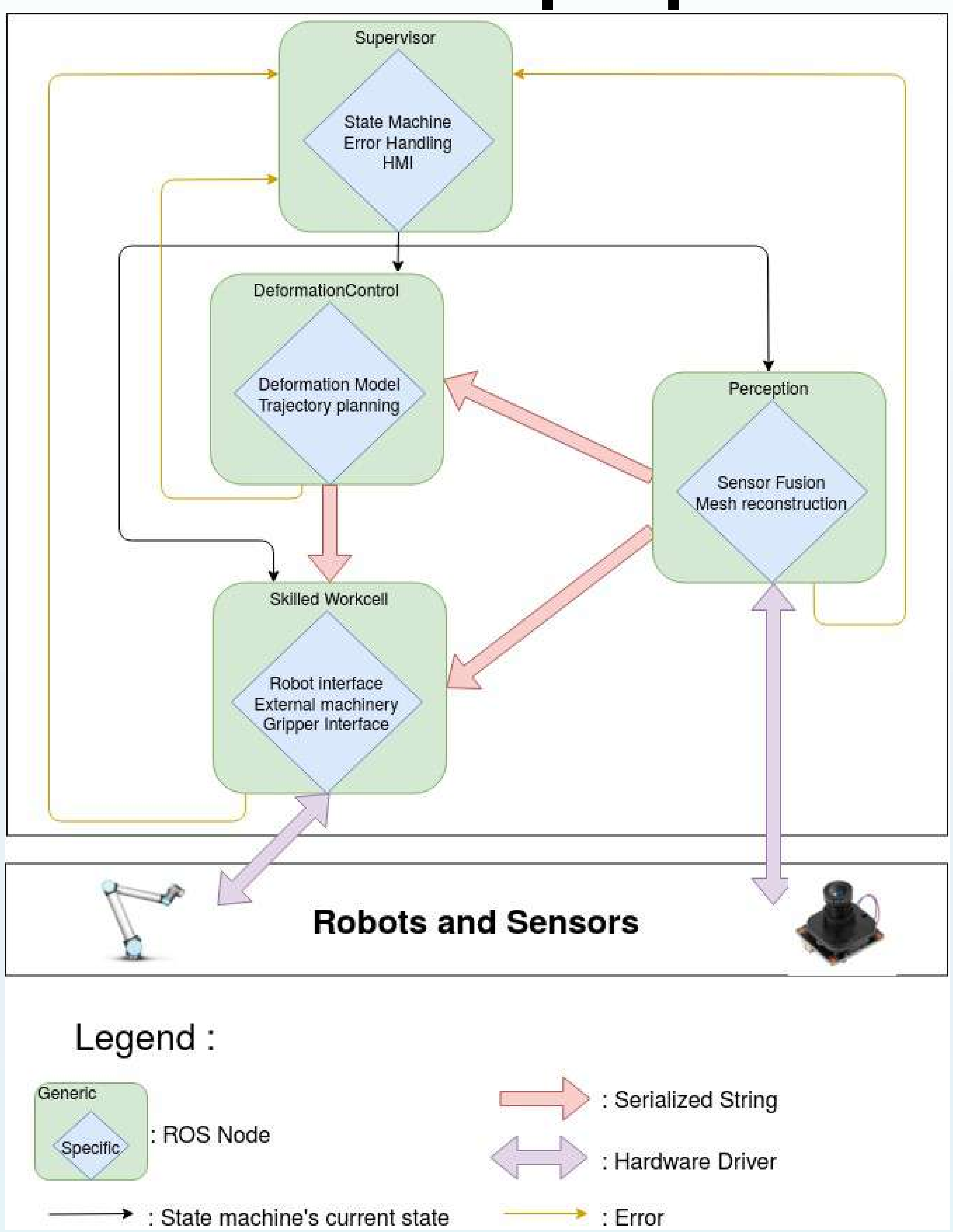

Résultats

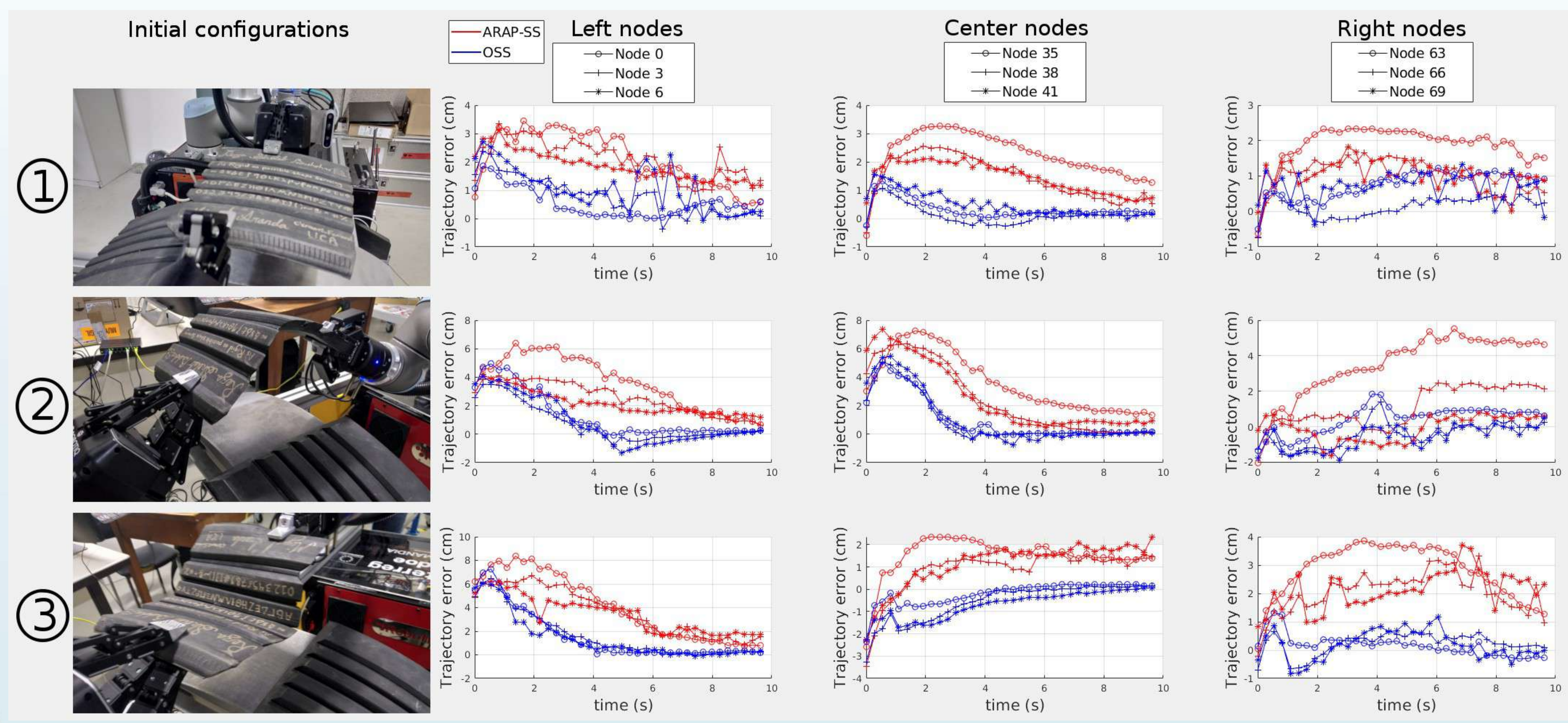

Conclusion

La commande optimale permet l'accomplissement de la tâche avec des contraintes. Ceci permet de maîtriser le temps de cycle, comment va évoluer la déformation dans le temps, et même empêcher certaines collisions avec l'environnement en utilisant des mouvements proches de ceux de l'humain. Les futurs travaux sont basés sur l'identifications des paramètres via démonstration humaine.

Bibliography

Victor H. Giraud, Maxime Padrin, Mohammadreza Shetab-Bushehri Chedli Bouzgarrou, Youcef Mezouar, Erol Ozgur, "Optimal Shape Servoing with Task-focused Convergence Constraints", Submitted for publication

EcoMobiCoin

Frédéric A. Hayek
Laboratoire d'Informatique, de Modélisation et d'Optimisation des Systèmes

Bitcoin and "traditional" cryptocurrencies...

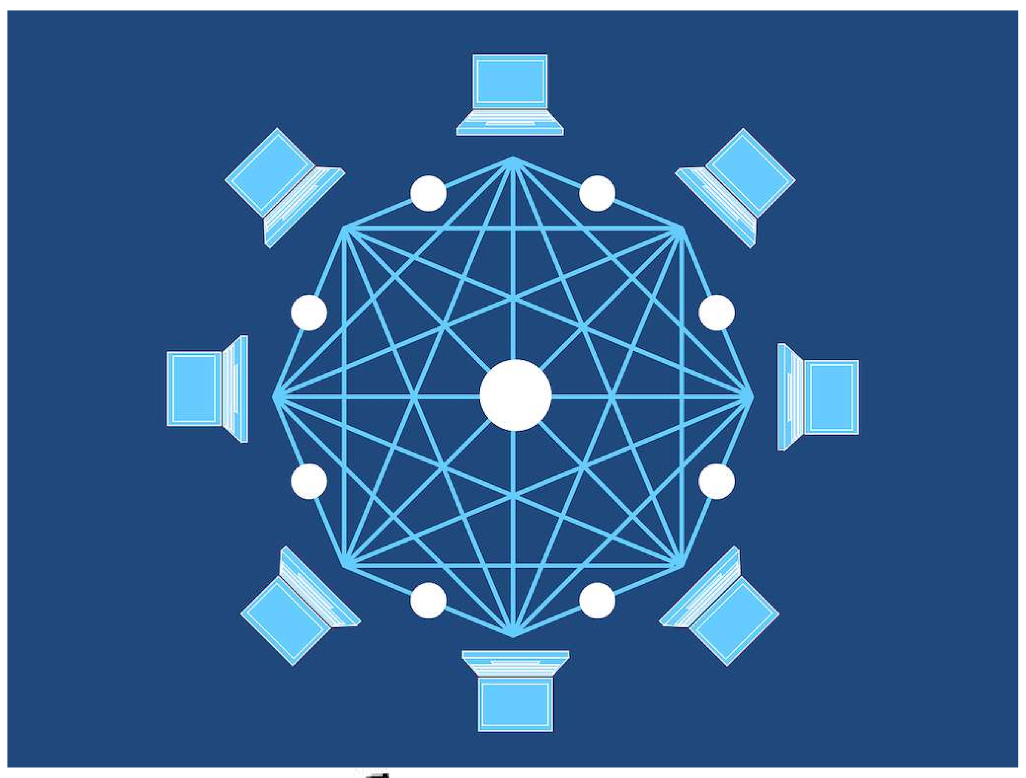

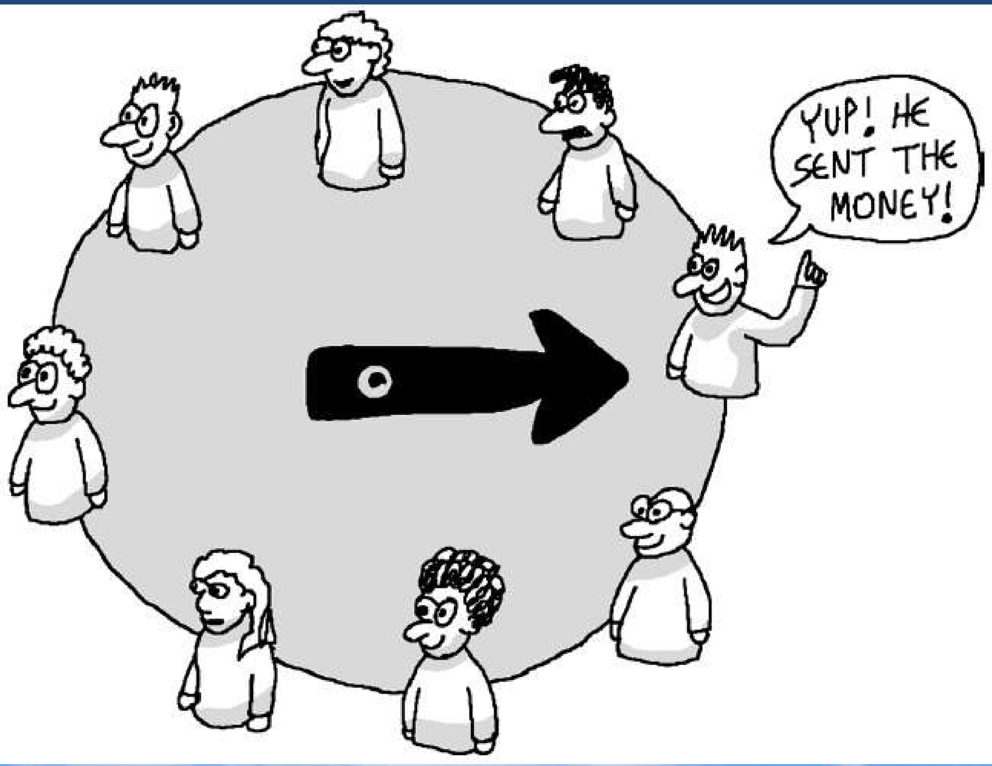

...Speculation...

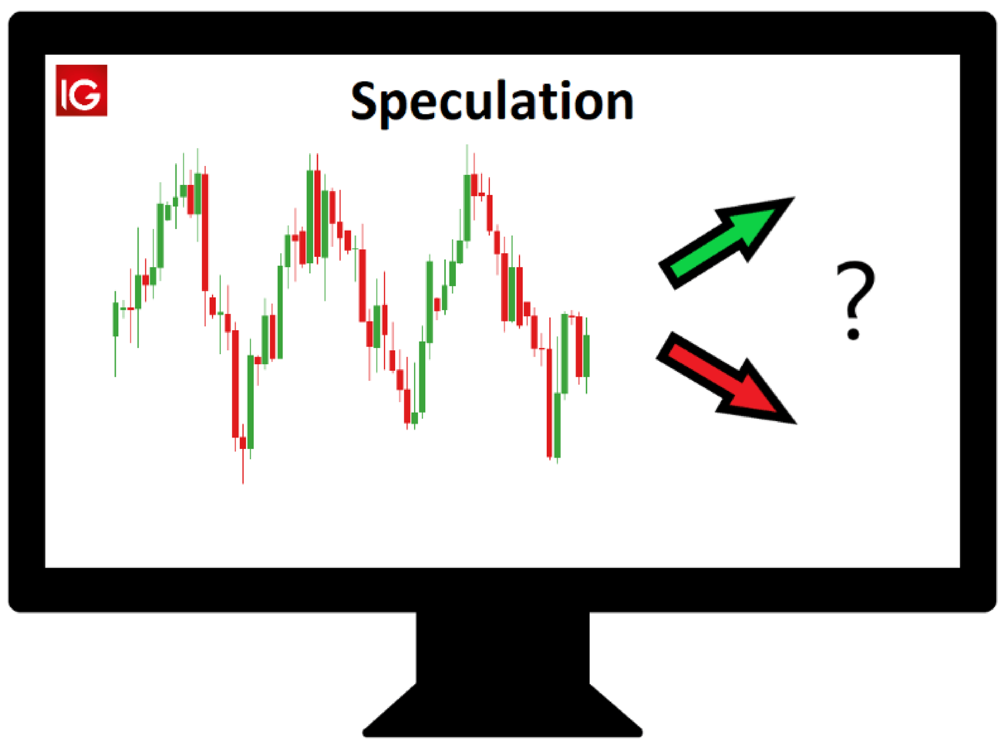

...Volatility

EcoMobiCoin...

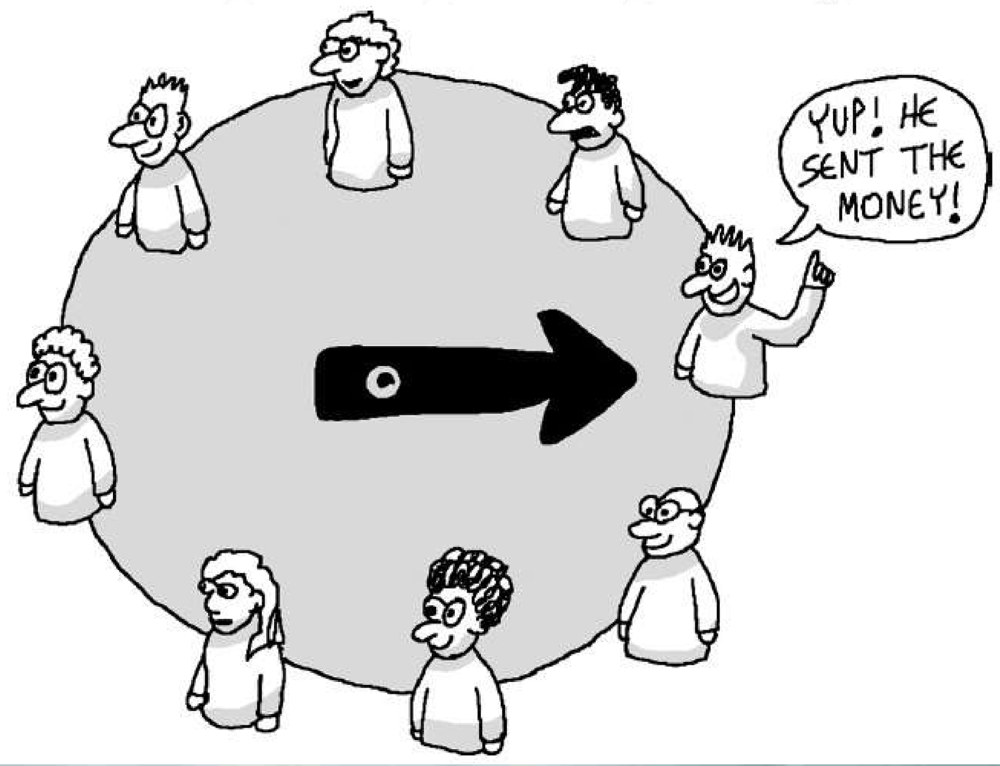

...Demurrage...

...Stability

frederic.hayek@uca.fr

Early Diagnosis of Lyme Disease by Recognizing Erythema Migrans Skin Lesion from Images

Ecole doctorale Sciences Pour l'Ingénieur

Sk Imran Hossain[1] — PhD student — sk_imran.hossain@uca.fr
Engelbert Mephu Nguifo[1] — Supervisor — engelbert.mephu_nguifo@uca.fr
Jocelyn de Goër de Herve[2] — Co-Supervisor — jocelyn.degoer@inrae.fr

[1]Université Clermont Auvergne, CNRS, ENSMSE, LIMOS, F-63000 Clermont-Ferrand, France
[2]Université Clermont Auvergne, INRAE, VetAgro Sup, UMR EPIA, 63122 Saint-Genès-Champanelle, France

Research Problem

Lyme disease is an infectious disease transmitted by ticks and caused by pathogenic bacteria of the *Borrelia burgdorferi* sensu lato group. In the early stage, the disease manifests itself in most cases with erythema migrans (EM) skin lesions. Better diagnosis of these early forms would allow improving the prognosis by preventing the transition to a severe late form thanks to appropriate antibiotic therapy. The goal of the thesis is to develop AI model to assist with the creation of diagnosis application as part of the DAPPEM project funded by European Union [1].

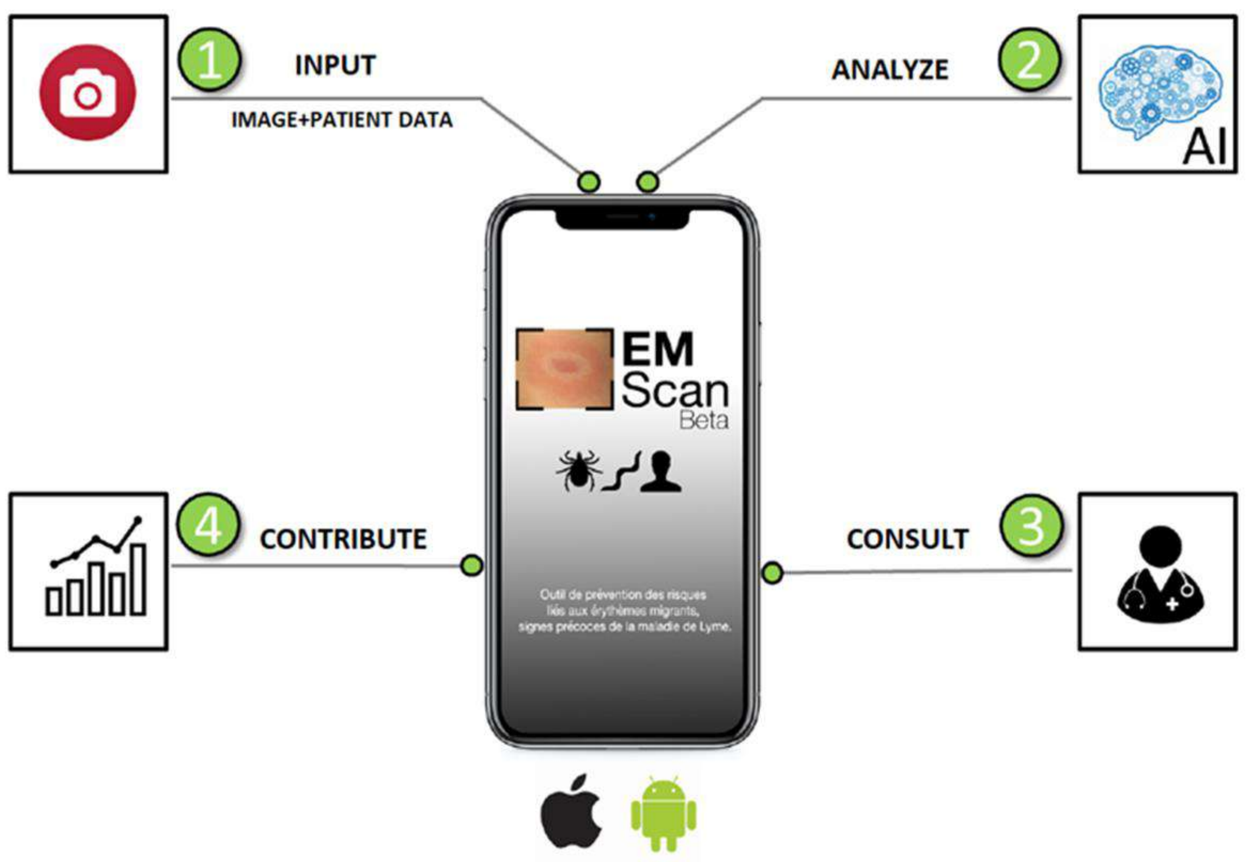

We are dealing with three research questions:
Q1: How to deal with the lack of a well-labeled publicly available dataset?
Q2: How to utilize patient metadata in the absence of enough training data?
Q3: How to efficiently deal with skin lesion hair?

Work Progress

1. We extensively analyzed the effectiveness of CNNs for diagnosing Lyme disease from images and to find out the best CNN architecture for the purpose. As there is no publicly available EM image dataset for Lyme disease predictions, we utilized an EM dataset created with the help of expert dermatologists and infectiologists from Clermont-Ferrand University Hospital Center. The study is published at [2].

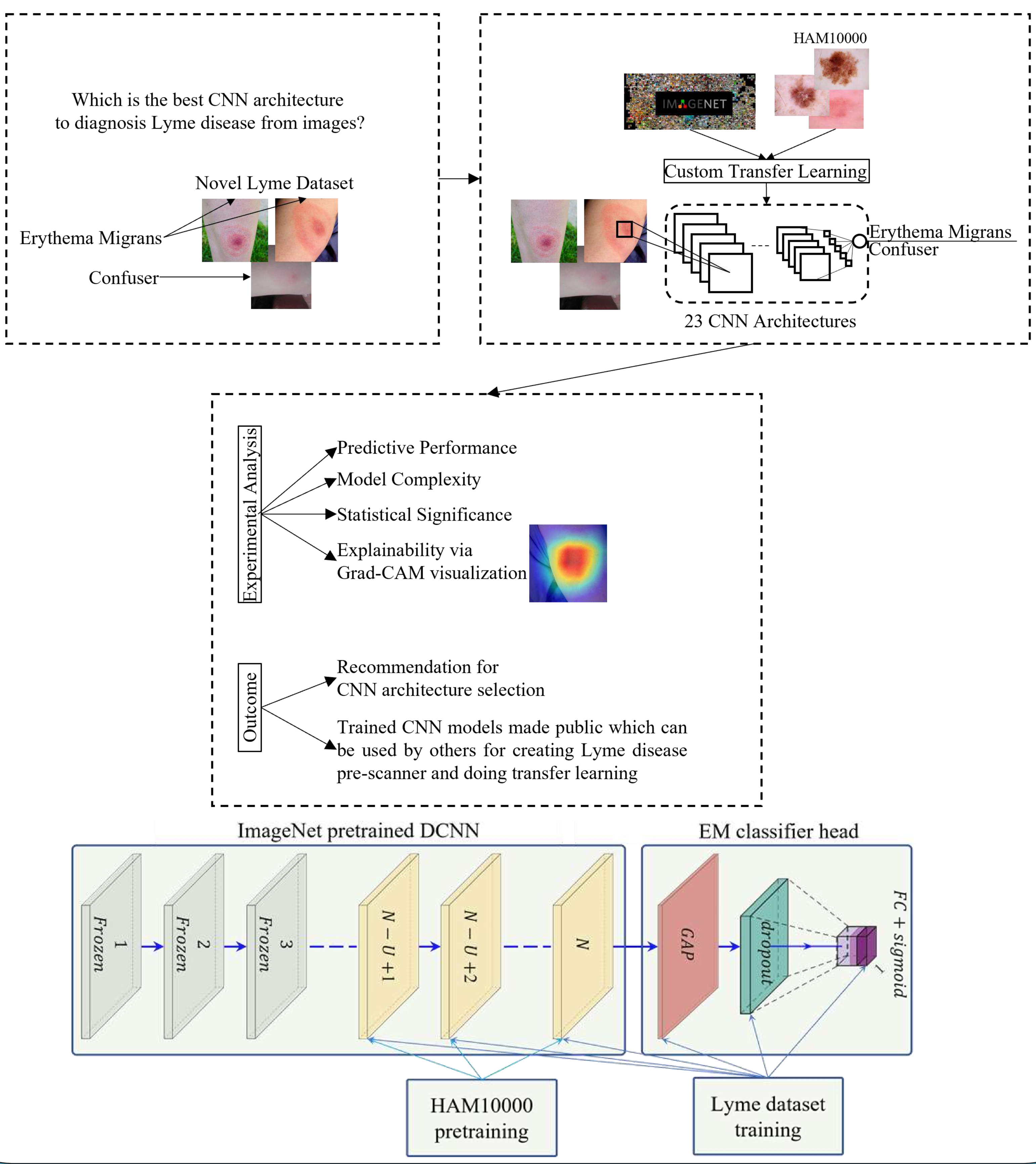

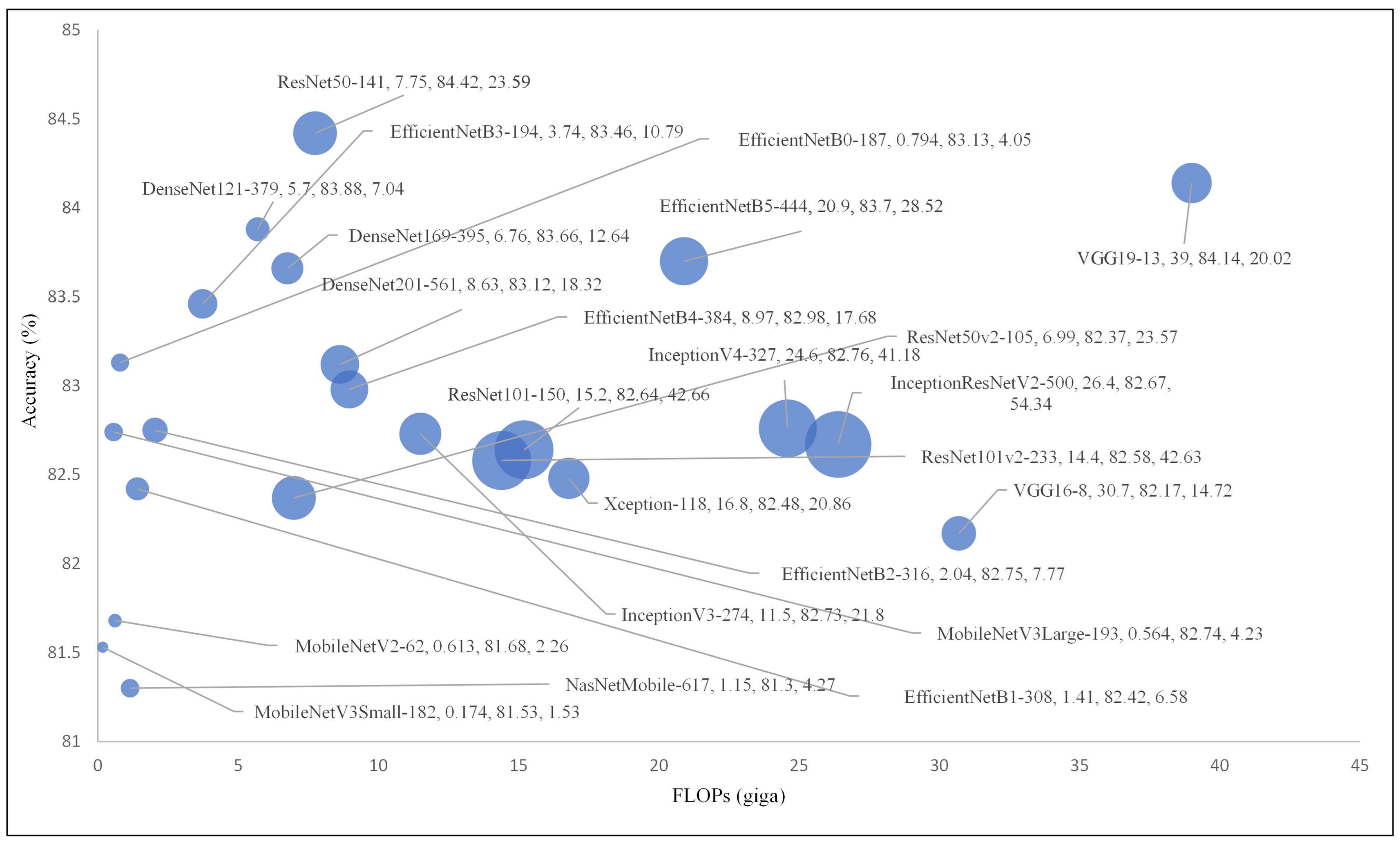

2. Existing works on Lyme disease prediction only utilize images of EM lesions whereas corresponding patient metadata can improve the predictive performance. We successfully elicited opinion form fifteen expert doctors to assist image based EM classifiers with additional patient metadata.

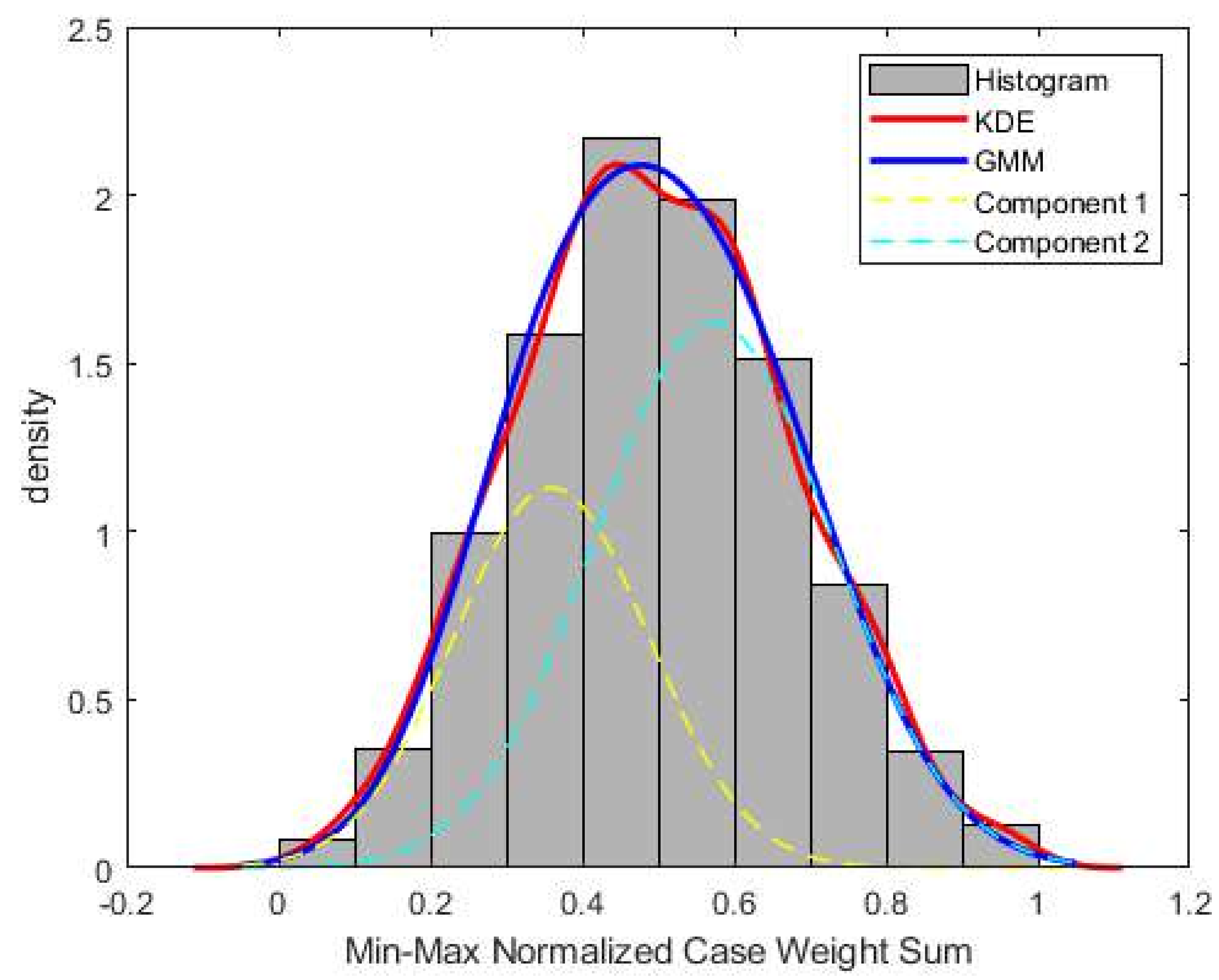

Research Plan

1. Standard image processing-based hair removal is not beneficial for real-time detection application and removing hair does not give new features to the network. So, augmenting images with skin hair can be of interest. Existing skin hair augmentation techniques require a hair mask to generate hair. These masks are created either manually, with random curves or lines and segmentation. Generative Adversarial Network can be utilized to automate the creation of hair masks.

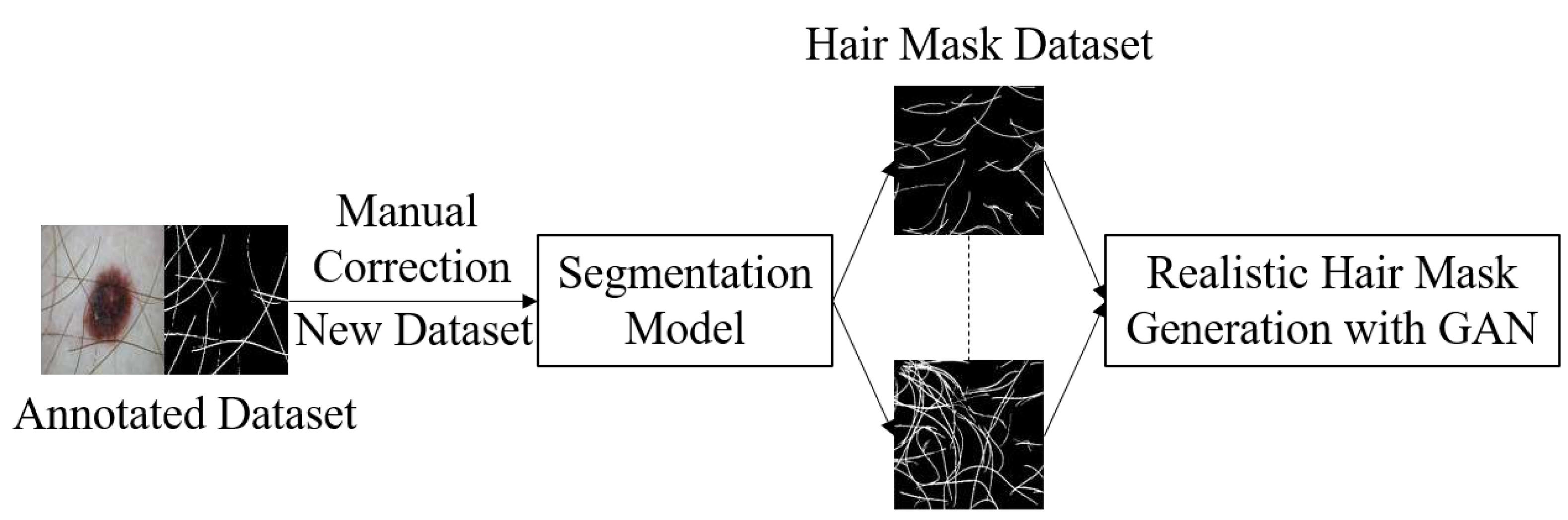

Bibliography

1. Isabelle Lebert, Jocelyn de Goër de Herve, Projet DAPPEM Développement d'une APPlication d'identification des Erythèmes Migrants. ⟨hal-02931682⟩
2. S. I. Hossain et al., "Exploring convolutional neural networks with transfer learning for diagnosing Lyme disease from skin lesion images," Comput. Methods Programs Biomed., vol. 215, p. 106624, Mar. 2022, doi: 10.1016/j.cmpb.2022.106624.

Acknowledgement: This research was funded by the European Regional Development Fund, project DAPPEM –AV0021029

Data quality evaluation

Ecole doctorale Sciences Pour l'Ingénieur

Roxane Jouseau, Sébastien Salva, Chafik Samir

Limos – Université Clermont Auvergne

Introduction

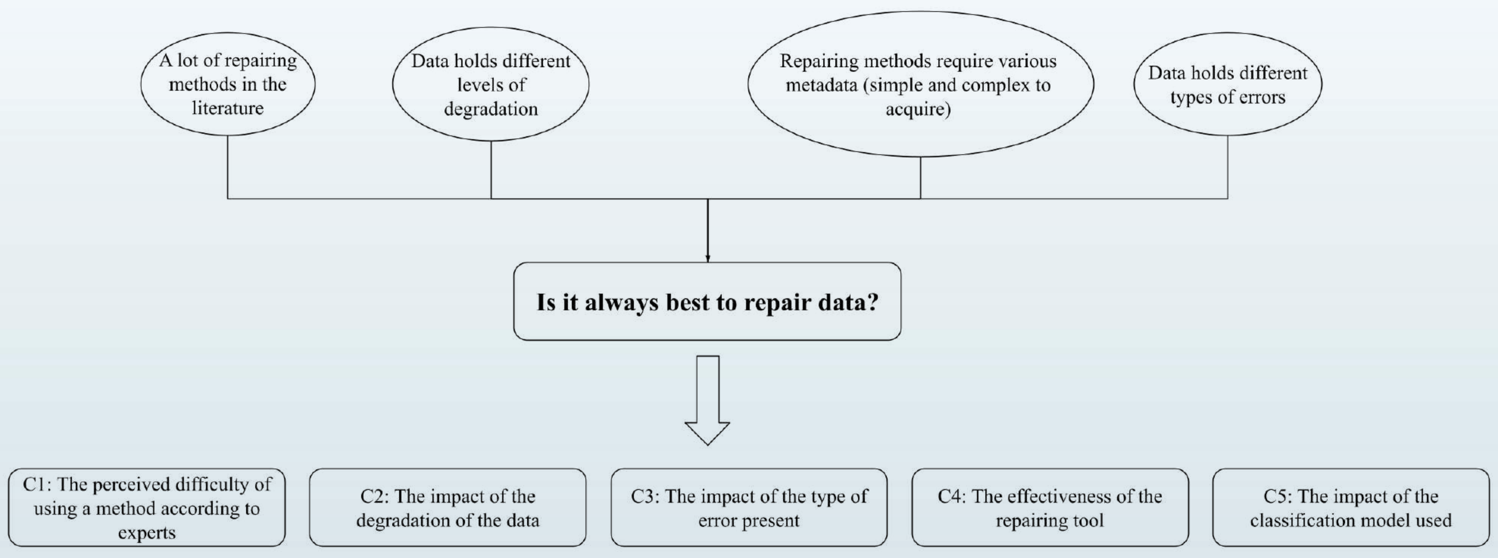

Figure 1. Research question and criteria of the study ([1], [2], [3])

The perceived difficulty of using repairing methods (C1)

We propose an evaluation process, that breaks down repairing methods into elementary tasks describing the actions executed to apply these methods, including creating the metadata needed. Given an error type, and a repairing method, we build a tree expressing the steps of the repairing method. For any other repairing method, we complete the tree when required.

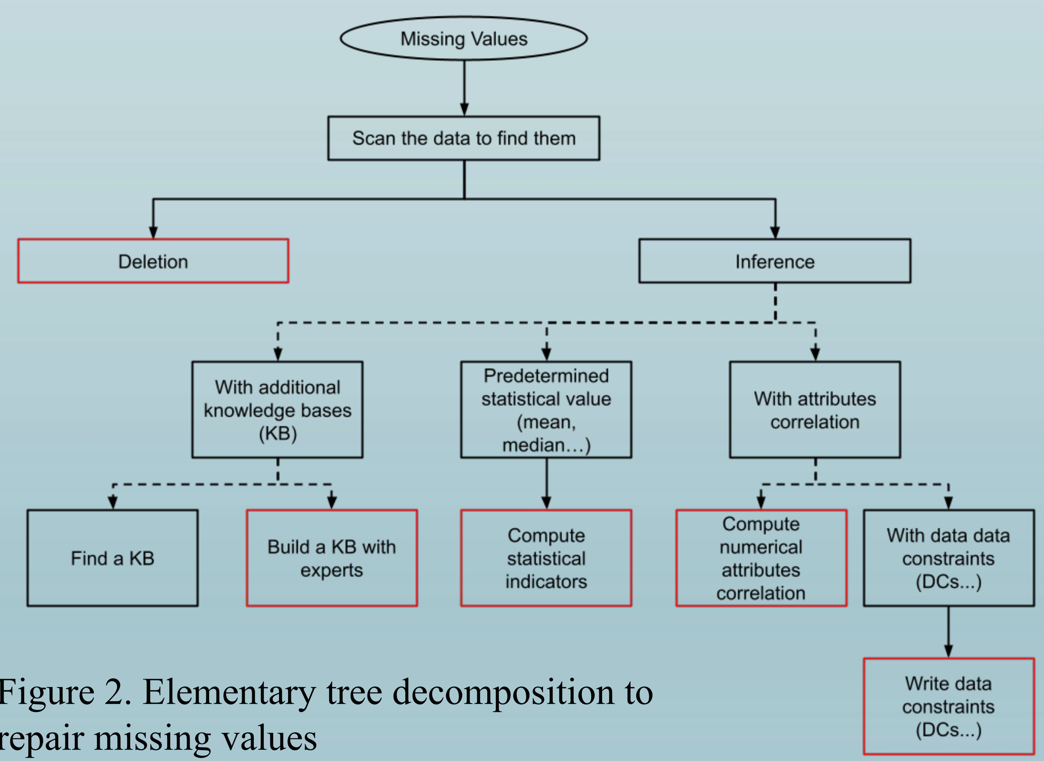

Figure 2. Elementary tree decomposition to repair missing values

The final nodes of the tree are elementary tasks. These elementary tasks are then evaluated by experts independently of the complete approaches. Figure 2 is the tree we built for the case of missing values. Additional trees were created for other types of errors such as duplicates, erroneous values, obsolete or irrelevant data attributes, pattern violations, miscodings, and outliers.

Delete the missing values	Impute using statistical indicators	Impute taking into account attribute correlation
1	1.89	1.89 + 1.75 = 3.64

Table 2. Difficulty evaluations of different methods for repairing missing values

To quantify the difficulty of each elementary task, we asked a panel of 8 industry data scientists to rank them on a four values scale: easy, medium, medium+, and hard. We registered the weighted average of each elementary task as its difficulty score Table 1. The weighting was 1, 2, 3, and 4 points for easy, medium, medium+, and hard. In Table 2 we show how these ratings can be used to evaluate the difficulty of different approaches used to repair missing values that we can find in Figure 2.

Elementary tasks	Estimated difficulty 1 (easy) to 4 (hard)
Compute statistical indicators	1.89
Delete data	1
Mining regexp	2
Mining data constraints	2.38
Write data conversion scripts	1.63
Compute attributes correlation	1.75
Write data harmonization scripts	2.44
Define similarity metrics	2.88
Data scientists check the data (for miscodings)	2.13
Write data format rules (regexp…)	2.44
Write data constraints (DCs…)	2.71
Build a knowledge base with experts	3.33
Set a threshold (for partial duplicates detection)	2.67
Write a probabilistic model	3
Define a metric (for outlier detection)	3.56

Table 1. Difficulty ratings of the elementary tasks of data repairing

The Experiment (C2 to C5)

In this experiment (summarized in Figure 3), we start by splitting the dataset into training and test. The test remains intact throughout the experience, while the training is subject to the modifications we describe below. We first inject the training dataset with one type of error at a percentage varying from 0 to 95% with increments of 5%. We apply each cleaning method to different copies of the deteriorated dataset to obtain cleaned datasets. We then use them to train several classification models. Finally, we compute the accuracy and f1-score on the test. We executed the complete process 30 times to reduce the bias for each percentage level.

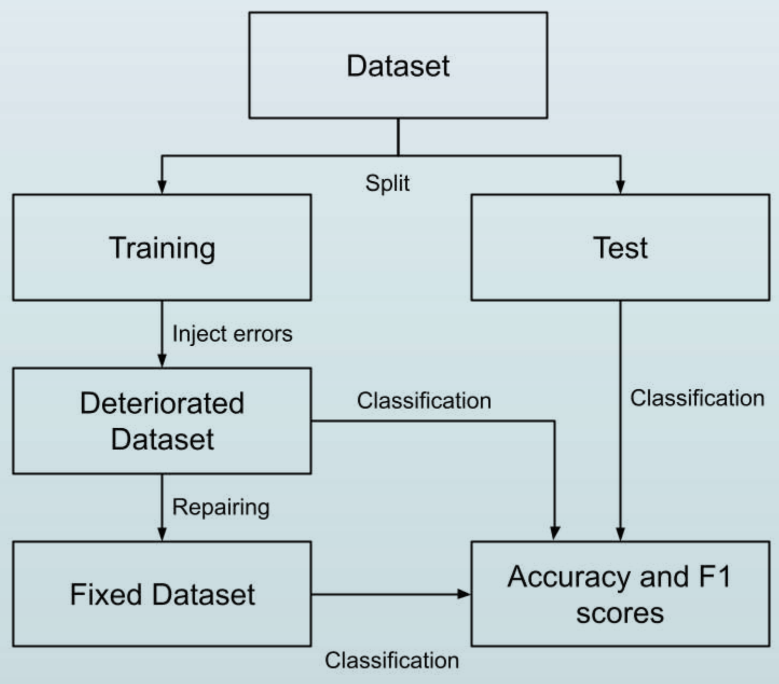

Figure 3. Structure of the experiment

We used 7 numerical datasets with various sizes, dimensions, and subjects: mnist, fashion-mnist, olivetti, iris, adult, breast cancer, and wine. We also have decided to include the following classification models: Logistic regression, K-Nearest Neighbors, Decision tree, Random forest, Ada boost, Naïve Bayes, XGboost, Support vector classification, Gaussian process, Multi-layer perceptron, Stochastic gradient descent, and Gradient boosting.

This protocol was conducted for the error types: missing values, domain value violations, exact duplicates, patrial duplicates, and outliers and to study the criteria C2, C3, C4, and C5 presented in Figure 1. We only present part of our results for C2 and C4 in this poster for space reasons. Figure 4 presents some of our experimental results for C2. It shows the mean accuracy obtained after repairing the data at different levels of degradation. Figure 5 showcases a part of our results for C4 with the mean accuracy for three different repairing methods as well as for the case where missing values were not repaired and just deleted.

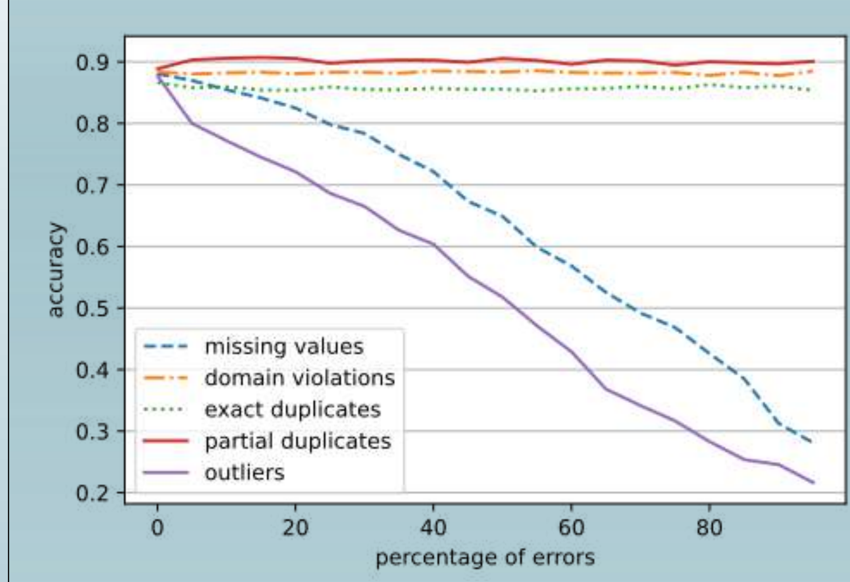

Figure 4. Accuracy after repairing by type of errors

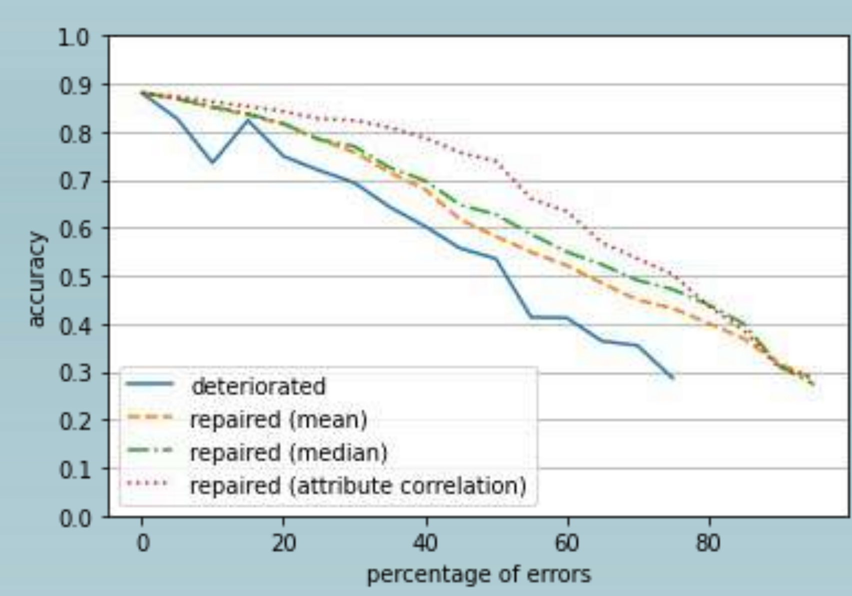

Figure 5. The example of missing values

Conclusions

In Figure 4 we identify 2 categories of error types: 1. the level of data degradation has little to no impact on the accuracy, and 2. the level of data degradation seems to have a big impact. For the case of missing values specifically, as we developed in figure 5 repairing data seems to be the best solution. Indeed, we can see that the repairing method with the overall best effectiveness is the one with the highest evaluated difficulty of the three. However, the three methods have similar effectiveness around 10% (and under) of missing values. This is a case where the difficulty evaluation of a method is particularly interesting since we can use a method with a lower difficulty score to achieve similar results. We can also identify a point around 80% of missing values where all the repairing methods perform equivalently poorly.
Extensions to other tasks are a possibility for future work as well as including more data types than numeric, especially more complex data types such as time series, which would imply more possible error types.

Bibliography

1. **Peng Li, Xi Rao, Jennifer Blase, Yue Zhang, Xu Chu, and Ce Zhang. Cleanml: A study for evaluating the impact of data cleaning on ml classification tasks. 36th IEEE International Conference on Data Engineering (ICDE 2020) (virtual), 2021.**
2. **C. BATINI, C. CAPPIELLO, C. FRANCALANCI, and A. MAURINO, "Methodologies for Data Quality Assessment and Improvement," *ACM Computing Surveys*, vol. 41, no. 3, p. article 16, Jul. 2009, doi: 10.1145/1541880.1541883.**
3. **Ziawasch Abedjan, Xu Chu, Dong Deng, Raul Castro Fernandez, Ihab F. Ilyas, Mourad Ouzzani, Paolo Papotti, Michael Stonebraker, and Nan Tang. Detecting data errors: Where are we and what needs to be done? Proceedings of the VLDB Endowment, 9(12):993–1004, 2016.**

Dynamic Wireless Charging System

Mincui LIANG, Khalil EL KHAMLICHI DRISSI, Christophe PASQUIER

Université Clermont Auvergne, Clermont Auvergne INP, CNRS, Institute Pascal

Objectives

1. to review resonance converters topology.
2. to review control strategies and identify the research gap in resonant converter control.
3. to propose a robust control strategy to achieve maximum power transmission with high tolerance for misalignment.

Introduction

Under the pressure of climate change and global warming, Electric Vehicles (EVs), as the most mature zero-emission vehicle technology, are developing accelerated. One of the limitations of EVs is the battery. However, Dynamic Wireless Charging System (DWCS) can solve the problem of battery dependence of the EVs by wireless charging the battery of the EVs when the EVs are driving to reduce the size of the battery. It used resonance technology to maximize the power transfer with high efficiency to achieve long-distance and various misalignment charging wireless. This research is focus on the control of the power electronic to apply for all kinds of resonance DWCS. The main reason why resonance DWCS is difficult to control, is that sensitive parameters are not fixed since the lateral and vertical displacements of EVs are changing.

Simulation

To address the difficulties of the resonance DWCS, it is necessary to simulate the developed control strategy before apply in real situation. The control should be fast transient responses, avoid voltage and current overshooting and transmit maximum power regardless of misalignment. The initial result of the control is shown in Figure 2. Figure 1 presents the system response in natural frequency without control. Moreover, Figure 2 presents the result with optimal control, and it can achieve our control goals.

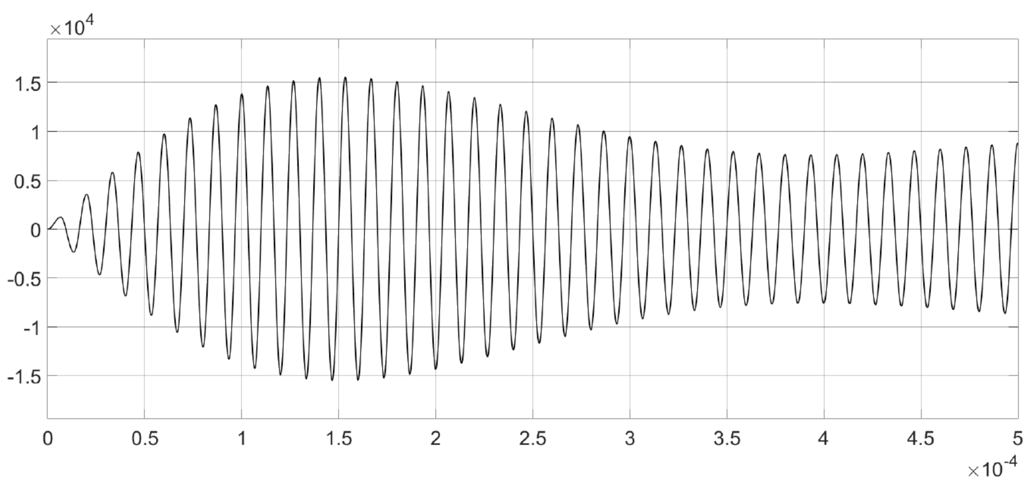

Figure 1:System response in natural frequency

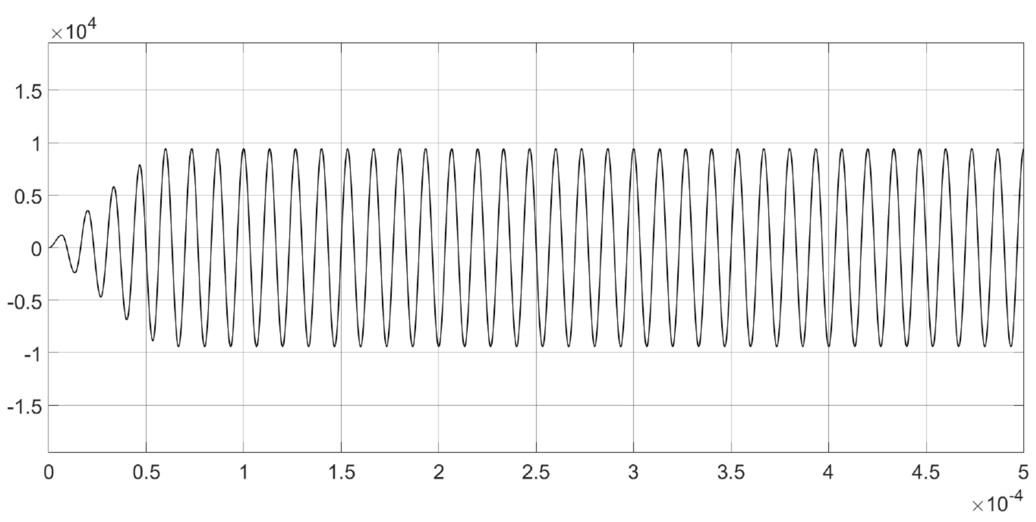

Figure 2:System response with optimal control

Experiment

After simulation, it is important to validate the theoretical and simulation results by conducting experiment. The FABRIC project [1] has conducted the experiment on a test road shown in Figure 3.

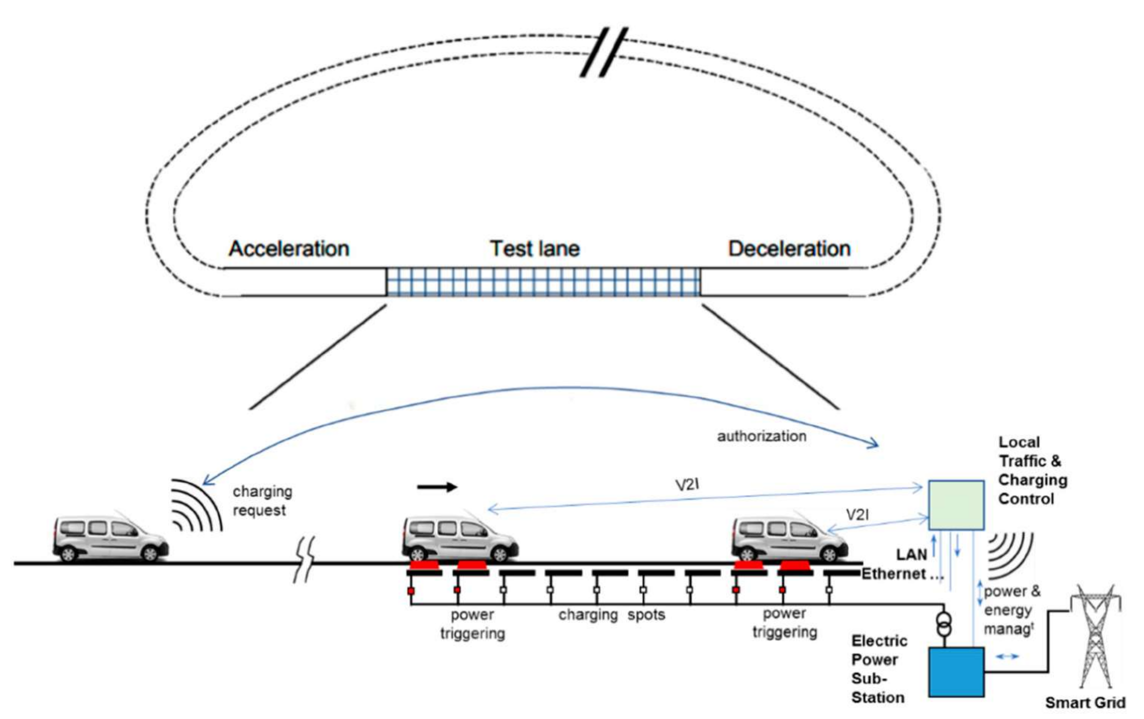

Figure 3:The FABRIC project demonstration

Theoretical model

In this section, a theoretical model of the SS-WPT shown in Figure 4 is thoroughly presented in order to understand how different parameters correlate and affect the system performances.

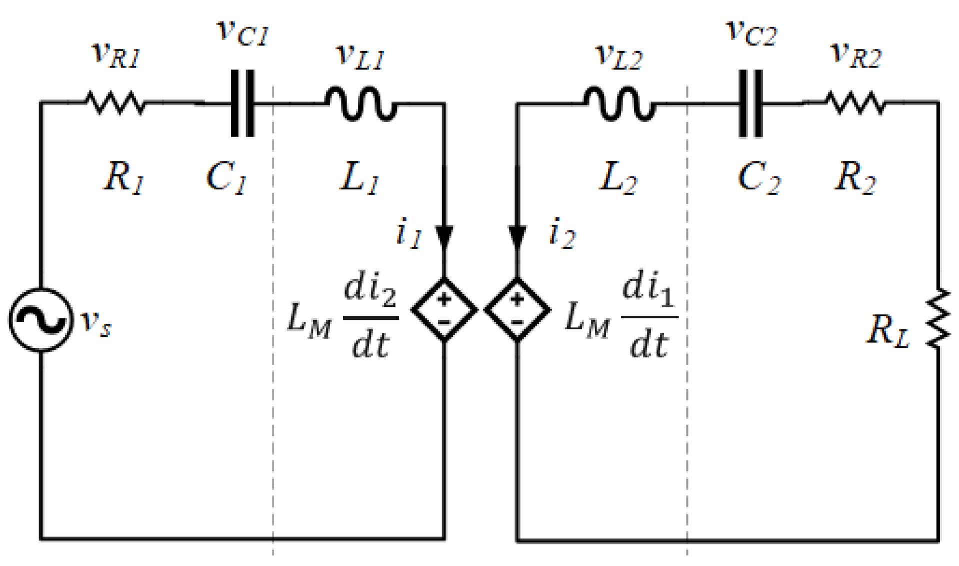

Figure 4:SS-WPT equivalent circuit

The mathematical relationship in time domain is given below in 1.

$$\begin{cases} v_s = v_{C1} + R_1 i_1 + v_{L1} + L_M \frac{di_2}{dt} \\ 0 = v_{C2} + (R_2 + R_L) i_2 + v_{L2} + L_M \frac{di_1}{dt} \\ i_1 = C_1 \frac{dv_{C1}}{dt} \\ i_2 = C_2 \frac{dv_{C2}}{dt} \end{cases} \tag{1}$$

Results: Figure

Figure 5 is the initial result of my project, and it shows that our theoretical results matches our simulation results very well.

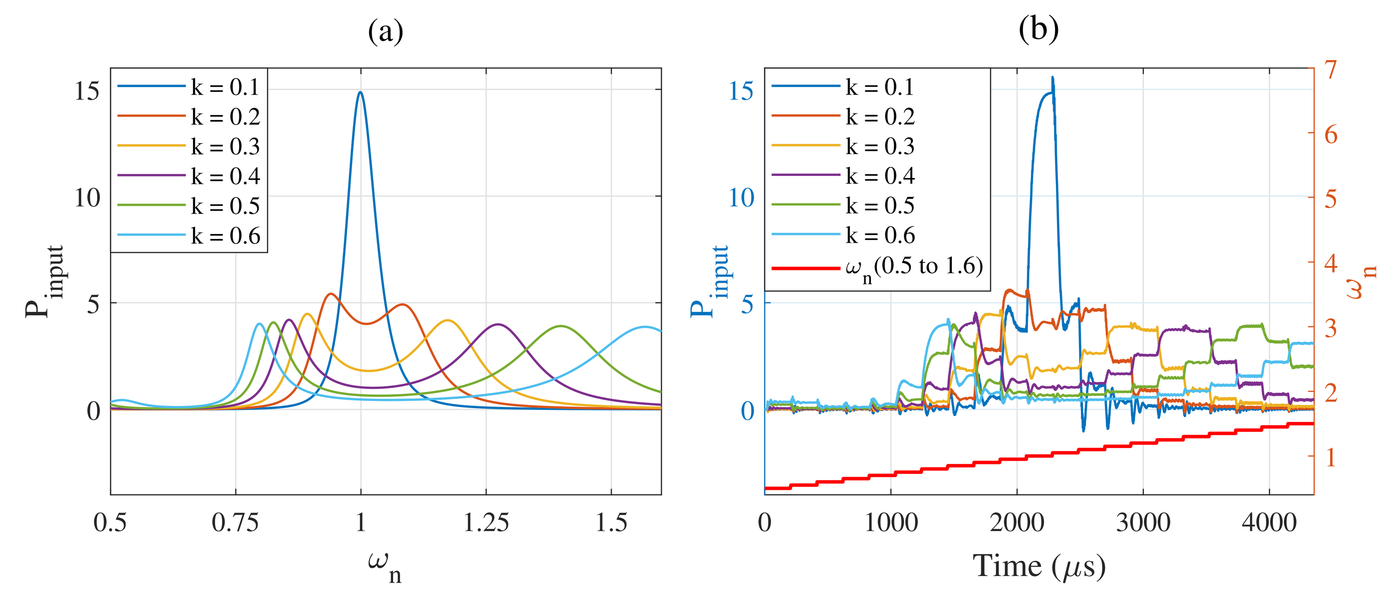

Figure 5:Result comparison: (a) Theoretical results; (b) Simulation results

Conclusion

This paper reviews briefly the DWCS system. It proposed a robust but simple controller to achieve maximum power transfer for different misalignment conditions and load variation situations without overshooting problem, with fast transient response feature. In the future, we will propose an experimental setup to evaluate the efficiency of our method and to apply this technique to multi-coil DWPT converters and adapt it to bi-directional WPT for Vehicle to Grid (V2G) applications.

References

[1] S. Laporte, G. Coquery, V. Deniau, A. De Bernardinis, and N. Hautière, "Dynamic Wireless Power Transfer Charging Infrastructure for Future EVs: From Experimental Track to Real Circulated Roads Demonstrations," World Electric Vehicle Journal, vol. 10, no. 4, p. 84, Nov. 2019, doi: 10.3390/wevj10040084.

Acknowledgments

This work was sponsored by a public grant overseen by the French National Research Agency as part of the "Investissements d'Avenir" through the IMobS3 Laboratory of Excellence (ANR-10-LABX-0016) and the IDEX-ISITE initiative CAP 20-25 (ANR-16-IDEX-0001).

Contact Information

- Web: https://fr.linkedin.com/in/mincui-liang
- Email: mincui.liang@uca.fr
- Phone: +33(0)663253433

Models and Algorithms for the Mangement of New Urban and Rural Mobility Services

Ecole doctorale Sciences Pour l'Ingénieur

Chijia LIU

D. FEILLET, A. QUILLIOT, H. TOUSSAINT

LIMOS, Université Clermont Auvergne

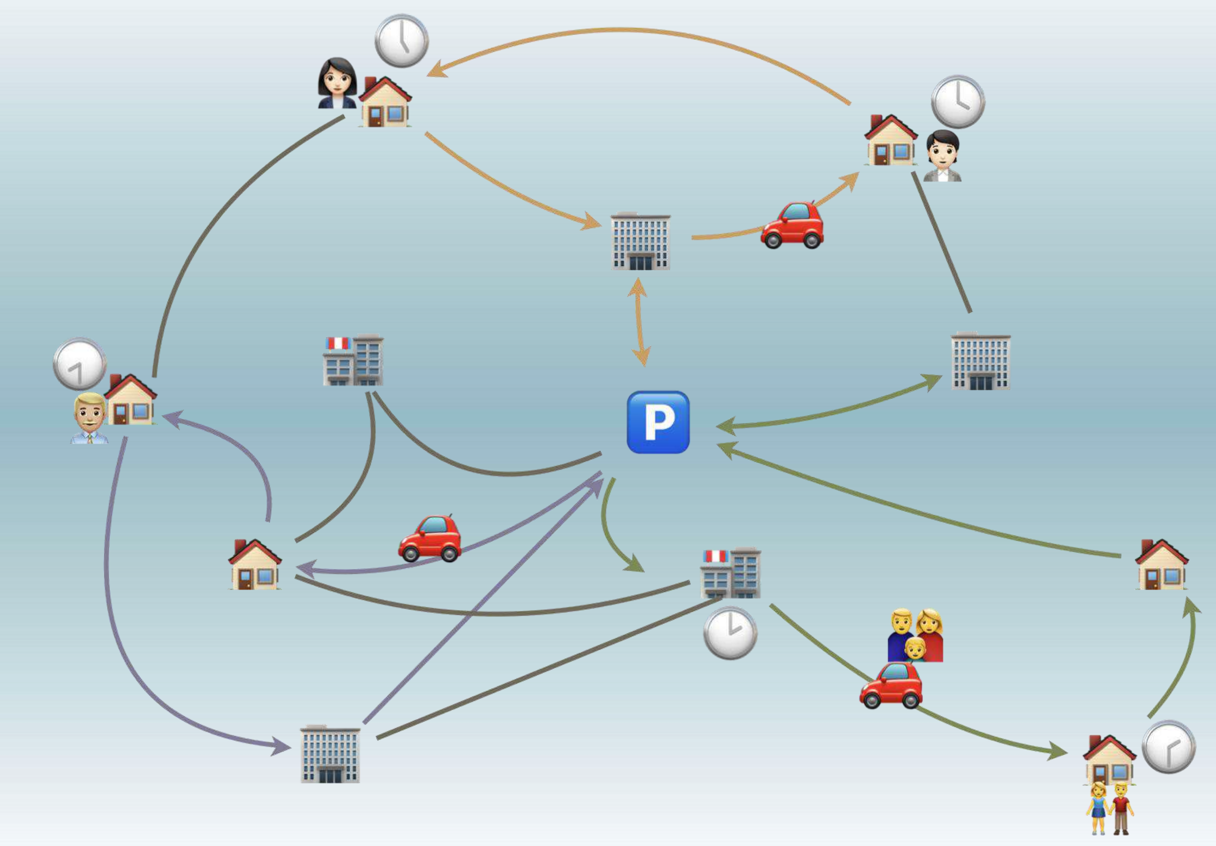

Objective

We aim to solve **a large-scale dynamic SAV** (Shared Autonomous Vehicle) **DARP** (Dial-A-Ride-Problem), where the system has to process a large number of passenger requests (at least 10,000) on-the-fly.

Therefore, one of the main objectives is to speed up the dispatching and scheduling process as much as possible while maintaining a good decision quality. For this, we have to introduce different techniques:

- The use of fleet filters in order to identify quickly a small subset of SAVs that are worth to be explored given a passenger reqeust;
- The use of insertion position filters in order to identify quickly a small subset of insertion points that are worth to be tested given a candidate SAV;
- An auxiliary model that helps to predict the possible requests and insertions by analyzing historical data.

Insertion process

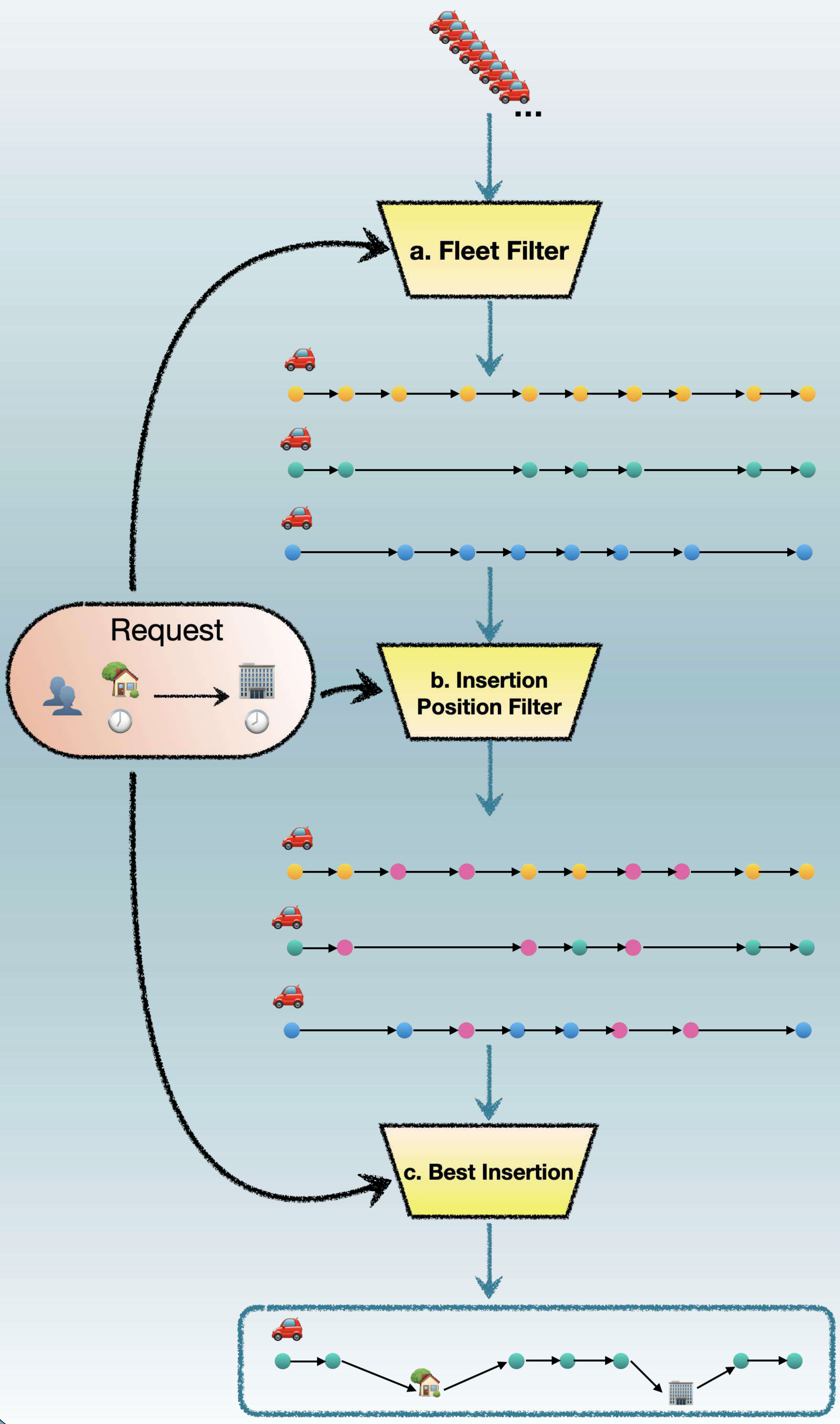

a. Screening Process

We introduce a screening process using two structures, which serves as a fleet filter that can provide us with a small subset of candidate SAVs very quickly. Both two structures, F and F^{idle}, are constructed and updated thanks to the spatial and temporal partition. F records the approximate schedules of the vehicle fleet, while F^{idle} records when and where the SAVs are "approximately" impossible to be tracked. Generally speaking, the screening process consists of identifying the vehicles scheduled to pass the zones during the periods related to the target request.

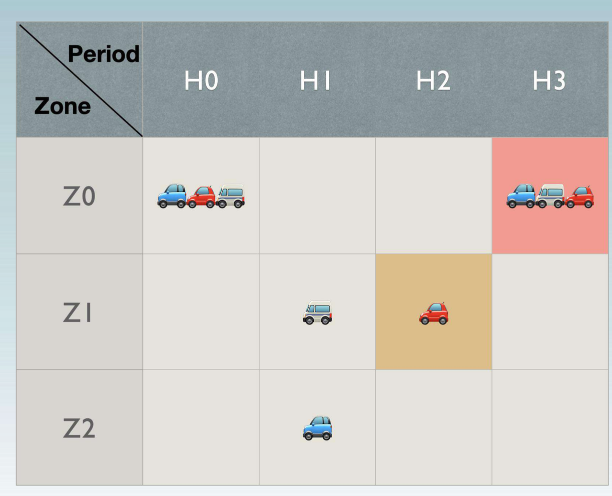

a.1 The zone-period matrix F

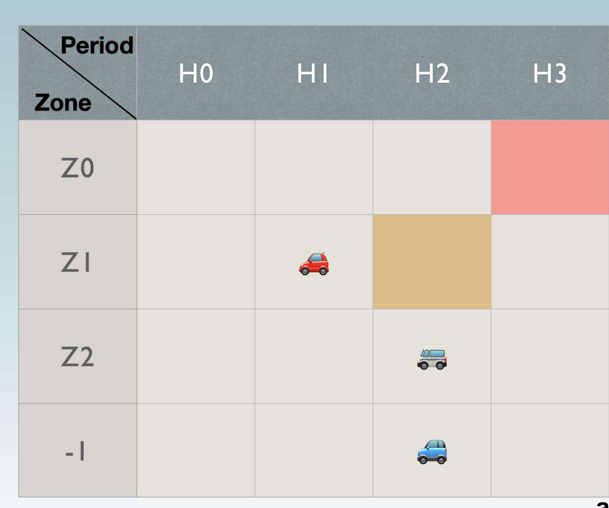

a.2 The complementary matrix F^{idle}

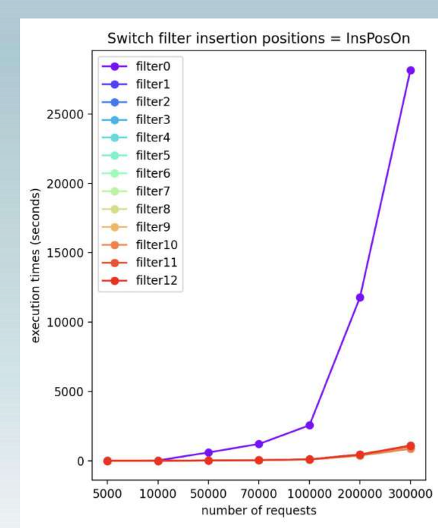

a.3 Execution time while using different combination of filters. (filter0 means no filter applied)

b. Insertion Position Filter

Given a candidate SAV with an indicator pointing to the first possible insertion position (which is also given by the step a.), the corresponding filter quickly selects a subset of points from the route of the SAV where the request is more likely to be successfully inserted. Essentially, we use the following creterion to quickly verify if from the current candidate position, it can arrive at the required position. ($t(z(v[p], z(X))$is the pre-calculated inter-zone travel time.)

$$v[p].dE + t(z(v[p], z(X))) \leqslant X.twL$$

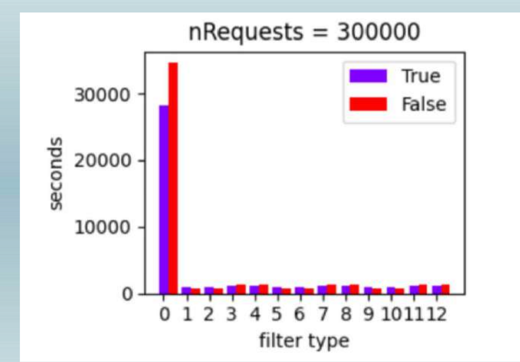

b.1 Execution time while using different combination of fleet filters. (True: using the insertion position filter; False: not using the insertion position filter)

c. Flexible Insertion

To insert the **origin** r.O at the position i:
- Feasibility check
  - load check
  - v can arrive at r.O on time from i
  - v can arrive at i+1 on time from r.O
- Update the loads and time windows

To insert the **destination** r.D at the position j:
- Feasibility check
  - load check
  - v can arrive at r.D on time from j
  - v can arrive at j+1 on time from r.D
  - the ride-time is less than the request's maximum ride-time
- Update the loads and time windows

Future works

- An auxiliary model that analyses massive historical data using learning techniques, in order to help speeding up further the dispatching and scheduling process.
- Management of congestion.
- Management of SAVs' batteries.

Bibliography

- Daniel J. Fagnant and Kara M. Kockelman. *Dynamic ride-sharing and fleet sizing for a system of shared autonomous vehicles in Austin, Texas.* Transportation, 45(1):143–158, January 2018.
- Michael W. Levin. *Congestion-aware system optimal route choice for shared au tonomous vehicles.* Transportation Research Part C: Emerging Technologies, 82:229–247, September 2017.
- Shuo Ma, Yu Zheng, and O. Wolfson. *T-share: A large-scale dynamic taxi ridesharing service.* In 2013 IEEE 29th International Conference on Data Engineering (ICDE), pages 410–421, Bris bane, QLD, April 2013.

École Doctorale des Sciences pour l'Ingénieur

SAMBA
Secure Federated Multi-Armed Bandits

Radu Ciucanu[1], Pascal Lafourcade[2], **Gael Marcadet**[2], Marta Soare[1]
Université Grenoble-Alpes, LIG (first.last@uga.fr)[1] Université Clermont-Auvergne, LIMOS (first.last@uca.fr)[2]

Secure Federated Multi-Armed Bandits

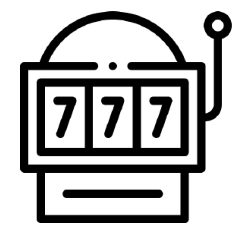

SAMBA enjoys the following properties:
- Multi-armed bandits in a Federated Learning setting.
- Confidentiality of data.
- Generic Framework.
- Small reasonable execution time overhead.

Federated Learning

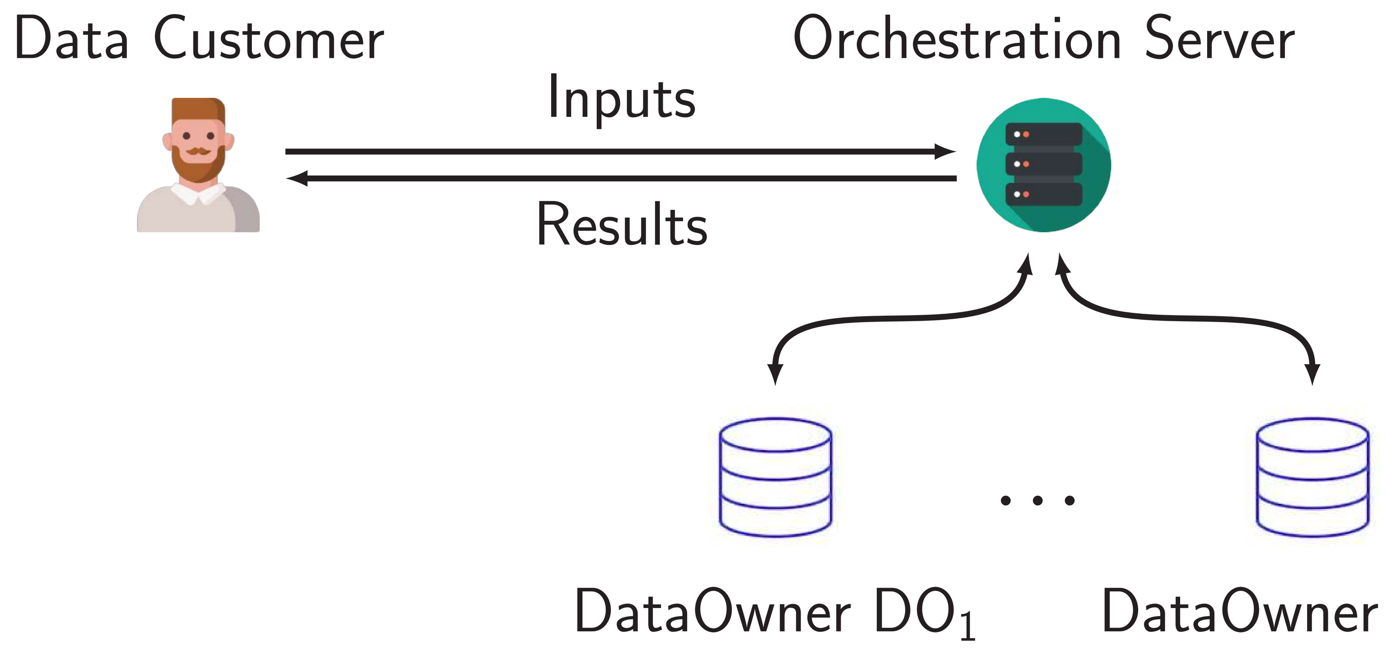

Multi-Armed Bandits

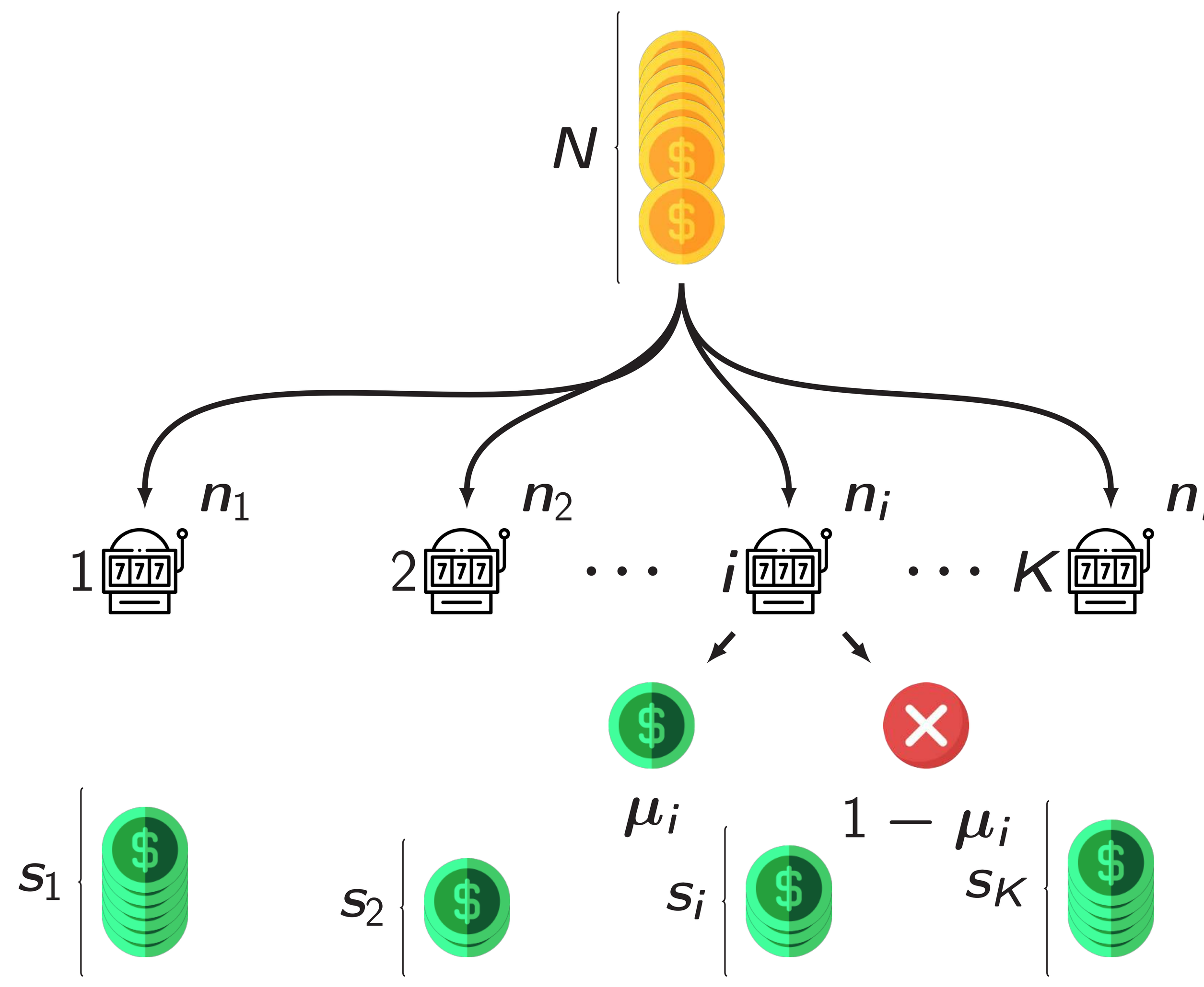

Vaccine Application

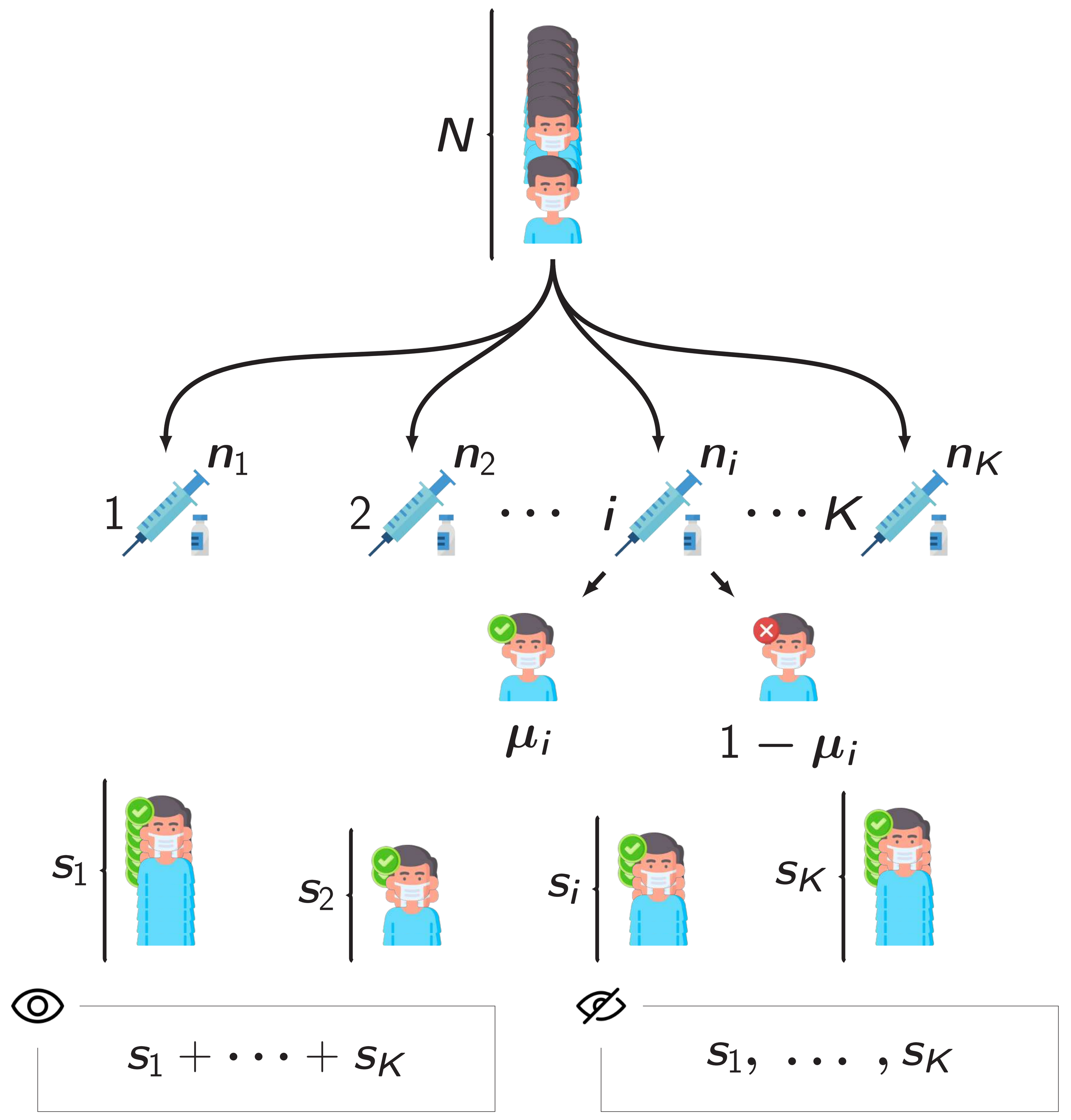

Symmetric Encryption Scheme (AES)

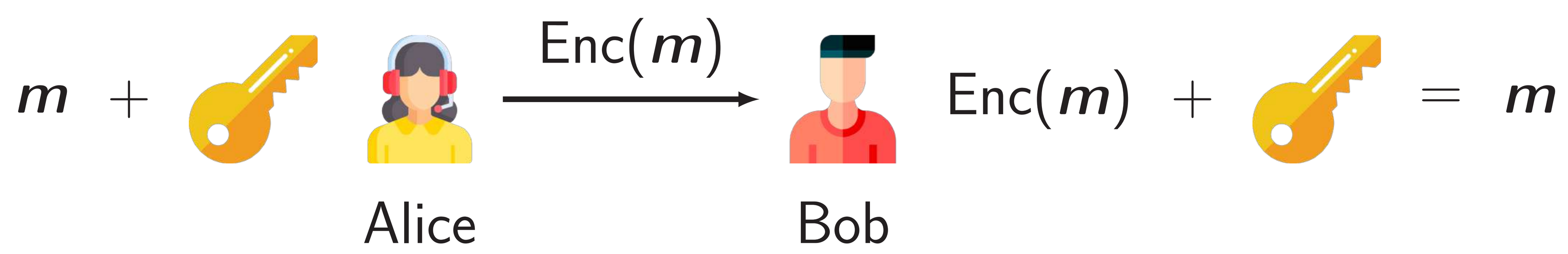

Asymmetric Encryption Scheme (Paillier Cryptosystem)

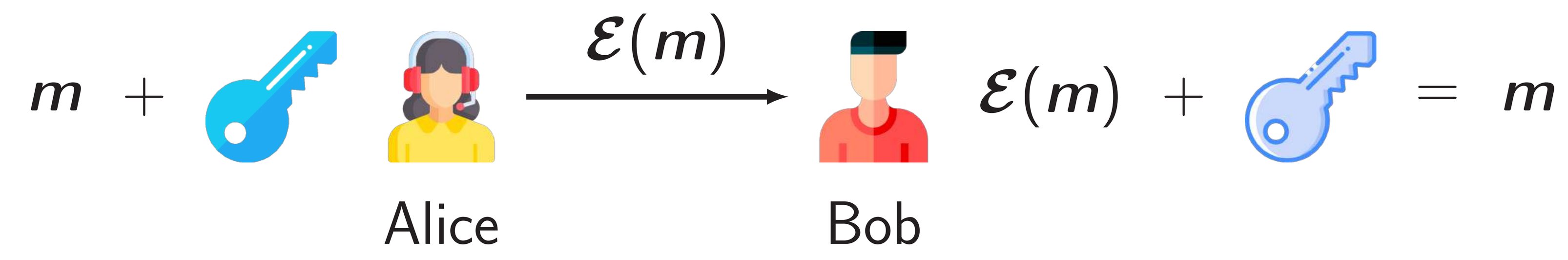

$$\forall a, b \in \mathbb{Z}, \mathcal{E}(a) \cdot \mathcal{E}(b) = \mathcal{E}(a+b)$$

SAMBA

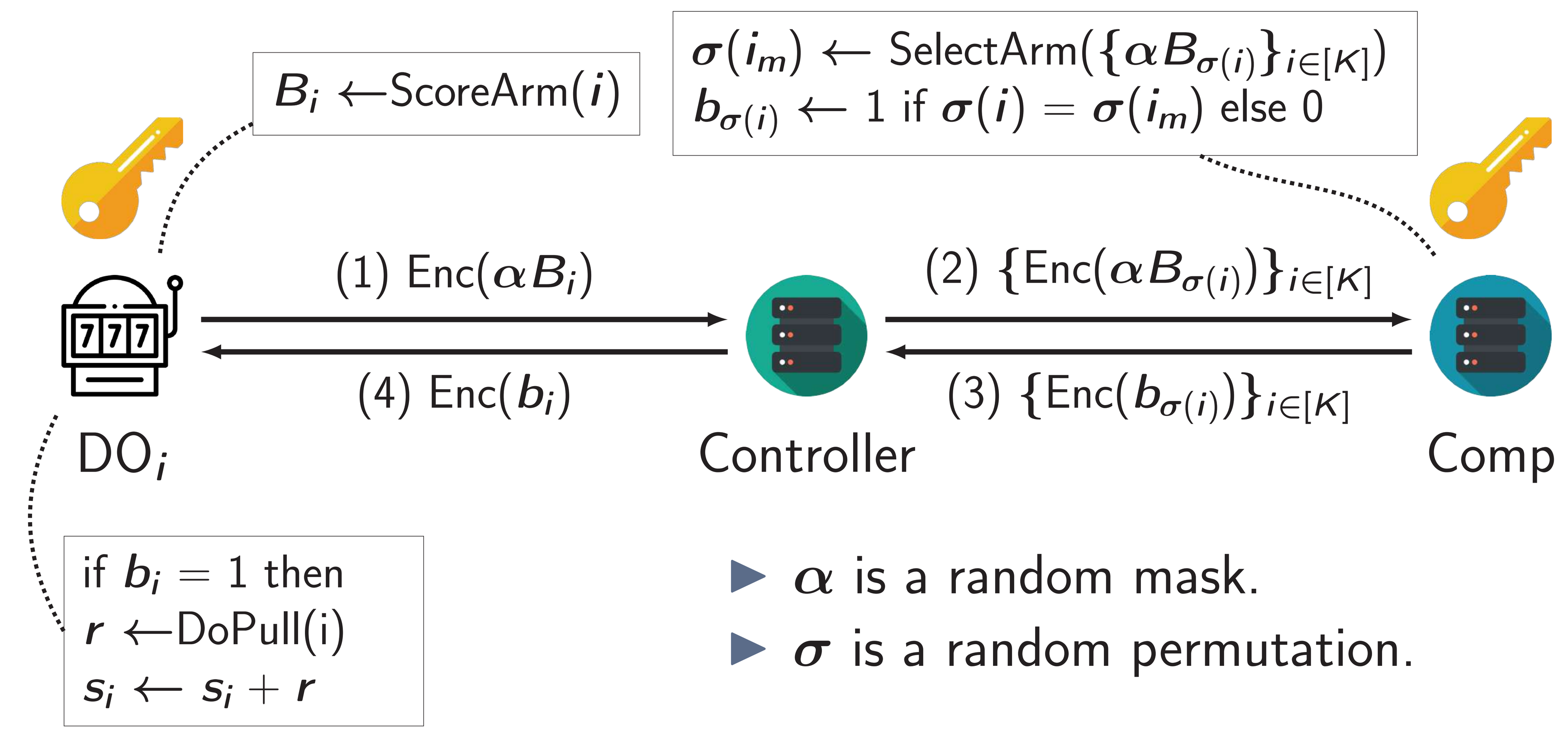

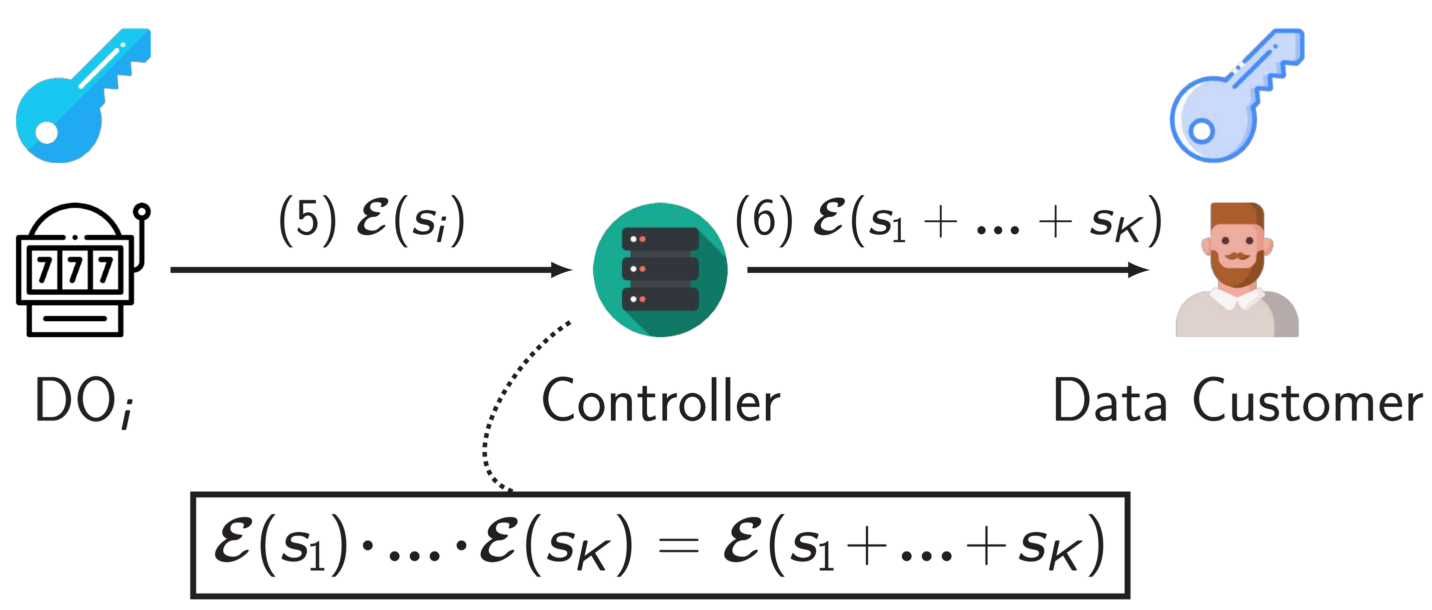

Genericity

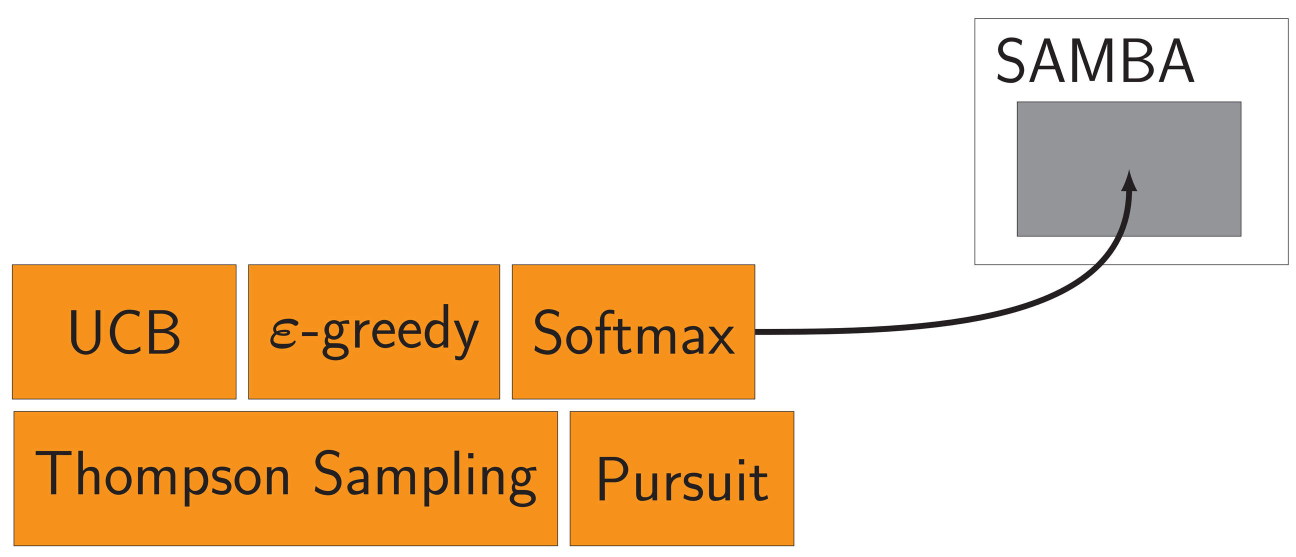

Efficiency

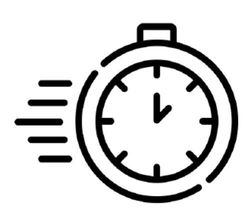

- $O(NK)$ AES Operations
- $O(K)$ Paillier Operations

Security

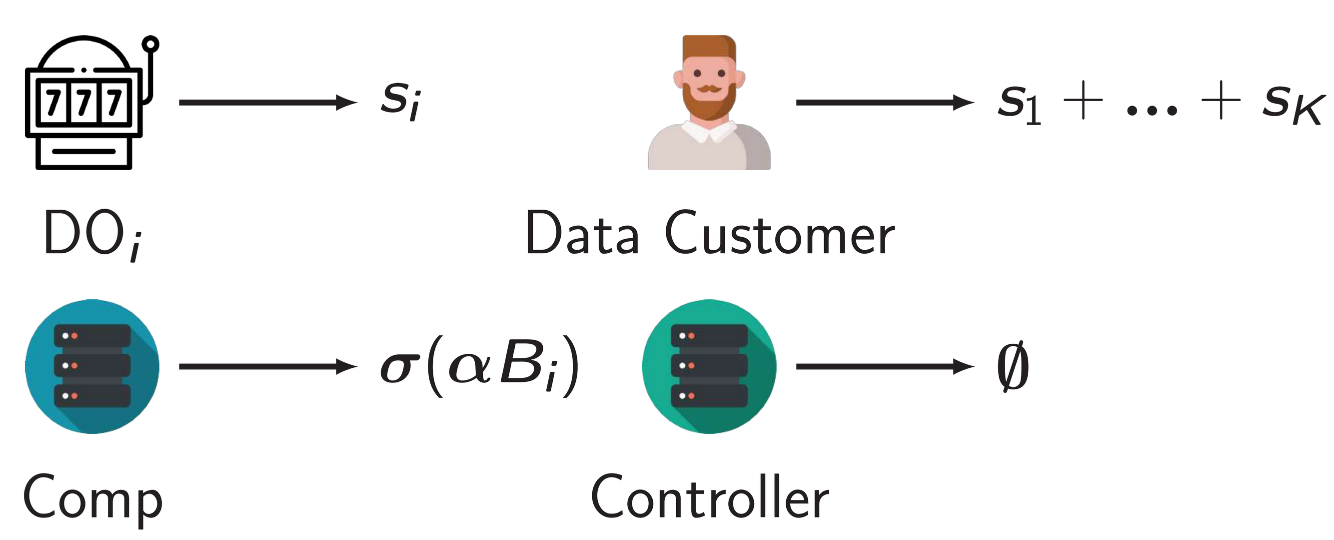

Résolution des problèmes de transport et de gestion de stock à l'aide de l'Intelligence Artificielle

Diego Perdigão Martino[1,2], Philippe Lacomme[1], Katyanne Farias de Araújo[1], Manuel Iori[3]

[1] Laboratoire d'Informatique, de Modélisation et d'Optimisation des Systèmes, Campus des Cézeaux, 63177
[2] Ecole Doctorale des Sciences pour l'Ingénieur
[3] Università degli Studi di Modena e Reggio Emilia, DISMI

INVENTORY ROUTING PROBLEM

L'*Inventory Routing Problem* (IRP) est défini comme un problème de routage de véhicules et de gestion de stock multi périodes. L'objectif est d'attendre les demandes des clients à un coût minimum de transport et stock en définissant des routes qui partent et reviennent au dépôt et les quantités à livrer [1].

Soit C l'ensemble des clients, F le fournisseur ($F = \{0\}$), $C' = C \cup F$, P l'horizon discret de temps et V l'ensemble de véhicules disponibles par période $p \in P$. Chaque client $c \in C$ possède, par période, des demandes d_{cp}, un niveau initial s_{c0}, un niveau minimal s_{min_c} et maximal s_{max_c} de stock qui doivent être respectés, ainsi qu'un coût unitaire de stockage $cout_c$ par période.

L'emplacement des clients et du fournisseur est défini par les coordonnées $[x; y]$ et les distances entre chaque pair de points (i, j) avec $i, j \in C'$ et $i \neq j$ sont considérées Euclidiennes. Le fournisseur dispose d'un stock initial s_{00}, d'un coût unitaire de stockage $cout_0$ par période de temps, ainsi qu'une capacité de production $prod_p$ par période. Un nombre V de véhicules est disponible par période et chaque véhicule possède une capacité cap de transport.

La figure 1 représente une solution pour le problème avec 10 clients, 3 périodes et 4 véhicules par période. Chaque tournée planifiée au sein d'une période possède on coût qui est déterminé par la distance totale parcourue par le véhicule ainsi que les coûts impliqués sur le stock vu la possibilité d'anticiper les demandes des clients à des périodes précédentes.

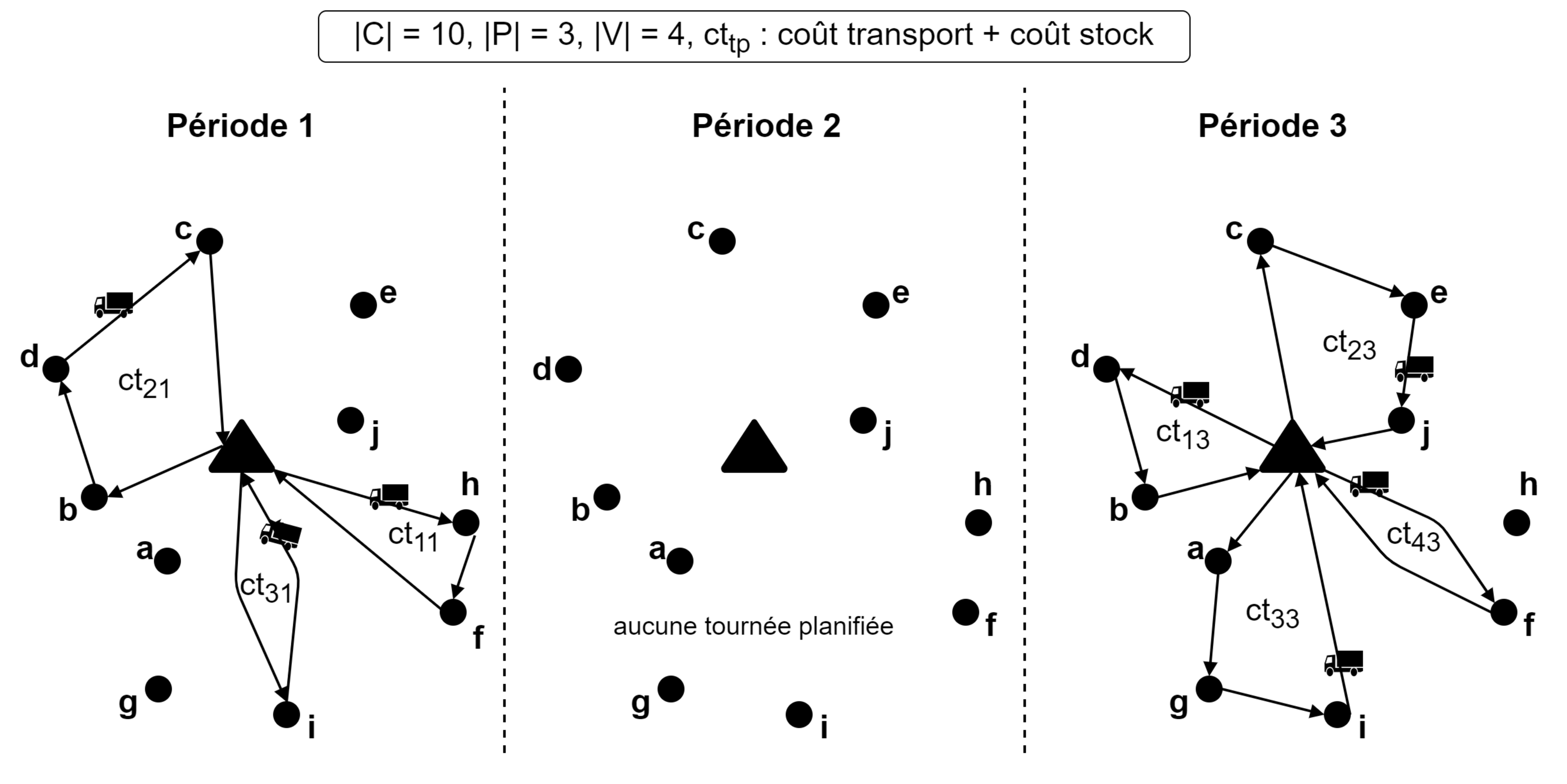

Figure 1: *Exemple de solution pour l'IRP*

OBJECTIFS

Dans le cadre de la thèse, l'objectif est de développer des algorithmes approchés (programmation dynamique, métaheuristiques), exactes (programmation linéaire) et hybrides (matheuristiques) pour résoudre l'IRP. Les méthodes proposées seront combinées à des techniques de l'intelligence artificielle pour résoudre de façon efficace les instances de la littérature, ainsi que des nouvelles instances plus réalistes à être proposées qui tiennent compte des véhicules hétérogènes, demandes et coûts variables et du dimensionnement des produits.

ALGORITME PROGRAMMATION DYNAMIQUE

Plusieurs méthodes ont été déjà proposées pour résoudre le problème [1, 2, 3, 5]. Cependant, nous avons proposé un nouvel algorithme à l'aide de la programmation dynamique efficace pour créer des solutions réalisables pour l'IRP. Sachant $\mathcal{S}_P = \{1, 2, ..., P\}$ l'espace de temps, $\mathcal{S}_\mathcal{E}$ l'espace d'états dont $|\mathcal{S}_\mathcal{E}| = N \times L$ avec N nœuds et L labels autorisées par nœud et $\mathcal{S}_D = ajouter(\{s_{1n}, s_{2n}, ..., s_{Ln}\}, s_{ln})$ l'espace de décision qui consiste à définir si un label candidat s_{ln} sera ou non ajouté dans le graphe selon les contraintes de visitation, niveaux de stock, capacité des véhicules ainsi qu'une règle de dominance qui consiste à déterminer si s_{ln} est dominé ou domine l'un des labels existants.

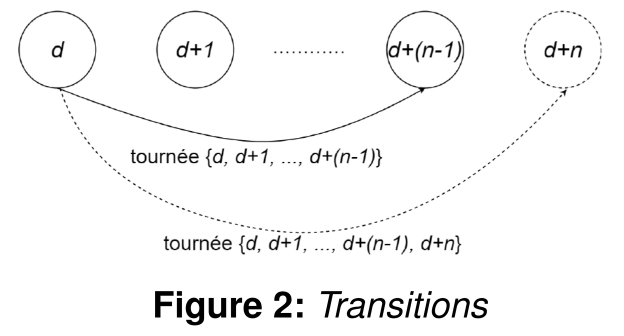

Figure 2: *Transitions*

Les transitions comprennent les coûts de transport et de stock des arcs entrants. Les coûts de transport sont exprimés par la distance Euclidienne $dist_{ij}$ entre deux points (i, j), où $i, j \in C'$ et $i \neq j$. Les coûts de stock dépendent de la quantité à livrer et les coûts de stockage chez les clients et le fournisseur.

Nous considérons également la possibilité d'insertion des labels dans les périodes précédentes afin de tester d'autres possibilités dont l'anticipation de la demande de la tournée concernée qui pourra éventuellement réduire le coût total de la solution.

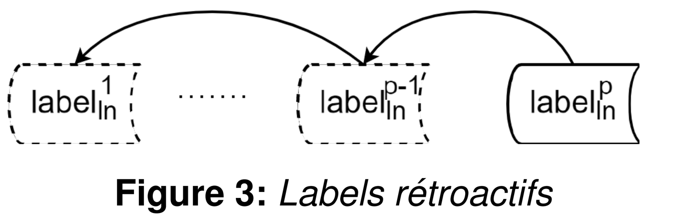

Figure 3: *Labels rétroactifs*

L'algorithme proposé est composé de deux étapes dont la première consiste à créer et ajouter des labels aux nœuds du graphe selon un parcours *forward* et la seconde à la définition du chemin critique grâce à un parcours *backward* en partant du label le moins coûteux sur le dernier nœud du graphe. Ces deux étapes sont illustrées par les figures 4 et 5.

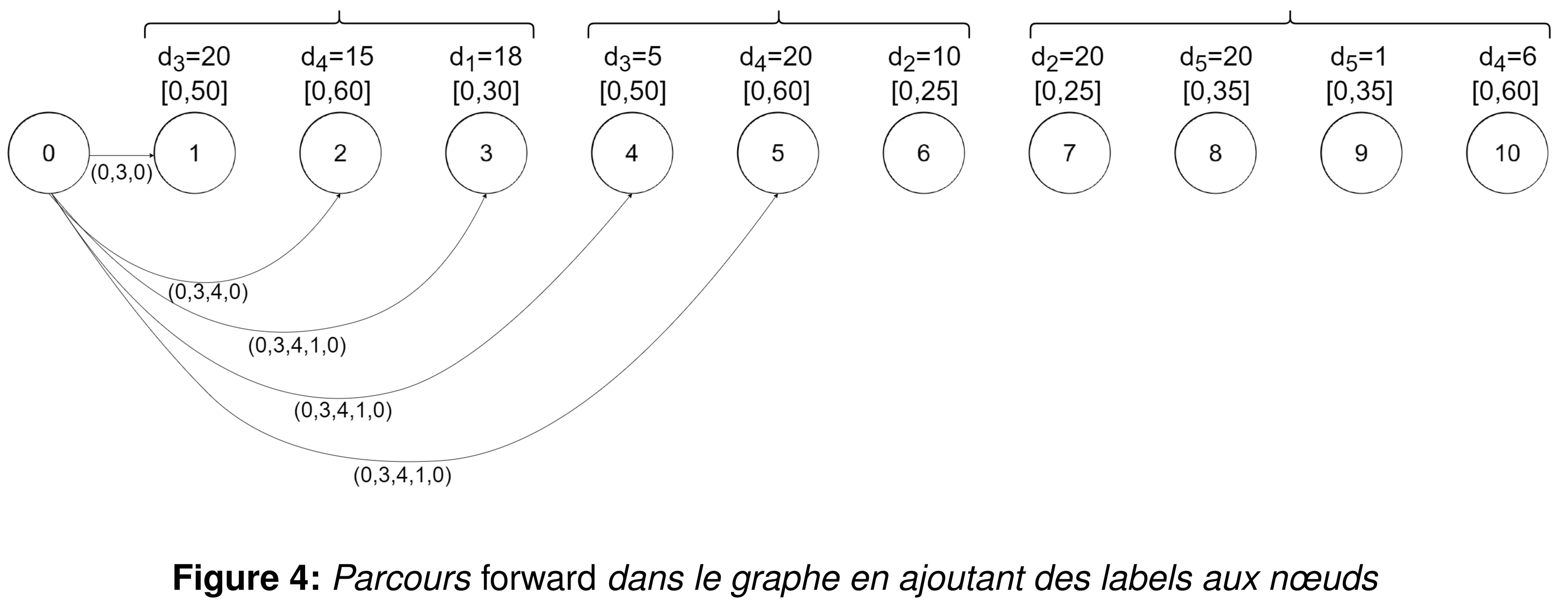

Figure 4: *Parcours* forward *dans le graphe en ajoutant des labels aux nœuds*

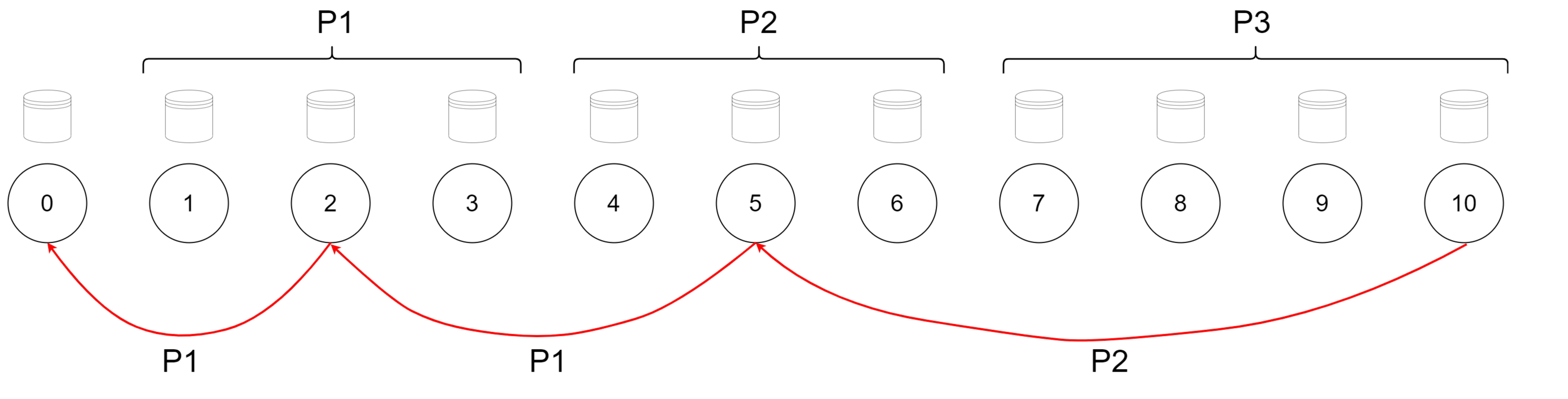

Figure 5: *Parcours* backward *pour trouver le chemin critique*

OPTIMISATION

Afin d'établir un schéma d'optimisation pour trouver des solutions pour le problème dans un temps raisonnable, la métaheuristique GRASP×ELS (*Greedy Randomized Adaptative Search Procedure* × *Evolutionary Local Search*) a été choisie (Figure 6). Celle-ci part d'une solution de départ et l'améliore à travers des niveaux ELS où chaque niveau consiste à générer des voisins et à appliquer des recherches locales dans le but d'améliorer le coût global.

La génération des solutions initiales ainsi que la reconstitution d'une solution après la création d'un voisin sont réalisées grâce à l'algorithme de programmation dynamique présenté précédemment. Les recherches locales comprennent des mouvements 2-OPT intra tournée, 2-OPT inter tournées, séparation et insertion. Ces mouvements de voisinage sont capables d'optimiser les tournées des véhicules pour les périodes.

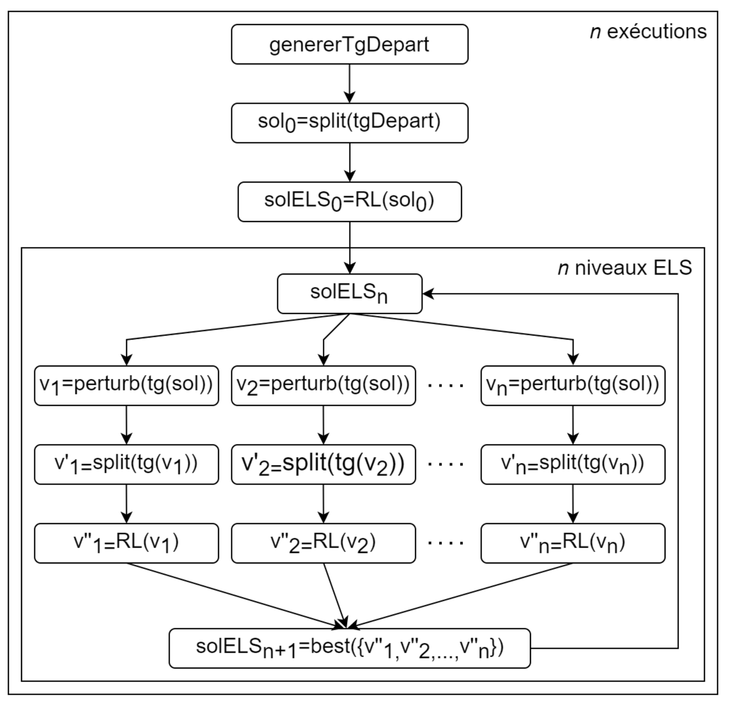

Figure 6: *GRASP×ELS*

RESULTATS PRELIMINAIRES

La métaheuristique a été testée sur 160 instances de la littérature proposées par [1]. Le jeu d'instances est décrit ci-dessous :

— 3 périodes
  highcost (50), *lowcost* (50)
  {5, 10, ..., 50} clients
— 6 périodes
  highcost (30), *lowcost* (30)
  {5, 10, ..., 30} clients

Le tableau 1 présente les résultats obtenus jusqu'à présent pour certaines instances dont le coût de stockage est élevé. Chaque ligne du tableau contient des valeurs moyennes pour cinq instances de même taille. La colonne $|C|$ contient le nombre de clients, le gap du coût obtenu par rapport à la solution optimale, t_{target} le *time to target* et t_{total} le temps total d'exécution de la métaheuristique.

$\|C\|$	*gap*(%)	t_{target}(s)	t_{total}(s)
5	4,62%	1,27	43,10
10	7,92%	13,72	45,77
15	9,19%	27,27	51,14
20	7,83%	29,86	61,22
25	10,34%	42,29	71,39
30	11,93%	67,49	89,67

Tableau 1 : $P = 3, V = 2, highcost$

CONCLUSION ET TRAVAUX FUTURS

Le métaheuristique proposée est à ce jour fonctionnelle est permet de trouver des solutions réalisables rapidement. Cependant, il est nécessaire l'incorporation d'autres mécanismes dont l'intelligence artificielle afin d'améliorer leur qualité. Un nouveau jeu d'instances sera proposé dans le but de représenter des caractéristiques plus proches de la réalité dont la flotte hétérogène est les demandes et coûts variables selon les périodes.

Une présentation orale de cet algorithme est prévue dans la Conférence EURO 2022 [4].

REFERENCES BIBLIOGRAPHIQUES

[1] Archetti, C., Bertazzi, L., Laporte, G., & Speranza, M. G. (2007). A branch-and-cut algorithm for a vendor-managed inventory-routing problem. Transportation science, 41(3), 382-391.
[2] Archetti, Claudia, et al. "Formulations for an inventory routing problem." International Transactions in Operational Research 21.3 (2014) : 353-374.
[3] Manousakis, Eleftherios, et al. "Improved branch-and-cut for the Inventory Routing Problem based on a two-commodity flow formulation." European Journal of Operational Research 290.3 (2021) : 870-885.
[4] Martino, D. P. ; Lacomme, P. ; Farias, K. ; Iori, M. A Split-based Dynamic Programming approach for the Inventory Routing Problem. 32nd European Conference on Operational Research. Finland, 2022.
[5] Vadseth, Simen T., Henrik Andersson, and Magnus Stålhane. "An iterative matheuristic for the inventory routing problem." Computers & Operations Research 131 (2021) : 105262.

CONTACT

https://perso.limos.fr/∼diperdigao
diego.perdigao_martino@doctorant.uca.fr
+33 (0) 4 73 40 53 68

REMERCIEMENTS

Ce travail a bénéficié d'une aide de l'État gérée par l'Agence Nationale de la Recherche au titre du programme "Investissements d'Avenir" dans le cadre du Laboratoire d'Excellence IMobS3 (ANR-10-LABX-0016) et de l'Initiative d'Excellence IDEX-ISITE CAP 20-25 (ANR-16-IDEX-0001).

Approach to exploiting industry 4.0 technologies for the implementation of production KPIs

Ecole doctorale Sciences Pour l'Ingénieur

Emna MASMOUDI[a], Laurent PIETRAC[a], Séverine DURIEUX[a]

a. UCA, Clermont Auvergne INP, CNRS, Institut Pascal

Contact : emna.masmoudi@sigma-Clermont.fr

Context

Production Key Performance indicators (KPIs) are the best tools that help to keep the performance in the production on the high level. But to calculate them, it requires :

- The reporting of the operator
- Time to collect the relevant data
- Observation in real time

Industry 4.0 related technologies and solutions are our object of interest to improve the accuracy of production KPIs calculations not only in real-time but also by predicting future performance degradations . The specific technologies that make this possible include digital twins and artificial intelligence.

Key words : production KPIs, Digital twins, Industry 4.0, Artificial intelligence

Problematic

How can digital twins and artificial intelligence contribute to improve the relevance of production KPIs in each phase of the production system lifecycle?

Method

In the first place, understanding the concept of digital twin, its definition, its technologies and its framework is essential in order to make sure that DT contributes effectively to the performance evaluation.

In the second place, implementing a digital twin for a real case study going from unit level to system level that will be able to define the actual state of the production system and to predict performance degradation through production KPIs.

The different utilization cases of the digital twin are illustrated in the following figure :

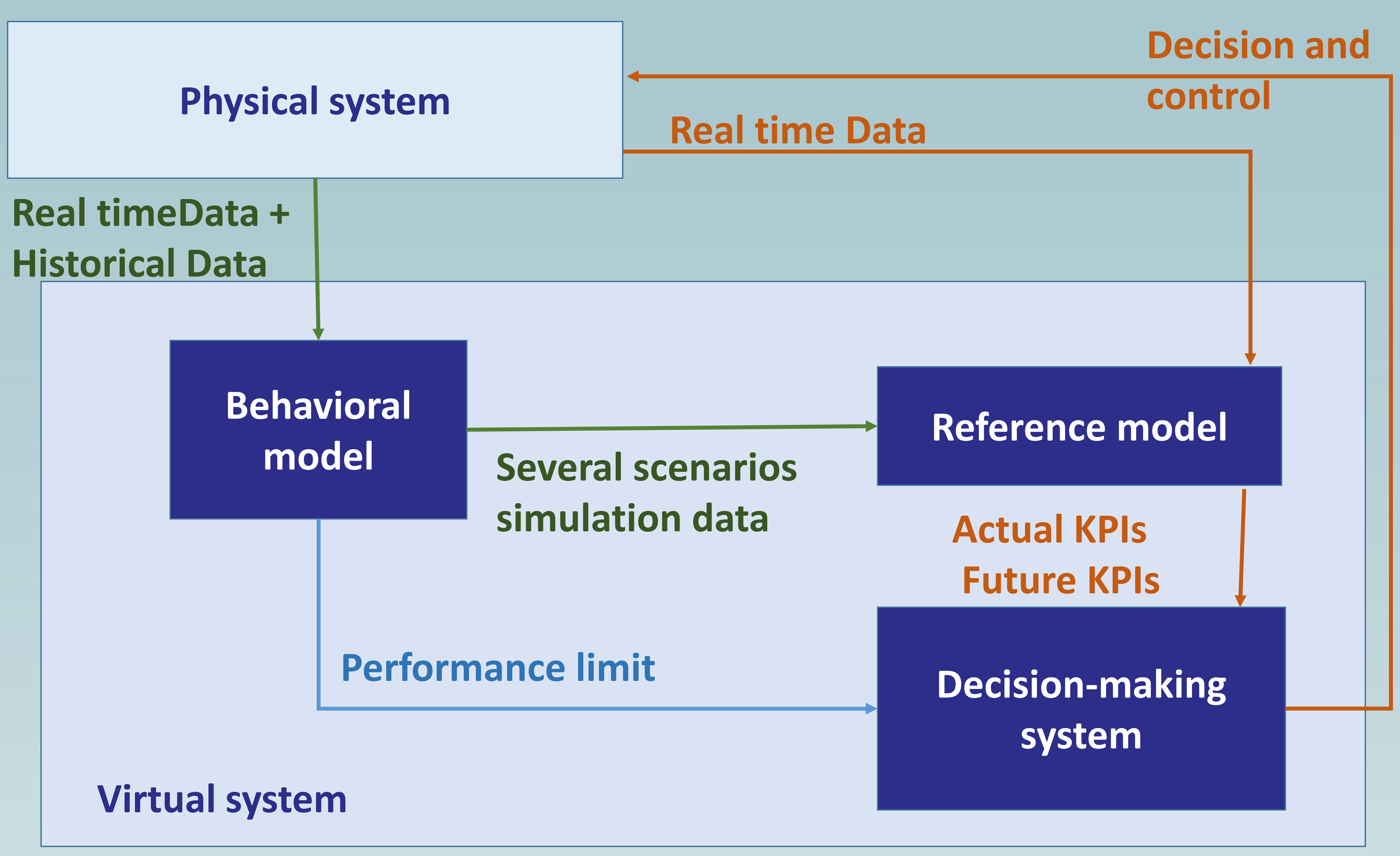

Determination of the reference model / Adaptation in case of reconfiguration, production change or context change
Observation and determination of the current state/ Predicting future state
Determination of the performance limits of the physical system

Current work

Defining digital twin :

In view of a literature review of scientific research [1] [2], what is digital twin can be summarized as follow :
DT provides virtual representations of a potential or actual physical system along its lifecycle which are continuously updated and synchronized.
It fuses historical data, real-time data and predicted data to track the past, monitor the present and predict the future [1] which helps to understand current state of physical systems and plays the role of a decision-making tool.

For a digital twin framework, we consider 5 dimensions : the physical system, the virtual models, the data, the services and the connections between all the elements[3].

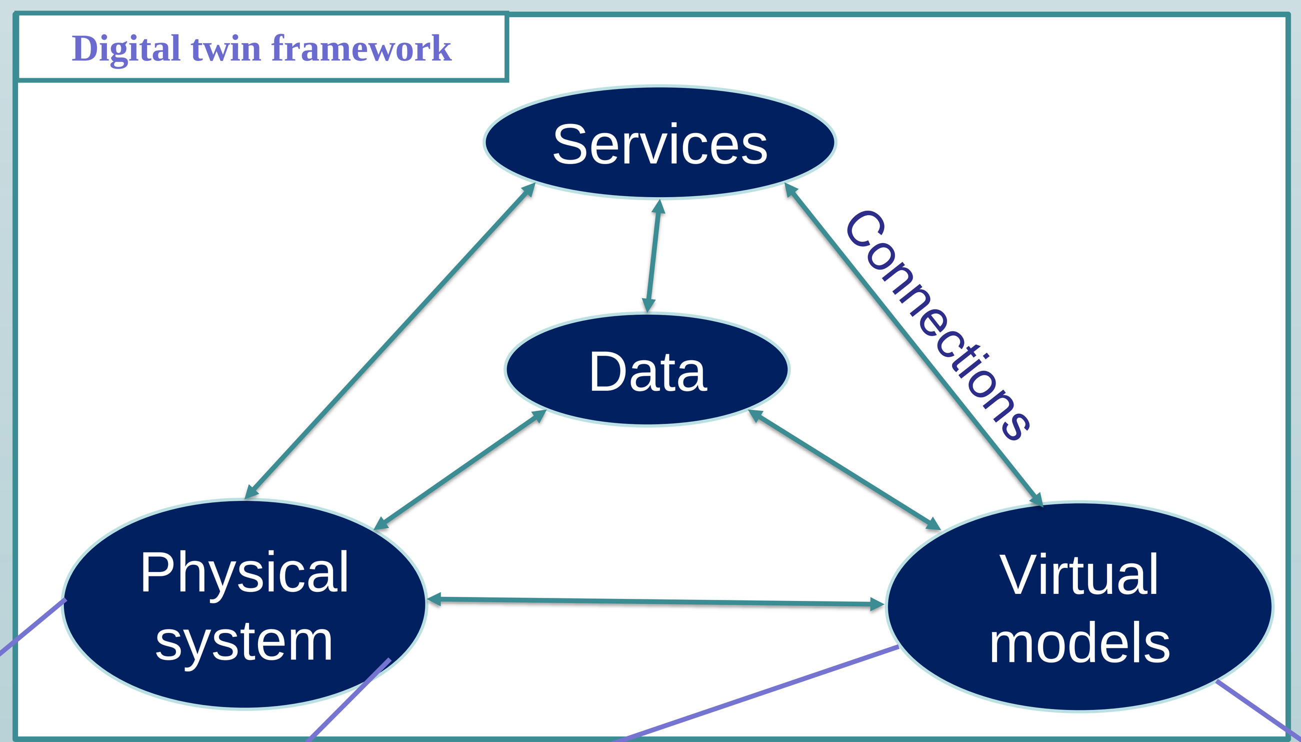

Real academic production system (Assembly line)

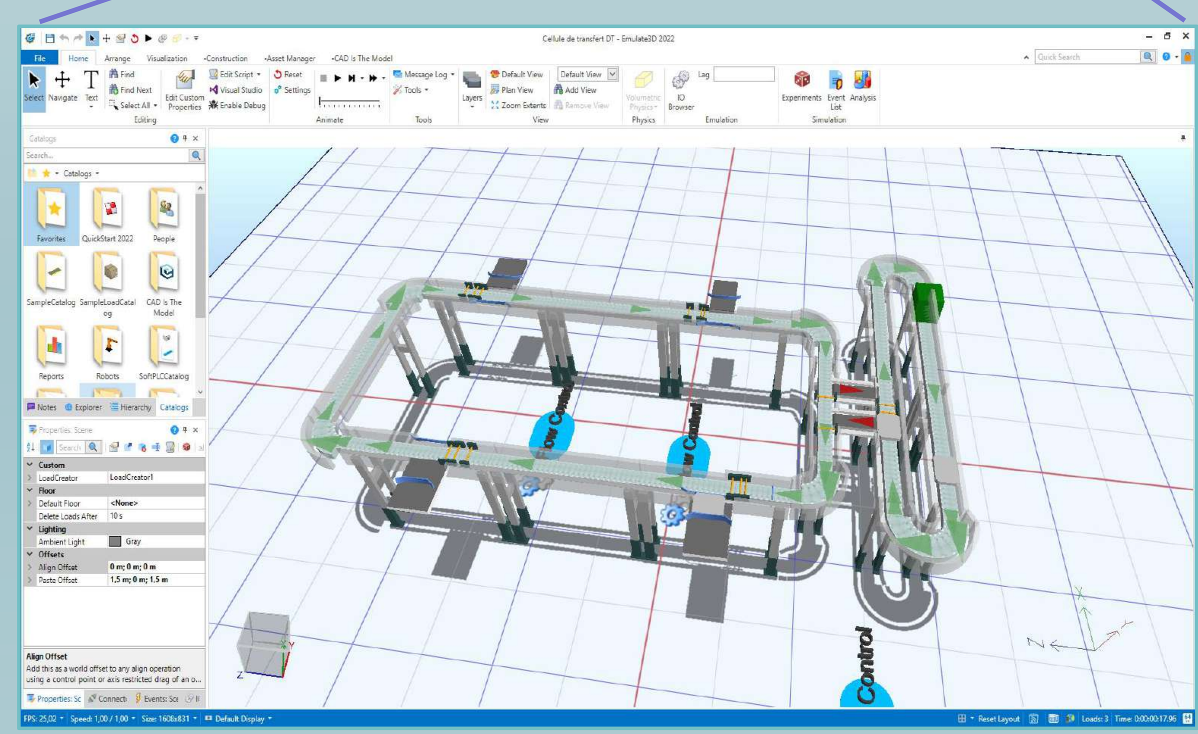

Behavioral model using Emulate3D

Future work

Next steps of the present research will be related to the implementation of the rest of the elements of the digital twin and their connections and insert the artificial intelligence algorithms to have an intelligent digital twin that is able to predict future performance of the physical system and auto adapt in case of context reconfiguration.

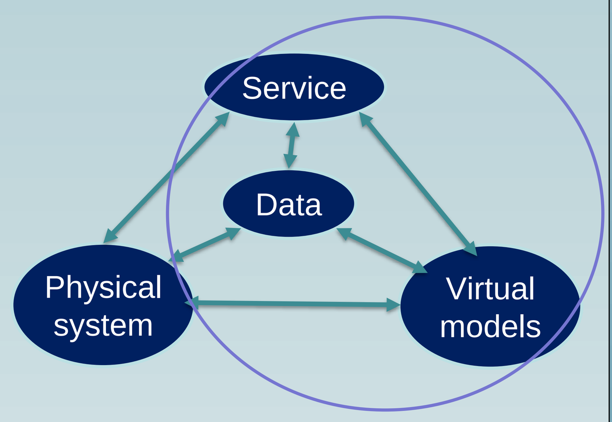

Bibliography

1. Liu et al. 2021. « Review of Digital Twin about Concepts, Technologies, and Industrial Applications ». Journal of Manufacturing Systems, Digital Twin towards Smart Manufacturing and Industry 4.0, 58 (janvier): 346-61. https://doi.org/10.1016/j.jmsy.2020.06.017.
2. Negri et al 2017. « A Review of the Roles of Digital Twin in CPS-Based Production Systems ». Procedia Manufacturing, 27th International Conference on Flexible Automation and Intelligent Manufacturing, FAIM2017, 27-30 June 2017, Modena, Italy, 11 (janvier): 939-48. https://doi.org/10.1016/j.promfg.2017.07.198.
3.Tao et al. 2017. « Digital Twin Shop-Floor: A New Shop-Floor Paradigm Towards Smart Manufacturing ». *IEEE Access* 5: 20418-27. https://doi.org/10.1109/ACCESS.2017.2756069.

Automation of Preoperative 3D Reconstruction for Laparoscopic Surgical Guidance

Ivan MIKHAILOV[1,2], Benoit CHAUVEAU[2], Nicolas BOURDEL[2] and Adrien BARTOLI[1]

[1]EnCoV, Institut Pascal, Université Clermont Auvergne, Clermont-Ferrand, France,
[2]SurgAR, Clermont-Ferrand, France

Context

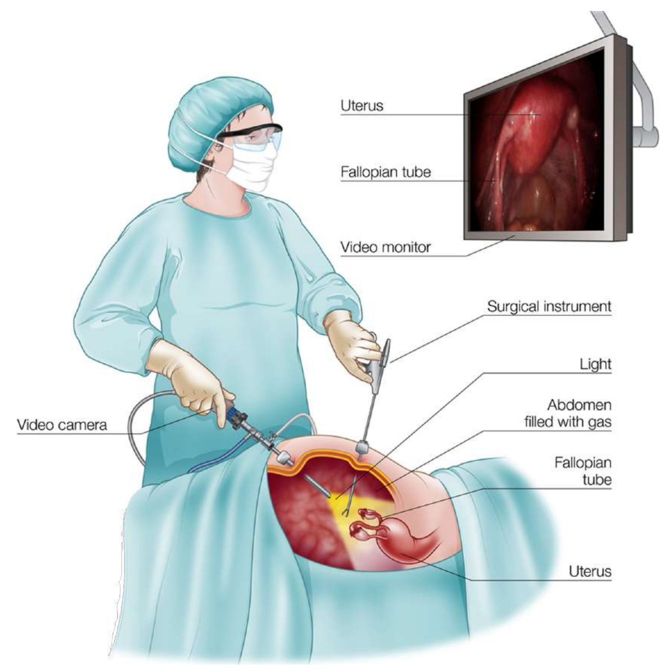

Figure 1:Gynecologic laparoscopy

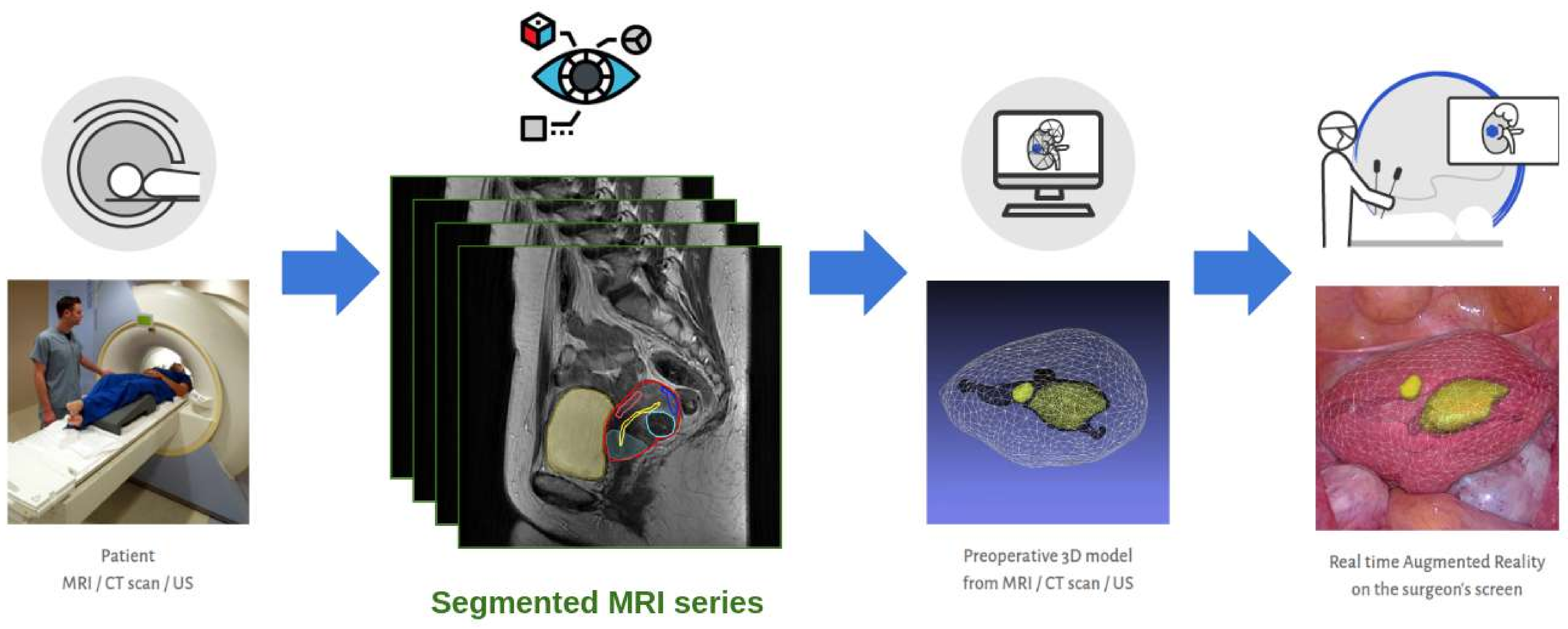

Figure 2:Pipeline: Augmented Reality software for computer-aided laparoscopic surgery

Scope

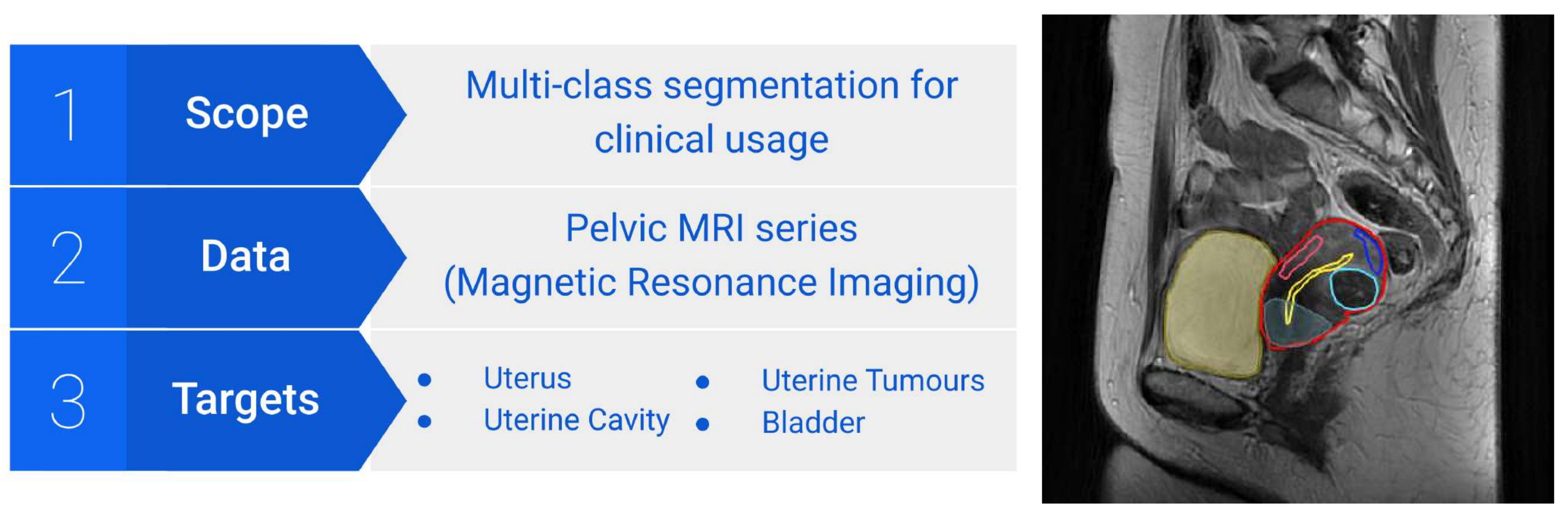

Figure 3:Left: defined project constraints; Right: an example of multi-class MRI segmentation in the sagittal view

Contribution

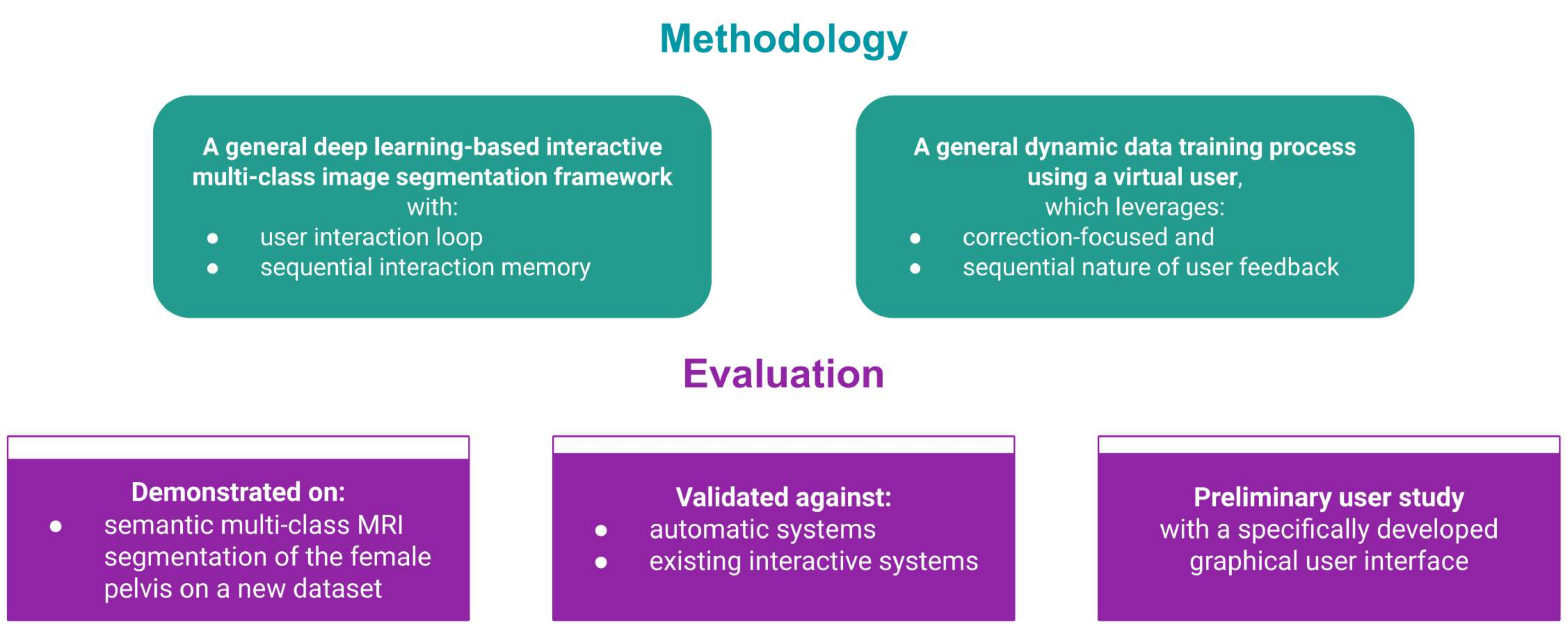

Figure 4:Top: Methodology contribution, Bottom: Evaluation directions

- Training Process & Data Generation
  - Existing approaches generate user interaction masks from labelled data, either via static data generation (SDG) before training or dynamic (DDG) during training. DDG improves performance, but is usually not representative of human user behaviour, which limits the system's generalisation and interaction effectiveness.
  - We introduce DDG method, which leverages the correction-focused and sequential nature of user feedback.
- Cumulative vs. Sequential Interaction Memory
  - Existing works employ cumulative interaction memory (CIM), which aggregates the raw system states by merging the successive interaction masks. This discards the ordering of interactions, hence the typical user sequentiality.
  - We introduce a sequential interaction memory (SIM), which, in contrast to CIM, preserves the past n system states, hence the user's sequential behaviour.

Methodology

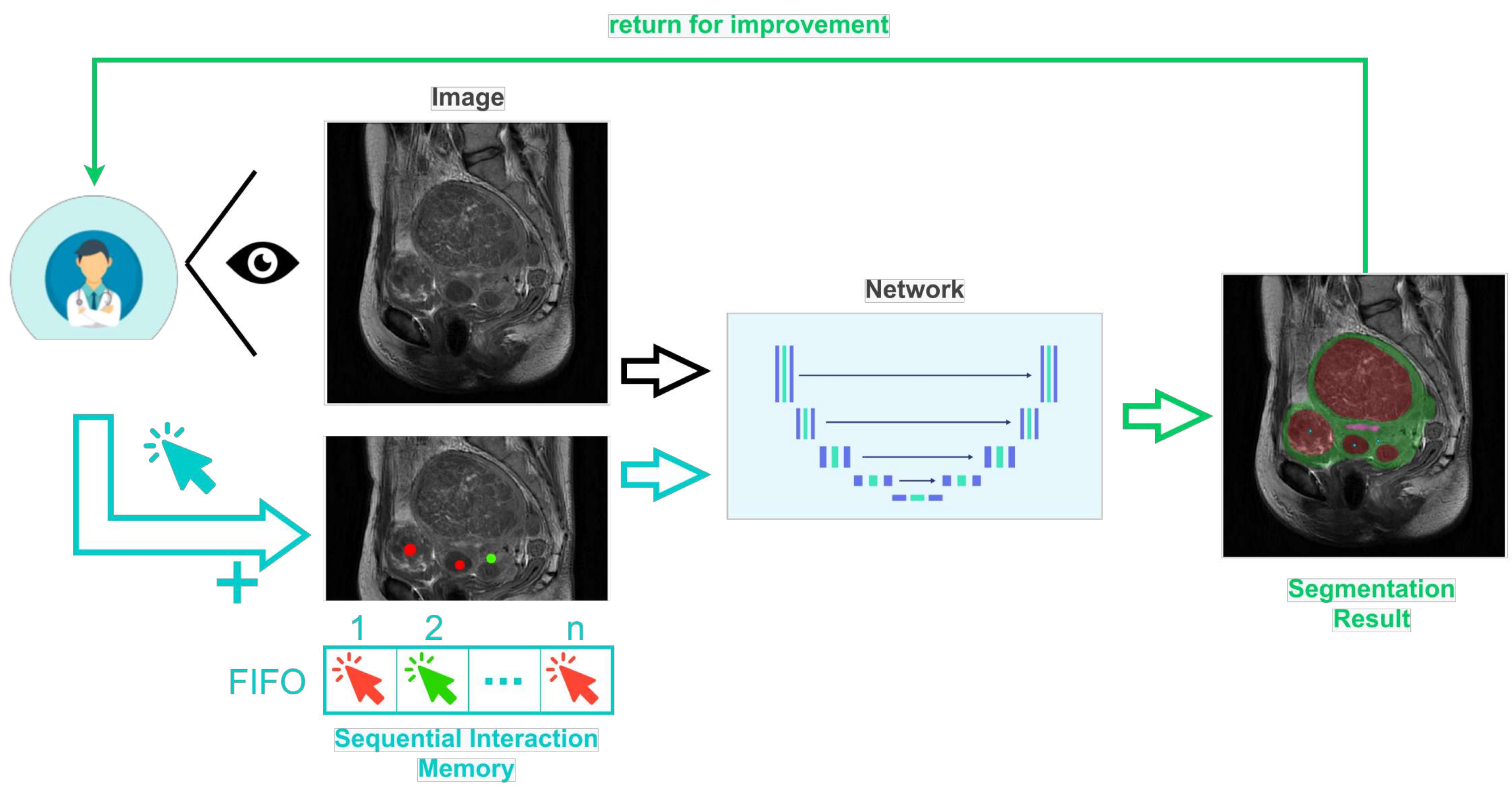

Figure 5:Schematic: Deep Learning-based Interactive Medical Image Segmentation Framework

Experimental Results

We compare one automatic method and four interactive methods in Table 1:

1. Auto: U-Net with ResNet34 encoder
2. SDG-base: memory-less system trained with SDG
3. SDG-CIM: network from Base+SDG used with a CIM overlay
4. DDG-CIM: system with CIM trained with DDG
5. DDG-SIM: complete proposed system with SIM trained with DDG

Table 1:Experimental evaluation results where bold means best.

Method	BGD		Uterus		Bladder		Tumours		Cavity	
	IoU	Dice	IoU	Dice	IoU	Dice	IoU	Dice	IoU	Dice
Auto	99.2	99.6	64.7	78.6	71.9	83.6	60.4	75.3	40.4	57.6
SDG-base	99.1	99.6	61.7	76.3	70.1	82.4	62.5	76.9	21.1	34.9
SDG-CIM	99.3	99.7	66.5	79.9	83.9	91.2	72.8	84.3	29.0	44.9
DDG-CIM	**99.6**	**99.8**	77.4	87.3	**87.4**	**93.3**	77.7	87.4	39.6	56.7
DDG-SIM	**99.6**	**99.8**	**79.8**	**88.7**	87.0	93.0	**79.0**	**88.3**	**57.8**	**73.3**

Table 2:User evaluation results given by IoU; 'A' and 'B' represent the two users.

Series	Time	BGD	Uterus	Bladder	Tumours	Cavity	mIoU
1-A	1'44"	99.7	69.5	92.0	-	44.0	76.3
1-B	3'00"	99.6	64.1	93.6	-	41.4	74.7
2-A	3'10"	99.3	67.0	79.4	71.7	35.0	70.5
2-B	2'42"	99.3	69.9	78.4	71.7	42.6	72.4
3-A	3'10"	99.6	70.3	76.1	-	38.5	71.1
3-B	2'50"	99.6	72.2	76.8	-	42.6	72.8
4-A	7'08"	98.1	63.0	71.9	81.0	44.0	71.6
4-B	8'30"	98.2	66.8	76.6	58.6	41.9	68.4
5-A	2'38"	99.8	61.0	93.2	-	24.9	69.7
5-B	4'17"	99.9	68.0	93.5	-	30.6	73.0

Results: Figure

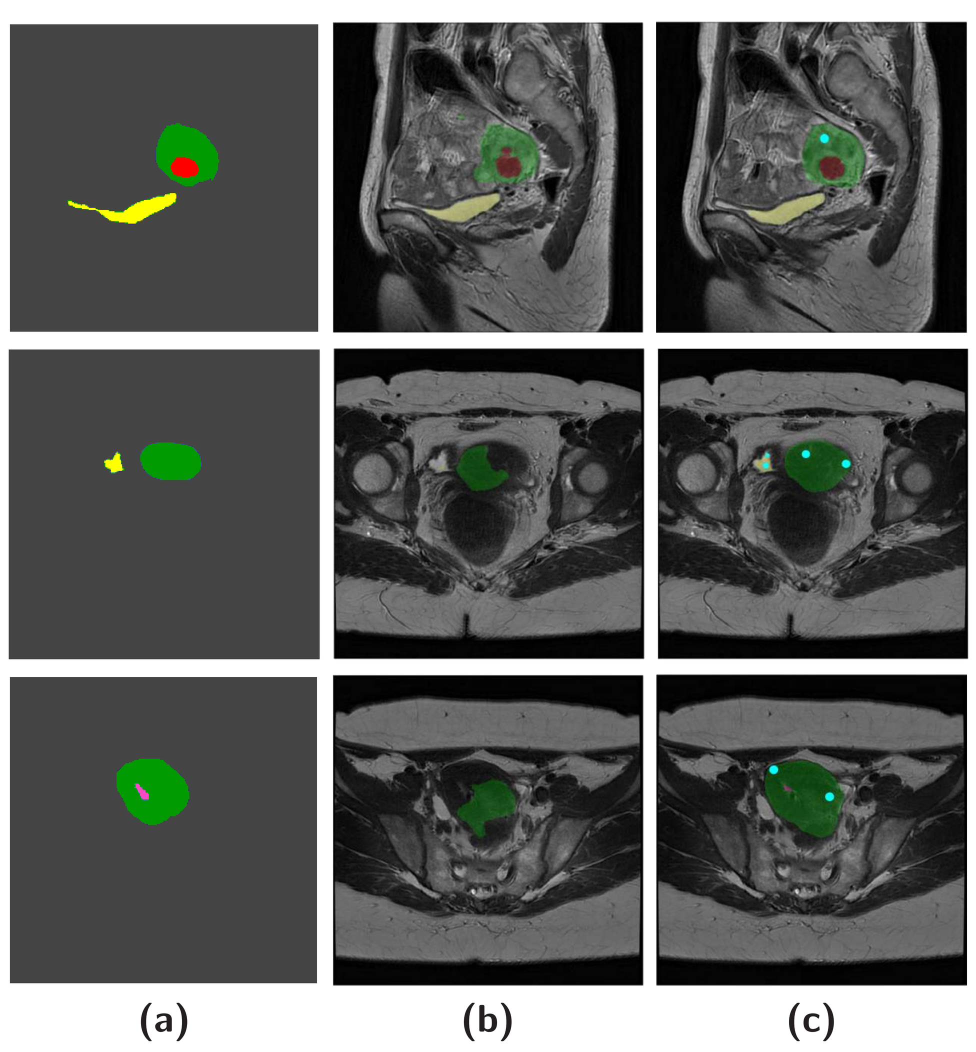

Figure 6:Comparison between the automatic segmentation and the human user-controlled proposed interactive system with uterus in green, bladder in yellow, tumour in red, cavity in pink and user interactions in the form of clicks in cyan: **(a)** ground truth; **(b)** automatic segmentation results; **(c)** interactive segmentation results.

ivan.mikhailov@doctorant.uca.fr, ivanmikhailov.mail@gmail.com

Toward a Generalized Risk Assessment Method on Occupancy Grids

Jérémy Morceaux[1,2], Johann Laconte[1], Elie Randriamiarintsoa[1], Ted Morell[1], Laurent Malaterre[1], Dieumet Denis[2], Romuald Aufrère[1], Roland Chapuis[1]

[1]Université Clermont Auvergne, Clermont Auvergne INP, CNRS, Institut Pascal, F-63000 Clermont-Ferrand, France

[2] Sherpa Engineering

Context & Motivations

- While occupancy grids are a good way to map the environment of a vehicle, they are not well-suited to assess risks of a specific path.
- Several recent works implemented a notion of risk in occupancy grids (e.g., [1]). In particular, [2] introduced the Lambda-Field, a mathematical theory where a physical risk can be computed for a specific path.

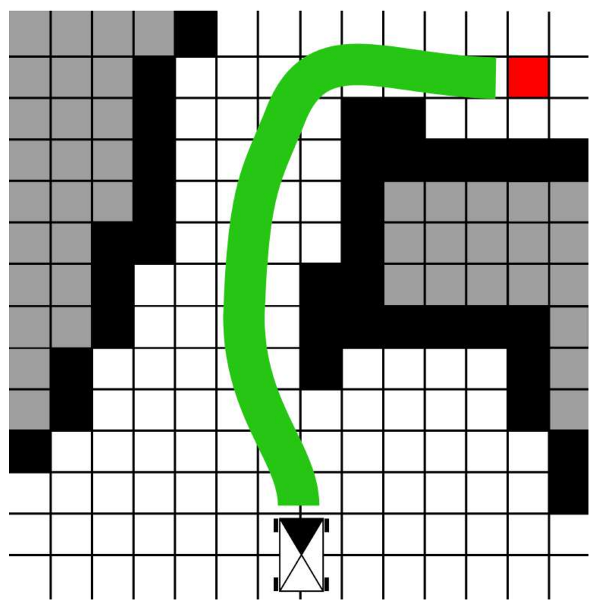

Figure: Even thought the Bayesian Occupancy grid can allow to compute a path to reach a goal, it cannot assess the physical risk for a specific path.

Lambda-Field

- Lambda-Field, instead of storing the probability of occupation, stores the intensity of an event. The intensity of a cell can be seen as the likelihood to create an event leading for example to a collision. For this work, we defined our event as the deformation of the wheel (assumed unique) due to a collision.
- For each cell c_i:

$$\lambda_i = p_i \cdot \frac{1}{e}\ln\left(1+\frac{u_i}{s_i}\right) \qquad p_i = \min\left(\frac{|H_i|}{R}, 1\right) \tag{1}$$

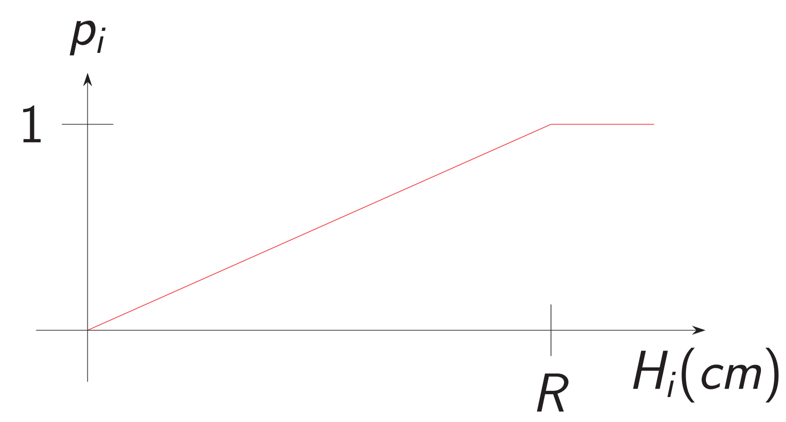

Figure: p_i, the probability to be harmful.

- To compute, s_i, u_i and H_i, we use a Digital Elevation Map (DEM).

H_i	Maximum elevation difference between the cell c_i and its neighbors
s_i	Cell c_i was measured s_i times safe ($< 5\,\text{cm}$).
u_i	Cell c_i was measured u_i times unsafe ($> 5\,\text{cm}$).
R	Radius of the wheel.

Table: List of parameters to compute the Lambda-Field.

Risk Function

- We use a spring to model the compression of the wheel during the collision.

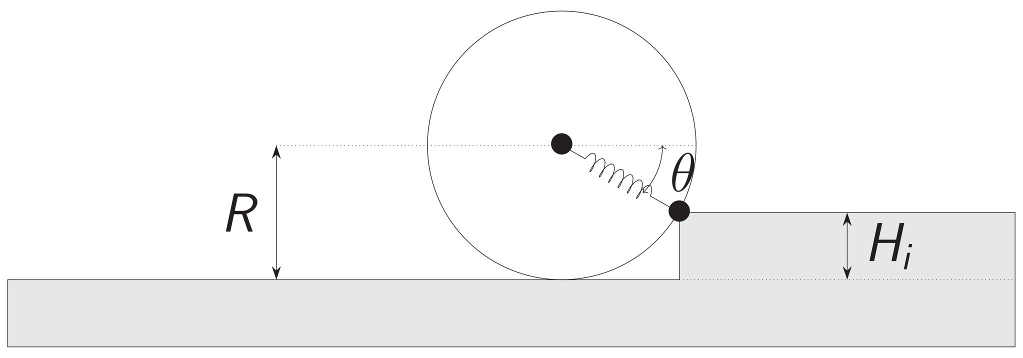

Figure: We model our wheel like a spring that will absorb the collision.

- Using the equation of an harmonic oscillator, we evaluate our risk function as the elastic energy absorbed by the spring:

$$r(v, H_i) = \frac{1}{2} \cdot k \cdot A(v, H_i)^2 \tag{2}$$

where A is the amplitude of the harmonic solution, v is the speed of the vehicle and k is the stiffness of the spring.
- As introduced in [2], we can compute the expected risk over a path with:

$$\mathbb{E}[r(\cdot)] = \sum_{i=0}^{N-1} K_i r(v, H_i), \quad \text{where}$$
$$K_i = exp\left(-\Delta a \sum_{j=0}^{i-1} \lambda_j\right)\left[1 - exp\left(-\Delta a \lambda_i\right)\right] \tag{3}$$

where Δa is the area of each cell.

Experimental Setup

- During this experiment, we used a 4-wheel drive robot equipped with a velodyne VLP-16.
- The VLP-16 is tilted with a 15° angle on the pitch axis in order to get a better representation of the road ahead.

Figure: Robot used for this experiment.

Results

- First, a DEM was created by accumulating several point clouds generated by a 3D LIDAR sensor.

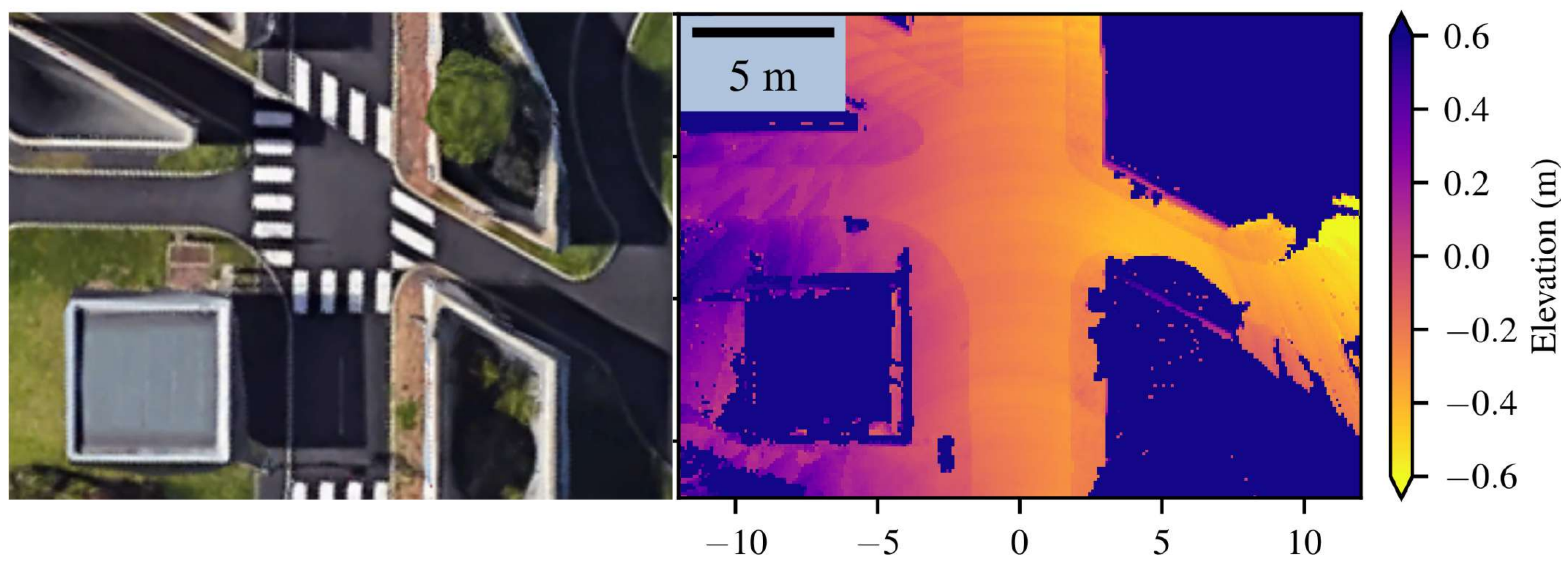

Figure: *Left*: Aerial view from our urban-like test site with sidewalks that may be hazardous. *Right*: DEM is computed from the accumulation of LIDAR points over time.

- Then, we constructed a Lambda-Field using a wheel radius of $R = 25\,\text{cm}$.

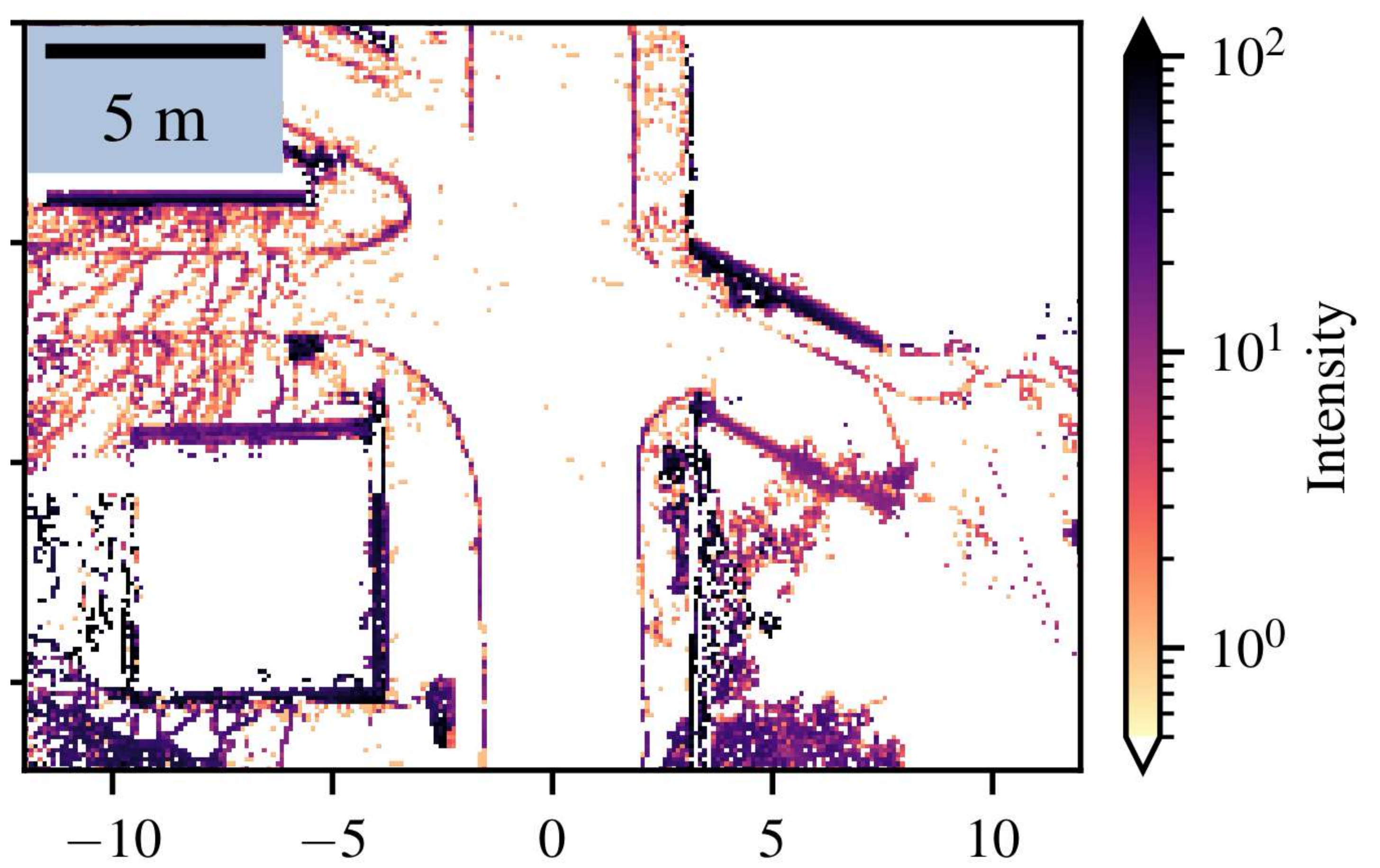

Figure: Lambda-Field computed from the DEM. We can see that curbs and walls have a high intensity, meaning that they are hazardous for the robot.

- Road curbs and walls have a high intensity, indicating that if the robot goes through, the event of collision will be very likely to occur. As our robot doesn't have any suspension, the VLP-16 experiences some vibration causing some cells (middle of the road) to appear higher/lower then they actually are.

Perspectives

- We intend to create different Lambda-Field to model different events such as roll over, lane invasion or high deceleration.
- After fusing several maps into the Lambda-Field for more generic risk assessments, we intend to provide it to a path planning algorithm and control our robot on our test site.

Acknowledgments and References

This work has been sponsored by Sherpa Engineering and ANRT (Conventions Industrielles de Formation par la Recherche).

[1] David D. Fan, Kyohei Otsu, Yuki Kubo, Anushri Dixit, Joel Burdick, and Ali-Akbar Agha-Mohammadi. STEP: stochastic traversability evaluation and planning for safe off-road navigation. *arXiv preprint arXiv:2103.02828*, 2021.

[2] Johann Laconte, Christophe Debain, Roland Chapuis, François Pomerleau, and Romuald Aufrère. Lambda-field: A continuous counterpart of the bayesian occupancy grid for risk assessment. *International Conference on Intelligent Robots and Systems*, pages 167–172, 3 2019.

 jeremy.morceaux@sherpa-eng.com

Traitement *in-vivo* des cellules cancéreuses de prostate par plasma froid

Maxime MOREAU, Karine CHARLET, Sébastien MENECIER, Frédéric PERISSE

Université Clermont Auvergne, Clermont Auvergne INP, CNRS, Institut Pascal, F-63000 Clermont-Ferrand, France

Introduction

L'utilisation du plasma froid est répandue dans l'industrie pour le traitement de surface, la stérilisation, *etc.* mais est aussi en développement dans le monde de la recherche médicale ou agronomique par exemple.

Depuis plusieurs années, le plasma froid est étudié comme traitement contre le cancer. En 2020, l'Institut Pascal en collaboration avec des biologistes du laboratoire du GReD a mené une étude *in-vitro* sur trois lignées de cellules de la prostate soumises à une exposition de quelques minutes au plasma froid [1]. Trois jours après, on mesure un taux de mortalité important chez les cellules cancéreuses là où les cellules saines sont peu touchées. De plus, les cellules meurent naturellement par apoptose : elles s'autodétruisent.

Cette différence d'efficacité entre les lignées est qualifiée de sélectivité. Même si ce point est encore mal compris, c'est un des enjeux principaux de la discipline.

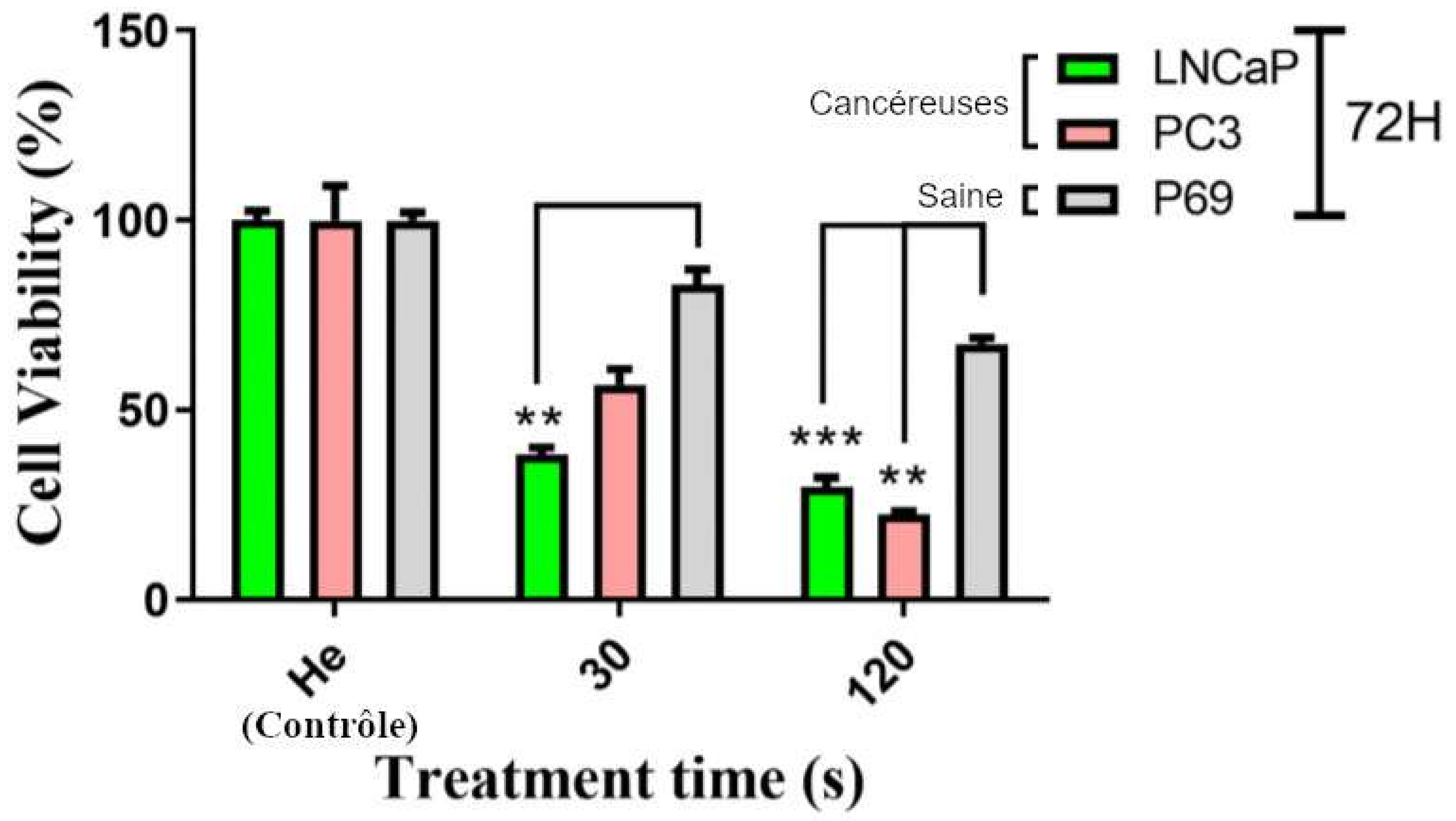

Figure 1 : Taux de viabilité des cellules de la prostate après exposition au plasma froid. D'après Fofana *et al.*

Plasma

Le plasma est le quatrième état de la matière. C'est un gaz ionisé, globalement neutre et très énergétique composé de molécules, d'atomes et d'ions à l'état fondamental ou excité mais aussi de particules élémentaires telles que des électrons ou des photons. Si l'énergie est transmise en majorité aux électrons, la température macroscopique ne varie pas : on parle alors de plasma froid.

Notre dispositif est constitué de deux parties : la torche où se forme le plasma qui est alimentée par un générateur haute tension.

- Paramètres électriques :
  - Torche : plasma gun
  - Tension : 5-10 kV
  - Fréquence : 20 kHz
  - Rapport cyclique : 20 %
- Autres :
  - Pression atmosphérique
  - Température ambiante
  - Gaz plasmagène : He
  - Débit : 1-10 L · min^{-1}

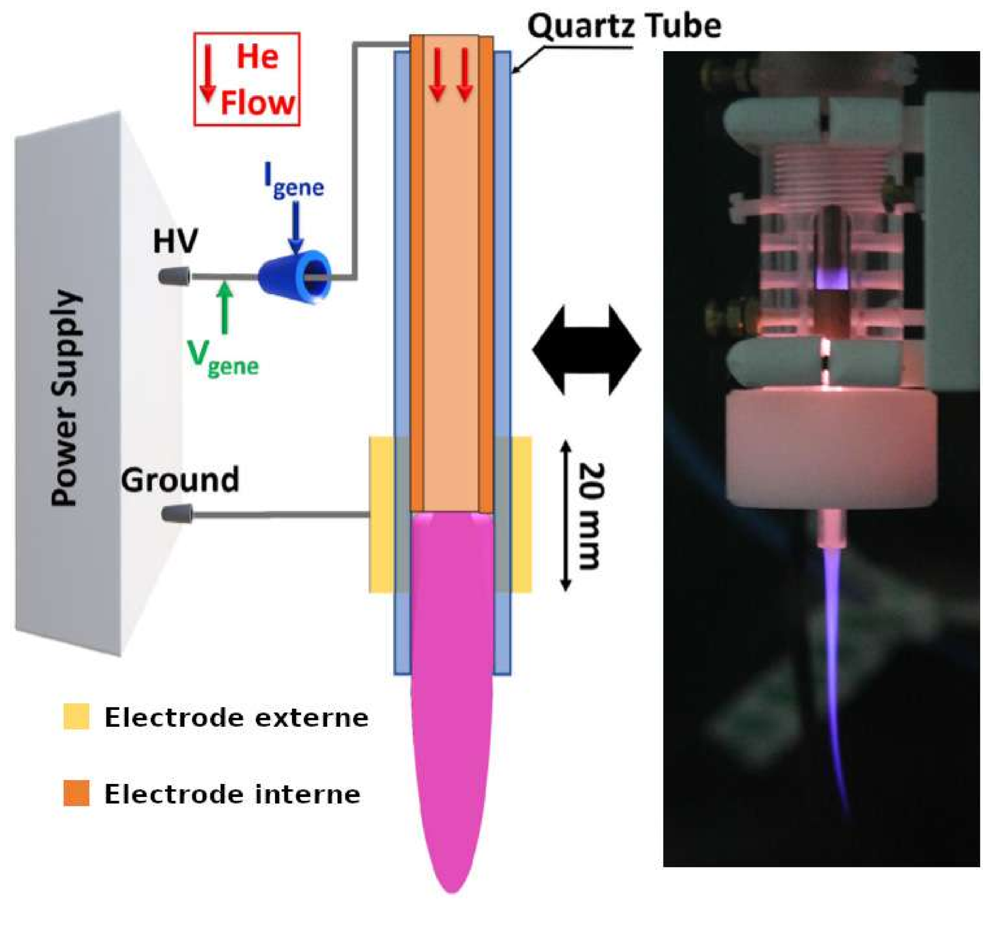

Figure 2 : Torche à plasma froid

La torche ci-dessus est du type plasma gun mais nous en avons une autre avec deux électrodes externes appelée plasma jet. Les propriétés du plasma sont dépendantes de la torche. Par exemple, en fonction de la cible étudiée, le plasma gun permet de générer un plasma d'une puissance de plus de 100 W alors qu'elle sera inférieure à 20 W pour le plasma jet [2].

References

[1] M. Fofana, J. Buñay, F. Judée, S. Baron, S. Menecier, M. Nivoix, F. Perisse, A. Vacavant, and X. Balandraud.
Selective treatments of prostate tumor cells with a cold atmospheric plasma jet.
Clinical Plasma Medicine, 2020.

[2] F. Judée, J. Vaquero, S. Guégan, L. Fouassier, and T. Dufour.
Atmospheric pressure plasma jets applied to cancerology: correlating electrical configuration with in vivo toxicity and therapeutic efficiency.
Journal of Physics D: Applied Physics, 52, 2019.

In-vitro

Une campagne d'expériences a eu lieu en mars/avril avec pour objectifs de :

- bénéficier d'une formation en culture cellulaire
- développer un modèle cellulaire *in-vitro* proche de l'*in-vivo*
- tester l'efficacité de la torche de type plasma jet

Le modèle cellulaire initial avait pour but de suspendre les cellules dans une matrice de collagène d'une épaisseur de quelques millimètres pour voir l'efficacité du traitement par plasma froid en profondeur. Malgré des premiers résultats intéressants, il a été mis de côté pour plusieurs raisons : une répartition des cellules peu homogène, une quantification difficile, *etc.*

Sur un modèle *in-vitro* classique, l'efficacité du plasma jet a été montrée. L'utilisation de cellules cancéreuses fluorescentes (lignée PC3-GFP) permet un suivi facile comme illustré sur les images ci-dessous. Trois jours après un traitement de 2 min au plasma froid, le taux de viabilité n'est plus que de 22 %.

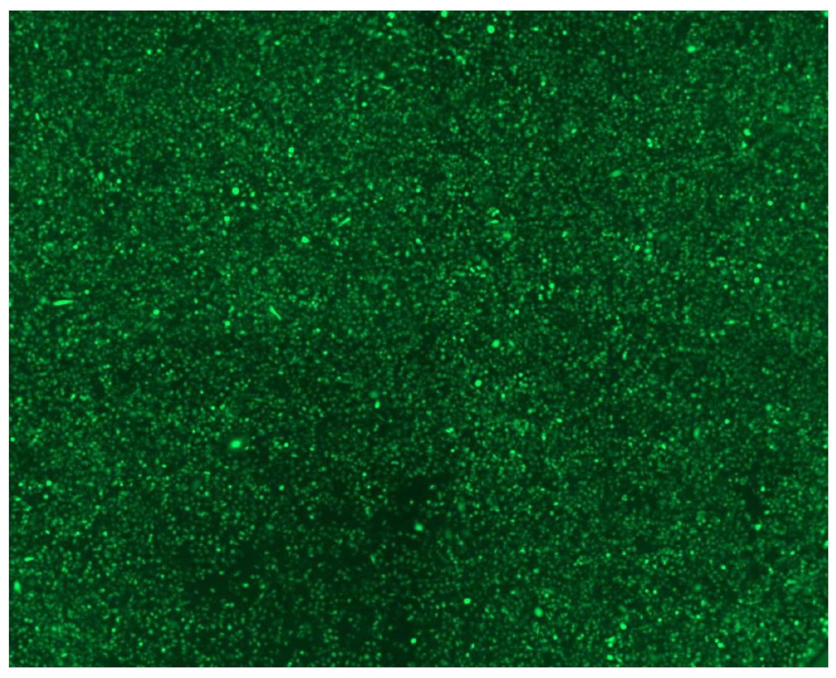

Figure 3 : Cellules avant exposition au plasma

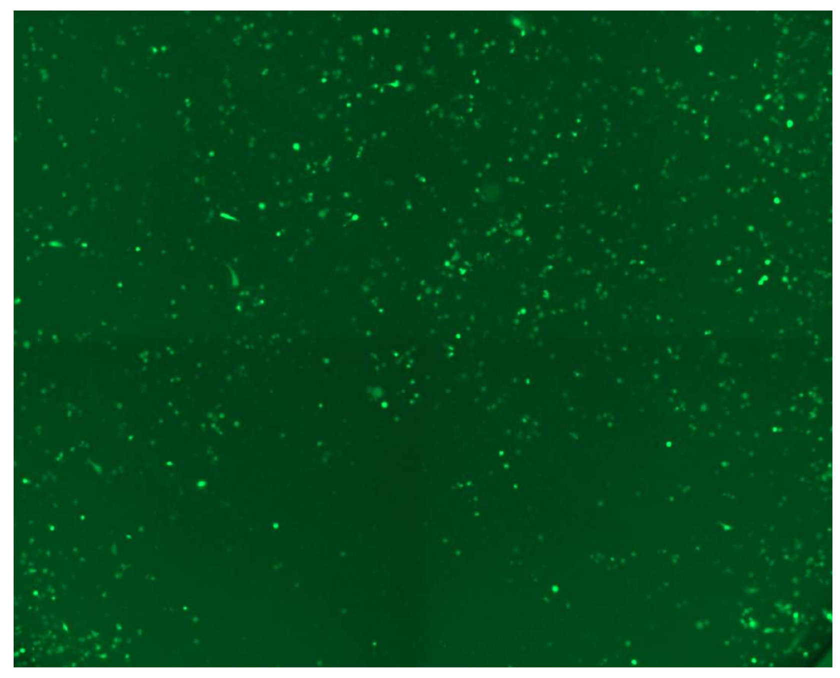

Figure 4 : Cellules 3 jours après 120 s d'exposition

In-vivo

Deux expériences pilotes *in-vivo* ont été réalisées en novembre et en mai. Les résultats sont très bons. Des souris porteuses de tumeurs au niveau de leurs deux prostates antérieures ont été traitées : l'une est exposée 10 min au plasma froid et l'autre 10 min à l'hélium pour servir de contrôle. La zone traitée est irriguée avec du milieu de culture toutes les 2 min pour éviter un assèchement des tissus. Une semaine après, les prostates sont récupérées et observées au microscope. Comme illustré par la perte de fluorescence sur l'image, les cellules tumorales de la zone exposées au plasma froid sont affectées par le traitement. Pour les différents individus, les résultats sont similaires, le reste de la prostate ainsi que celle exposée à l'hélium reste intacte avec une persistance de la fluorescence. Cela prouve une efficacité du traitement *in-vivo* par plasma froid.

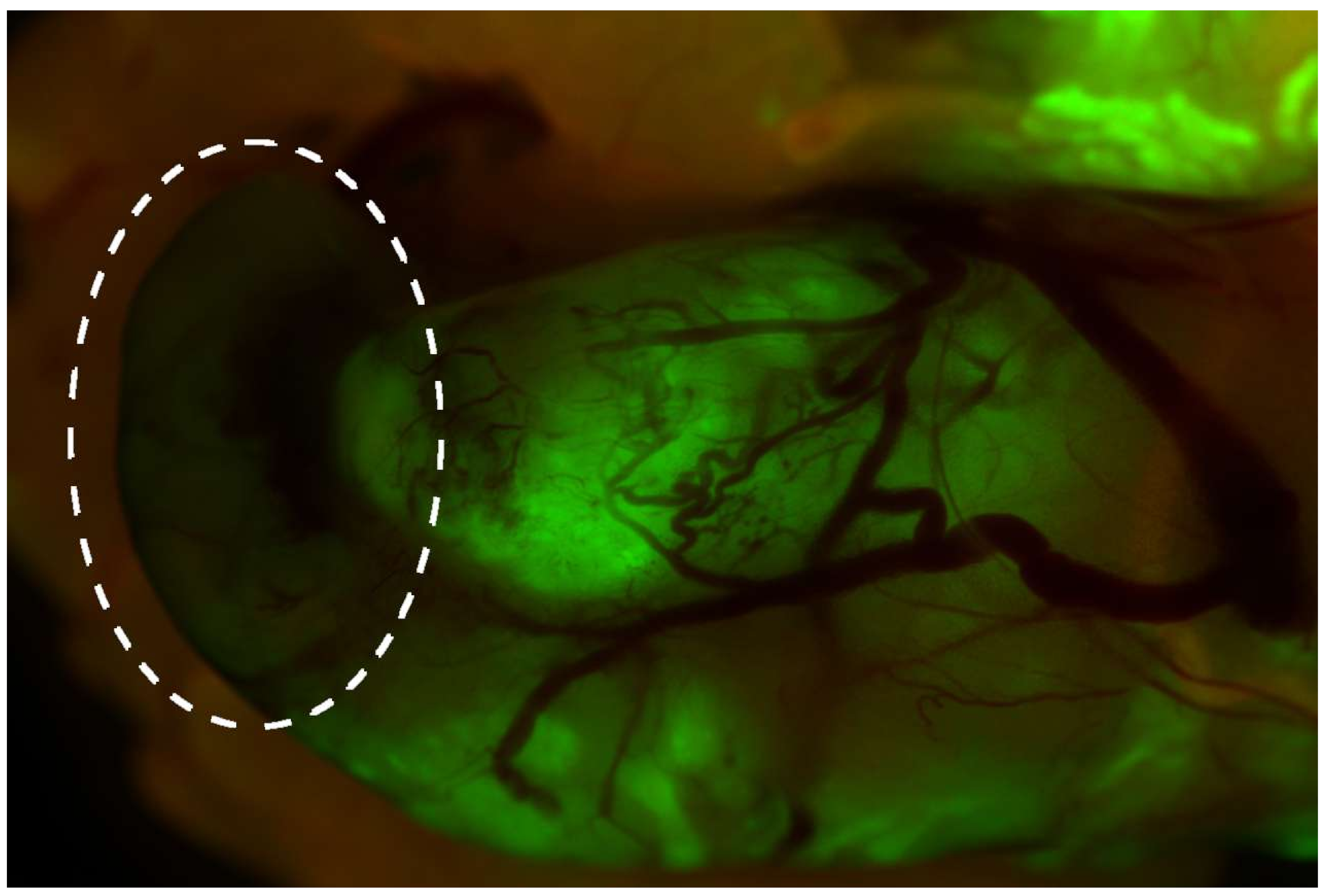

Figure 5 : Prostate antérieure gauche traitée 10 min par plasma froid (souris PTEN)

Objectifs

- Protocoles de mesures électriques et spectroscopiques à améliorer
- Optimisation des torches : CEM, sécurité, plasma via cathéter
- Nouvelles campagnes *in-vitro* : maximiser l'efficacité, comprendre les mécanismes cellulaires, perfectionner la quantification par analyse d'images
- Nouvelles expériences *in-vivo* en fonction des résultats *in-vitro*
- Adaptation du dispositif au milieu hospitalier

Design of an intelligent multi-sensor medical device for the detection of low mobility.

Aimé Cedric MUHOZA, Emmanuel BERGERET, Corinne BRDYS and Francis GARY
Université Clermont Auvergne, CNRS/LPC, F-63000, Clermont-Ferrand, France
{aime-cedric.muhoza, emmanuel.bergeret, corinne.brdys, francis.gary} @uca.fr

Context and Objectives

In the context of chronic pain management, there is a need for a secure, autonomous, non-invasive wearable device able to collect sedentary data and monitor patients daily.

1. Detect and quantify sedentary and physical activity levels for patients with chronic pain.
2. Patient surveillance and evaluation of medical intervention efficiency.
3. Detailed result interpretation based on quantitative data.
4. Provide a learning tool that can be used to detect similar physiological patterns, characteristic behaviour or bio-markers from different subjects.

Methods and Materials

- Physical activity detection and data collection:
  - Activity detection using an Inertial Measurement Unit (IMU)
- Data processing and analysis:
  - An ARM-based (Cortex-M family) Micro-controller processes data and runs them through an embedded deep learning model for activity classification.
- Data transmission:
  - The model output is transmitted to a sink using a low energy module. *i.e Bluetooth Low Energy (BLE), LoRa*

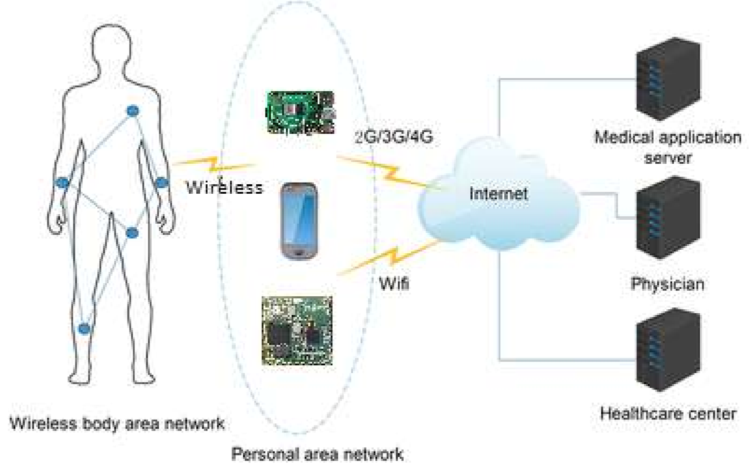

Figure 1:Body Area Network

Deep learning

The first model was built using a public dataset of data collected on smartphone with different subjects [1]

- Characteristics:
  - Multiple sensor data (Accelerometer, Gyroscope and Magnetometer)
  - Multiple positions (pockets, belt, upper-arm and wrist)
  - Collected at a frequency of 50Hz
- Feature Engineering and Extraction:
  - Data preparation and train-test split (80% - 20 % respectively)
  - Model training and accuracy evaluation using a DCNN Model (Deeep Convolutional Neural Network).[2]
- Deployment:
  - Model conversion to a C++ library using TensflowLite [3]
  - Inference run directly on Micro-controller

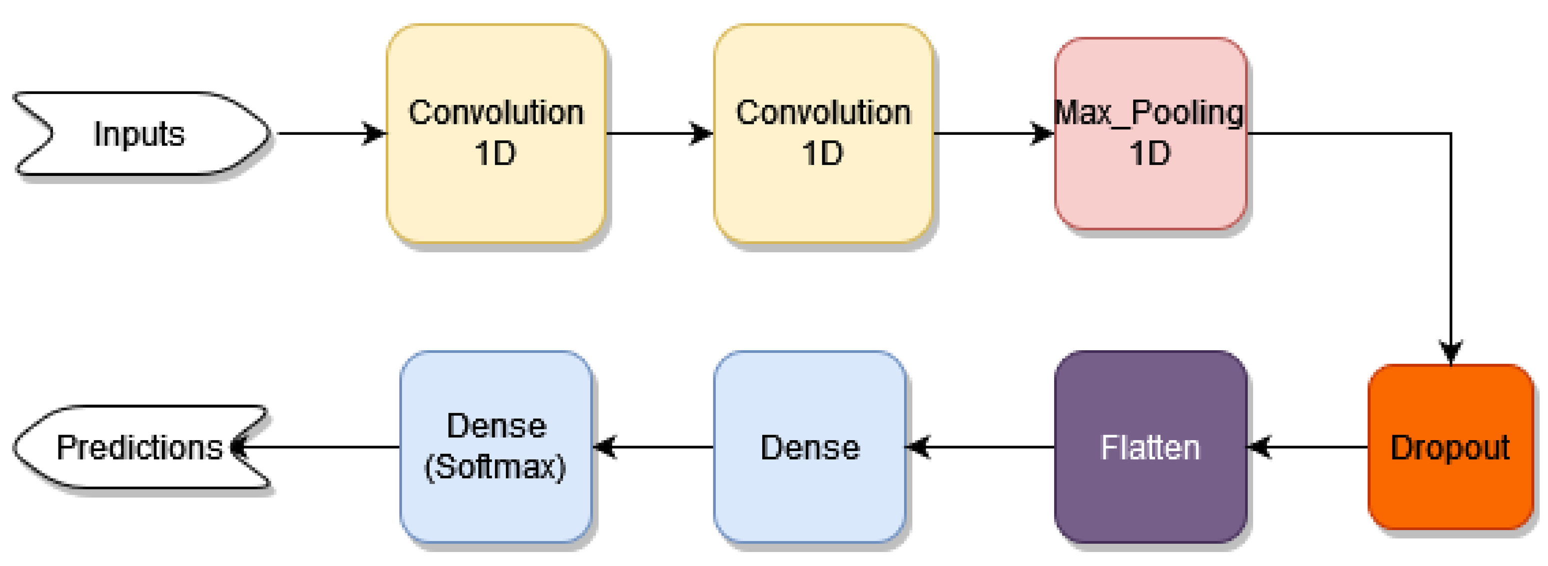

Figure 2:Model structure

Results: Model Features

- Feature selection:

Acc(x,y,z)	‖Acc‖	Gyr(x,y,z)	‖Gyr‖	Results
•	•	•	•	✗
		•	•	✗
•	•			✓

Table 1:Feature selection

**The use of magnetometer data in combination with accelerometer based data does not necessarily improve classification accuracy.*

- Model performance on a single position:

Position	Pockets	Belt	Upper-arm	Wrist
Accuracy	98.8%	95.7%	90.3%	94.6%

Table 2:Model accuracy on different positions

Results: Model Evaluation

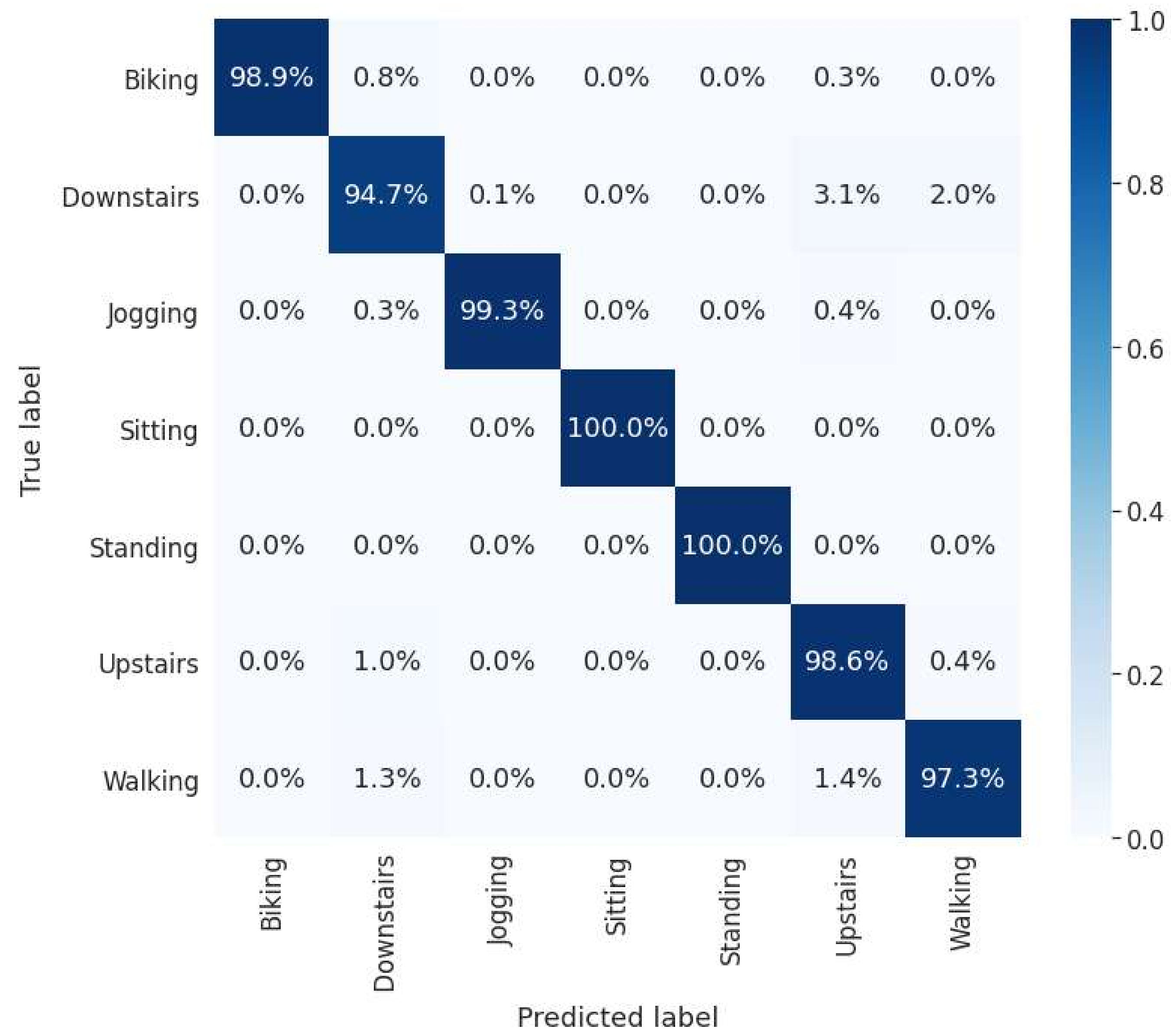

Figure 3:Inferences on test data

Data Collection

After a successful inference run using the model generated from public dataset, we conducted multiple data acquisition sessions on different participants performing complex daily activities.

- Data Collected:
  - Accelerometer data on 3 positions (Belt, Wrist and ankle)
  - High-Resolution video, Optical Motion data (Qualisys Track Manager)

Conclusion

- We proved that deep-learning algorithms can be used for human activity recognition even on resource constrained embedded systems whith good accuracy.
- Power consumption reduction by 10% using Embedded-AI versus Remote AI
- Creation of a custom dataset with complex gestures and multiple nodes, this dataset will be used in future studies.
- Future Work:
  - Defining an energy consumption model.
  - Generating a deep learning model with our data.
  - Use of distributed DCNN model on multiple sensors forming a BAN (Body Area Network)
  - Designing and building a custom device with optimized memory and enrgy consumption

References

[1] M. Shoaib, S. Bosch, O. D. Incel, H. Scholten, and P. J. M. Havinga, "Fusion of smartphone motion sensors for physical activity recognition," *Sensors*, vol. 14, no. 6, pp. 10146–10176, 2014.

[2] A. Mhalla and J.-M. Favreau, "Toward personalized human activity recognition model with auto-supervised learning framework," in *2021 IEEE International Conference on Multimedia and Expo (ICME)*, pp. 1–6, 2021.

[3] D. S. Pete Warden, *TinyML*. O'Reilly Media, Inc., 2019.

[4] M. Muaaz, A. Chelli, A. A. Abdelgawwad, A. C. Mallofré, and M. Pätzold, "Wiwehar: Multimodal human activity recognition using wi-fi and wearable sensing modalities," *IEEE Access*, vol. 8, pp. 164453–164470, 2020.

Algorithms for lattices

Thanh Loan NGUYEN

LIMOS, Universite Clermont Auvergne

Motivation

- Graph coloring problems with predictive learning in machine learning [Farber and Jamison, 1986]
- Finding two maximal "meta-concepts" separating two set of concepts $\mathcal{C}_\infty$ and $\mathcal{C}_\in$ formal concept analysis [Ganter et al., 2005]
- Generalization and specialization of first-order clauses in inductive logic programming [Nienhuys Cheng and Wolf, 1997]

Introduction

- Given a ground set, a closure system is a family of set that containing the ground set and closing under intersection. Its factors are referred to as closed sets. Closure structures are utilized in several fields of laptop technology such as propositional logic, database idea, combinatorial optimization or argumentation idea. Because of their size, closure structures are frequently encoded with representations like implication bases or meet-irreducible set.
- The half-space separation problem on a closure system, which has a wide range of applications including machine learning, formal concept analysis, inductive logic programming, etc. Unfortunately, however, Seiffarth et al. proved that this problem cannot be solved in polynomial time unless $NP = P$.
- The thesis aims at developing new techniques for half-space separation problem based on presentations of closure system and some parameters. Also, in order to improve time complexity, we build an approximation algorithm for feasible solutions.

Research objects

- Closure system $(X, \mathcal{C})$: finite ground set X with $\mathcal{C} \subseteq 2^X$ such that
  - $X \in \mathcal{C}$
  - $A \cap B \in \mathcal{C} \quad \forall A, B \in \mathcal{C}$
- Closure operator $\phi : 2^X \to 2^X$
  - $A \subseteq \phi(A)$
  - if $A \subseteq B$ then $\phi(A) \subseteq \phi(B)$
  - $\phi(\phi(A)) = \phi(A)$
- H closed if $H \in \mathcal{C}$.
- H is a half-space if H and $H^c = X \setminus H$ are closed.
- A and B are separable if there exists two disjoint closed sets $H_A, H_B \subseteq \mathcal{C}$ such that $A \subseteq H_A, B \subseteq H_B$.
- A and B are half-space separable if there is a half-space $H \in \mathcal{C}$ such that $A \subseteq H, B \subseteq H^c$.
- $M \in \mathcal{C} \setminus X$ is meet-irreducible if $M = C_1 \cap C_2$ where $C_1, C_2 \in \mathcal{C}$ implies $M = C_1$ or $M = C_2$.
- $\mathcal{C}$ can be reconstructed from the set $\mathcal{M}$ of all meet-irreducible elememts of $\mathcal{C}$.

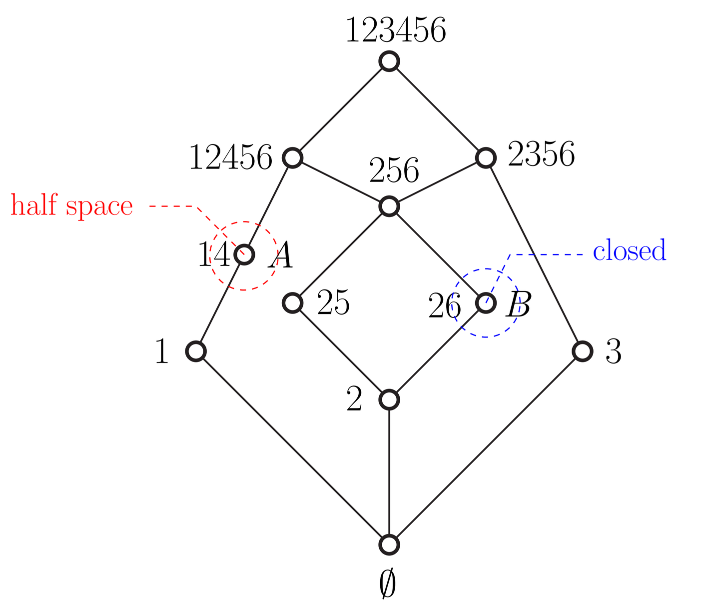

Figure 1: A closure system with two set A and B are half-space separable.

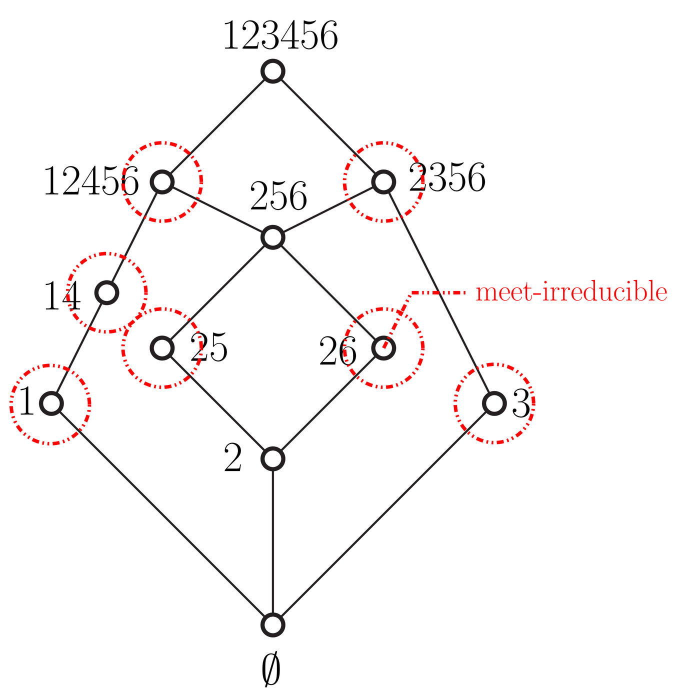

Figure 2: All meet-irreducible elements of a closure system.

Area of investigation

- Original problem: Half-space separation (HSS) problem (Seiifarth et al., 2019)
  - Given a closure operator (X, ϕ) and two subsets $\emptyset \neq A, B \subseteq X$.
  - Decide if A and B are half-space separable in $\mathcal{C}_\phi$.
- Hardness: The HSS problem is NP-complete.
- Methods to improve the problem:
  - Researching classes of closure systems where HSS is polynomial.
  - Using presentations of a closure system such as implication bases and meet-irreducible set.

Results

- Half-space separation problems using meet-irreducible (HSSM) problem:
  - Given a ground set X, meet-irreducible set $\mathcal{M}$ corresponding with closure operator ϕ and two disjoint subsets $\emptyset \neq A, B \subseteq X$.
  - Decide if A and B are half-space separable.
- Strategy
  - Construct a bipartite graph $G = (X, \mathcal{M}, E(G))$ with an edge $e \in E(G)$ connecting $x \in X$ and $M \in \mathcal{M}$ if $x \notin M$. (G. Markowski, 1975).

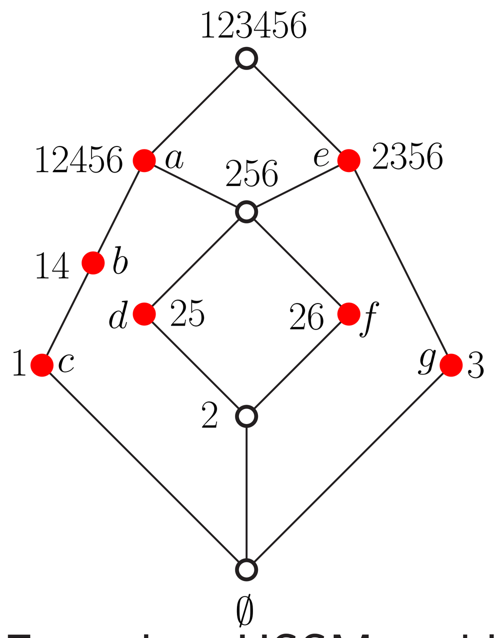

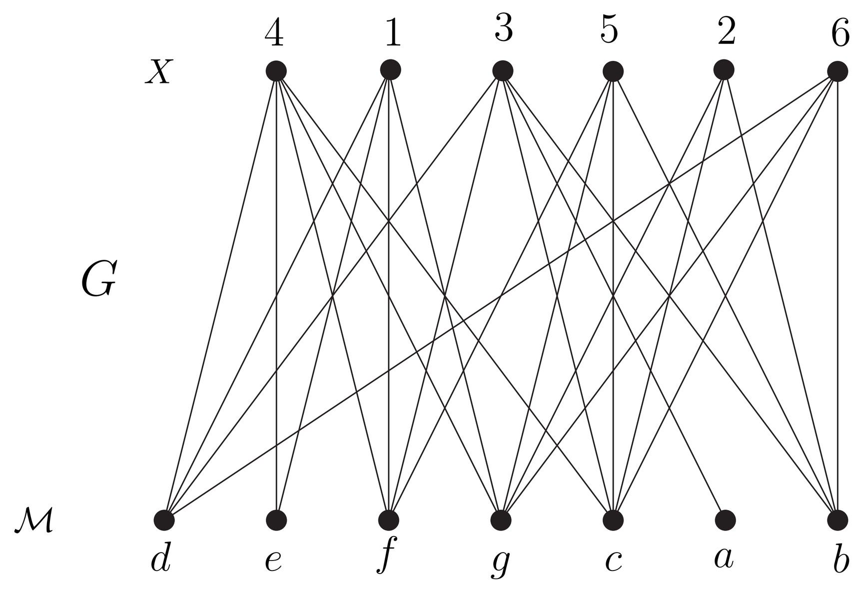

- Formulate HSSM problem as equivalent in bipartite graph.

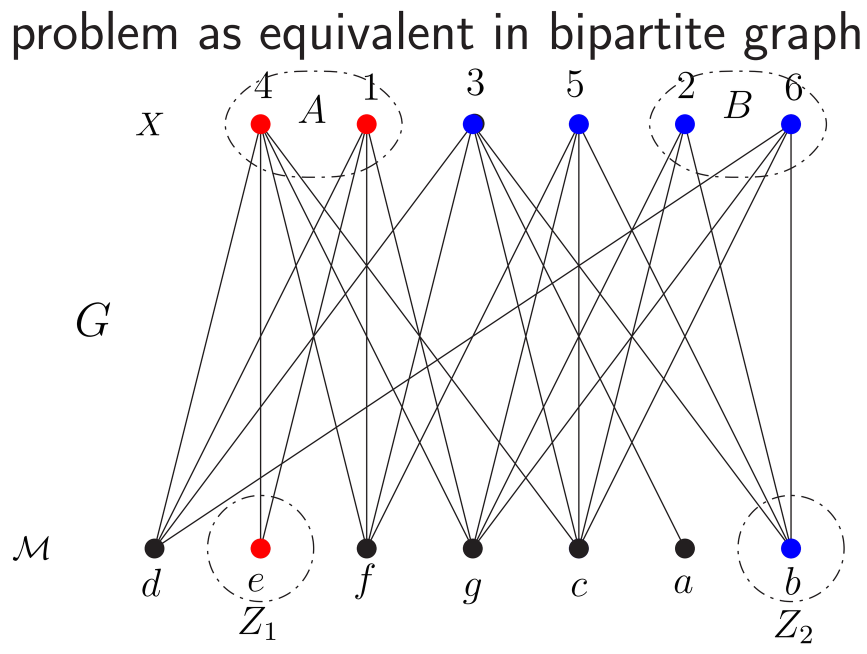

- Then, HSSM problem can be solved in polynomial time.

Further work

- From HSS problem to HSSM problem:
  - (Lawler et al., 1980) Enumerating all meet-irreducible $\mathcal{M}$ from closure operator (X, ϕ) can not be in polynomial time. This mean $|\mathcal{M}|$ can be exponential to $|X|$.
- Reduce the memory space of $|\mathcal{M}|$ by $|X|$:
  - Formulate HSSM problem: which constraints?
- Is there an approximation algorithm for HSS problem?

References

[1] Ganter, B.; Stumme, G. Wille, R., Formal Concept Analysis: Foundations and Applications, *Springer*, *Heidelberg*, 3626 (2015).

[2] Markowski. G, The factorization and representation of lattic, *Tran. AMS, 185-200*, 203 (1975).

[3] Seiffarth, F., Horvath, T., Wrobel, S.: Maximal closed set and half-space separations in finite closure systems, *In: Machine Learning and Knowledge Discovery in Databases - European Conference*, ECML PKDD 2019. LNCS, vol. 11906, 21 -37 Springer (2019).

Contact

- Mail: thanh_loan.nguyen@uca.fr
- Téléphone: 06.76.91.29.46

Generic Construction for Identity-based Proxy Blind Signature

Xavier Bultel[1], Pascal Lafourcade[3], **Charles Olivier-Anclin**[2,3], Léo Robert[3]

[1]LIFO, INSA Centre Val de Loire, Université d'Orléans, France [2]Be-Ys Pay

[3]Université Clermont Auvergne, CNRS, Mines de Saint-Étienne, LIMOS, France

École Doctorale des Sciences pour l'Ingénieur | Contact: charles.olivier-anclin@uca.fr

Contribution

This is a new generic construction for Identity-Based Proxy Blind Signature. Build upon two signatures schemes: a EUF-CMA blind signature and a SUF-CMA unique signature. This construction is practical and proven secure under the previous assumptions.

Signature and Unique Signature

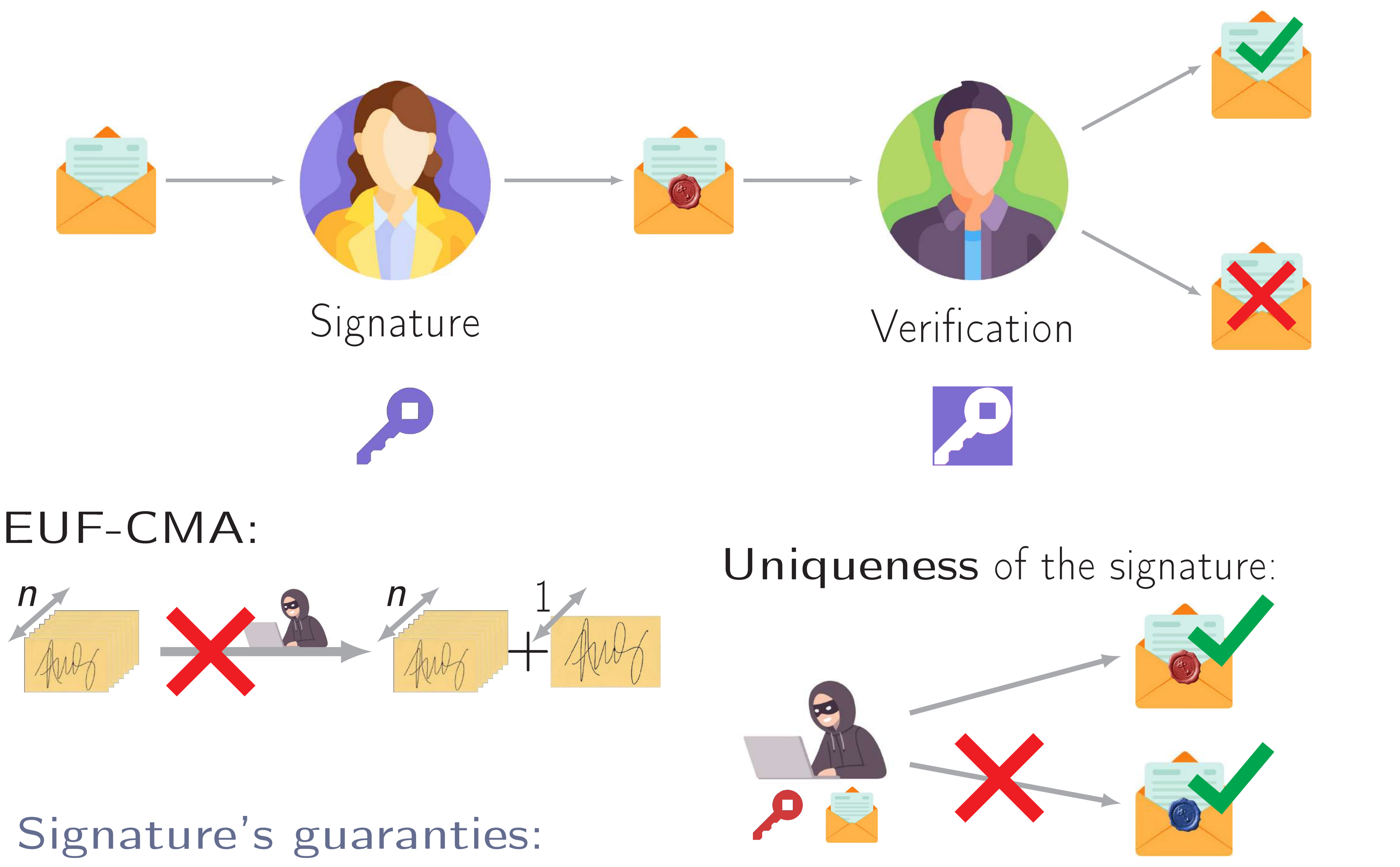

Signature's guaranties:

Authentication
Integrity
Non-repudiation

+ **Uniqueness** : computationally hard to output two different signatures for a message.

Identity-Based Cryptography [Shamir 1984]

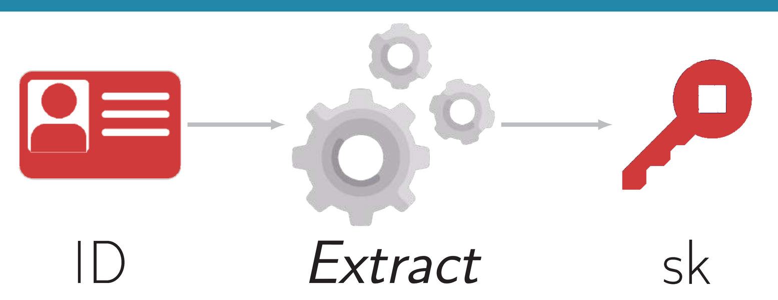

Blind Signature, *signature on a secret* [Chaum 1982]

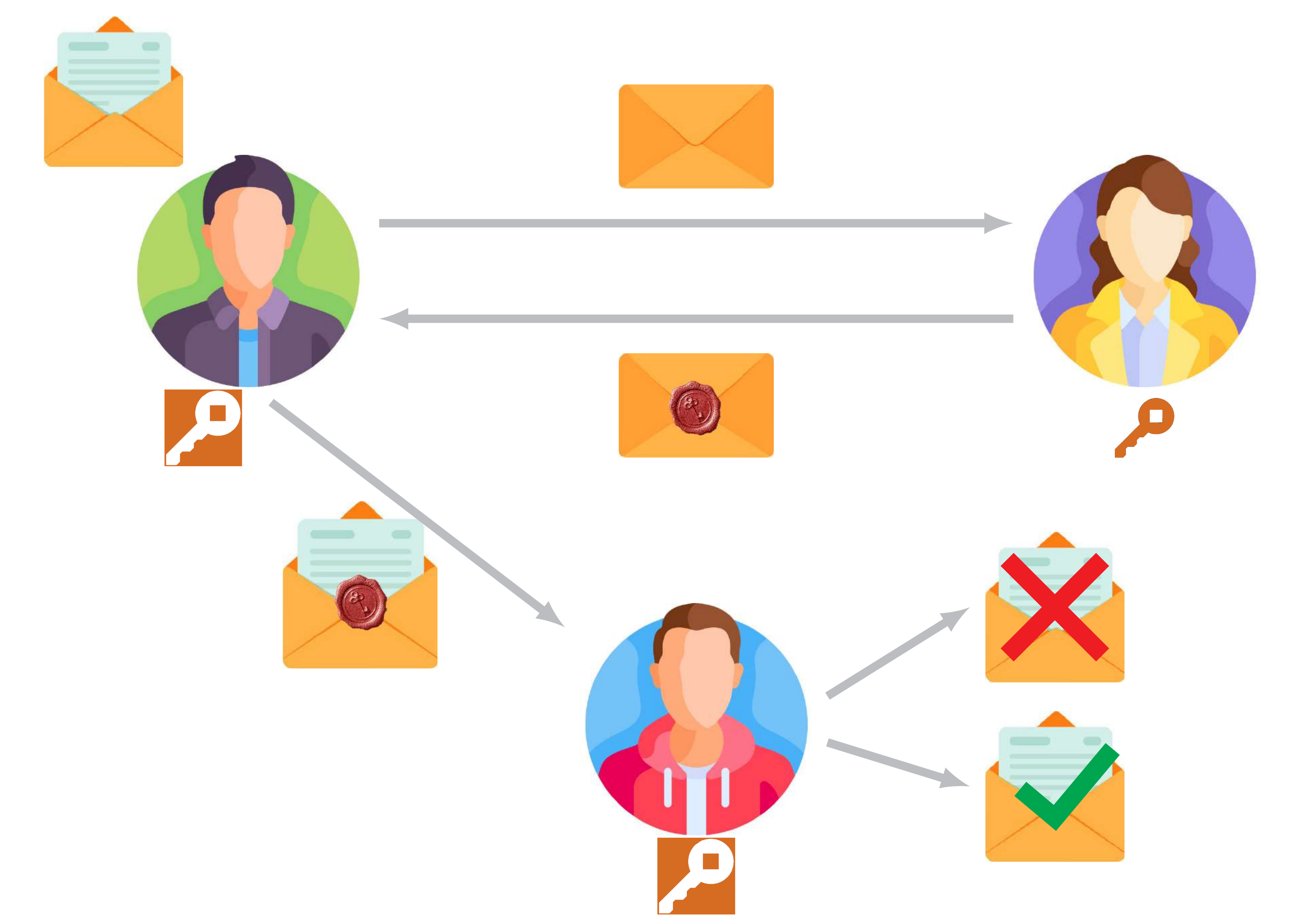

Security: **EUF-CMA** and **Blindness**

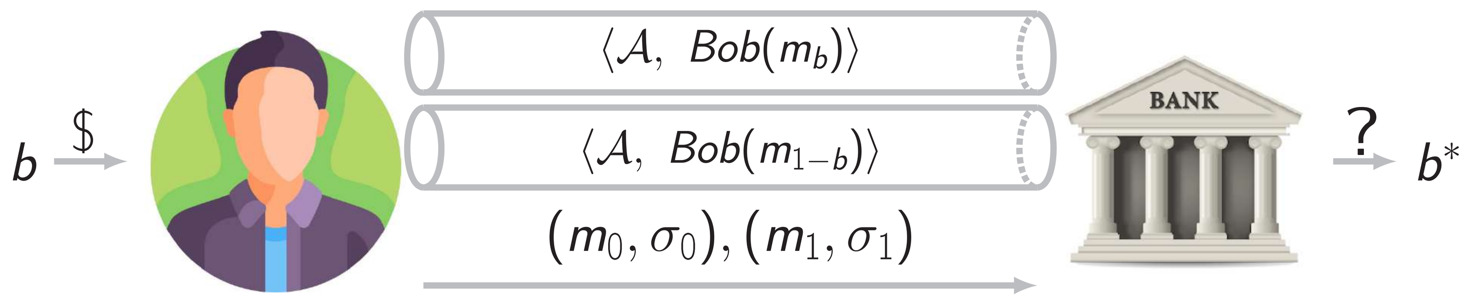

Unlinkability of **Alice** with respect to a **Message**, from the point of view of the **Bank**.

Constructions in the Literature

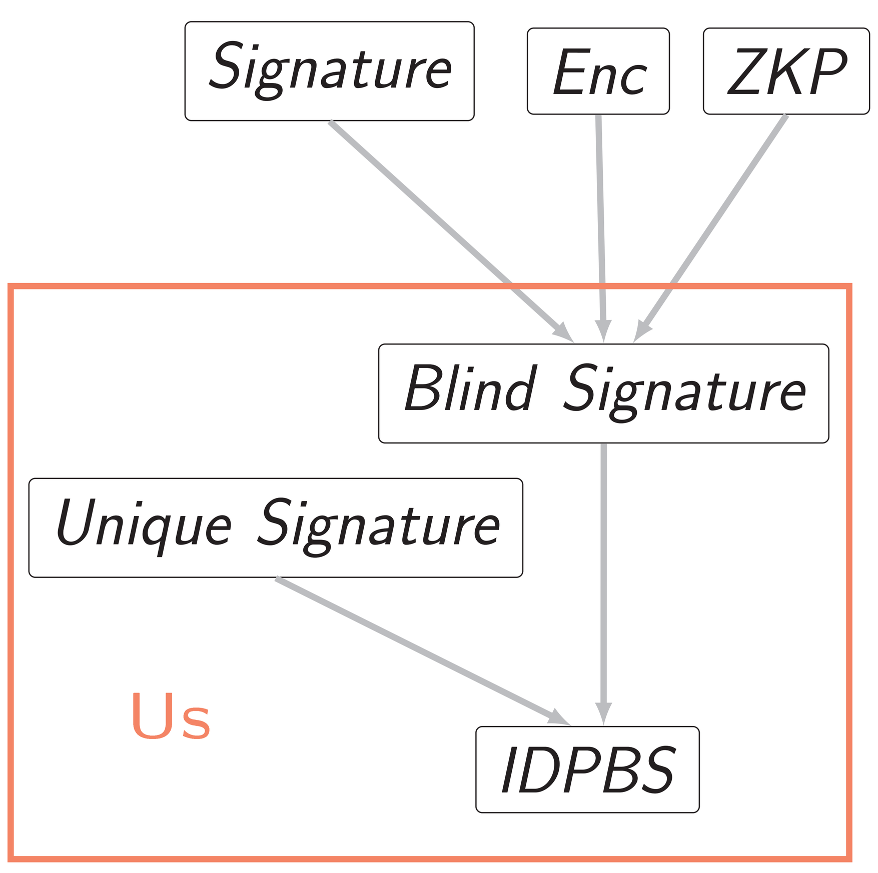

Security of the building blocks
$\implies$ Security of the construction.

Enabeling Proxy

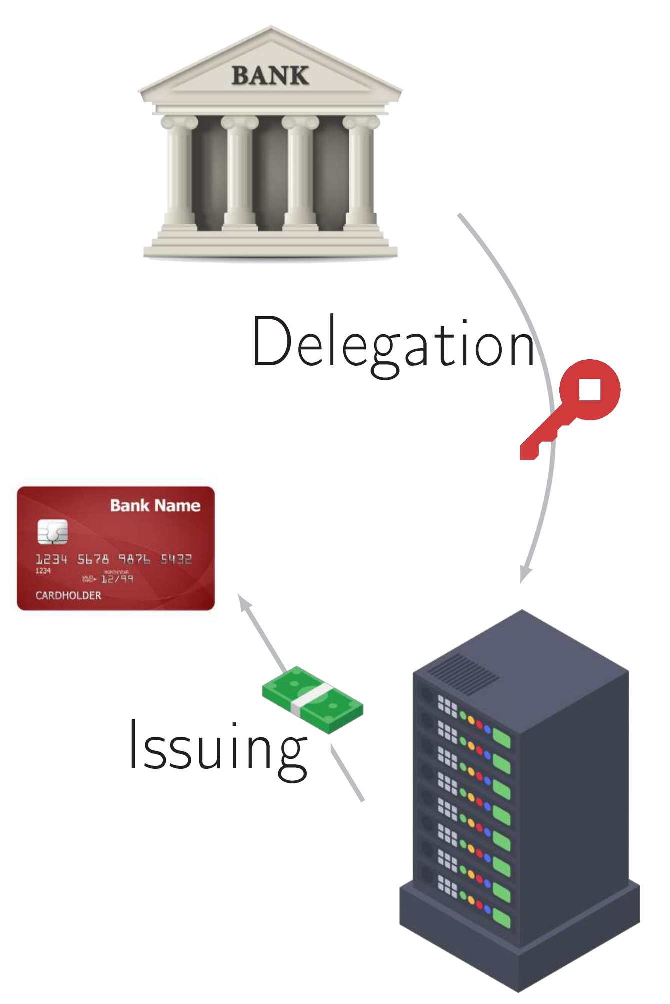

Generic Construction

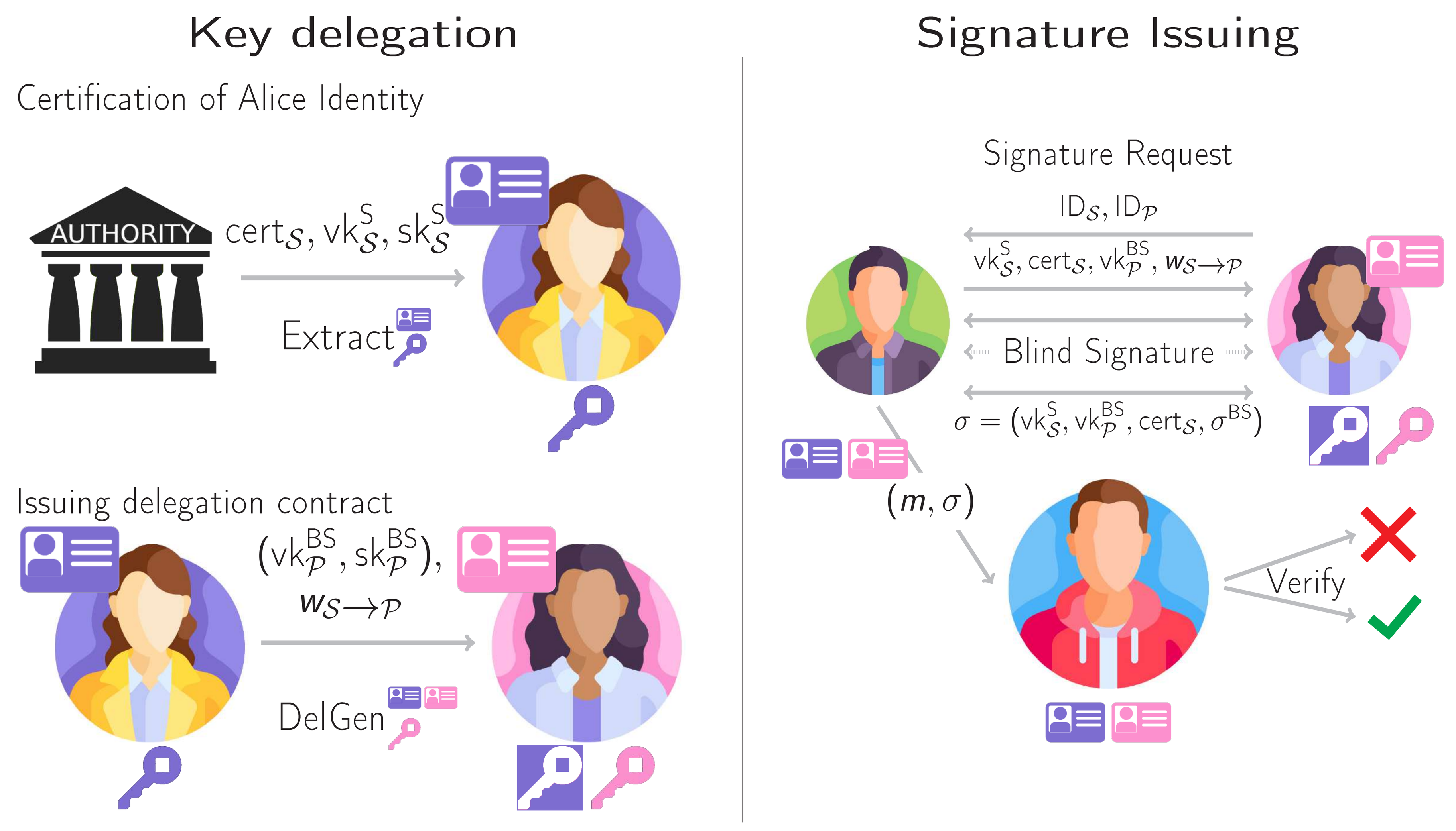

Formal Security Properties

Verifiability

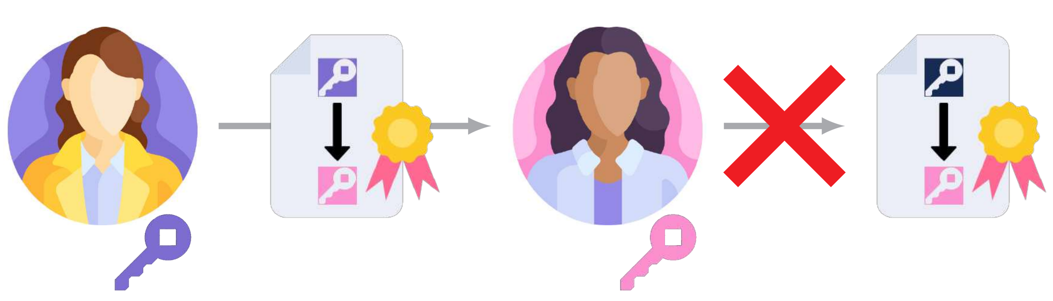

Prevention of Misuse

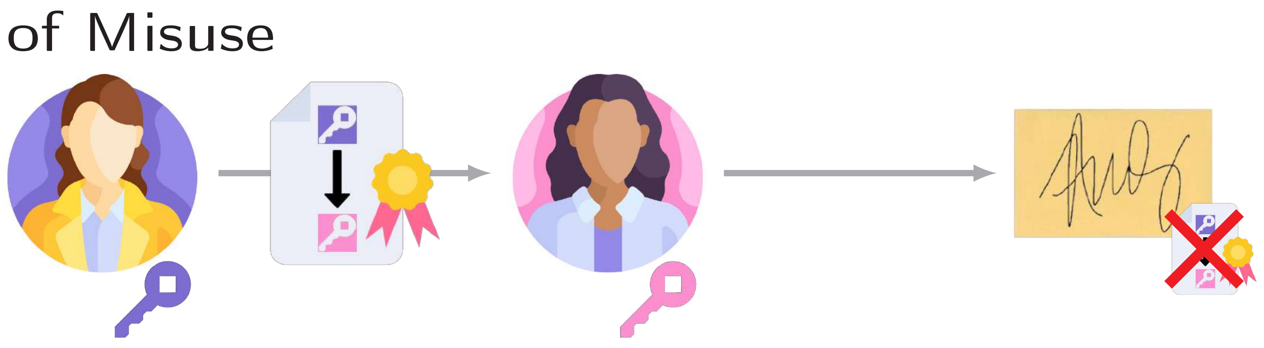

Strong Identifiability

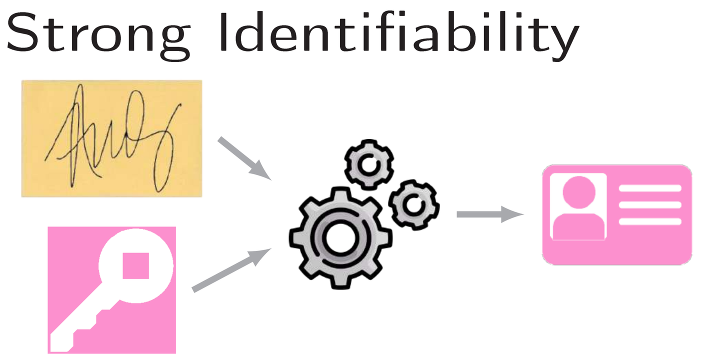

Strong Undeniability

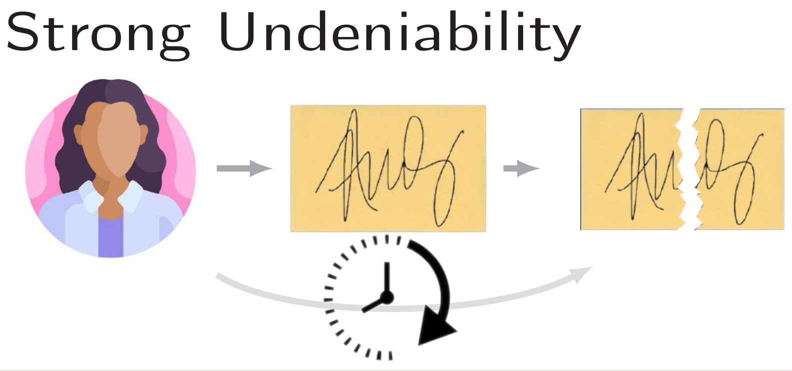

Efficiency

Signature issuing: (in number of execution)

	$\mathsf{Verif}_{\mathsf{S}}$	$\mathsf{Commit}_{\mathsf{BS}}$	$\mathsf{Blind}_{\mathsf{BS}}$	$\mathsf{Sign}_{\mathsf{BS}}$	$\mathsf{Unblind}_{\mathsf{BS}}$
User	2		1		1
Proxy signer		1		1	
Total	2	1	1	1	1

Verification:

	$\mathsf{Verif}_{\mathsf{S}}$	$\mathsf{Verif}_{\mathsf{BS}}$
Verifier	2	1

Notations:

$$\mathsf{BS} = (\mathsf{KeyGen}_{\mathsf{BS}}, \mathsf{Protocol}_{\mathsf{BS}}, \mathsf{Verif}_{\mathsf{BS}})$$

$$\mathsf{BlindSignature}_{\mathit{Protocol}} = (\mathsf{Commit}_{\mathsf{BS}}, \mathsf{Blind}_{\mathsf{BS}}, \mathsf{Sign}_{\mathsf{BS}}, \mathsf{Unblind}_{\mathsf{BS}})$$

Improvements:

- Boxes in Orange can be *executed only once* for a proxy signer.
  $\rightarrow$ Reduced computation
  $\rightarrow$ Less data to transmit
- *Round optimal* : minimum of communication can be reached.

Soft Robotics and Smart Materials

PhD Student:
Manuela OTTI

BACKGROUND: The thesis **"Smart materials for robotic dexterous manipulation"** aims at designing a multimaterial soft gripper which is capable of dexterous manipulations. The gripper integrates smart materials that optimize its functioning.

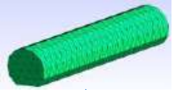

WORKFLOW:

- FEM model of 1 finger → Simulations and control using SOFA → Design of 1 finger
- Simulations and control using SOFA:
  - Inverse model control
- Design of 1 finger:
  - 3D printing
  - Molding and casting
- Real time control of designed finger:
  - Interfacing SOFA and arduino
- Repeat finger design process → Assembling of fingers to form the gripper:
  - Non anthropomorphic form
  - With an active palm
- Test and évaluations of the manipulations:
  - Real dexterity evaluation
  - Potential dexterity evaluation
  - Evaluation of the manipulator

A Soft Dexterous Manipulator integrating Smart Materials

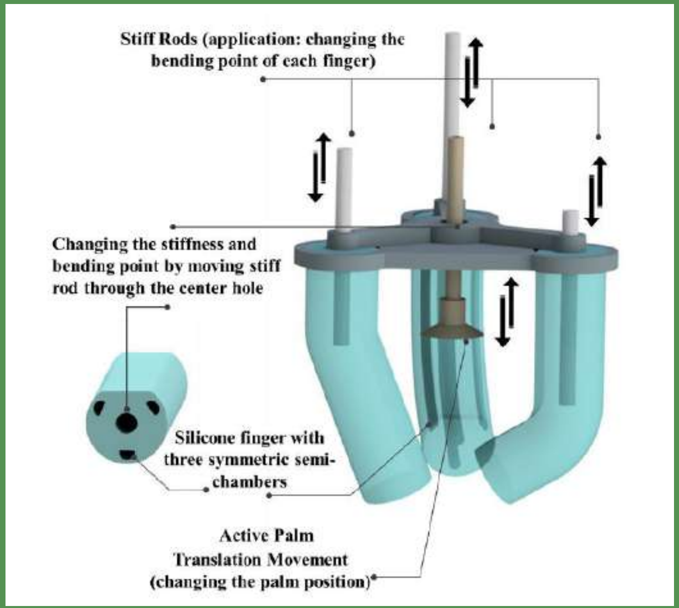

DOI: 10.1109/MRA.2020.3024283. Design and Optimization of a Dexterous Robotic Finger: Incorporating a Sliding, Rotating, and Soft-Bending Mechanism While Maximizing Dexterity and Minimizing Dimensions

Architecture:
- Non anthropomorphic artifiacial hand
- At least three soft fingers

Multimaterial structure for:
- Varying the form
- Varying the stiffness
- Auto perception

Tools:
- Catia v6 / FreeCAD
- Gmsh & Meshlab
- SOFA framework
- Python, C++, arduino

MANIMAT project supported by the ANR under the identifier : ANR-20-CE33-0005

What is Dexterity ?

The skillfull performance of tasks especially with the hands.

Types of Manipulations

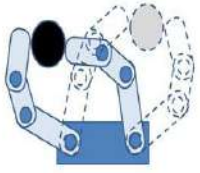

In-grasp manipulation

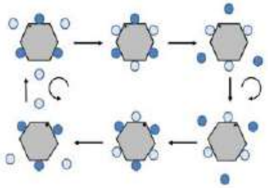

Finger gaiting

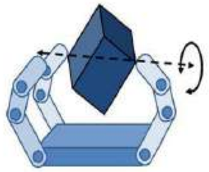

Finger pivoting

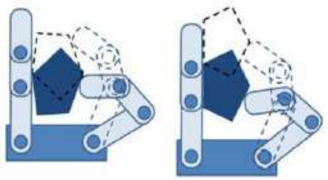

Rolling and Sliding

R. R. Ma y A. M. Dollar, «On dexterity and dexterous manipulation», en *2011 15th International Conference on Advanced Robotics (ICAR)*, Tallinn, Estonia, jun. 2011, pp. 1-7. doi: 10.1109/ICAR.2011.6088576.

Manuela OTTI, Frédéric CHAPELLE, Chedli BOUZGAROU, Yuri LAPUSTA.
Université Clermont Auvergne, CNRS, Clermont Auvergne INP, Institut Pascal, F-63000, Clermont-Ferrand, France

Proposal for a diagnostic methodology for railways tracks based on the fusion of data from multiple information sources

Ecole doctorale Sciences Pour l'Ingénieur

Jorge ROJAS VIVANCO [1, 2]

Pierre BREUL [1], Aurélie TALON [1], Sébastien BARBIER [2], Miguel BENZ-NAVARRETE [2]

[1] CNRS, Institut Pascal, Civil Engineering Department, Université Clermont Auvergne, Clermont-Ferrand

[2] Sol-Solution, Research and Development Department, Riom

Introduction

Under the effect of repeated solicitations, environmental problems (geotechnical and/or climatic), ageing, the railway infrastructures undergo a degradation which results in a loss of their initial mechanical characteristics. The consequences of these degradations are essentially geometrical defects which reduce the comfort of the users, the operation of the track and even the safety.

Exploitation → Geometrical defects

Problem

Railways diagnostic

The established diagnostic methods to take any action on the railway tracks are based on geometry measurements. They do not make clear the defects' origin of the track in terms of the participation of the elements that compose it.

Data Fusion

Several information, point and linear measurements, are available with specific uncertainty. More over the measurements are carried ont in different time, that can influence the evolution of the global state of railways.

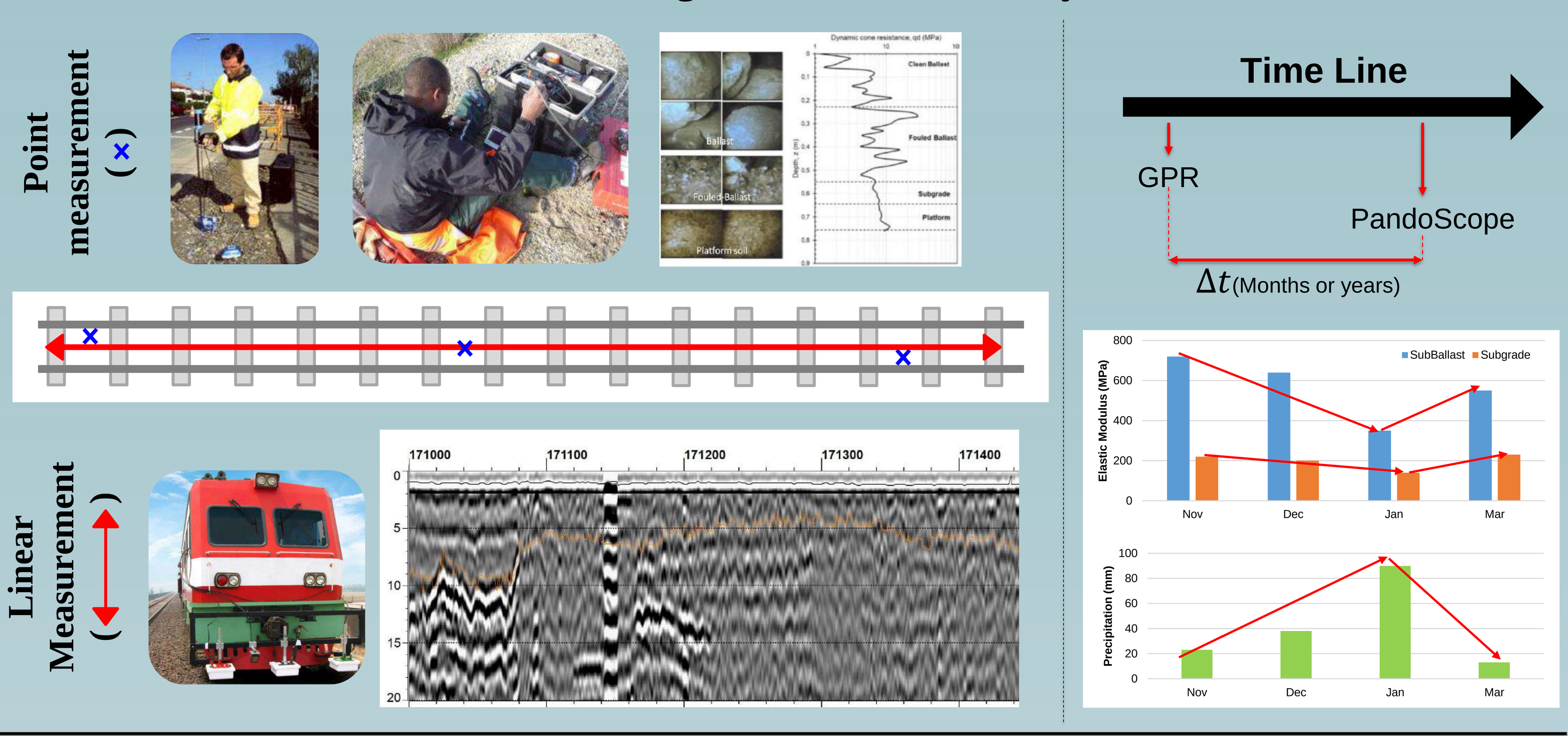

Objectives

Principal objective :

Proposal for a diagnostic methodology for railways tracks based on the fusion of data from multiple information sources.

Secondary objectives :

- ✓ To know the parameters influencing the behavior of the track + zone of influence + variability / uncertainties.
- ✓ To know the material, the processing methods, the interpretation methods + inaccuracies; to be associated to each parameter.
- ✓ To know the criteria and the associated thresholds, as well as the maintenance decision making methods (French and international).
- ✓ To propose a track condition index taking into account the knowledge of the three previous points.
- ✓ To develop a methodology leading to this index.
- ✓ To calibrate on cases where maintenance has been triggered.
- ✓ To validate on cases where maintenance has been triggered.

General methodology

Data acquisition

Geotechnical background information for data fusion | Other sources of information

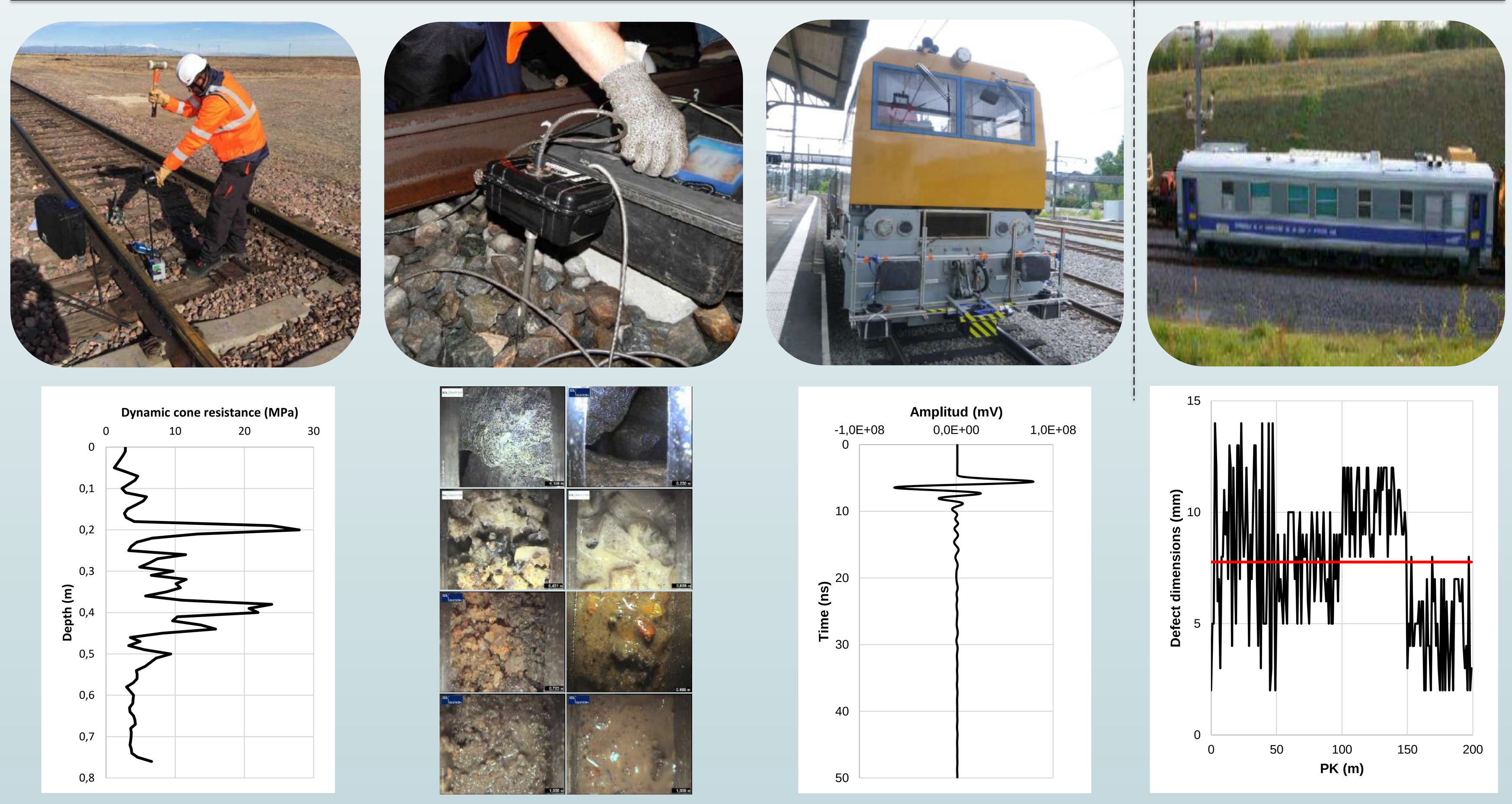

Data processing

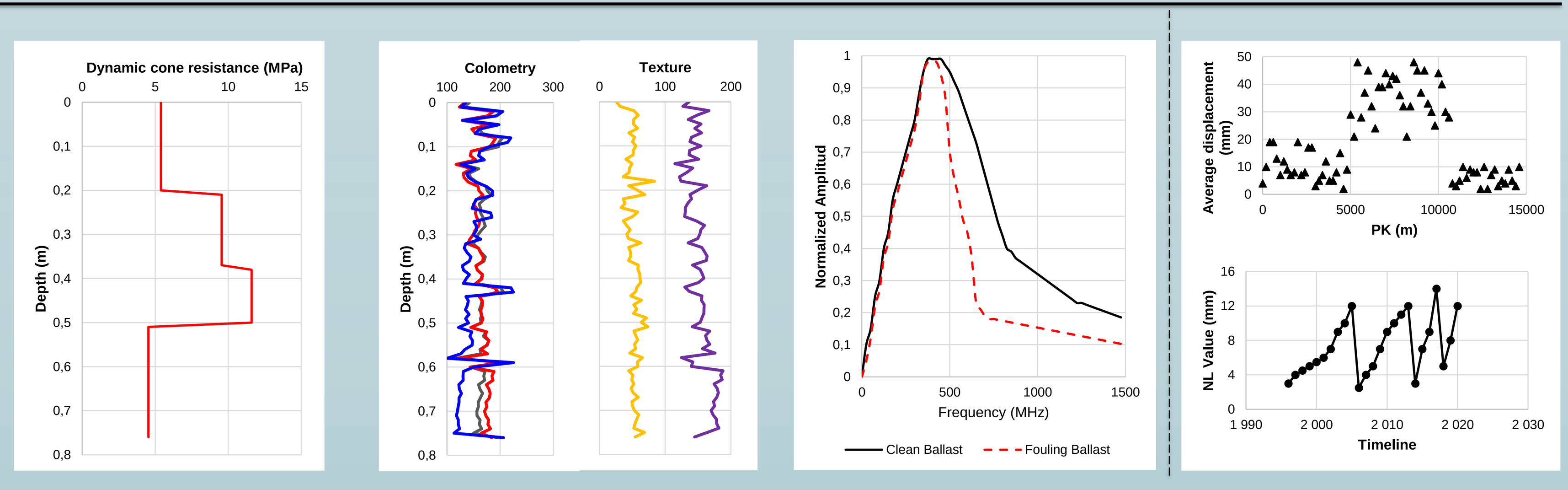

Data fusion

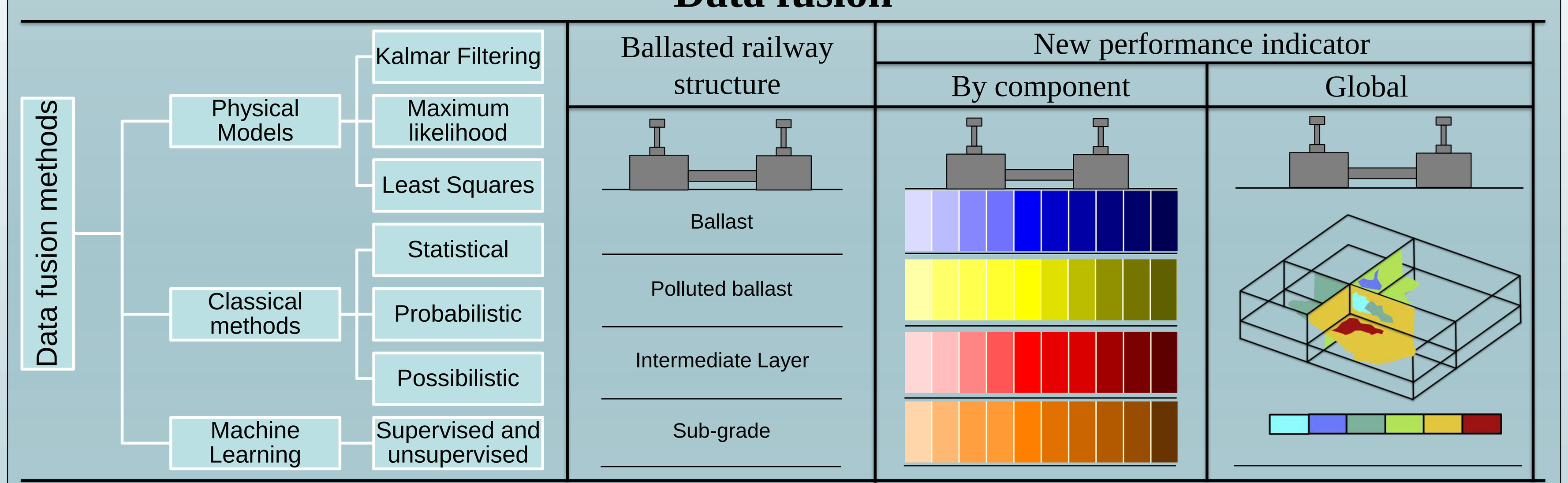

Work plan

First year

1. State of the art on railway diagnostic methods and data fusion methods.
2. Data processing and analysis.

Second year

Application of the different methods of fusion and geospatialization of information.

Third year

1. Validation of the methodology developed with the database and field campaigns.
2. Thesis writing.

Bibliography

1. Dezert, T. (2019). Combinaison d'informations ponctuelles et volumiques pour le diagnostic d'ouvrages en terre soumis à des risques hydrauliques. Ecole doctorale Ecologie, Géosciences, Agronomie et Alimentation - Université de Nantes.
2. Li, D; Hyslip, J; Sussmann, T; Chrismer, S. (2016). Railway Geotechnics. ISBN 9781119130536.
3. Duong, T; Cui, Y; Tang, A; Calon, N; Robinet, A. (2014).Assessment of conventional French railway sub-structure: a case study. Bulletin of Engineering Geology and the Environment. Doi: 10.1007/s10064-014-0575-y.
4. Sussman, T, Thompson, H. (2010). Methods to assess the impact of ballast condition on the track structure. ASTM Special Technical Publication. Doi: 10.1520/STP160520170036.
5. Klein, L. 2012. Sensor and data fusion: A tool for information assessment and decision making. SPIE PRESS. ISBN: 9780819491343.
6. Fourati, H; Iniewski, K. (2017). Multisensor data fusion: From algorithms and architectural design to applications. Taylor & Francis Group. ISBN: 9781482263756.

Graph learning methods to analyze and support industrial resilience

Kévin CORTIAL

Supervisors : Adélaïde ALBOUY KISSI – Frédéric CHAUSSE

Open Studio – Institut Pascal – Université Clermont Auvergne - CNRS - Clermont Auvergne INP

Context

Graphs are increasingly used to describe interactions between entities. They are based on a simple formalism that nevertheless allows complex systems to be modelled. Thus, in many domains, graphs can represent different aspects of the real world. In this context and **based on open source data, knowledge graphs representing industrial ecosystems have been built.**

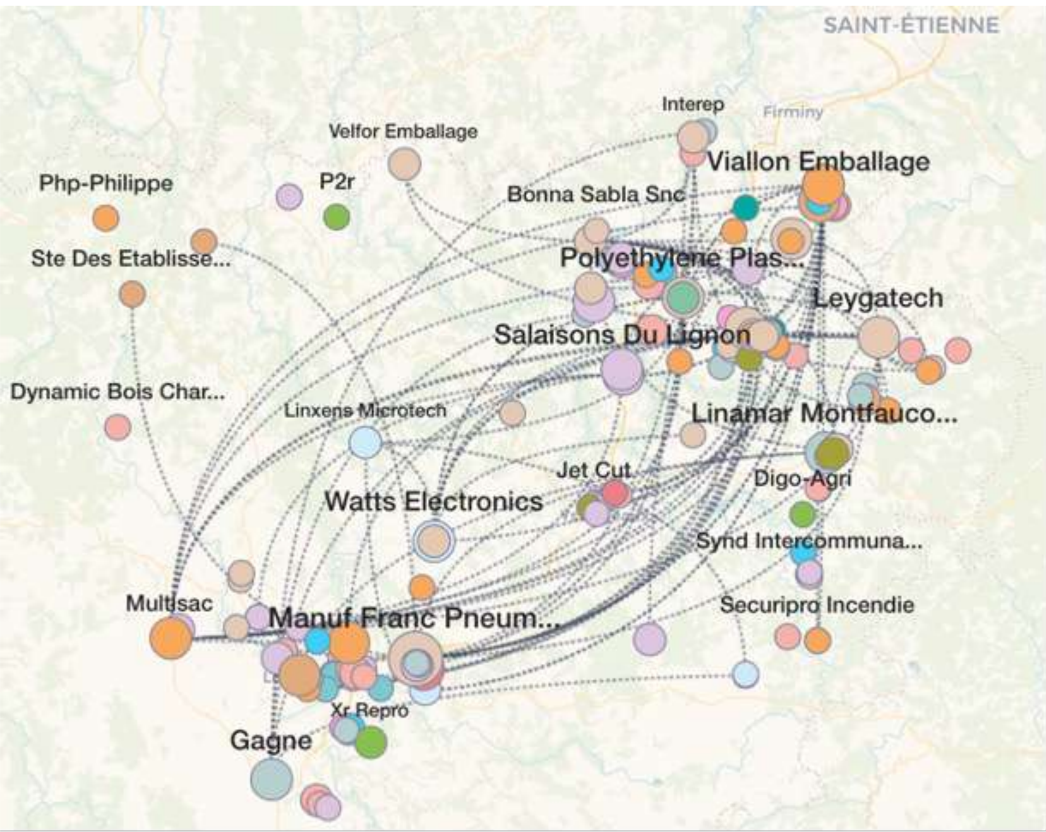

Learning on graphs requires **revisiting the usual artificial intelligence methods, as these unstructured data are complex to analyse.** Economics already uses methods from graph theory to describe and study the relationships between economic agents in networks. In this PhD, **we develop new learning methods for economic graphs** with the latest advances in graph learning.

Objectives

– **Classification of nodes** will allow identification of key players in economic network.

– **Clustering** to group and detect industrial communities with similar properties.

– **Prediction of links** that do not yet exist between two nodes. Predicting a connection between two entities could be seen as a recommendation system.

Methods

Machine and deep learning methods for graphs compute vector embeddings for each node to obtain better representations in their environment. With this new data for each node, graph learning is effective for many tasks, such as link prediction, community detection and node classification.

Graph Neural Networks

GNNs have made the hypothesis that many pieces of node's information reside in its neighborhoods. To store this data, we use node embedding which gathers the neighborhoods information with neural network.

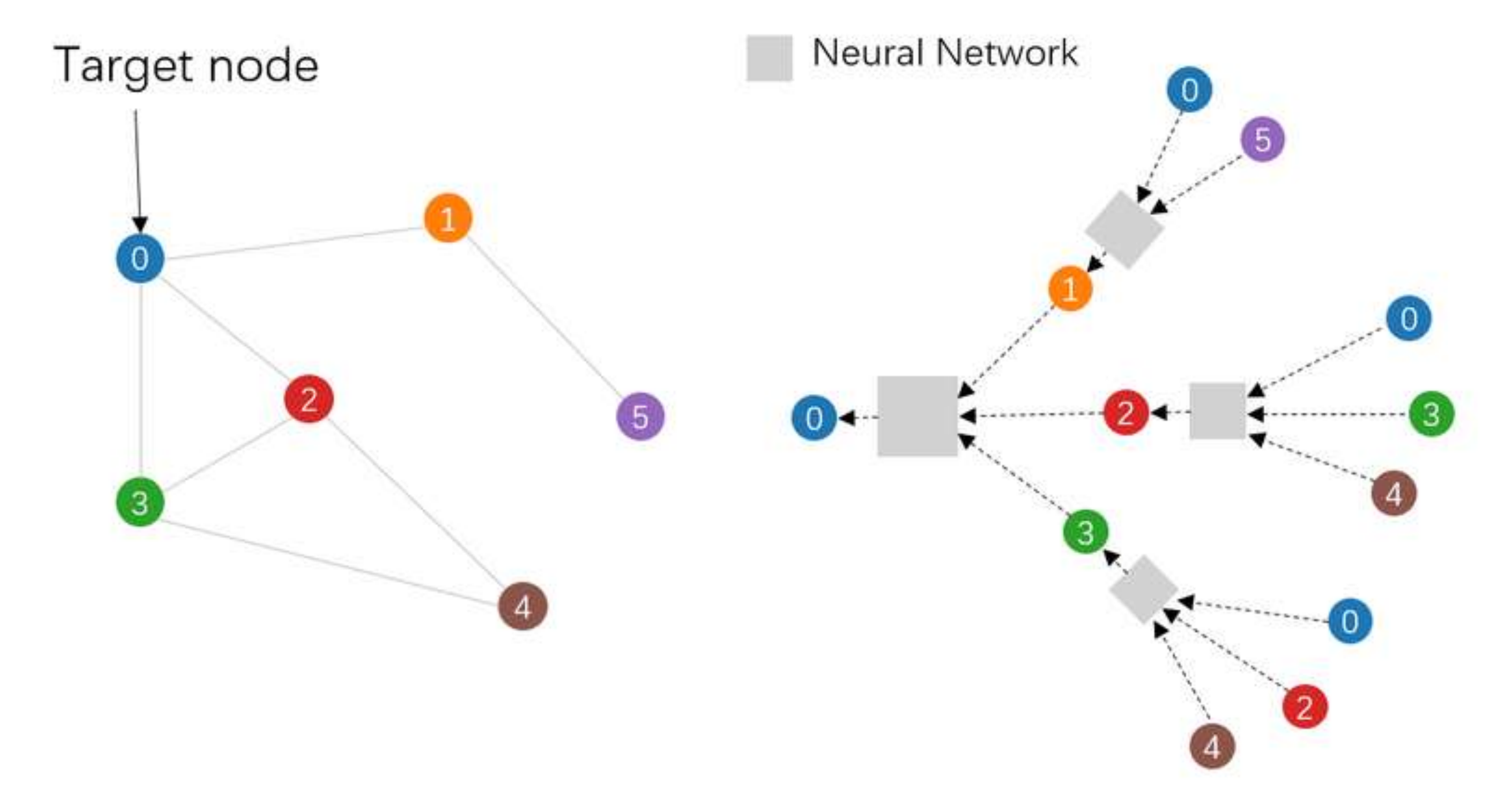

(a) Input graph

(b) Neighborhood aggregation

Graph Attention Networks

Like GNN, Graph Attention Networks (GAT) use data contained in these neighbors to create embeddings for each node. The difference in GATs is the use of the **attention mechanism to select the importance to be given to each neighbor** (like Transformer models).

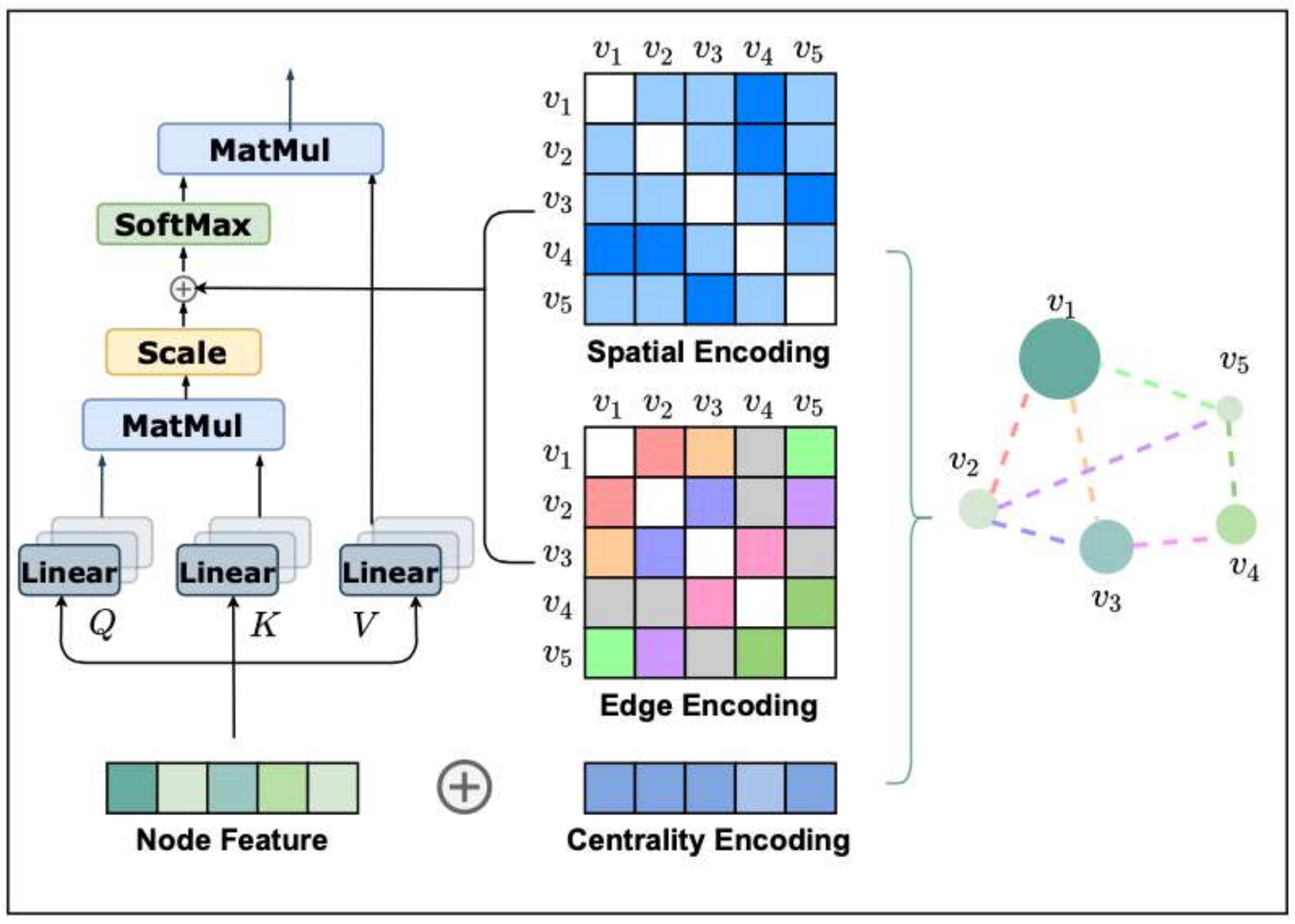

GAT aggregates information present in the neighborhood of a node by a weighted sum as an attention mechanism.

- First, GAT calculates an attention coefficient for each neighbor of the node in question (node features).
- Then, GAT must integrate edge data according to their number (centrality).
- Finally, if the nodes position in the graph is important, GAT will consider this position data (spatial encoding).

The adaptation of the GAT architecture, presented above, requires the addition of all graph's information at self-attention layer.

Perspectives

If we have historical data over several years, we can work on the analysis and evolution over time of economic graphs. In this context, we could investigate **Temporal Graph Networks** (TGNs), a deep learning model on dynamic graphs represented as sequences of timed events.

During this PhD, we could test combinations of new artificial intelligence or statistical concepts into GNN. The goal would be to improve the performance perhaps but especially to make graph learning models more explainable and interpretable for the economic world.

There are many research perspectives on these methods and their fields of application. For example, chemistry and biology use these models to analyse molecular graphs. **Social networks** are already using these methods for their **recommendation systems** but also in e-commerce.

Bibliography

Kipf, Thomas N., et Max Welling. 2017. « Semi-Supervised Classification with Graph Convolutional Networks »

Schlichtkrull, Michael et al. 2018. « Modeling Relational Data with Graph Convolutional Networks »

Vaswani, Ashish et al. 2017. « Attention Is All You Need »

Veličković, Petar et al. 2018 « Graph Attention Networks »

Ying, Chengxuan et al. 2021. « Do Transformers Really Perform Bad for Graph Representation ? »

Zhang, Muhan et Yixin Chen. 2018. « Link Prediction Based on Graph Neural Networks »

Analyzing of microservice-based systems, repairing for better reliability, performance and security

Ecole doctorale Sciences Pour l'Ingénieur

Jarod SUE

Phd Supervisor : Sebastien SALVA

Co Supervisor : Laurent PROVOT

Introduction

- Microservice is a ccomplex web architecture composed of small interdependant programms interacting together.
- Testing them is known to be hard.
- Developping new approach to generate tests automatically
- Using them to automaticallyy repair microservices based on reliability tests, performance tests, security tests.

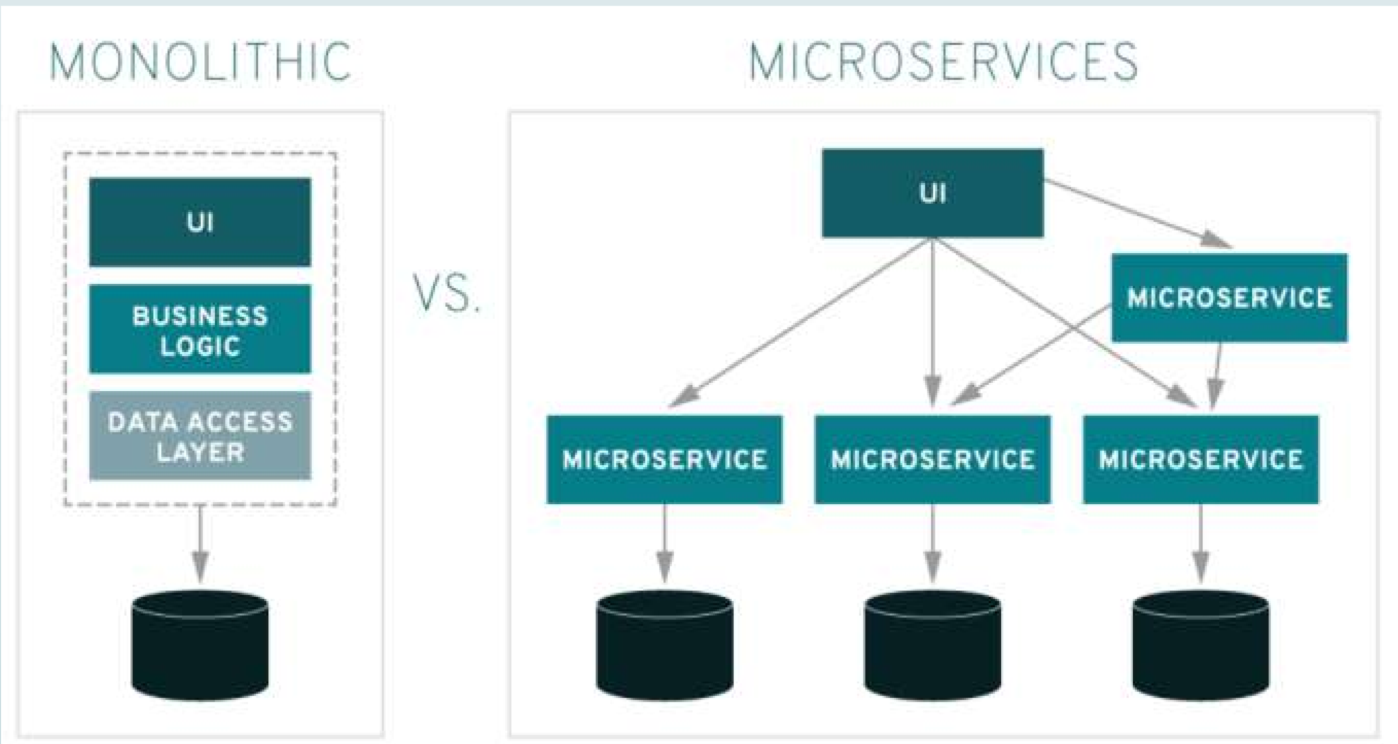

Example of a microservice architecture compare to a monolith one

The approach

- New approach : generate tests directly from event logs
- Mutate this tests in order to test their quality and create new logs
- Use them to improve the system

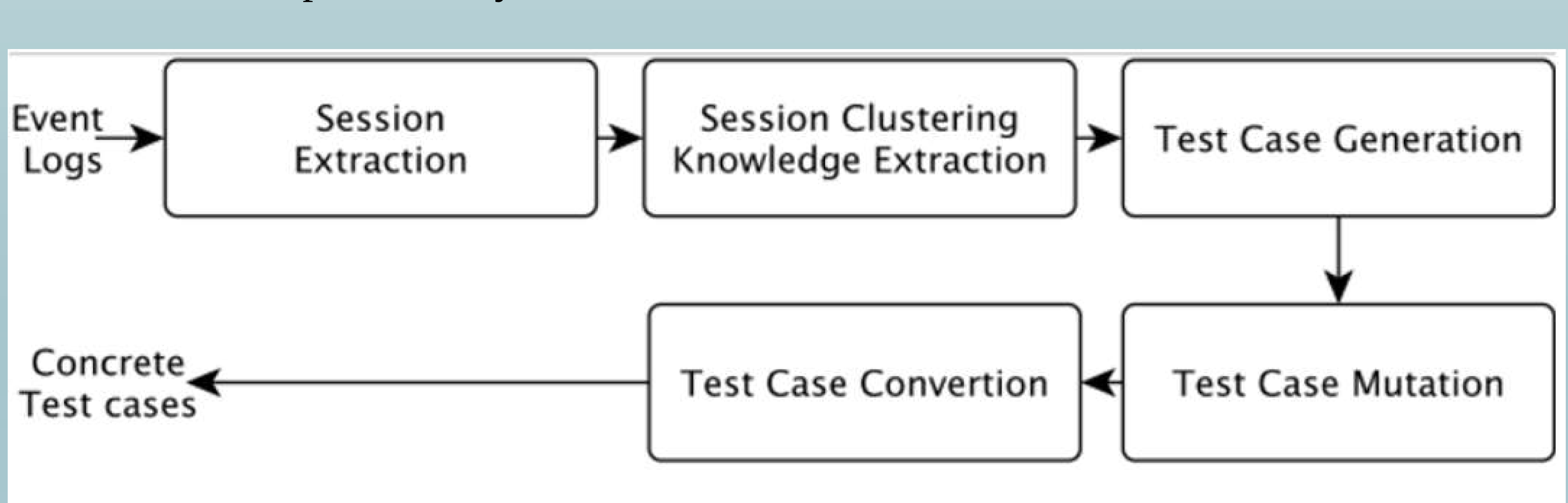

Action plan to create tests

Session Extraction

- Logs are not processed
- Find the sessions by means of correlation patterns and correlation keys
- Use a quality meter to get the most interessant one

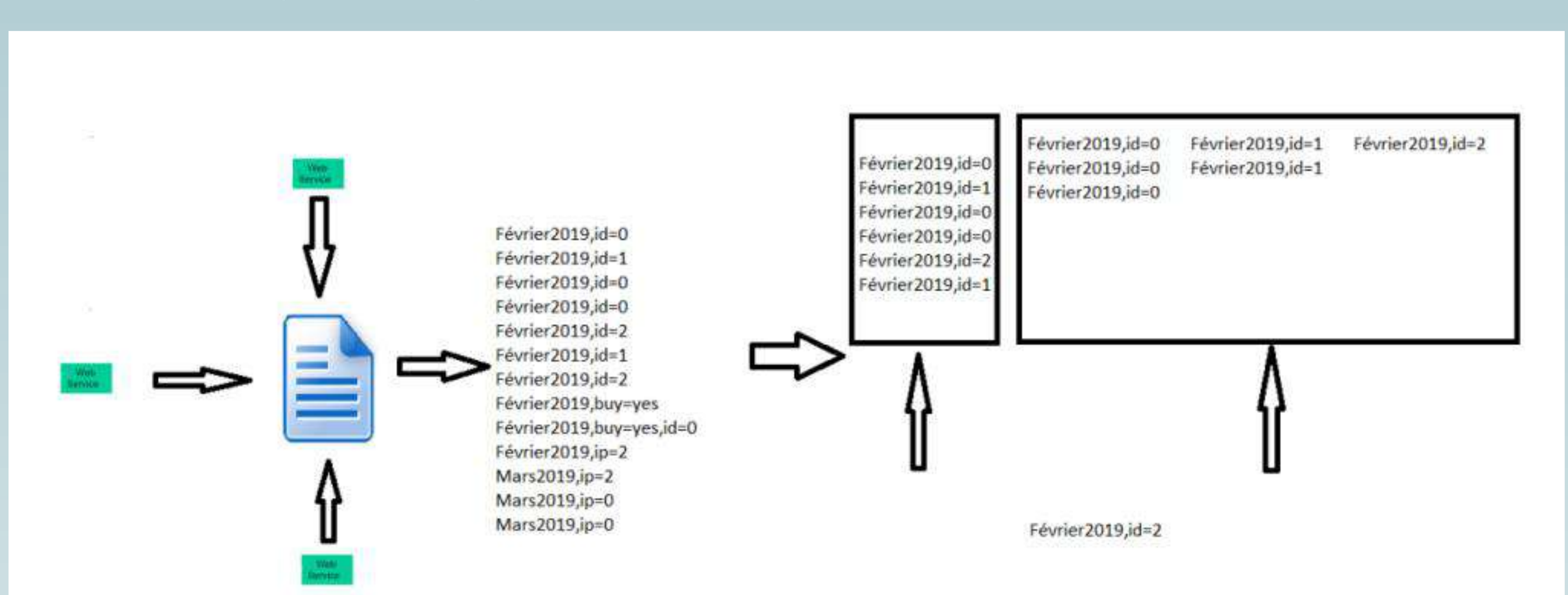

Example of a conversation extraction

Session Clustering and Data extraction

- Use business knowledge and rules following a When something happen, then it is something pattern.
- Cluster the sessions by this knowledge.
- Abstract the sessions.

Test Case generation

- Sort the clusters by their quality.
- Create tests from the cluster with the most quality.
- Repeat

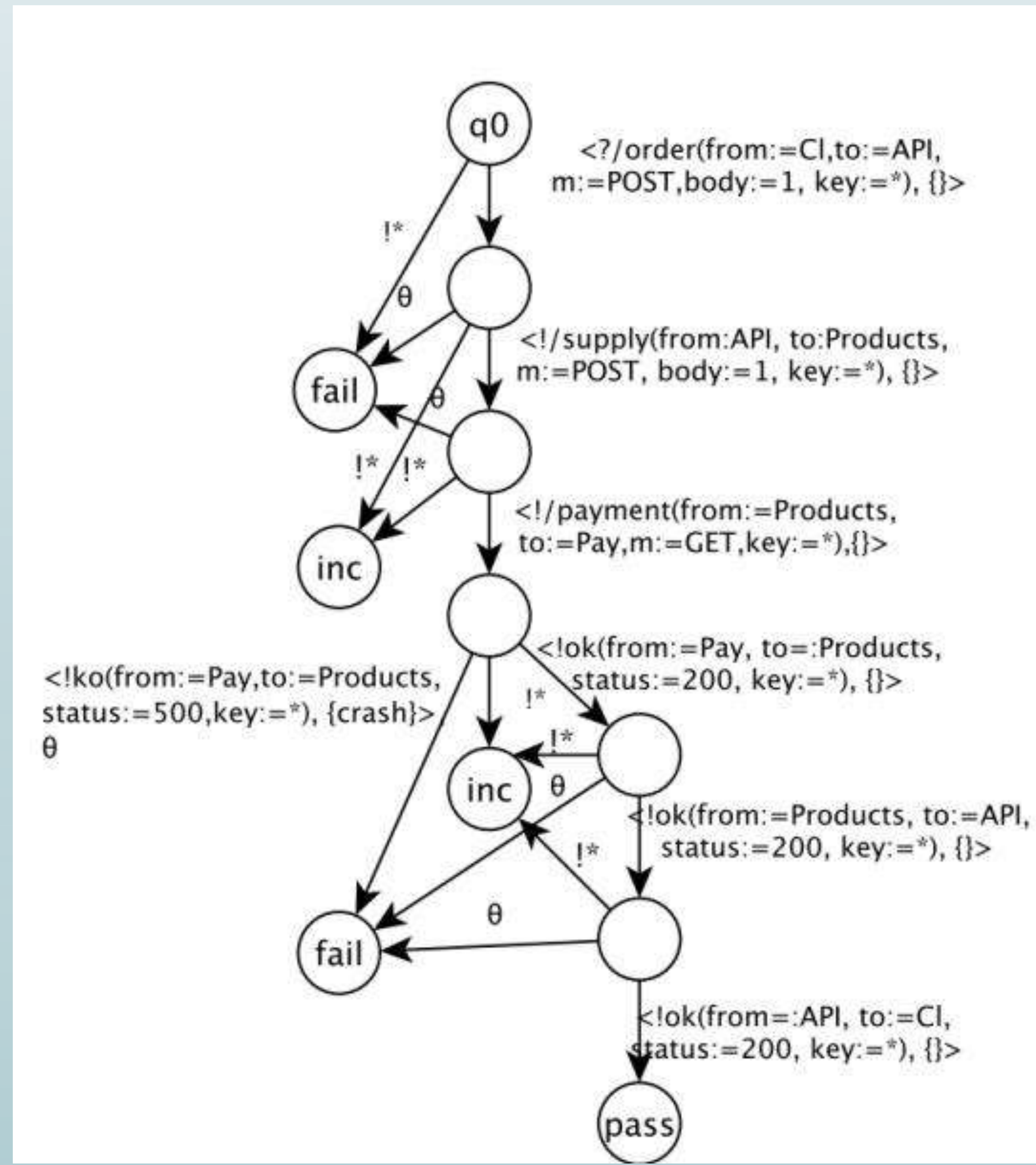

Example of a test case

Test Case Mutation

- Use mutation operators to mutate the test case
- Mutation operators are small changements to the tests case : event duplication, event removal ...

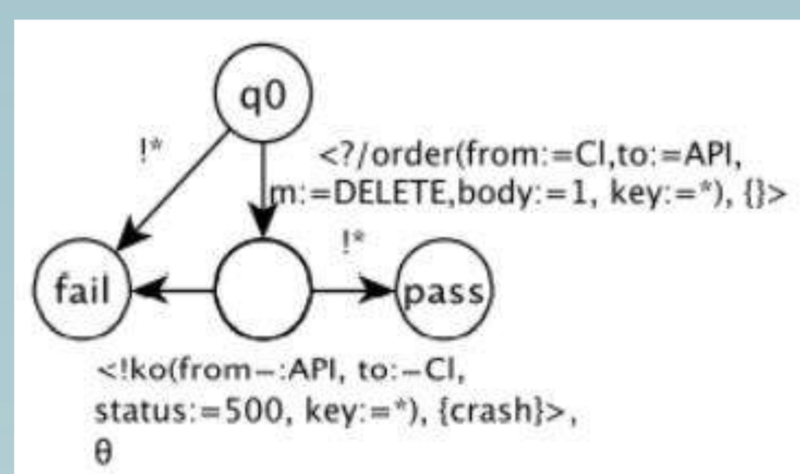

Same test case as before but with a mutation operator "Verb Change" applied

Results

- Already 2 scientific papers published
- Experimentations show that our approach perform well in practice
- Need more testing for the generation

	Correlation Key Set Recall	Correlation Key Set Precision
S1	100%	81%
S2	100%	76%
S3	100%	80%
S4	100%	100%
S5	100%	100%
S6	100%	90%

Table representing the performance of our session extraction

Conclusions

- Entirely new approach at Test Case Generation
- Algorithms performs well in practice
- Future work can be in a variety of fields ranging from security to robustness

Evaluation of inner soil behavior in head-fixed double sheet-pile method using X-ray CT

Hideharu Sugimoto[1)3)], Ayaka Nasu[2)] Hideki Nagatani [2)]Jun Otani[1)]

1) Graduate school of Science and Technology, X-earth center, Kumamoto University, Japan

2) Kajima institute research, Tokyo, Japan

3) Université Clermont Auvergne, CNRS, Institut Pascal, Clermont Ferrand, France

Directeur de thèse : Pierre BREUL, Bastien Chevalier

Introduction

As the new construction method in Japan, double sheet-pile construction method is developping[1)]. This method is that the head of two sheet-piles are connected, and we aim more the twice displacement control effect compare with than only two sheet-pile. In the case of using this method, soils between two sheet-pile (called 'inner soil') is very important to consider the entire strength. In this research, using microfocus X-ray CT, the behavior of inner soil was observed and quantitative evaluation with image analysis.

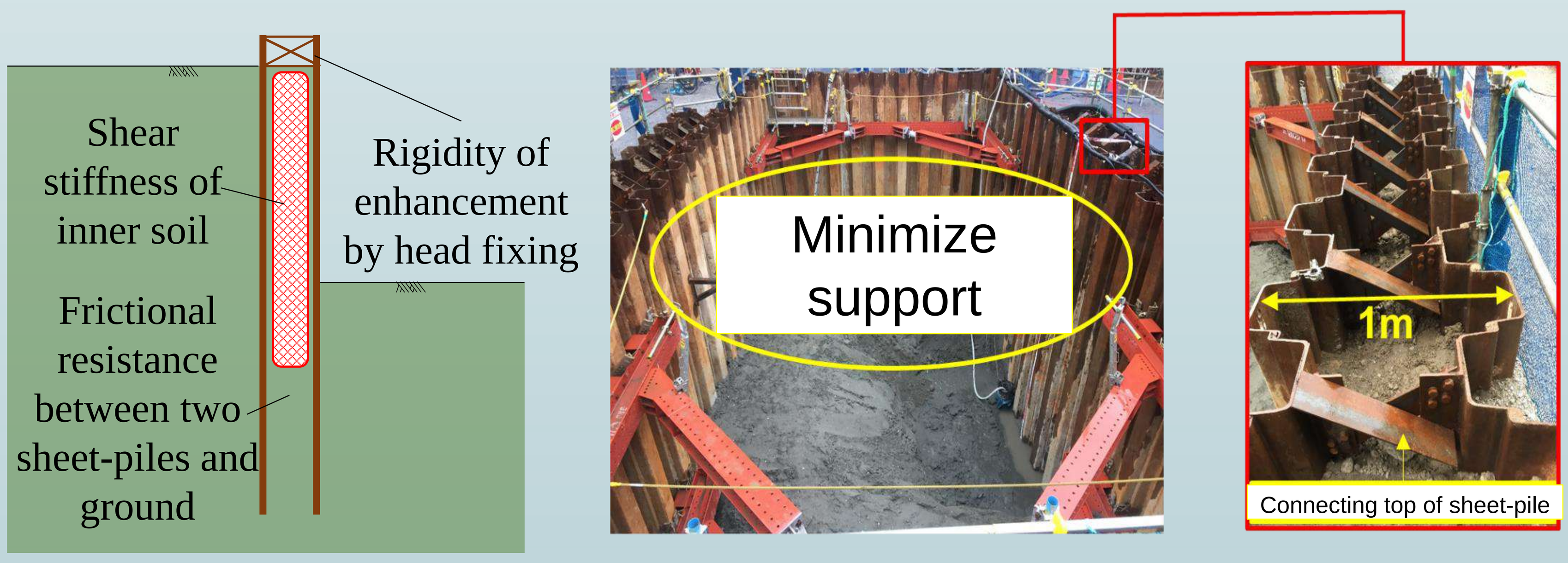

Methods

What is X-ray CT ??

X-ray CT method is a computer tomography method that utilizes the X-ray absorption rate and permeability of an object[2)].(Computed tomography) Since there is an approximate linear relationship between the X-ray attenuation coefficient after passing through the object and the density of the object, it is possible to visualize the density distribution inside the object.

For example, in the geotechnical engineering, we can observation the behavior inside soil and specimen as the difference the density. Images are made black and white colar. And from obtained image, we can apply the image analysis and calculate the displacement and strain (Degital Image corralation).

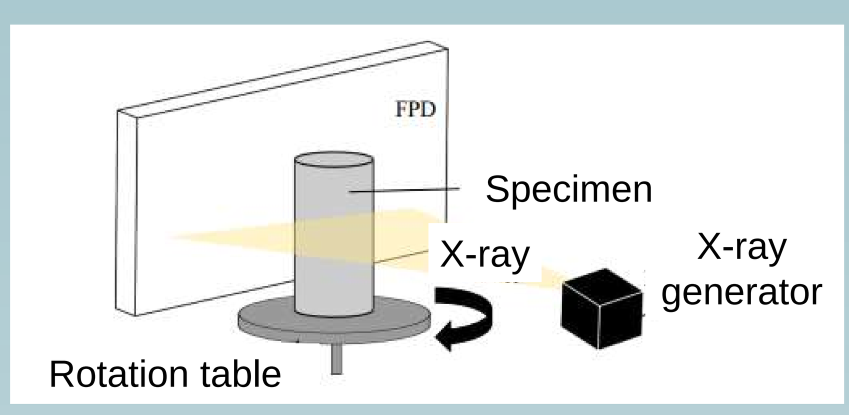

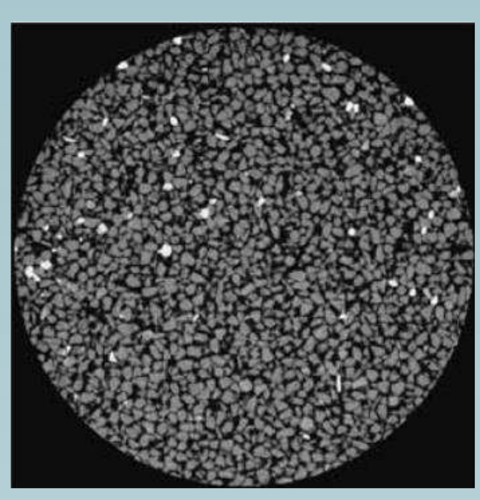

Dry sand image by X-ray CT

Experiment method

In this research, to observate behavior of inner soil, horizontal loading test with modeled sheet-pile and inner soil were did. Firstly, set the sheet-pile and making the specimen. After that, we applied confining pressure to reproduction real stress state on ground. Finally, horizontal loading test were did with X-ray CT par 2mm displacement.

The experimental case were set with consideration the effect of entire strength. In this poster, we introduce the results that the difference of relative density of inner soil.

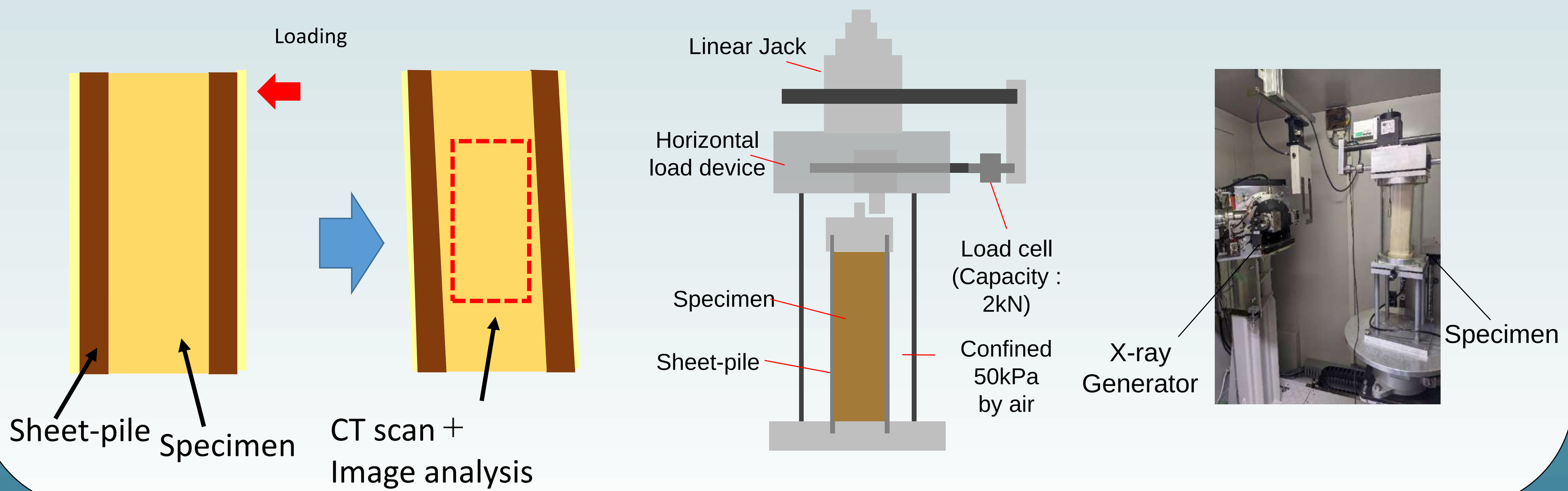

Results

Loding test

- Each case, the horizontal load increases up to a horizontal displacement of about 4 mm, after which the load increase slows down.
- In the case of Dr=60%, strain softening is observed → Suggesting that shear failure occurs in the inner soil due to horizontal loading.

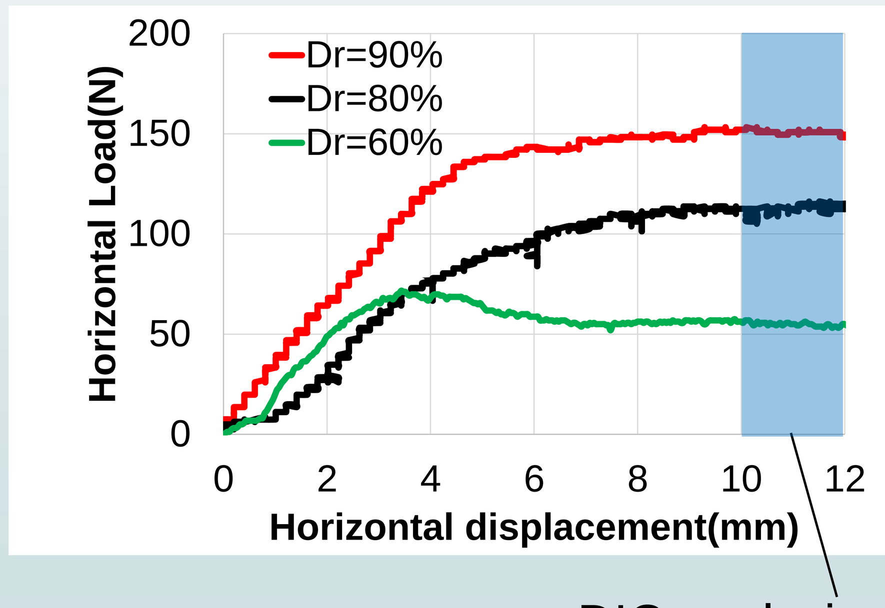

DIC analysis area

X-ray CT Scan and image analysis

- From the X-ray CT image, it was confirmed that the entire specimen behaved as a result of loading on the sheet pile head.
- Density change areas could not be seen from the CT images.

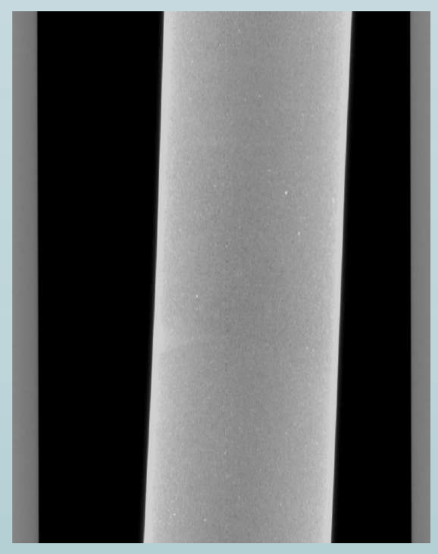

CT image of 12mm horizontal loading on the Dr=80%

Apply the image analysis

- DIC[3)] (Degital image corralation) image analysis was applyed with CT image to evaluate the displacement and strain on the specimen while loding.
- From the DIC results between 10mm-12mm loading, shear strain were apeear, but the appearing place and size were different among the case.
- The location of the strain may have affected the overall sttiffness of the specimen.

Shear strain

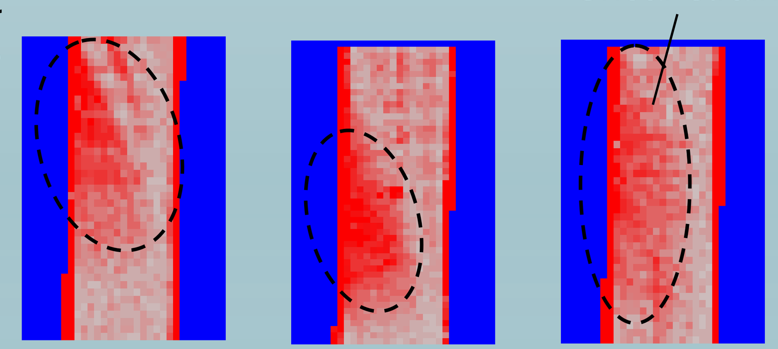

(a) Dr=80% (b) Dr=60% (c) Dr=90%

Shear strain on the 10-12mm loading

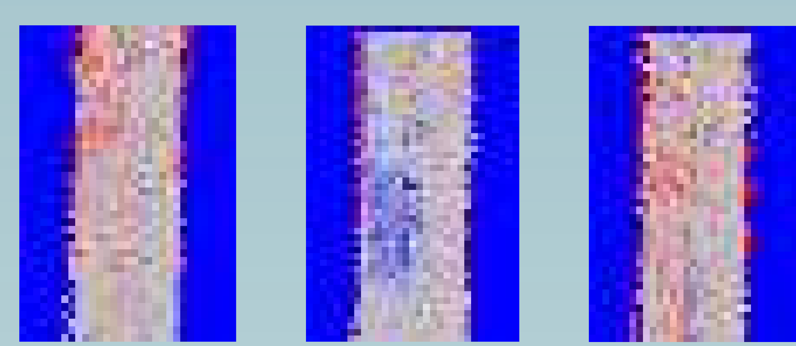

(a) Dr=80% (b) Dr=60% (c) Dr=90%

Volumetric Strain on the 10-12mm loading

By increasing the relative density of the inner soil, deformation of the inner soil can be suppressed

Conclusions

- In order to investigate the mechanism of strength development of double sheet pile structures, a newly developed model experimental apparatus was used in conjunction with X-ray CT.
- The results of DIC image analysis showed the appearing place and size were different among the case. This difference affect the entire stiffness.

Bibliography

1) Sugimoto et al., (2021) Model test on double sheet-pile method for excavation works using X-ray CT. Proceeding of Second International Conference Press-In Engineering 2021, Kochi, Japan, 312–322.
2) Otani et al, (2000) Application of X-ray CT method for characterization of failure in soils. Soils Found. 40, 111-118.
3) Stamati et al., (2020). spam: Software for Practical Analysis of Materials. Journal of Open Source Software, 5(51), 2286,

CLERMONT AUVERGNE INP
Ecole doctorale Sciences Pour l'Ingénieur

Evaluation of inner soil behavior in head-fixed double sheet-pile method using X-ray CT

Hideharu Sugimoto[1)3)], Ayaka Nasu[2)] Hideki Nagatani [2)]Jun Otani[1)]

1) Graduate school of Science and Technology, X-earth center, Kumamoto University, Japan
2) Kajima institute research, Tokyo, Japan
3) Université Clermont Auvergne, CNRS, Institut Pascal, Clermont Ferrand, France
Directeur de thèse : Pierre BREUL, Bastien Chevalier

INSTITUT PASCAL
熊本大学 Kumamoto University
X-Earth Center

Introduction

As the new construction method in Japan, double sheet-pile construction method is developping[1)]. This method is that the head of two sheet-piles are connected, and we aim more the twice displacement control effect compare with than only two sheet-pile. In the case of using this method, soils between two sheet-pile (called 'inner soil') is very important to consider the entire strength. In this research, using microfocus X-ray CT, the behavior of inner soil was observed and quantitative evaluation with image analysis.

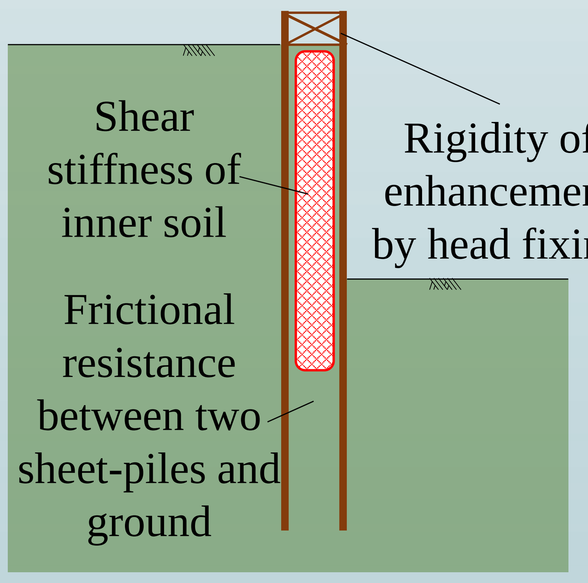

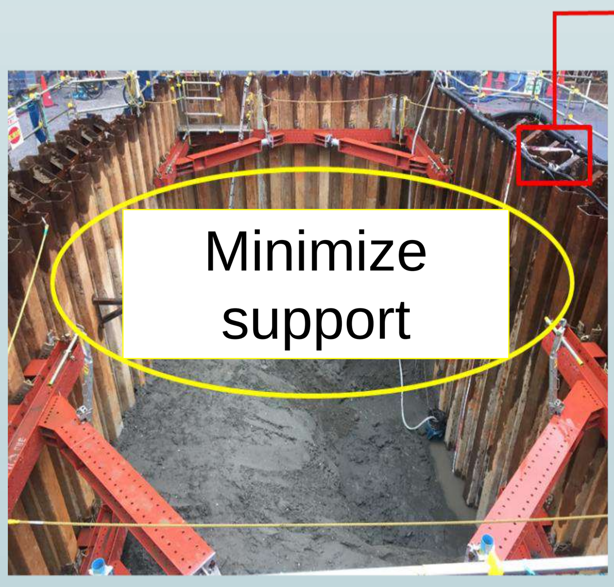

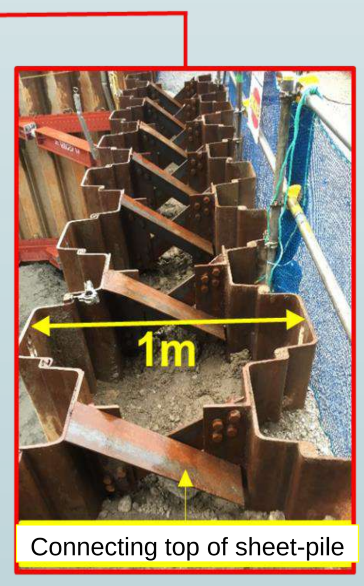

Methods

What is X-ray CT ??

X-ray CT method is a computer tomography method that utilizes the X-ray absorption rate and permeability of an object[2)].(Computed tomography) Since there is an approximate linear relationship between the X-ray attenuation coefficient after passing through the object and the density of the object, it is possible to visualize the density distribution inside the object.

For example, in the geotechnical engineering, we can observation the behavior inside soil and specimen as the difference the density. Images are made black and white colar. And from obtained image, we can apply the image analysis and calculate the displacement and strain (Degital Image corralation).

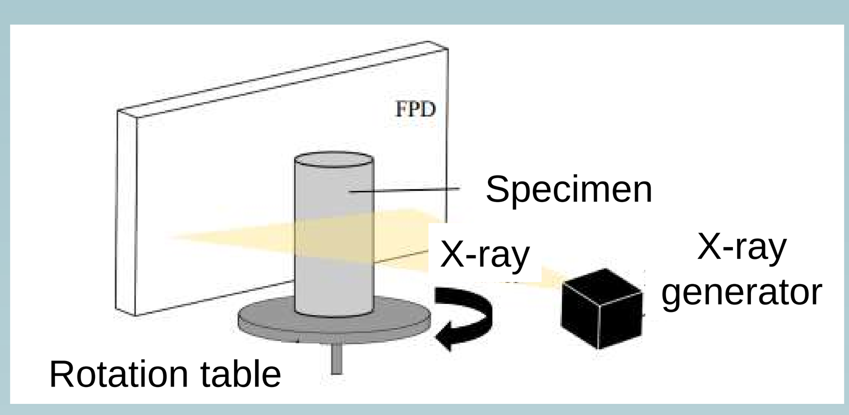

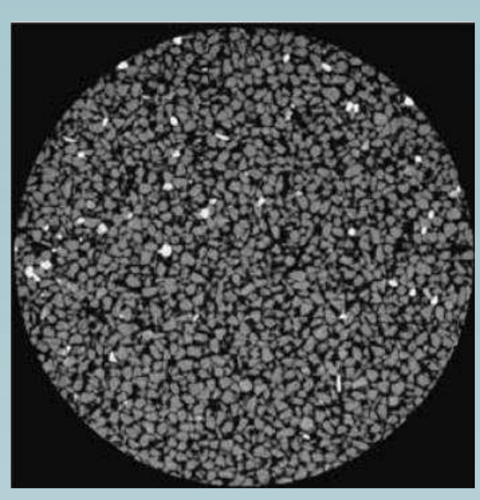

Dry sand image by X-ray CT

Experiment method

In this research, to observate behavior of inner soil, horizontal loading test with modeled sheet-pile and inner soil were did. Firstly, set the sheet-pile and making the specimen. After that, we applied confining pressure to reproduction real stress state on ground. Finally, horizontal loading test were did with X-ray CT par 2mm displacement.

The experimental case were set with consideration the effect of entire strength. In this poster, we introduce the results that the difference of relative density of inner soil.

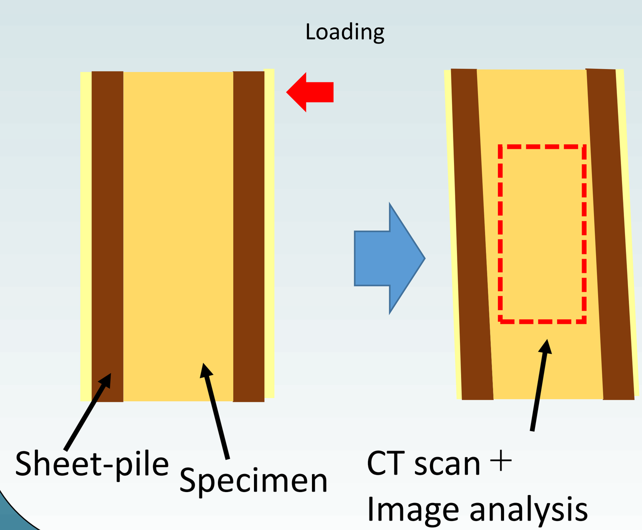

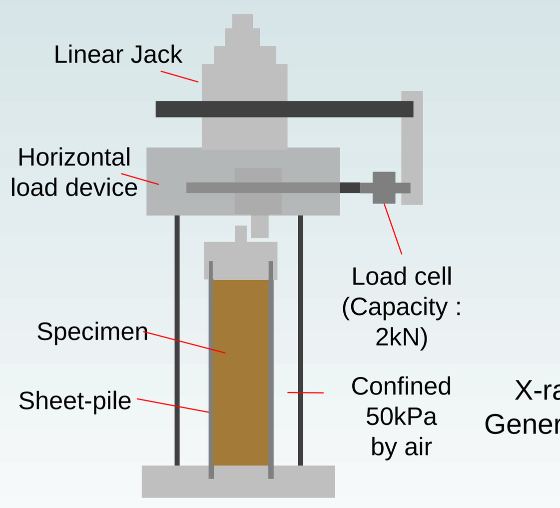

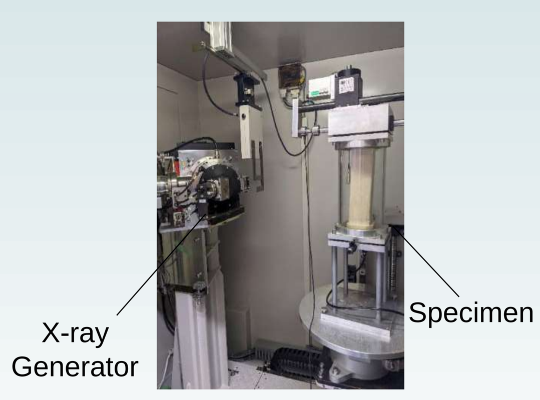

Results

Loding test

- Each case, the horizontal load increases up to a horizontal displacement of about 4 mm, after which the load increase slows down.
- In the case of Dr=60%, strain softening is observed → Suggesting that shear failure occurs in the inner soil due to horizontal loading.

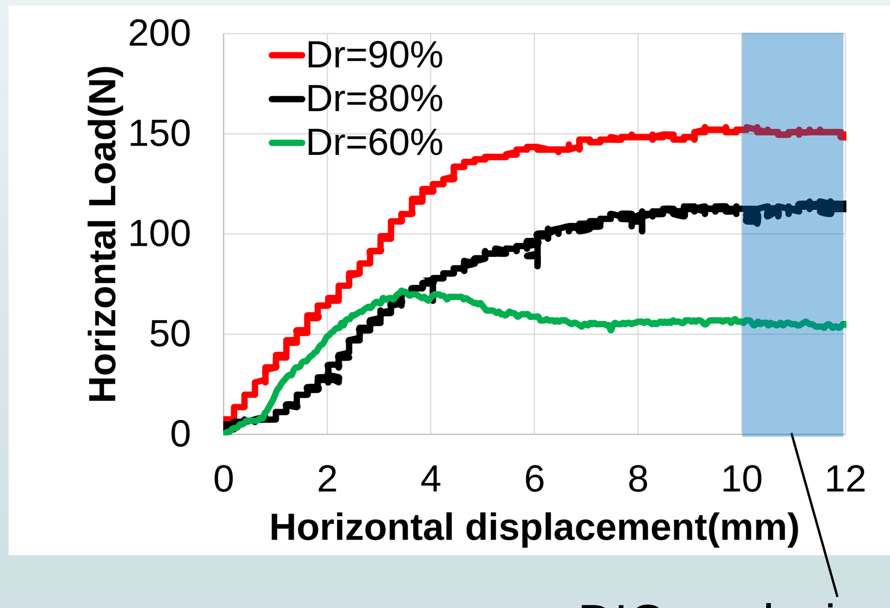

DIC analysis area

X-ray CT Scan and image analysis

- From the X-ray CT image, it was confirmed that the entire specimen behaved as a result of loading on the sheet pile head.
- Density change areas could not be seen from the CT images.

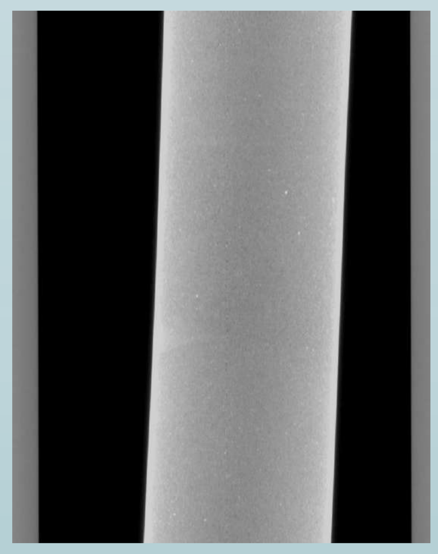

CT image of 12mm horizontal loading on the Dr=80%

Apply the image analysis

- DIC[3)] (Degital image corralation) image analysis was applyed with CT image to evaluate the displacement and strain on the specimen while loding.
- From the DIC results between 10mm-12mm loading, shear strain were apeear, but the appearing place and size were different among the case.
- The location of the strain may have affected the overall sttiffness of the specimen.

Shear strain

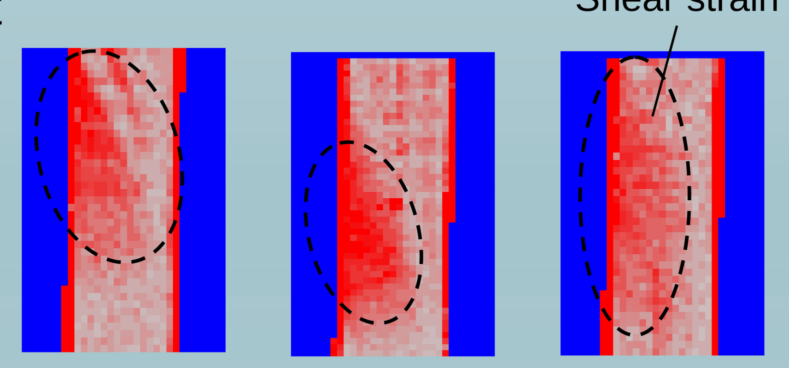

(a) Dr=80% (b) Dr=60% (c) Dr=90%

Shear strain on the 10-12mm loading

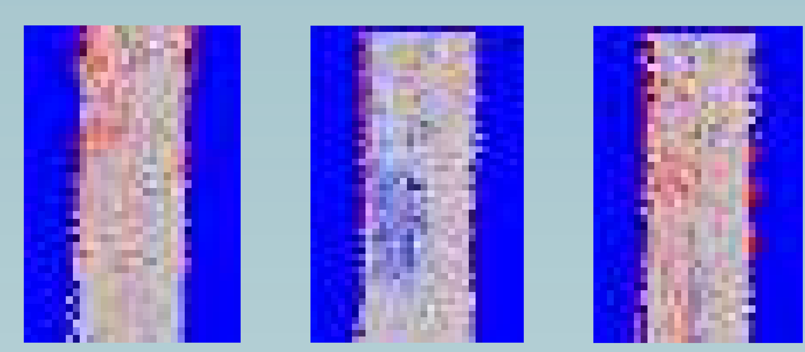

(a) Dr=80% (b) Dr=60% (c) Dr=90%

Volumetric Strain on the 10-12mm loading

By increasing the relative density of the inner soil, deformation of the inner soil can be suppressed

Conclusions

- In order to investigate the mechanism of strength development of double sheet pile structures, a newly developed model experimental apparatus was used in conjunction with X-ray CT.
- The results of DIC image analysis showed the appearing place and size were different among the case. This difference affect the entire stiffness.

Bibliography

1) Sugimoto et al., (2021) Model test on double sheet-pile method for excavation works using X-ray CT. Proceeding of Second International Conference Press-In Engineering 2021, Kochi, Japan, 312–322.
2) Otani et al, (2000) Application of X-ray CT method for characterization of failure in soils. Soils Found. 40, 111-118.
3) Stamati et al., (2020). spam: Software for Practical Analysis of Materials. Journal of Open Source Software, 5(51), 2286,

Sensitivity to statistical estimation uncertainties and probabilistic model identification

Charles Surget[1,2] – Sylvain Dubreuil[1] – Jérôme Morio[1] – Cécile Mattrand[2] – Jean-Marc Bourinet[2] – Nicolas Gayton[2]

charles.surget@onera.fr

Context

Uncertainty propagation in engineering problems:

$$\phi : \left| \begin{array}{ccc} \mathcal{X} \subseteq \mathbb{R}^d & \longrightarrow & \mathbb{R} \\ \boldsymbol{X} := (X_1, ..., X_d) \sim f_{\boldsymbol{X}} & \longmapsto & Y \end{array} \right. . \quad (1)$$

Quantity of Interest (QoI):

One could be interested in assessing a given expectation of a function τ of Y by *Monte Carlo Simulation* (MCS):

$$\mathbb{E}_{f_{\boldsymbol{X}}}\left[\tau\left(\phi(\boldsymbol{X})\right)\right] = \int_{\mathcal{X}} \tau\left(\phi\left(\boldsymbol{x}\right)\right) f(\boldsymbol{x}) \mathrm{d}\boldsymbol{x} \approx \frac{1}{N_{\boldsymbol{X}}} \sum_{j=1}^{N_{\boldsymbol{X}}} \tau\left(\phi\left(\boldsymbol{X}^{(j)}\right)\right). \quad (2)$$

Industrial context:

$f_{\boldsymbol{X}}$ is estimated from a sample $\widetilde{\boldsymbol{D}}$ of limited size N_D [1]. The estimator (2) is subject to a bi-level uncertainty [2]:

- a first uncertainty source from the estimate $\hat{f}_{\boldsymbol{X}|\widetilde{\boldsymbol{D}}}$ of $f_{\boldsymbol{X}}$,
- a second uncertainty source from the MCS estimate.

Problem

Where the investment should be made in order to reduce the variance of the estimator?

INVESTMENT

DATABASE ? $\rightarrow N_D \nearrow$

SIMULATION ? $\rightarrow N_{\boldsymbol{X}} \nearrow$

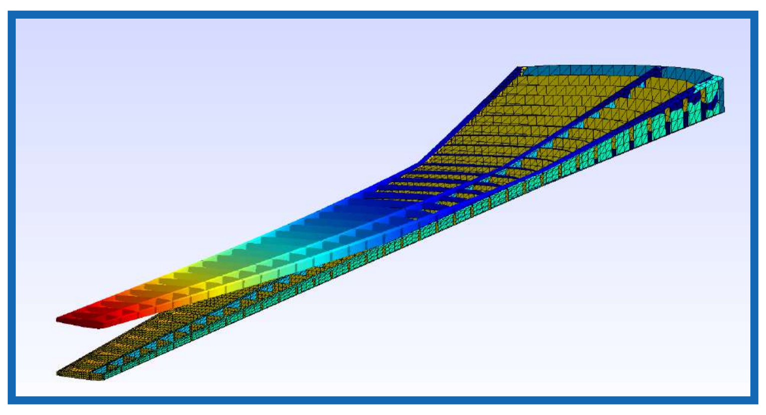

The test-simulation trade-off is made based on a sensitivity analysis where the predominant indice indicates which is the leading uncertainty source on the variance of the estimator.

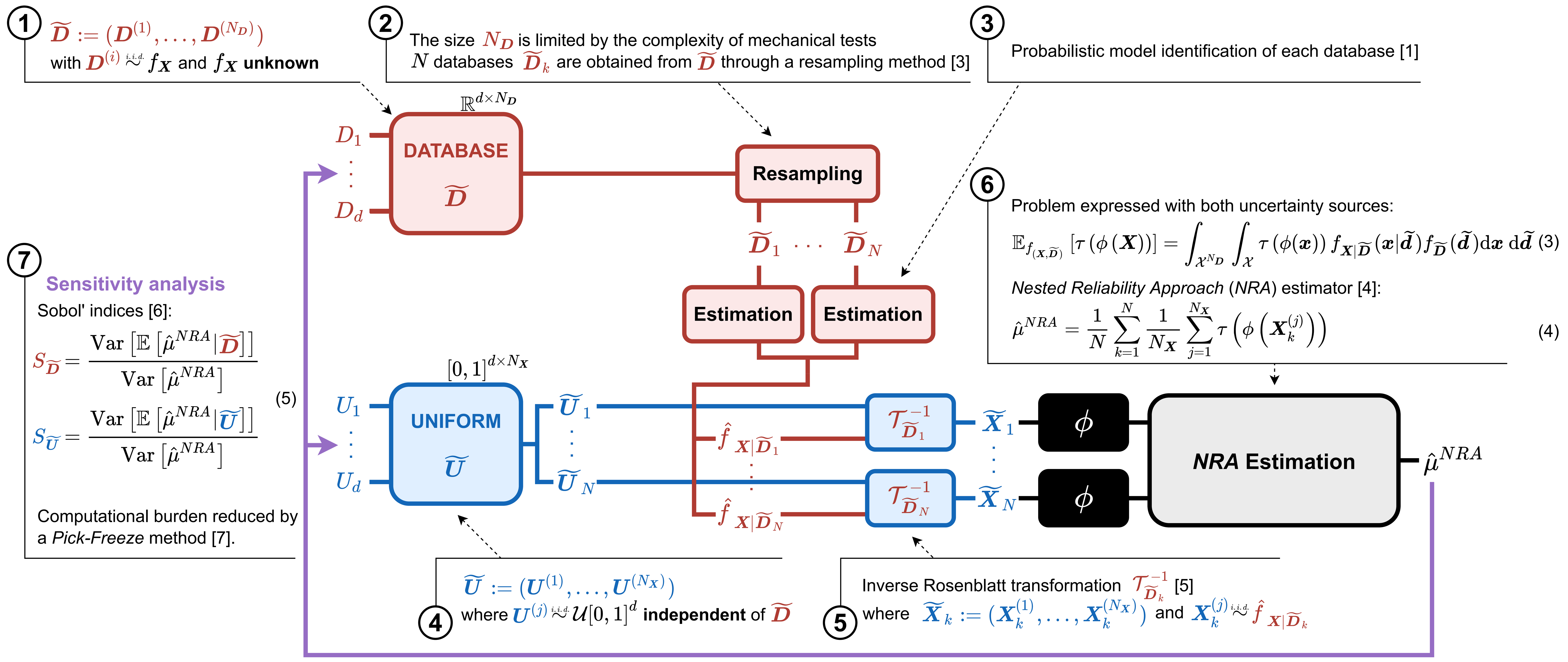

Application

Mean deflection of a cantilever beam:

$$\phi\left(F, L, E, b, h\right) = \frac{4FL^3}{Ebh^3} \quad , \quad (3)$$

where F is the transverse load applied on the free end of the beam of length L, Young's modulus E and cross-section $b\ h$ [8].

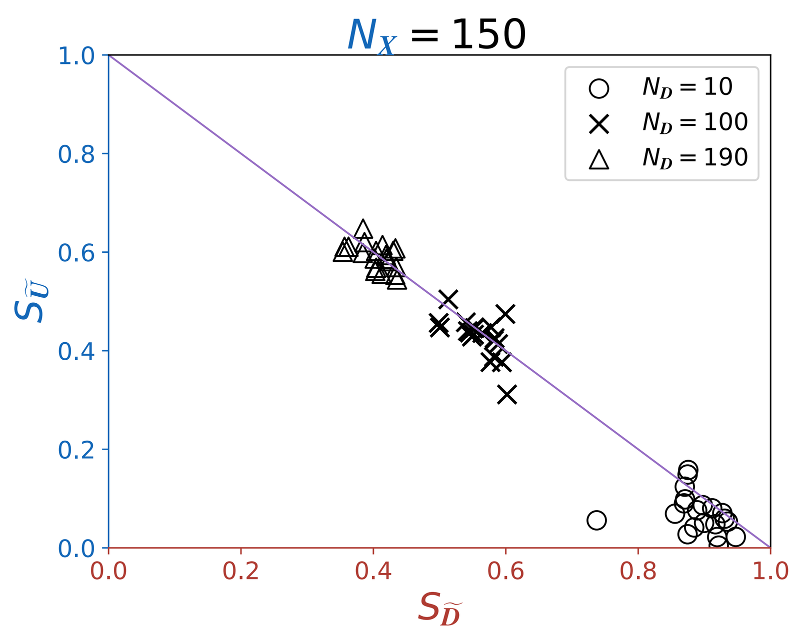

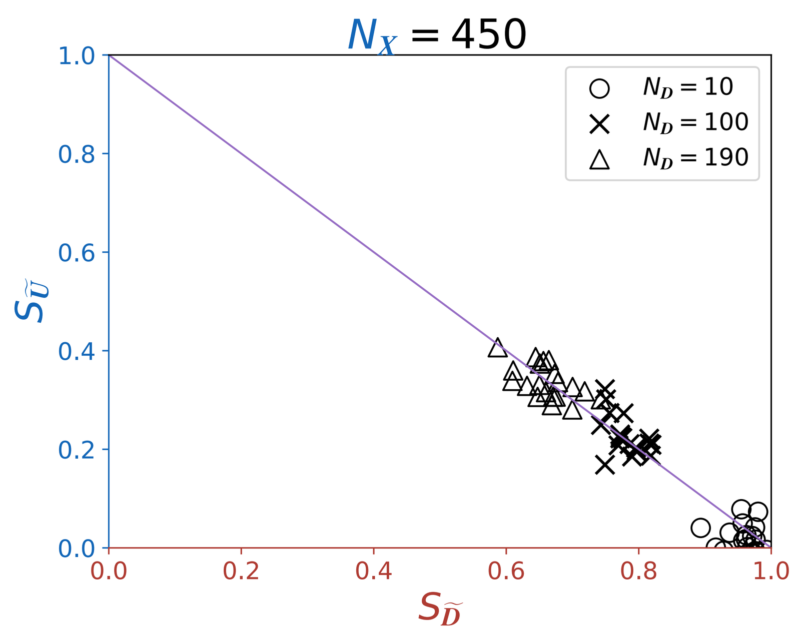

References

[1] Nils-Bastian Heidenreich, Anja Schindler, and Stefan Sperlich. Bandwidth selection for kernel density estimation: a review of fully automatic selectors. *AStA Advances in Statistical Analysis*, 97(4):403–433, 2013.

[2] Gabriel Sarazin. *Analyse de sensibilité fiabiliste en présence d'incertitudes épistémiques introduites par les données d'apprentissage.* PhD thesis, Toulouse, ISAE, 2021.

[3] Chong Ho Yu. Resampling methods: concepts, applications, and justification. *Practical Assessment, Research, and Evaluation*, 8(1):19, 2002.

[4] Vincent Chabridon. *Analyse de sensibilité fiabiliste avec prise en compte d'incertitudes sur le modèle probabiliste-Application aux systèmes aérospatiaux.* PhD thesis, Université Clermont Auvergne(2017-2020), 2018.

[5] Régis Lebrun and Anne Dutfoy. Do rosenblatt and nataf isoprobabilistic transformations really differ? *Probabilistic Engineering Mechanics*, 24(4):577–584, 2009.

[6] Ilya M Sobol. Sensitivity analysis for non-linear mathematical models. *Mathematical modelling and computational experiment*, 1:407–414, 1993.

[7] Fabrice Gamboa, Alexandre Janon, Thierry Klein, Agnès Lagnoux, and Clémentine Prieur. Statistical inference for sobol pick-freeze monte carlo method. *Statistics*, 50(4):881–902, 2016.

[8] Baoyu Li, Zhang Leigang, Xuejun Zhu, Xiongqing Yu, and Xiaodong Ma. Reliability analysis based on a novel density estimation method for structures with correlations. *Chinese Journal of Aeronautics*, 30(3):1021–1030, 2017.

[1] Onera, ONERA/DTIS, F-31055 Toulouse, France [2] SIGMA Clermont, F-63000 Clermont–Ferrand, France

Growth of GaN nanostructures on GaAs(111)A substrate by Droplet Epitaxy : a theoretical and experimental characterizations by XPS spectroscopy

Ministry of Higher Education and Research and Innovation (MESRI)
Doctoral School of Engineering Sciences

Guy TSAMO, *Luc BIDEUX, Guillaume MONIER, Philip HOGGAN, Christine ROBERT-GOUMET, Matthieu PETIT, Alain RANGUIS*

Université Clermont Auvergne, Clermont Auvergne INP, CNRS, Institut Pascal, F-63000 Clermont-Ferrand, France

Aix Marseille Université, CNRS, CINaM UMR 7325, 13288, Marseille, France

- ❑ **Optimization of the growth parameters of GaN/GaAs(111)A quantum dots by droplet epitaxy technique(DE)**
- ❑ **Development of an in-situ XPS modeling to characterize morphologically the fabricated nanostructures**
- ❑ **Complementarity between in-situ (XPS model) and ex-situ (SEM and AFM) morphological characterizations**

Potential applications

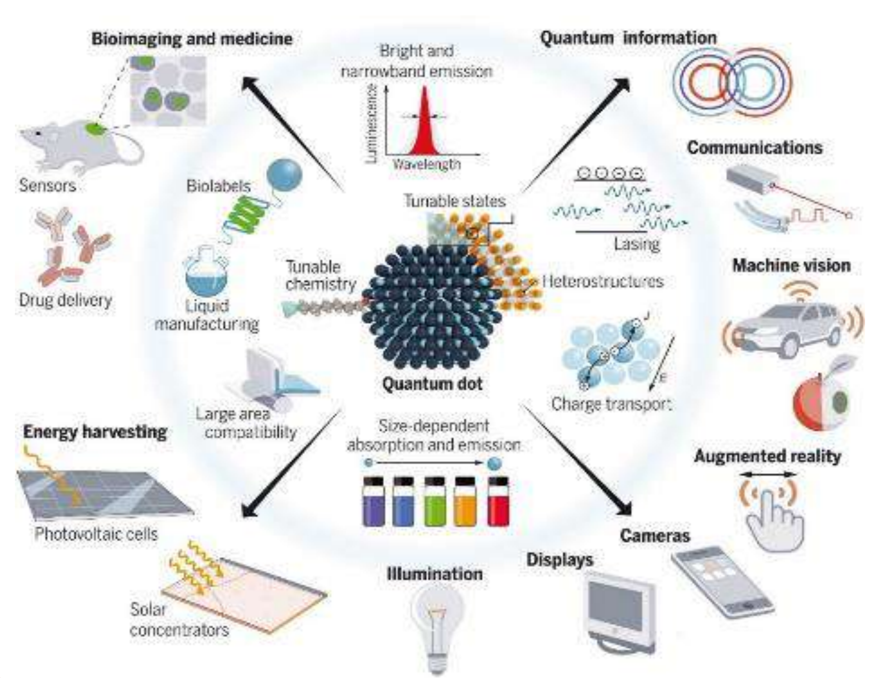

Droplet epitaxy technique growth

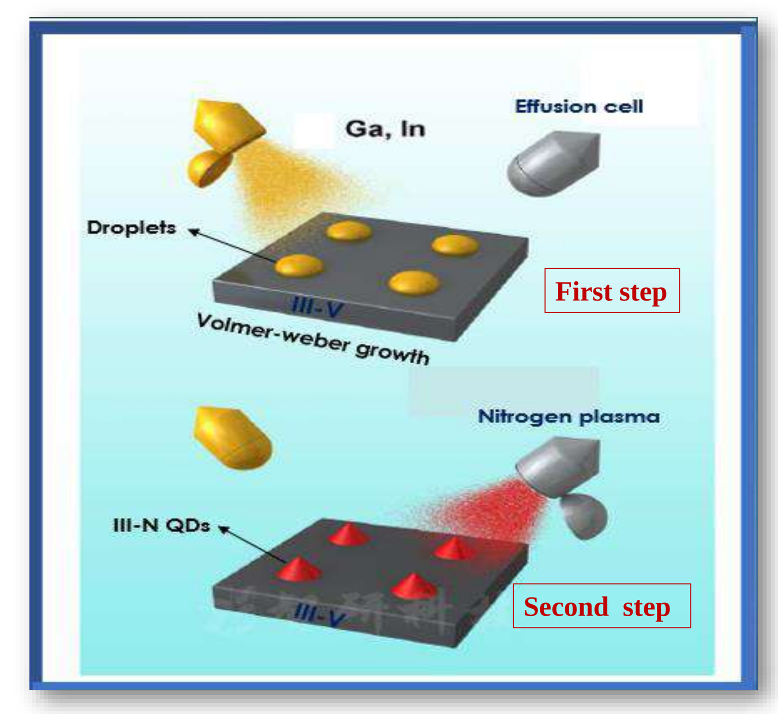

First step: gallium droplets deposition

In-situ XPS modeling

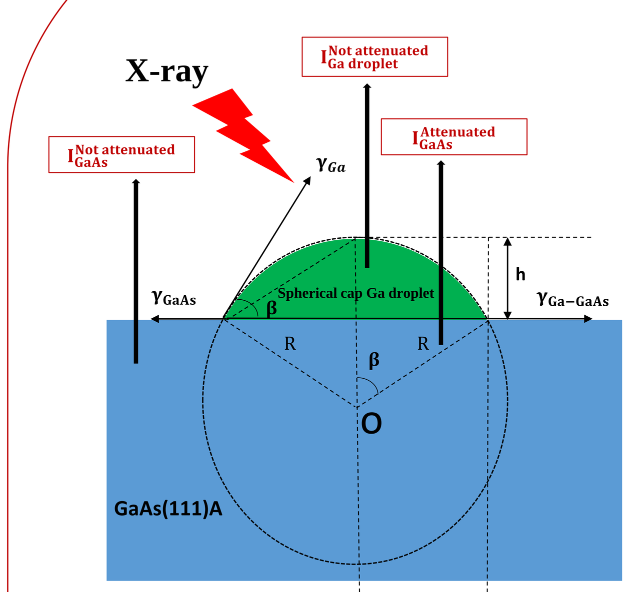

- Young Dupré law: $\cos\beta = \frac{\gamma_{GaAs} - \gamma_{Ga-GaAs}}{\gamma_{Ga}}$
- Hydrophilic substrate: $\beta \leq 90°$

XPS modeling imput parameters:

- q_{ML}: amount of material deposited in number of monolayer
- Tiotical droplet density:

$$n_{th} = jF^p\left[v^{-1}\exp\left(\frac{-E_a}{k_BT}\right) + t_r \exp\left(\frac{-E_a - E_r}{k_BT}\right)\right]^{-1} \text{ in cm}^{-2}$$

➢ Height: $h = \sqrt[3]{\frac{q_{ML}}{\pi n_{th}\left(\frac{1}{1-\cos\beta} - \frac{1}{3}\right)}}$

➢ Radius: $r = \frac{h}{\tan\left(\frac{\beta}{2}\right)} = \frac{h \sin\beta}{1-\cos\beta}$

➢ Coverage rate : $\theta = n_{th}\pi r^2 = \frac{r^2 q_{ML}}{h^3\left(\frac{1}{1-\cos\beta} - \frac{1}{3}\right)}$

XPS experiment in-situ under ultra high vacuum

Mg K_α X-ray (1253.6 eV)

After 3ML Ga deposition: T=300°C, F=0.1ML/s

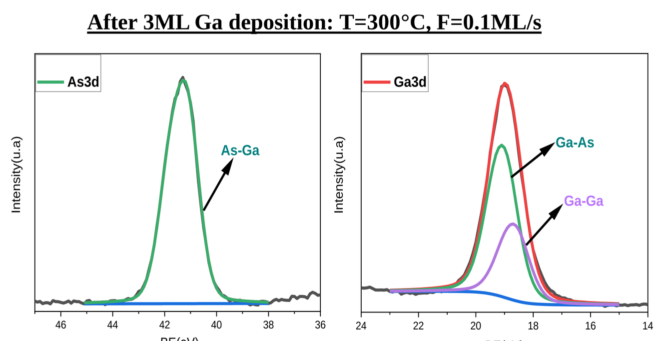

$$R_{1ex} = \frac{I^{GaAs}_{Ga3d} + I^{Ga}_{Ga3d}}{I^{GaAs}_{As3d}} = 1, \quad R_{2ex} = \frac{I^{Ga}_{Ga3d}}{I^{GaAs}_{Ga3d}} = 0.45$$

XPS modeling

After 3ML Ga deposition, T=300°C, F=0.1ML/s

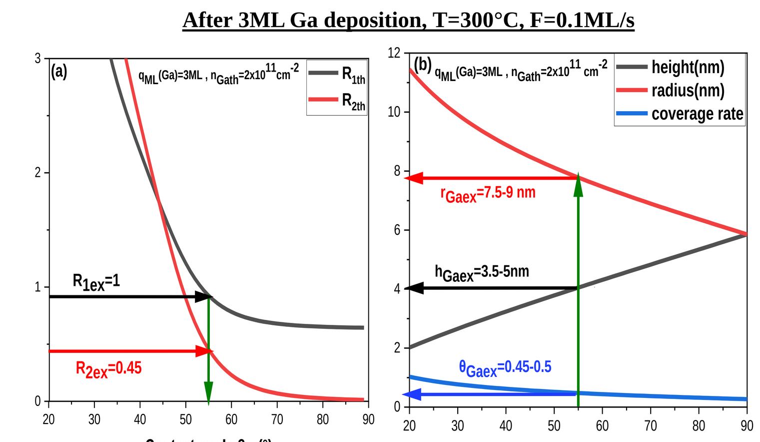

Complementarity between experimental and theoretical XPS signal ratios for a contact angle of 55° ➡ Determination of radius , height and coverage rate for a contact angle of 55°

In-situ XPS morphological characterization:

$r_{Gath} = 7.9$ nm ; $h_{Gath} = 4$nm ; $\theta_{Gath} = 0.5$; $\beta_{Gath} = 55°$; $n_{Gath} = 2X10^{11}cm^{-2}$

Ex-situ characterization: SEM and AFM

After 3ML Ga deposition, T=300°C, F=0.1ML/s

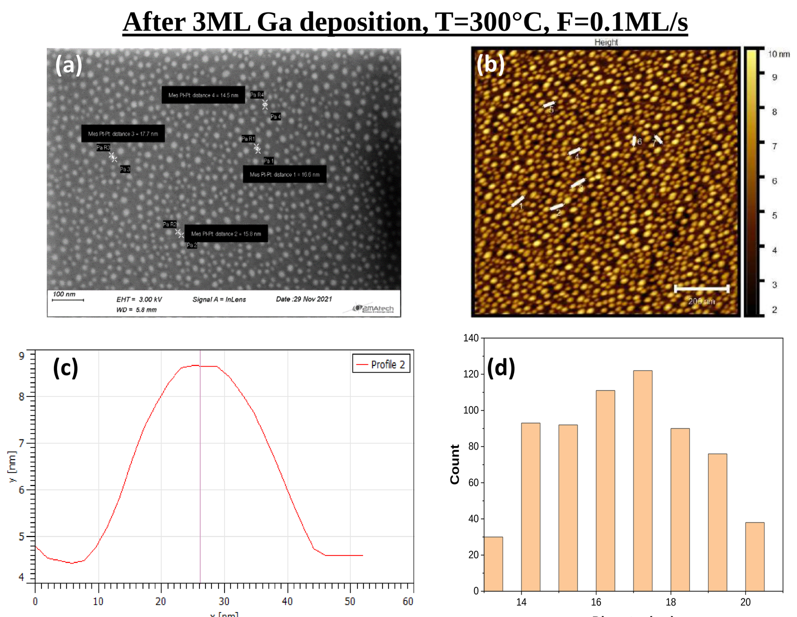

Ex-situ SEM and AFM morphological characterization:

r_{Gaex}=7.5-9 nm ; h_{Gaex}=3.5-4.5nm ; θ_{Gaex}=0.45-0.5 ; $\beta_{Gaex} = 52 - 58°$; $n_{Gaex} = 2X10^{11}cm^{-2}$

=

Complementarity between in-situ XPS and ex-situ(SEM and AFM) morphological characterization

Second step: nitridation of gallium droplet

In-situ XPS modeling

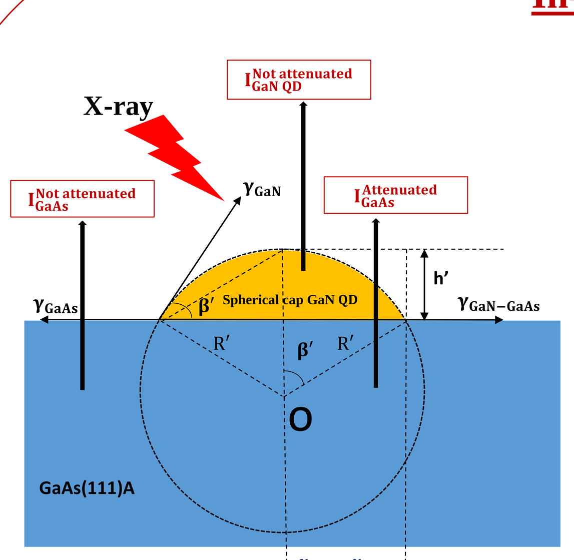

- Young Dupré law: $\cos\beta' = \frac{\gamma_{GaAs} - \gamma_{GaN-GaAs}}{\gamma_{GaN}}$
- Hydrophilic substrate: $\beta' \leq 90°$

➢ Height : $h' = \sqrt[3]{\frac{V'}{\pi\left(\frac{1}{1-\cos\beta'} - \frac{1}{3}\right)}}$

➢ Radius : $r' = \frac{h'}{\tan\left(\frac{\beta'}{2}\right)} = \frac{h' \sin\beta'}{1-\cos\beta'}$

➢ Coverage rate: $\theta' = n'\pi r'^2$

Hypothesis:

➢ All the gallium atoms of droplet are nitridate

➢ $V_{GaN} = \delta_1 V_{GaN} = 1.15V_{Ga}$

➢ $r_{Gath} = r_{GaNth}$, $n_{Gath} = n_{GaNth}$ → $\theta_{GaNth} = \delta_2\theta_{Gath}$ → $\theta_{GaNth} = \theta_{Gath}$

XPS experiment in-situ under ultra high vacuum

Mg K_α X-ray (1253.6 eV)

After nitridation: $P_N = 7X10^{-5}$mbar:

T = 100°C(15min), 200°C(15min), 300°C(15min)

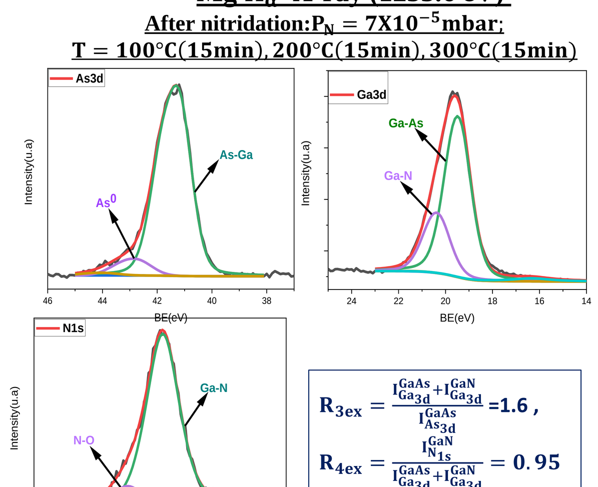

$$R_{3ex} = \frac{I^{GaAs}_{Ga3d} + I^{GaN}_{Ga3d}}{I^{GaAs}_{As3d}} = 1.6, \quad R_{4ex} = \frac{I^{GaN}_{N1s}}{I^{GaAs}_{Ga3d} + I^{GaN}_{Ga3d}} = 0.95$$

XPS modeling

After nitridation: $P_N = 7X10^{-5}$mbar:

T = 100°C(15min), 200°C(15min), 300°C(15min)

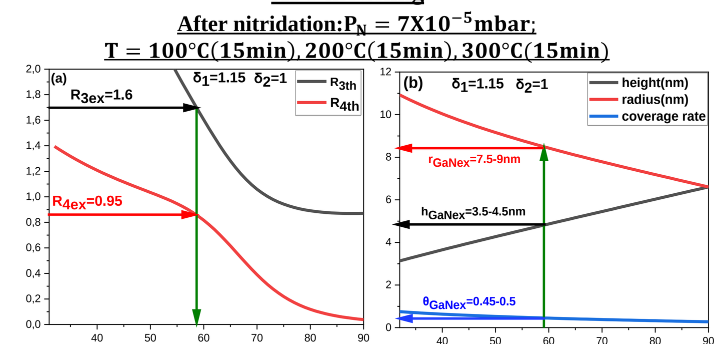

Complementarity between experimental and theoretical XPS signal ratios for a contact angle of 58° ➡ Determination of radius , height and coverage rate for a contact angle of 58°

In-situ XPS morphological characterization:

$r_{GaNth} = 7.9$ nm ; $h_{GaNth} = 3,73$nm ; $\theta_{GaNth} = 0.5$; $n_{GaNth} = 2X10^{11}cm^{-2}$

=

Ex-situ characterization: SEM and AFM

After nitridation: $P_N = 7X10^{-5}$mbar:

T = 100°C(15min), 200°C(15min), 300°C(15min)

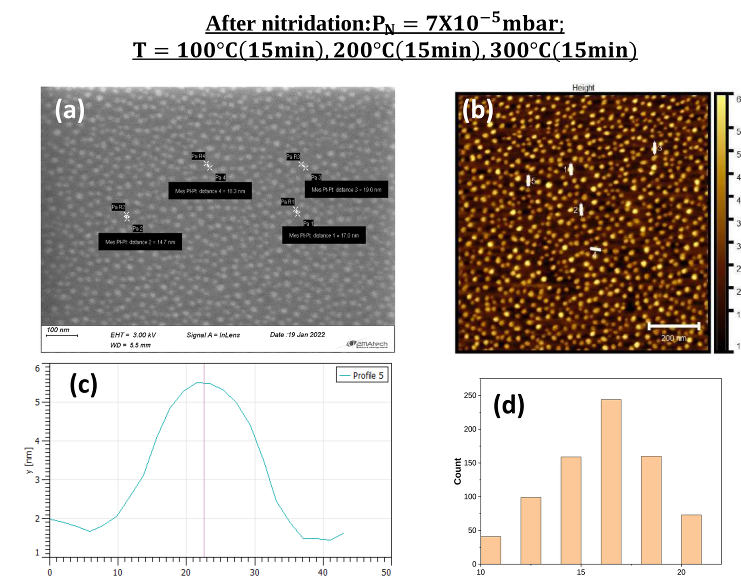

Ex-situ SEM and AFM morphological characterization:

r_{GaNex}=7.5-9 nm ; h_{GaNex}=3.5-4.5nm ; θ_{GaNex}=0.45-0.5 ; $n_{GaNex} = 2X10^{11}cm^{-2}$

Fabrication and characterization of high density nanometrics GaN quantum dots by droplet epitaxy technique

Excitons Generation, Charges Transfer and Transport in Photosynthesis

Daniel Yaacoub[†*], Jean-François Cornet[†], Jérémi Dauchet[†],
Thomas Vourc'h[†], Richard Fournier[‡], Fabrice Gros[†], Stéphane Blanco[‡]
[†]Université Clermont Auvergne, Clermont Auvergne INP, CNRS, Institut Pascal, F-63000 Clermont-Ferrand, France
[‡]Université Toulouse III-Paul Sabatier, CNRS, Laboratoire Plasma et Conversion d'Energie, F-31000 Toulouse, France
[*]http://www.danielyaacoub-physique.fr

Journées Scientifiques des Doctorants SPI 2022

Context

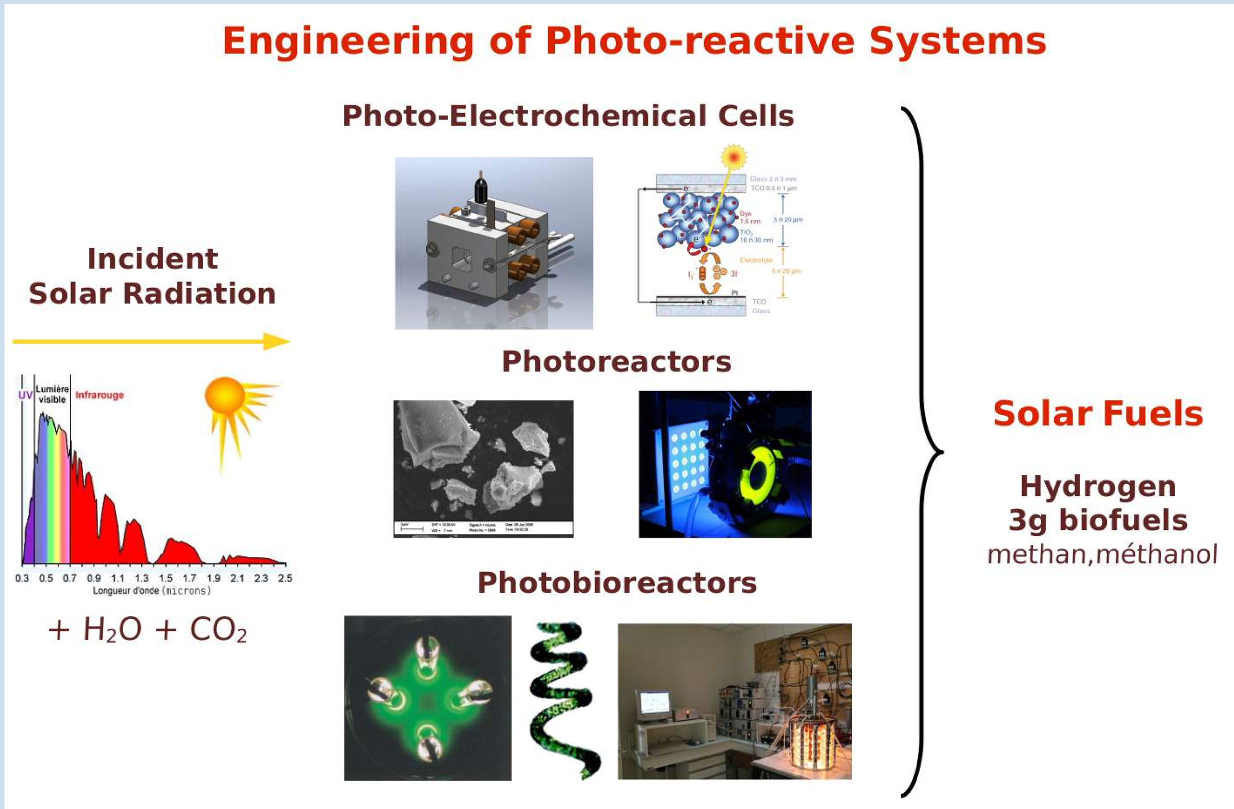

- Need to **Reach** 80% **of biofuels**
- ⇒ Develop **Multi-scale models** of photoreactive systems
- ⇒ Build detailed models of **Thermokinetic couplings**

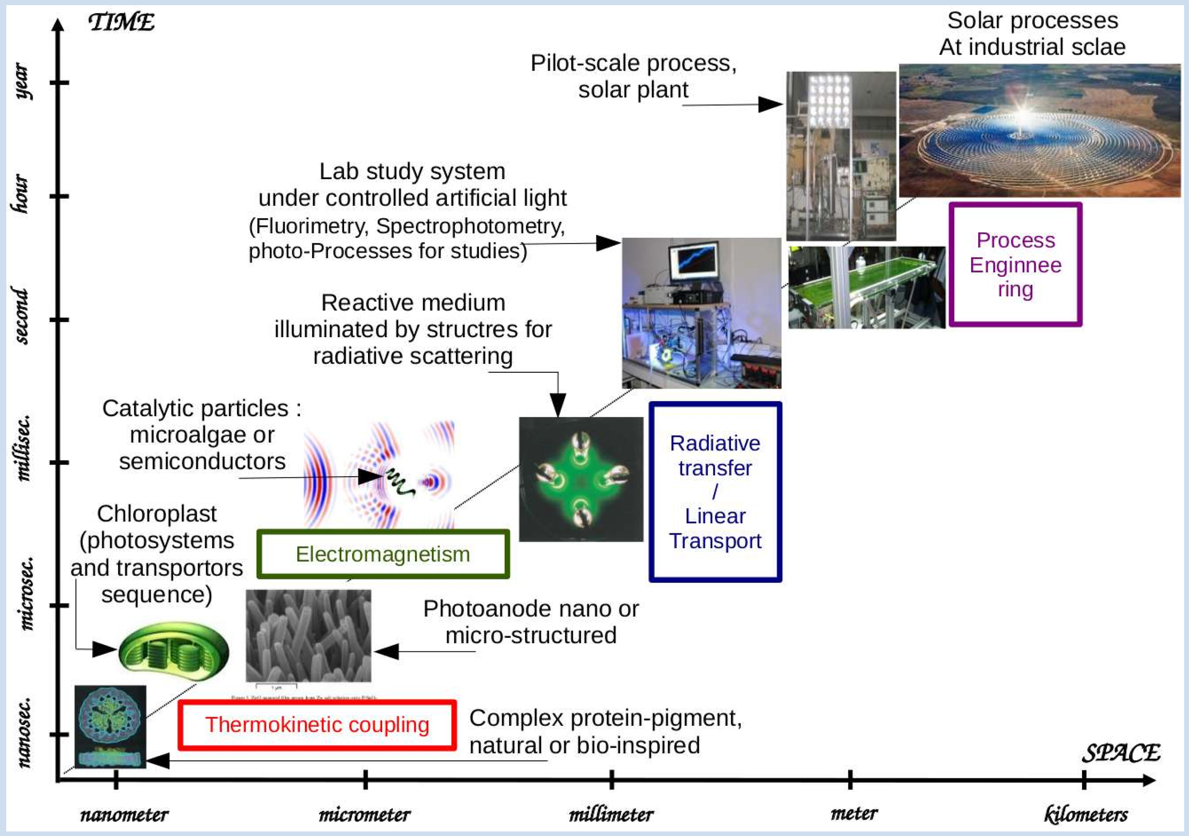

Framework and Issues

Artificial photosynthesis :

- High thermodynamical efficiency
- Synthesis of bio-inspired photo-catalysts

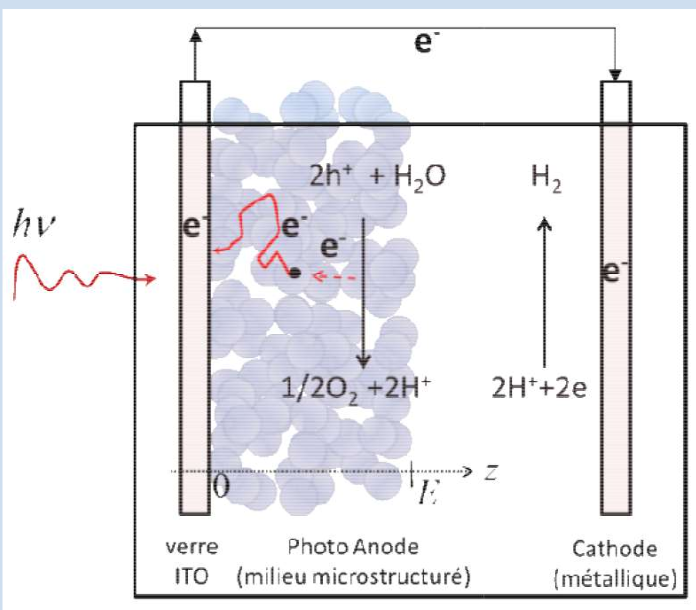

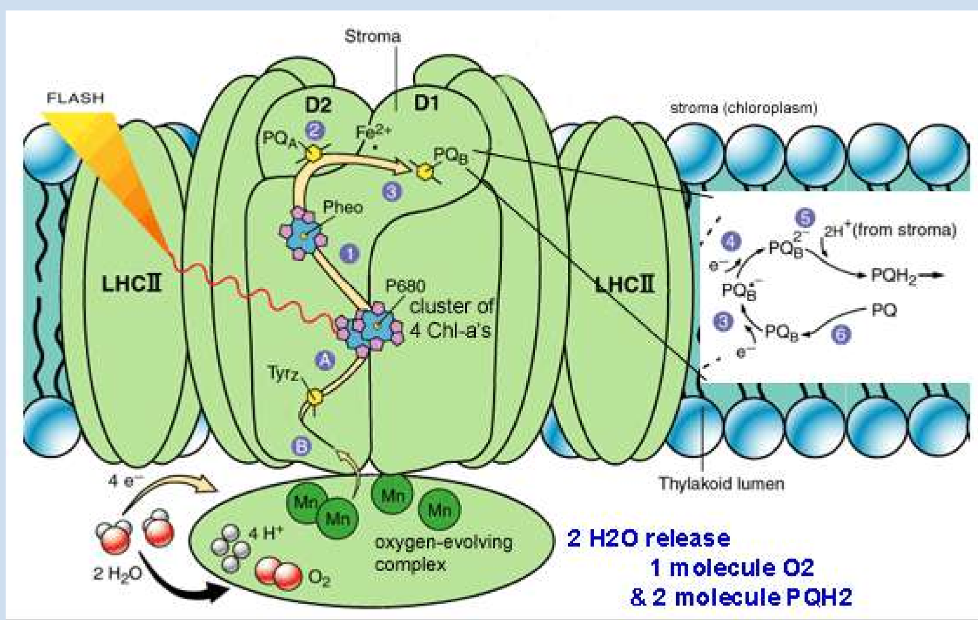

Natural photosynthesis :

- Improved photo-catalysts
- Low thermodynamical efficiency

- Theoretical **physical modeling** and simulation of **thermokinetic** couplings in photosynthesis : **from light absorption to chemical reactions**
- **Unified approach** based on **analogies** between primary steps of **natural** photosynthesis and **artificial** Photo-ElectroChemical cells.

⇒ **Issues** : Describe [1] Excitons photogeneration and charges transfert, [2] charges transport

Excitons Generation/Transfer

Bio-inspired cells ⇔ Thylakoid membranes

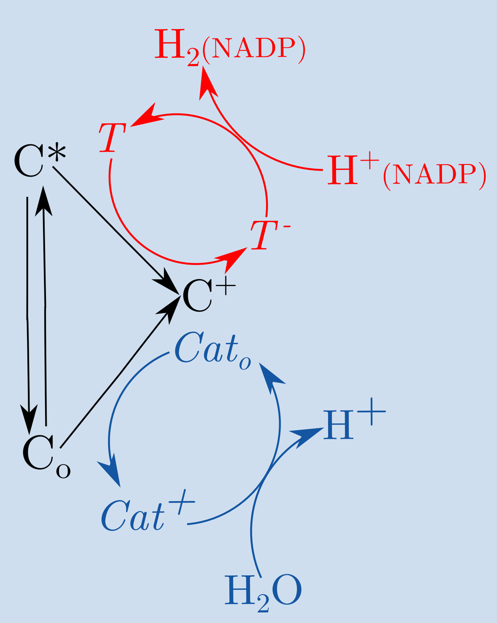

$C \equiv$ pigment
$Cat \equiv$ catalyst
$T \equiv$ transfer chain

Charges Transport

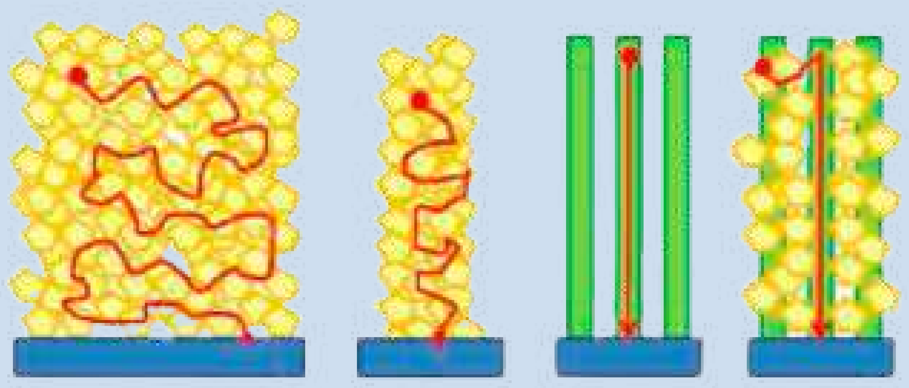

$$\begin{cases} \partial_t q^\gamma &= -\nabla\cdot\left(-D\nabla q^\gamma - \mu z q^\gamma \nabla\Phi\right) - kq^\gamma \\ \nabla^2\Phi &= -\frac{ze}{\varepsilon}q^\gamma \end{cases}$$

- Diffusion
- Electro-migration
- Recombination losses

⇒ Search for **Integral Formulations** (charges collection yield)

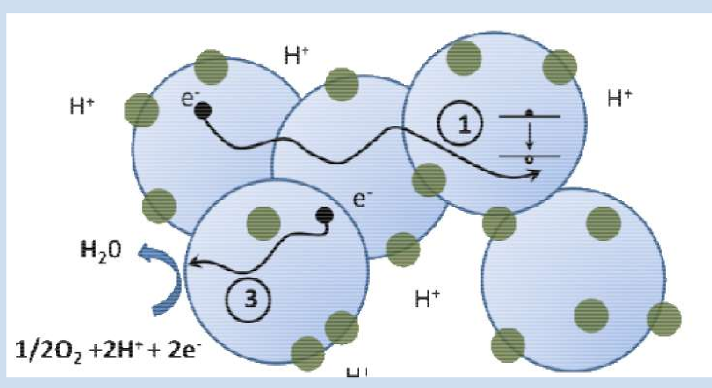

Approach and Methods

Probabilisation and **Integral formulation** of thermokinetic couplings compatible with **process optimisation** by **Monte Carlo** simulations and **path-spaces** analysis.
Powerful and meaningful :

- ∀ Geometrical complexity.
- ∀ Phenomenological complexity of photogeneration-transfert-transport couplings.

Expected Results

Short-term Results :

- Build **detailed models** of **thermokinetic processes** in photosynthesis.
- Provide physical pictures based on the **visualisation of** excitons/**charges paths** during the photo-conversion

Long-term Results :

- **Inverse design** to optimize bio-inspired photoreactive processes and reach thermodynamical optima.

Système de mesure de champs denses pour la caractérisation de matériaux quasi-fragiles aéronautiques soumis à des sollicitations dynamiques rapides

TIXIER Damien, GREDIAC Michel(1), BLAYSAT Benoît(1), FOUREST Thomas(2), LANGRAND Bertrand(2)

(1) M3G, Institut Pascal, Clermont-Ferrand, France

(2) DMAS, ONERA, Lille, France

Financement ONERA / AID

Contexte et Démarche

La nature quasi-fragile de certains composites rend délicats les essais de caractérisation mécanique notamment à grande vitesse de déformation.

Objectifs :
- Proposer un système de mesure de champs
- Limiter le bruit et les biais de mesure
- Avoir une résolution spatiale satisfaisante

Démarche :

Marquage
↓
Essai
↓
Traitement d'image (LSA)
↓
Principe des travaux virtuels

Méthodes

Marquages :
- Motif en damier
- Utilisation d'une graveuse laser

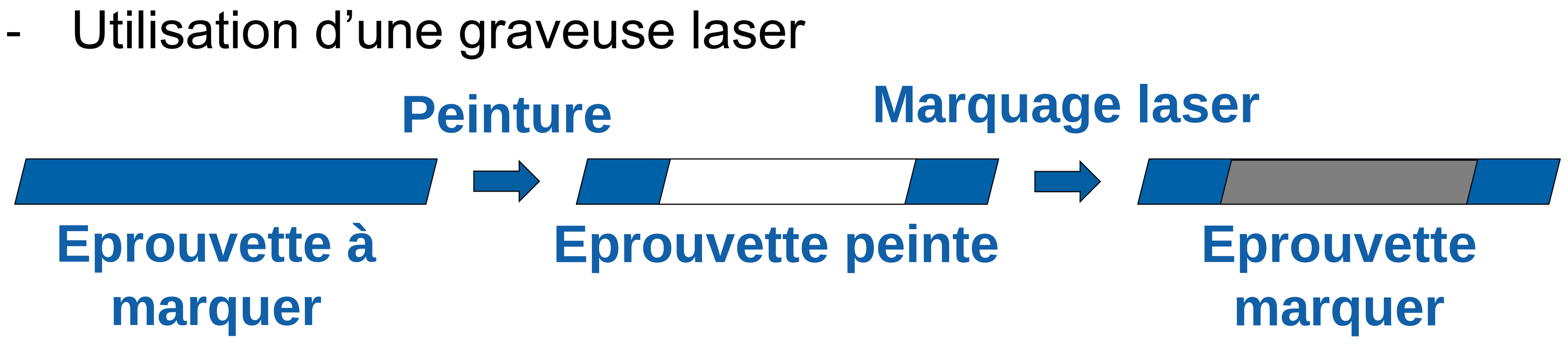

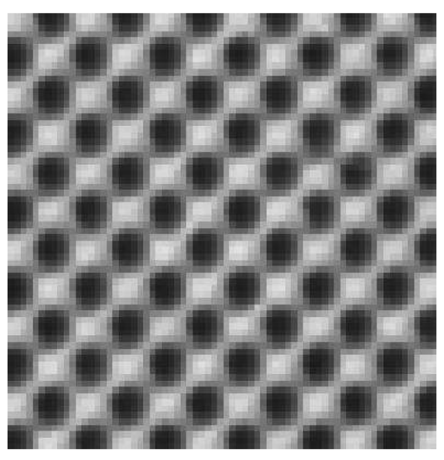

Avantages :
- Motif périodique
- Répétabilité du marquage
- Rapidité et facilité de mise en œuvre
- Adaptable
- Evite l'utilisation de colle

Traitement d'image (LSA) [1] :

Transformée de Fourier fenêtrée *(eq.1)*

$$\widehat{s_g}(x,y,\theta)=\int_{-\infty}^{+\infty}\int_{-\infty}^{+\infty} s(\eta,\xi).g(x-\eta,y-\xi).e^{-2i\pi f(x.\cos(\theta)+y.\sin(\theta))}.d\eta.d\xi \quad (eq.1)$$

Calculs des phases *(eq.2)*

$$\phi_x(x,y)=\arg\left(\widehat{s_g}(x,y,0)\right) \quad et \quad \phi_y(x,y)=\arg\left(\widehat{s_g}\left(x,y,\frac{\pi}{2}\right)\right) \qquad (eq.2)$$

Déplacements proportionnels au déphasage entre 2 images *(eq.3)*

$$\begin{pmatrix} u_x(x,y) \\ u_y(x,y) \end{pmatrix} = \begin{pmatrix} -\frac{p}{2.\pi}.\left[\phi_x^{déf}\left(x+u_x(x,y),y+u_y(x,y)\right)-\phi_x^{réf}(x,y)\right] \\ -\frac{p}{2.\pi}.\left[\phi_y^{déf}\left(x+u_x(x,y),y+u_y(x,y)\right)-\phi_y^{réf}(x,y)\right] \end{pmatrix} \qquad (eq.3)$$

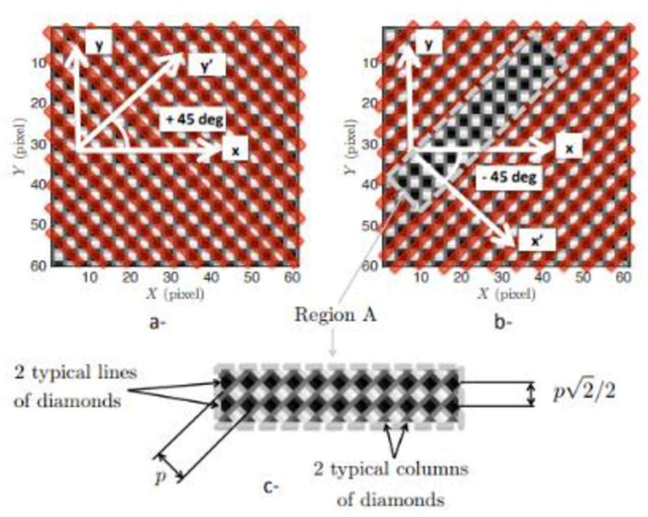

Dans le cas d'un motif en damier les axes de la grille se trouvent suivant les bissectrices du damiers [2]

Résultats

Réalisation d'un essai de traction quasi-statique afin de tester le système de mesure :

- Traction quasi-statique
- Composite unidirectionnel
- Fibre de carbone/matrice époxy
- Orientation des fibres de 30°

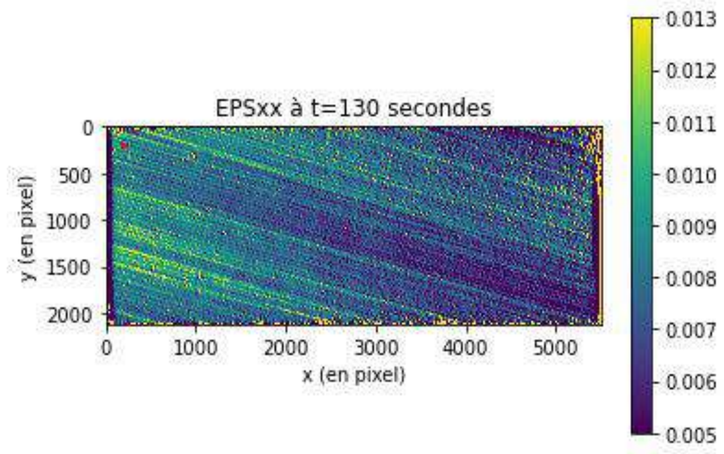

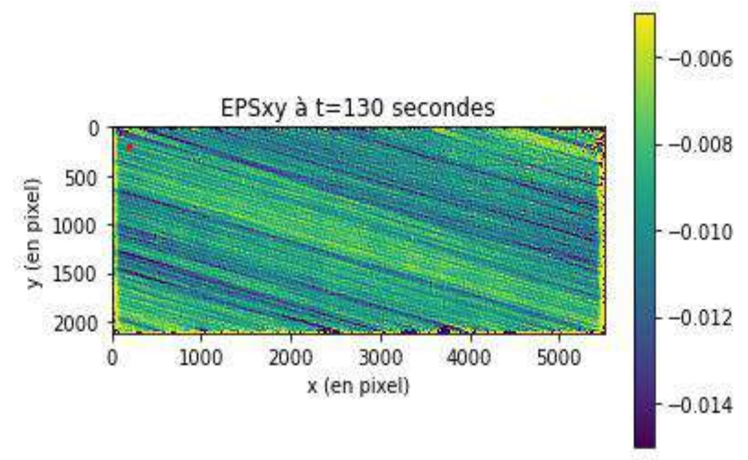

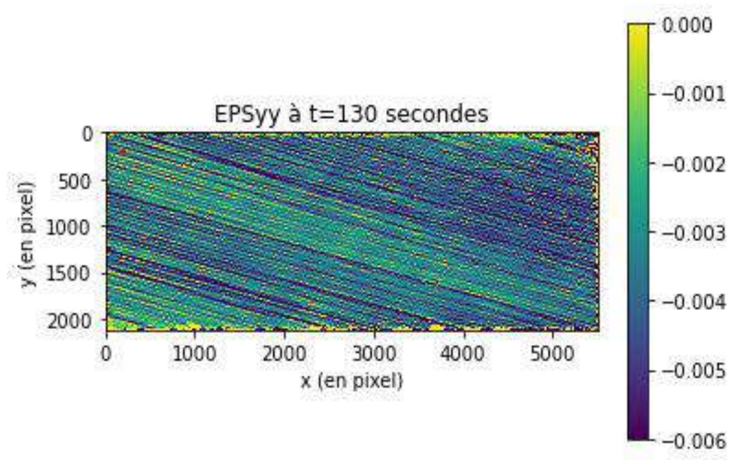

Conclusion :

Obtention de cartes de champs de déformations hétérogènes dont les hétérogénéités semblent liées à la structure interne (fibres, matrice) du composite.

Visualisation de la structure de l'éprouvette par tomographie RX :

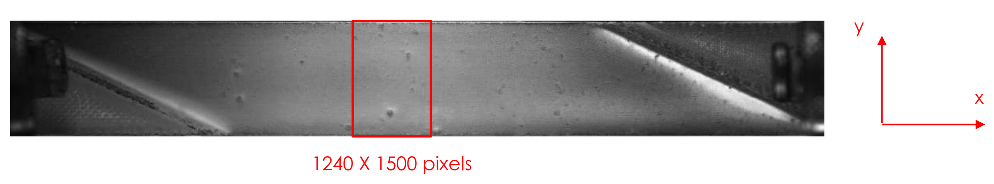

80 images de la profondeur (suivant z)

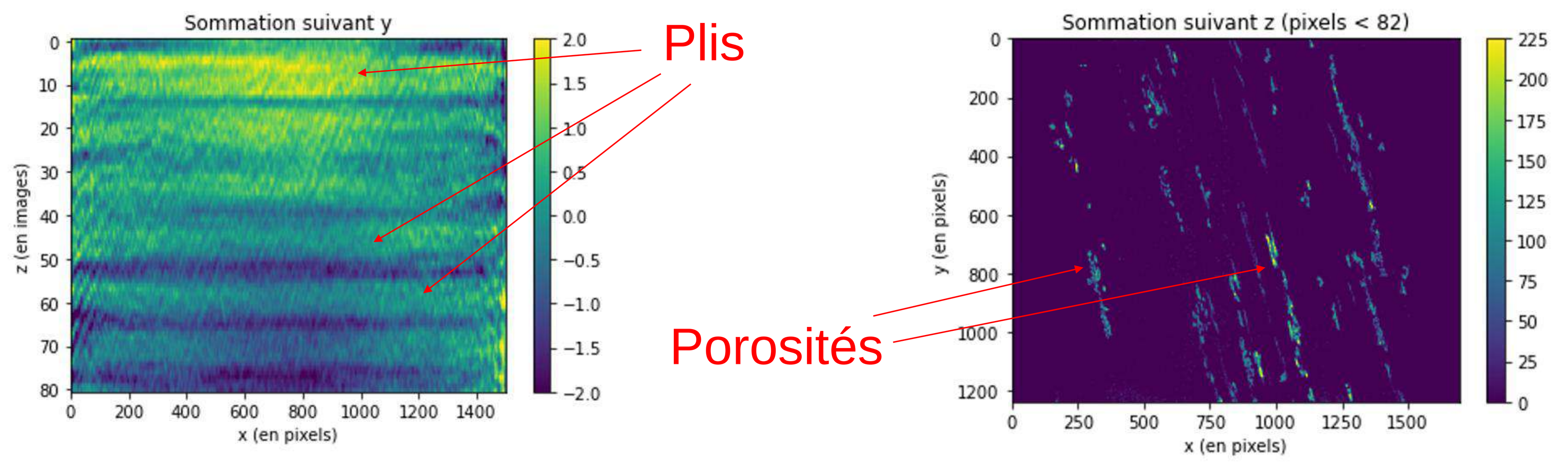

Perspectives :
- Réalisation d'un 2nd essai sur une éprouvette visualiser au préalable par tomographie pour faire une comparaison carte de champs de déformations et structure du composite
- Utilisation du système de mesure dans le cas d'un essai de dynamique rapide

[1] M.Grediac, F.Sur, B.Blaysat, « The grid method for in-plane displacement and strain measurement: a review and analysis », 2016.
[2] M.Grediac, B.Blaysat, « Extracting displacement and strain fields from checkerboard images with the localized spectrum analysis », 2018.